

*Proceedings from  
Faroe Islands Exploration Conference 2004*

---

## Contents

***Heri Ziska***

Introduction

### ***Scientific papers***

***Robert S. White, Roman Spitzer, Philip A.F. Christie, Alan Roberts, Zoë Lunnon,***

***Jennifer Maresh and iSIMM Working Group***

Seismic Imaging through Basalt Flows on the Faroes Shelf.

***Wayne C. Crawford and Satish C. Singh, Thomas Hulme and John R. Smallwood***

Applications of Seafloor Compliance Measurements in the Faroes-Shetland Basin.

***Stephen Linnard and Rob Nelson***

Effects of Tertiary Volcanism and later Events upon the Faroese Hydrocarbon System.

***Mark Woodfin, Jon Seedhouse, Giacomo Spadini and Maurizio Cardamone***

Elastic Impedance Inversion to aid lithology prediction in the Palaeocene of the Judd sub-basin.

***John R. Smallwood***

Lithology prediction from velocity data: Paleocene sediments in the Faroe-Shetland area.

***John R. Smallwood***

Quantity, distribution and provenance of Paleocene sediments in the Faroe-Shetland area.

***Dirk Frei, Thomas Rasmussen, Christian Knudsen, Michael Larsen, Andrew Whitham  
and Andrew Morton***

New methods and techniques for innovative, integrated provenance studies.

***Stephen Cawley, Hamish Matheson and Gordon Stalker***  
An Updated View of the Faroes-Shetland Petroleum System.

***Judith Keser Neish***  
Faroeese Area: Structural Interpretation of Seismic Data in a Basalt Environment.

***Heri Ziska and Claus Andersen***  
Exploration Opportunities in the Faroe Islands.

*Extended abstracts.*

***Marion Jegen-Kulcsar and Richard Hobbs***  
Outline of a Joint Inversion of Gravity, MT and Seismic Data.

***Rupert Hoare, Phil Schearer, Andrew Langridge, Emmanuel Saragoussi, WesternGeco, Philip Christie, Schlumberger and the iSIMM team***  
Imaging sub-basalt with deep towed streamer: A case study from the Faroe Islands.

***Nick Terrell, Huw Edwards, Perry Scoffield and Mark Martin***  
PGS Faroe Shetland Basin Mega Survey – the key to new discoveries in a maturing frontier area?

# Introduction

Hydrocarbon exploration on the Faroese Continental Shelf has to date a short but hectic history since the rights to the resources in the subsoil were finally handed over to the Faroese Government in 1992. The Foinaven field was discovered the same year and an intense focus for exploration for the Foinaven-analogous trap was initiated, with a few similar discoveries being found nearby in the following years.

However, there was going to be eight years before the first Faroese licensing round was opened. These years saw a lot of seismic activity, with large areas being covered by 3D seismic data. Some of these are presented by **Terrell et al** in “*PGS Faroe Shetland Basin Mega Survey – the key to new discoveries in a maturing frontier area?*”

The first licensing round on the Faroese Continental Shelf took place in 2000 and was a big success with eight wells committed on four of the seven awarded licenses. The licenses with well commitments were all located in the Judd basin or to the adjacent Sjørður Ridge.

Different lithology prediction tools were used prior to the wells being spudded, two of these are documented in this volume; **Woodfin et al** in “*Elastic Impedance Inversion to aid lithology prediction in the Palaeocene of the Judd sub-basin.*” and **Smallwood** in “*Lithology prediction from velocity data: Paleocene sediments in the Faroe-Shetland area.*” The wells did, however, demonstrate that there is an active hydrocarbon system and **Cawley et al** are discussing the implications of this in “*An Updated View of the Faroes-Shetland Petroleum System*” where they focus primarily on the Judd basin. **Linnard and Nelson** in “*Effects of Tertiary Volcanism and later Events upon the Faroe Hydrocarbon System*” discuss what effect the volcanism has had on the petroleum system.

Three of the four wells that are drilled to date have demonstrated an active hydrocarbon system in the basin, but it did also demonstrate that there

was a lot more sand in the basin than previously thought as discussed by **Smallwood** in “*Quantity, distribution and provenance of Paleocene sediments in the Faroe-Shetland area.*” The high influx of clastic sediments meant that the stratigraphic element in the Foinaven play was severely challenged.

The results from the first four wells resulted in a shift of focus from the Foinaven play to a more basic and robust structural play. There were already three licenses outside the Judd basin in an area which had a varying thickness of basalt cover compared to the very thin to absent basalt cover in the Judd basin. These areas contain more traditional structural targets, but are in real frontier areas from an exploration point of view.

One of the key issues when exploring the Faroese Continental Shelf outside the Judd basin is sub basalt imaging. Early seismic data indicate that there were structures under the basalt cover, but confidence in the mapping varied considerably and de-risking of prospects to a drillable level was unlikely. There has, however, been made a lot of progress in respect to seismic imaging as demonstrated by **Hoare et al** in “*Imaging sub-basalt with deep towed streamer: A case study from the Faroe Islands.*” and **White et al** in “*Seismic Imaging through Basalt Flows on the Faroes Shelf.*” **Neish** in “*Faroese Area: Structural Interpretation of Seismic Data in a Basalt Environment*” shows what can be done with conventional data through her presentation of seismic interpretations and TWT maps of sub basalt sections over much of the Faroese Continental Shelf. Other more unconventional approaches have been tried in order to support conventional seismic data as demonstrated by the **Jegen-Kulcsar and Hobbs** contribution on joint inversion of different data types in “*Outline of a Joint Inversion of Gravity, MT and Seismic Data*”, while **Crawford et al** suggests a new approach “*Applications of Seafloor Compliance*

*Measurements in the Faroes-Shetland Basin.*”, which attempts to utilize long wavelength surface waves through their loading effect on sub basalt sediments.

Another key issue has been reservoir provenance, with Greenland long being favoured as a key candidate. **Ziska and Andersen** do however, suggest that a Faroese basement and intrabasinal ridges are the primary provenance areas in “*Exploration Opportunities in the Faroese Continental Shelf*”. The key problem with this suggestion is that it cannot be tested because of lack of samples, but **Frei et al** do in “*New methods and techniques for innovative, integrated provenance studies*” suggest a new way of assessing provenance area, which can help solve this discussion, although samples from Faroese Basement are still required in order to be included in the analysis.

Recent developments have lifted the optimism considerably. These developments include the rumoured Cambo discovery, the Rosebank/Lochna-

gar discovery and a rumoured successful well test on the Laggan discovery. Cambo and Rosebank/Lochnagar are immediately adjacent to the Faroese/UK Boundary. These discoveries have, most likely, had an influence on the interest in the second licensing round, where awards were announced in January 2005. Here, ChevronTexaco and partners were awarded acreage across the boundary from their Rosebank/Lochnagar discovery, while Statoil with partners were awarded one license next to their held license no. 006. Statoil did also receive two more licenses. Føroya Kolvetni received one license on the Wyville-Thomson Ridge where no licenses were previously held. Geysir and Atlantic Petroleum were also awarded a couple of licenses in the Faroe Shetland Channel.

There is thus optimism regarding the future of hydrocarbon exploration on the Faroese Continental Shelf.

*Heri Ziska*



# Seismic Imaging through Basalt Flows on the Faroes Shelf

ROBERT S. WHITE<sup>1\*</sup>, ROMAN SPITZER<sup>1</sup>, PHILIP A.F. CHRISTIE<sup>2</sup>, ALAN ROBERTS<sup>1</sup>, ZOË LUNNON<sup>1</sup>, JENNIFER MARESH<sup>1</sup> AND iSIMM WORKING GROUP<sup>3</sup>

1: Bullard Laboratories, Madingley Rd., Cambridge CB3 0EZ, UK.

\*Email: rwhite@esc.cam.ac.uk; Tel: +44 1223 337187; Fax: +44 1223 360779

2: Schlumberger Cambridge Research Ltd., High Cross, Madingley Road, Cambridge CB3 0EL, UK.

3: iSIMM Working Group comprises N.J. Kusznir, R.S. White, A.M. Roberts, P.A.F. Christie, R. Spitzer, N. Hurst, Z.C. Lunnnon, C.J. Parkin, A.W. Roberts, V. Tymms and D. Healy.

## Abstract

Massive magmatism occurred on the North Atlantic margins when the continents broke apart in the presence of the Iceland mantle plume. The extrusive basalts on the Faroes Shelf create a considerable problem for seismic imaging by causing extensive scattering from the multiple lava flows and by attenuating the higher frequencies in the seismic signal. We have made considerable advances in imaging through the basalts and into the underlying sediments and basement by focussing on the generation and recording of low-frequency energy centred on ~10 Hz and by making use of the additional information available from long-offset data. We show how such low frequency seismic signals can be generated and recorded, and how long-offset data can be acquired using currently available technology. We outline the processing and imaging strategies we have developed and show results that illustrate these techniques from two recent seismic experiments (FLARE and iSIMM), shot across the Faroes Shelf and adjacent continental margin. Combination of normal incidence and wide-angle seismic data, together with the use of sources and receivers tuned to the low frequencies required for intra- and sub-basalt penetration enable us to see structure both within and below the basalts.

## Introduction

Extrusive igneous rocks dominate the northwestern flank of the Faroes-Shetland Basin and the Faroes Shelf. Flood basalts created at the time of breakup between the Faroe Islands and east Greenland extend over 250,000 km<sup>2</sup>, at least 40,000 km<sup>2</sup> of which lie in the Faroe-Shetland Basin (Naylor *et al.*, 1999). They attain a thickness of more than 7 km on the Faroe Islands themselves, and extend some 150 km eastwards from the islands to feather out in the Faroe-Shetland Trough (Figure 1). Their thickness and distribution in the Faroes area has been reported by White *et al.* (2003) and Sørensen (2003). The volcanic rocks in the Faroes region are

part of a much larger igneous province with up to 10 million km<sup>3</sup> of rock generated when the North Atlantic Ocean opened above a thermal anomaly in the mantle caused by a mantle plume which currently lies beneath Iceland (White and McKenzie, 1989; Eldholm and Grue, 1994). This larger igneous province extends from the northern tip of Norway to the southern part of Rockall Plateau on the eastern side of the North Atlantic, and down the east coast of Greenland on the conjugate margin.

Regionally, both the sediment supply and the availability of accommodation space within the Faroes-Shetland Basin through the Paleocene and Eocene were controlled primarily by the uplift caused by the Iceland mantle plume beneath the

lithosphere and by the volcanism in the Paleocene. So there is a complex and intimate link between the rifting, subsidence, sedimentation and igneous histories of the Faroes region (Doré *et al.*, 2002).

Early Palaeocene sedimentation in the basin was controlled initially by the underlying end-Cretaceous fault-induced topography (Ebdon *et al.*, 1995), until these fault basins were infilled. Subsequently a period of deep-water fan sand progradation across the basin developed, attributed by White and Lovell (1997) to enhanced erosion and base level changes caused by uplift of the shelf and hinterland by the proto-Icelandic mantle plume. Following the end of the Paleocene rifting, an abundant supply of clastic material, derived from the uplifted Scottish Highlands, built two major progradational packages out across the basin, the Lamba and Flett Formations. Clinoforms 500 m high in the Lamba, and at least 300 m high in the Flett Formation indicate the paleo-water depth and show the scale of the depositional systems. The major extrusive igneous activity which generated the first basalts on the Faroes commenced during deposition of the Flett Formation (White *et al.*, 2003).

The end of the basalt extrusion is marked by the culmination of a major uplift event and development of a regional unconformity, which forms the base to the overlying Balder Formation. The Balder Formation itself progressively onlaps the top basalt surface to the northwest as marine transgression proceeded and deep marine conditions were re-established across the basin in the Lower Eocene. A suite of sills in the centre of the Faroe-Shetland basin is thought to have been intruded mainly around the time of the Balder Formation (Smallwood and Maresh, 2002).

Overall, the Eocene and following periods were dominated by post-rift thermal subsidence. This general subsidence during the Cenozoic was punctuated by several periods of both local and regional uplift (Nadin *et al.*, 1997). A number of compressional events formed inversion structures in the Faroe-Shetland Basin between the late Paleocene and the Miocene, events which are now reflected in the shape of the top basalt surface (Boldreel and Andersen, 1993).

The extrusive lavas pose a particular problem for seismic imaging through to the underlying, possibly prospective, sediments and basement

structure. In this paper we discuss the main causes of these problems. We show that by focussing on the production and recording of low-frequency seismic energy, improved sub-basalt images can be obtained. We then discuss practical ways of increasing the low-frequency response of seismic profiling systems. Another helpful approach for sub-basalt imaging is to record seismic data to very long offsets, which provide additional refractions and wide-angle reflections at angles approaching the critical angles. By using new processing techniques, these wide-angle arrivals can be used to help identify deep reflections from the base of thick basalt sequences and the underlying structure.

We illustrate these techniques using data from two novel surveys on the Faroes Shelf. The first

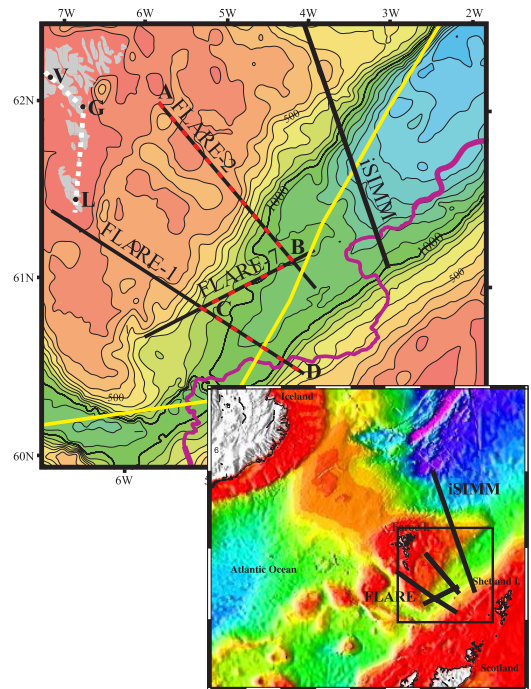


**Figure 1.** Map showing location of long-offset two-ship FLARE and single-ship, 12 km iSIMM profiles used in this paper. Main map covers the same area as basalt thickness map in Figure 9. Purple line marks southeastern limit of Tertiary basalt flows. Yellow line marks boundary between UK and Faroes waters. Bathymetric contours every 100 m. Red dashes mark the location of the composite seismic profile illustrated in Figure 8. Borehole locations marked by G - Glyvursnes; L - Lopra 1/1A; V - Vestmanna with white dotted line joining them showing line of cross-section in Fig. 2. Inset shows regional setting, area of main map and complete length of iSIMM profile.

is the Faroes Large Aperture Research Experiment (FLARE), which was acquired by the Amerada Hess Limited Partner Group. By using flip-flop firing from two seismic vessels, each towing streamers, profiles with offsets of up to 38,000 m were acquired. The second is the iSIMM (integrated Seismic Imaging and Modelling of Margins) profile, which extends 400 km across the northern Faroes Shelf and continent-ocean boundary (Figure 1).

### The requirement for low frequencies to penetrate basalts

Layered sequences of lava flows act as effective high-cut filters to seismic energy transmitted through them. This means that the higher frequency energy is attenuated rapidly, so most reflections from sub-basalt horizons are therefore rich only in the lower frequency energy.

There are now several good determinations of the effective seismic quality factor,  $Q$ , from basalt sequences on the Faroe Islands themselves, and from elsewhere in the North Atlantic, including the northern Rockall Trough (Maresh *et al.*, 2003). In addition, there are some measurements from both sub-aerial (Columbia River basalts) and submarine (Juan de Fuca Ridge) extrusive lavas elsewhere (Table 1). Most of the measurements of  $Q$  have been made by spectral analyses of seismic energy recorded from vertical seismic profiles (VSPs) in

boreholes. The spectral ratio method (Toksöz *et al.*, 1979), for estimation of  $Q$  works by comparing the spectrum of the waveform incident on the basalt layer with the spectrum after transmission through the basalt, so it is dependent on the incident waveform having a broad spectrum to start with.

Strictly speaking, the processes causing loss of the higher frequency energy are not primarily absorption, because massive basalt is not strongly absorptive. For massive basalts, the intrinsic  $Q$  is typically within the range 100–400. However, the effective  $Q$  values derived by spectral analysis provide a convenient measure of the effect of the basalt layers on the transmitted energy. The effective  $Q$  probably comprises a small component of intrinsic absorption, and a larger effect from scattering. The scattering disperses the energy, and preferentially scatters the higher frequency components for the velocity structure of typical lava flow sequences, and so removes it from the coherent first arriving reflections.

Part of the scattering is caused by the strongly layered nature of the basalt flows. Typically an individual lava flow has a massive interior, with vesiculated, weathered or even rubbly tops that exhibit lower seismic velocities (Planke, 1994). There may also be soil or sediment horizons between the flows which often have even lower seismic velocities. Since the individual flows are usually relatively thin (a few metres to a few tens

Location	$Q$	Reference
Columbia Plateau Basalts	48	Pujol and Smithson, 1991
Upper Basalt Series, Vøring Plateau, Norwegian Sea	~40	Rutledge and Winkler, 1987
Juan de Fuca Ridge, Pacific Ocean	20–50	Jacobsen and Lewis, 1990
Tertiary basalts, Northern Rockall Trough, North Atlantic	15–35	Maresh <i>et al.</i> , 2003
Lower Basalt Series, Lopra Borehole, Suðuroy, Faroe Is.	35	Christie <i>et al.</i> , in press
Upper and Middle Basalt Series, Glyvursnes borehole, Streymoy, Faroe Is.	~10–45	Shaw <i>et al.</i> , 2004

**Table 1.** Summary of Effective Seismic Quality Factor,  $Q$ , from Basaltic Flow Sequences

of metres thick), a typical stack of lava flows may contain hundreds of sub-horizontal interfaces with large impedance contrasts. These readily cause numerous intra-basalt multiples, which scatter the energy (Christie *et al.*, in press).

Within the Faroe Islands themselves, three scientific boreholes penetrate portions of the Lower, Middle and Upper Basalt formations. These are the Lopra, Vestmanna and Glyvursnes boreholes (Figure 2), and all three have been extensively cored, logged and studied by VSPs and wide-angle seismic experiments (Japsen *et al.*, 2005). Quality factors of  $\sim 10$ – $45$  have been reported (Christie *et al.*, 2002, and in press; Shaw *et al.*, 2004), with typical values being 35–40. There is some indication in the Glyvursnes borehole that  $Q$  increases with depth, which may partly be caused by the difference between the Upper and the Middle Basalt formations (Figure 2), and partly due to increasing depth beneath the surface correlating with a smaller percentage of open pore space and fractures. In offshore basalt sequences on the Faroes Shelf, velocity gradients ranging from 0.1 to 0.7 km/s per km are found (Flidner and White, 2001a; Spitzer *et al.*, 2004). Such velocity gradients are also indicative of a decrease in the amount of cracking and pore space with depth which would tend to correlate with an increase of  $Q$  with depth.

In Figure 3a we show theoretical calculations of the effect on the frequency content of waveforms that have undergone two-way transmission at normal incidence through a 1-km-thick basalt sequence with an average seismic velocity of 4 km/s for a range of different realistic values of  $Q$ . The incident wave has an amplitude of unity at all frequencies and this diagram shows the effect of

attenuation without including any other factors that might affect the amplitude, such as geometric spreading or interference between reflections off different interfaces. The high frequencies are extremely rapidly attenuated. For example, if  $Q$  is 25, then a 10 Hz signal will lose slightly less than half of its amplitude in two-way transmission through a 1-km-thick basalt layer, while a 50 Hz signal will lose 96% of its amplitude. Or, in other words, a perfect reflection from the base of the basalts will retain 53% of the incident amplitude for a 10 Hz signal, but only 4% of the incident amplitude for a 50 Hz signal.

So if we wish to see seismic reflections from beneath thick basalts, there is little alternative than to use low frequencies. The unfortunate corollary is that the low frequencies limit the resolution, but it is better to lose some resolution and to obtain interpretable sub-basalt reflections than to use higher frequencies and as a result to record no reflected sub-basalt energy above the noise levels.

### Generation and recording of low-frequency seismic energy

In the context of imaging sub-basalt structure, seismic sources rich in energy at about 10 Hz are required, although it is also important to retain as great a bandwidth as possible to ensure maximum resolution until the signal becomes swamped by noise. Conventional airgun sources, typically peak-tuned, towed at 5–8 m depth, with volumes of  $\sim 70$  litres (c. 4,000 cu. in.), and centre frequencies of  $\sim 50$  Hz still produce some energy at low frequencies, and have proven to be capable of penetrating at least thin sections of basalts. The FLARE profiles provide an example of this (White *et al.*,

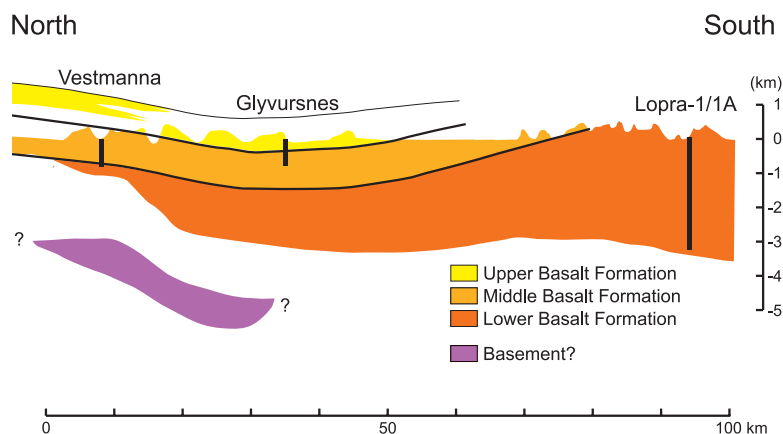


**Figure 2.** Stratigraphic position of boreholes through basalt on the Faroe Islands, superimposed on cross-section passing through the boreholes (modified from Waagstein, 1988). For location of cross-section and boreholes, see Figure 1.

2003), although the signal-to-noise ratio and hence the confidence of interpretations of weak sub-basalt reflectors are much poorer than with sources designed to be rich in low frequencies (Lunnon *et al.*, 2003; Spitzer *et al.*, 2004).

Using conventional airgun technology there are three main ways of producing low frequencies with significant energy at ~10 Hz using marine sources.

#### *Use big airguns*

At a given depth and air pressure, the larger the airgun volume, the lower the frequency of the bubble pulse. So the simplest way to produce lower frequencies is to increase the chamber volume. This is not completely trivial, because the larger the chamber, the more difficult it is to evacuate the air quickly through the vents once the gun is triggered. But this concept has been used by Ziolkowski *et al.* (2003), to produce low-frequency energy centred at 20 Hz by using 'large' chambers (the chamber size is not specified in their paper). The disadvantage of using a limited number of very large guns is that the source may become rather monochromatic, which can be deleterious to resolution. But it is arguable that the low-pass filtering effect of thick basalt flows only allows a limited range of frequencies to penetrate the basalt in any case, so this may be less of a drawback than it at first appears.

A more conventional way to increase the overall airgun volume is to use standard arrays of airguns, but with more guns, perhaps biased toward the larger conventional chamber sizes. Using this approach, the FIRE (Faroes-Iceland Ridge Experiment) profiles shot in 1994 across the continental margin northwest of the Faroe Islands achieved a total volume of 153 litres (9,324 cu. in.), with 48 guns, the largest of which was 8.2 litre (500 cu. in.). The source was towed at a depth of 10 m. Good arrivals were recorded at ranges up to 160 km after propagation through the basaltic crust and upper mantle beneath the 35-km thick Faroe-Iceland Ridge (White *et al.*, 1996; Smallwood *et al.*, 1999; Staples *et al.*, 1999). One of the disadvantages of simply increasing the power of the source array, however, is that the source-generated 'noise' due to multiples and water-wave 'wrap-round' (McBride *et al.*, 1994) is also increased. It may then become necessary to increase the interval be-

tween shots to allow the source-generated noise to decay, and this of course has the deleterious effect of reducing the fold of cover.

#### *Tow airguns deep*

The sea-surface acts as an almost perfect reflector, because there is such a large impedance contrast between water and air. It also causes a phase reversal in the downward reflected wave. Since airgun arrays radiate energy in all directions, the downward-travelling wave which is used for seismic imaging is supplemented by the surface reflected wave, which is phase-inverted and delayed in time by an amount dependent on the depth of the source beneath the surface. Constructive interference occurs if the source is towed at a depth of one quarter of a wavelength. So, for example, since the speed of sound in water is close to 1500 m/s, the optimum depth for constructive interference is 19 m at 20 Hz, or 38 m at 10 Hz.

However, there is a counter-effect of increasing the tow depth of airguns. Because the ambient pressure is higher at greater depth, the frequency of oscillation of the bubble pulse increases as a gun of any given volume is towed deeper. So there is a trade-off in increasing the tow depth of airguns between enhancing the constructive interference from the sea-surface reflection by going deeper, while preventing the primary bubble frequency increasing too much by not going too deep.

In practice, this trade-off is optimized at an airgun tow-depth of 15–20 m, and several surveys designed for low frequencies have used arrays at such depths. They include the survey reported by Ziolkowski *et al.* (2003), mentioned above and the FLARE survey, from which we show extracts later in this paper, which both used airgun depths of 15 m. The iSIMM profiles, which are also discussed later used 18–20 m airgun depths (Lunnon *et al.*, 2003). An airgun array depth of up to 20 m is operationally attractive because it can usually be accommodated within the normal towing arrangements of the airgun array on a seismic acquisition vessel. It is also worth noting that although the peak enhancement at 19 m depth occurs at a frequency of 20 Hz, which is somewhat higher than our optimum of 10 Hz, as Figure 3b shows, the sea surface reflection enhances the source signal over a bandwidth of 2.32 octaves up to the first notch at which destructive interference reduces the signal



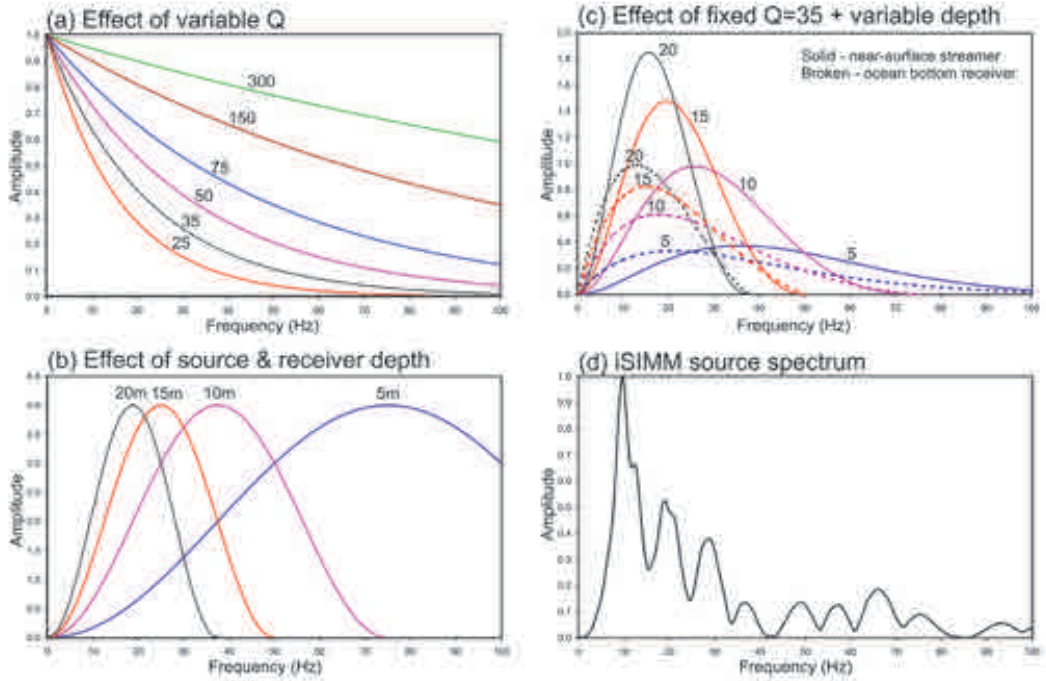


**Figure 3.** Theoretical calculation of effect of quality factor  $Q$ , and depth of source and receiver on frequency-dependent amplitudes of seismic waves passing through basalt. All calculations are for two-way transmission at normal incidence through a 1 km thick basalt layer with an average seismic velocity of 4 km/s and do not include any other sources of amplitude variation, such as geometric spreading or interference between multiple reflectors. Incident wave has an amplitude of 1.0 across all frequencies from 0–100 Hz. Panels (b) and (c) only show the response up to the first notch where destructive interference occurs. (a) effect of varying  $Q$ ; (b) effect of varying the source and receiver depth (both kept identical); (c) effect of holding  $Q$  fixed at the geologically typical value of 35 (black line in Fig. 3(a)), solid lines show effect of different source and receiver depths (both identical), broken lines show effect of different source depths with a deep water ocean bottom receiver; (d) far-field source spectrum including the source ghost used for iSIMM seismic reflection profiles, with bubble-tuning and source at 18 m depth.

to its minimum, at whatever depth the source is towed (Lunnon *et al.*, 2003). So towing the source deeper than the conventional depth of 5–8 m always enhances the low-frequency response. At 19 m depth there is a significant enhancement at 10 Hz in addition to the maximum enhancement at 20 Hz.

There is a marked effect of combining the low-frequency filtering effect of the basalts with the tow depth of the source and receivers. This is shown in Figure 3c, where we assume a typical value of 35 for the quality factor,  $Q$  based on observational results from basalts in the Rockall and the Faroes regions (Table 1), and demonstrate the interaction of this with the low-frequency enhancement of towing deep. The overall result is that the window for energy to propagate through the basalts is centred on the low-frequency part of the spectrum, so to make full use of this it is important to tune the

source to match as far as possible the frequency pass band of the basalts, while maintaining as large a bandwidth as possible for the source to optimise the achievable resolution.

#### *Use bubble tuning rather than peak tuning*

A novel way to enhance the low frequency energy in an airgun source is to set the individual firing delays on the airguns such that the first bubble pulse of the different airguns is enhanced rather than to use the conventional firing method which enhances the first peak. This was first suggested by Avedik *et al.* (1993), based on earlier work by Safar (1980), together with a refinement that different sized airguns might be towed at different depths so as to individually optimize the enhancement of their bubble frequencies by towing close to their individual optimum depths for reinforcement by the sea-surface reflection. In designing

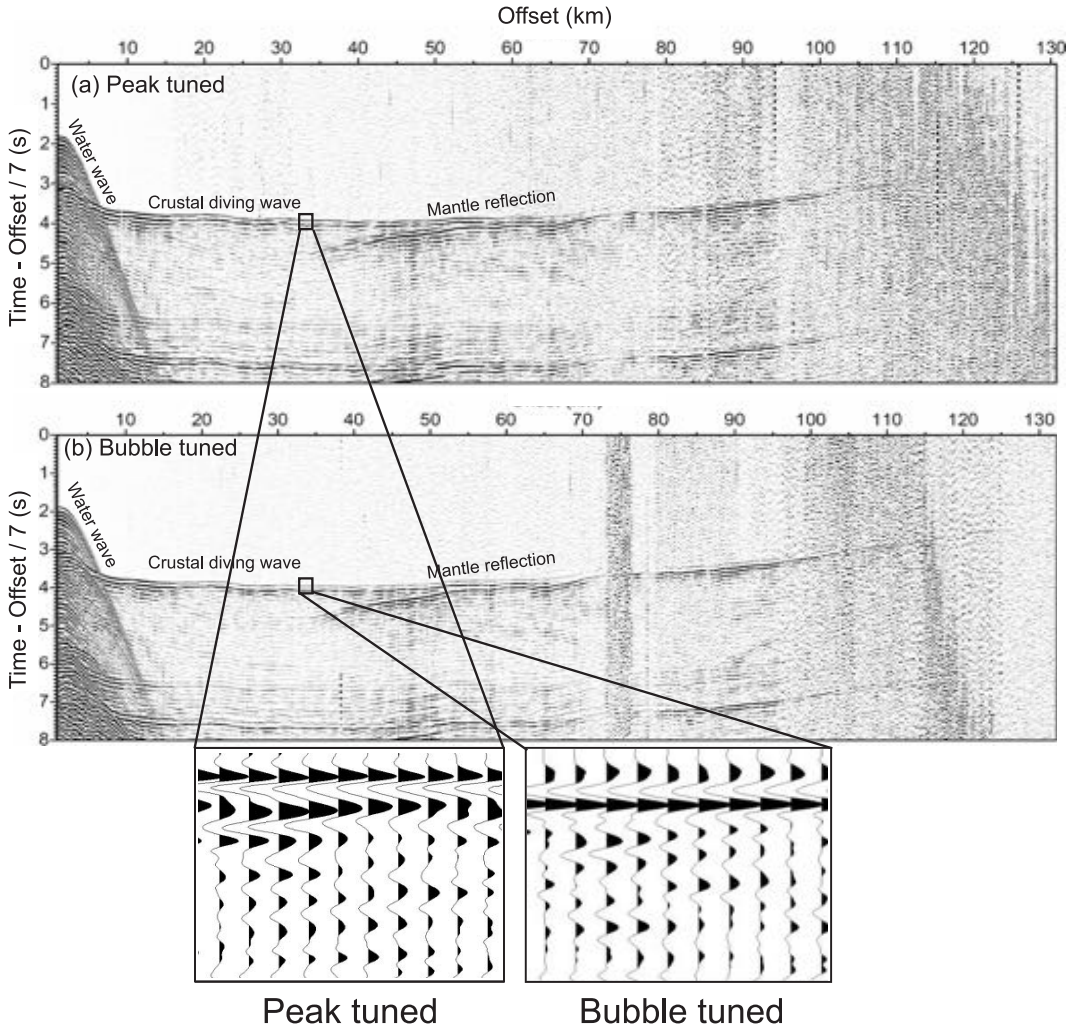


**Figure 4.** Receiver gathers from an OBS on the iSIMM profile to show the difference between (a) peak tuning, and (b) bubble tuning. Location of OBS is shown on Figure 10, with shots fired toward the southeast. Both profiles use the same airgun configuration of a 104 litre, (6,360 cu in.) array of 14 guns towed at 20 m depth, with the only difference being the tuning method. Note the sharp wide-angle Moho reflection, which attains high amplitude beyond 35 km offset as the critical distance is approached. Data are band-pass filtered 3–18 Hz, and only every second trace is displayed after a running trace mix. Reduction velocity (equivalent to linear moveout) of 7 km/s means that arrivals with a phase velocity of 7 km/s are horizontal in this display. Enlargements show the more compact nature of the bubble-tuned source. Figure after Roberts *et al.* (in press).

the source for the iSIMM profiles we took a similar approach of tuning on the first bubble pulse. From far-field monitoring of the wavefield using vertical arrays we have shown that the iSIMM bubble-tuned source contains significantly more low-frequency energy than an identical source fired with conventional peak-pulse tuning (Lunnon *et al.*, 2003). From repeat firing into fixed ocean bottom seismometers deployed along the iSIMM profile using first peak tuning and then bubble tuning, we have also found that the long-range propaga-

tion of low-frequency seismic energy is markedly better for the bubble-tuned sources (White *et al.*, 2002; Roberts *et al.*, in press). Another advantage of the bubble-tuned source, reported by Lunnon *et al.* (2003), is that after it has propagated through the earth filter produced by the subsurface, the bubble-tuned waveform is more compact than the peak-tuned waveform, so is capable of producing better resolution of deep structure, a characteristic which is of particular importance with wide-angle ocean bottom seismometer data (Figure 4).

The iSIMM source for the Q-streamer profile data, from which we show extracts later, used a 48-gun, 167 litre (10,170 cu in.) array towed at 18 m depth with bubble-tuning (White *et al.*, 2002; Hoare *et al.*, this volume). Individual airgun chamber sizes ranged from 1.7 to 4.8 litres (105 to 290 cu in.), with some of the guns clustered to produce an effective volume of 9.6 litres (580 cu in) from the clusters. The resultant waveform is rich in low frequencies (Figure 3d), producing considerable energy in the window which allows propagation through the basalts and making it well matched to the geological requirements. Operationally, an advantage of bubble-tuning is that it can use conventional airgun arrays with just a minor change to the firing control parameters.

#### *Source signature*

Whatever source is used, the Common Mid-Point stack is improved if shot-by-shot designature is applied before stacking. This is better than a purely statistical approach to source deconvolution which optimizes some chosen statistical measure, and is also better than the normal assumption that the source signature is invariant along the profile. However, there is a practical problem in recording the far-field signature of every shot. One approach is to tow a hydrophone at depth to record the outgoing waveform from each shot. This is difficult to do because at a normal acquisition ship speed of about 5 knots, it is not easy to hold a hydrophone both at sufficient depth, and sufficiently close to the ship to record the downgoing far-field waveform. There is, in addition, often a practical problem in that the water depth may be insufficient to allow recording of the far-field waveform in the water column. Another experimental approach for assessing the far-field waveform for each shot, reported by Hobbs and Jakubowicz (2000), is to fire a small reference source immediately prior to the main airgun array, and from that to calibrate the main source using the seabed reflection as a signal common to both.

An alternative approach to shot designature is to record the waveforms at individual pressure sensors or accelerometers close to each airgun, and then to reconstruct the far field source signature from these individual near-field measurements (Ziolkowski *et al.*, 1982). This approach was used for the iSIMM towed streamer profiles shown

here, using calibrated sensors near to each gun. An advantage of shot-by-shot designature is that small changes in the airgun source can be accounted for on every shot. In the case of the bubble-tuned, deep-towed source, we had no prior calibrated library signature and so the use of shot-by-shot signature monitoring was a key enabler in deconvolving the complex source signature into a standard, simple wavelet for further processing.

#### *Receiver optimisation*

The major control which can be applied to the normal streamer configuration so as to enhance the low-frequency response is to tow it deeper, as the sea surface ghost enhances the low-frequency response. In the iSIMM profiles displayed in this paper, the source and streamer were both towed at 18 m below the sea surface, because this doubles the effect of constructive interference. At the frequency corresponding to the optimum depth the amplitude is increased by a factor of four (Figure 3b). An additional benefit of towing the streamer deep is that it is less susceptible to wave noise from rough seas. Since the wave noise is generally at the low-frequency end of the spectrum, this proves to be an important benefit because it gives a much lower noise level in precisely that part of the spectrum that we have to use for detecting sub-basalt returns.

If bottom receivers are available, either as ocean bottom seismometers or as a bottom cable, the bandwidth available is further enhanced, because the signal at the receiver detectors (at least in deep water), do not suffer the notches created by the sea-surface interference. This is demonstrated in Figure 3c: the solid lines show the effect of towing both the source and the receiver at a range of (identical) depths, while the broken lines show the response of a seabed receiver, with only the source at varying depths. Although the amplifying effect of the sea-surface reflection due to constructive interference is greater when the receiver is near the surface (solid lines), the bandwidth is considerably greater when the receiver is on the sea bottom (broken lines). Since the limiting noise level is often signal-generated (multiples and scattering), rather than the ambient background level, the absolute signal level is probably of less importance than the ability to record low frequencies, so the greater bandwidth available from a bottom cable is likely



to have a highly beneficial effect on sub-basalt imaging.

## Long-offset acquisition

Acquisition of wide-angle data, which requires long offsets, provides considerable additional information that is useful for sub-basalt imaging. In this section we first examine the theoretical basis for this assertion and the types of additional or supplementary information that can in principle be derived from wide-angle data, then we discuss practical ways of acquiring long-offset data, and finally show examples of its use in practice in the Faroes region.

In almost all conventional processing of multichannel seismic reflection profiles, one of the first steps is to mute all the energy outside the water-wave cone. This is partly because a large part of this energy at larger offsets comes from diving waves (sometimes called refractions), with close to linear moveout. If they were to be included in the normal hyperbolic moveout correction that is used in stacking the data, they would not stack properly (because they have linear rather than hyperbolic moveout), and so would generate coherent noise on the stacked section. A further problem is that at large offsets the wide-angle reflections from closely-spaced layers, such as those in sediments, converge with increasing offset. When these arrivals are brought back to normal incidence along a hyperbolic moveout curve, they are stretched. If the stretch becomes unacceptably large this degrades the image, so for this reason, too, a mute is often applied to the longer offset data. However, there is considerable information, particularly on the velocity field, in these wide-angle arrivals, so if they are used in conjunction with the better imaging characteristics of the conventional near-offset field, the combined result is both improved imaging and a better understanding of the sub-surface geology.

### Theoretical Considerations

The resolution of the stacking velocity in deeper parts of conventional seismic profiles decreases with increasing depth, simply because the moveout of the hyperbolic reflections decreases. At wide angles the velocity resolution improves markedly,

partly because diving waves are travelling sub-horizontally and so have much greater moveout with offset than do the near offset reflected waves, and partly because the increased spatial recording aperture of long-offset data provides a larger distance over which to record moveout. There is, however, another significant effect which is of particular importance in sub-basalt imaging, especially when basalt layers overlies sediments with lower seismic velocities. This is that the low-velocity sediments beneath basalts produce a distinctive and easily recognised step-back in the travel times of diving waves as they pass through the low-velocity layer. This is demonstrated in Figure 5, which is a full-waveform synthetic seismogram from a simple 1-D velocity model with a 1.5 km thick basalt layer. A step-back of about 1 sec in the first arriving energy occurs at about 20 km offset. The ray-diagram in the lower panel of Figure 5 shows the reason for this. As the rays (shown in green on Figure 5) pass through the base of the basalts they are refracted away from the normal by the lower underlying velocities, and are only refracted back toward the surface when they enter the higher velocity material of the basement.

The size of the travel-time step-back is determined by the product of the thickness of the low-velocity zone and its velocity, and the two cannot be calculated independently just from the magnitude of the step-back. However, on long-offset data the moveout of the top-basement reflection (solid green line on Figure 5) may be used to determine the sub-basalt sediment velocity and hence its thickness.

The synthetic seismogram in Figure 5 also illustrates another common problem with sub-basalt imaging, which is that there is a great deal of multiple and mode-converted energy present. This is a very simple 1-D model, yet contains many non-primary arrivals: in the real world with laterally varying structure, the complexity of such arrivals only increases. But this example also illustrates another important feature of long-offset arrivals: the first arriving energy is always a primary p-wave, and not a multiple. This means that we can have confidence in using these arrivals to identify primary features of the profile. As discussed later, our approach is to migrate these wide-angle arrivals back to normal incidence, and to use them to 'tag' reflectors that we can then image with better

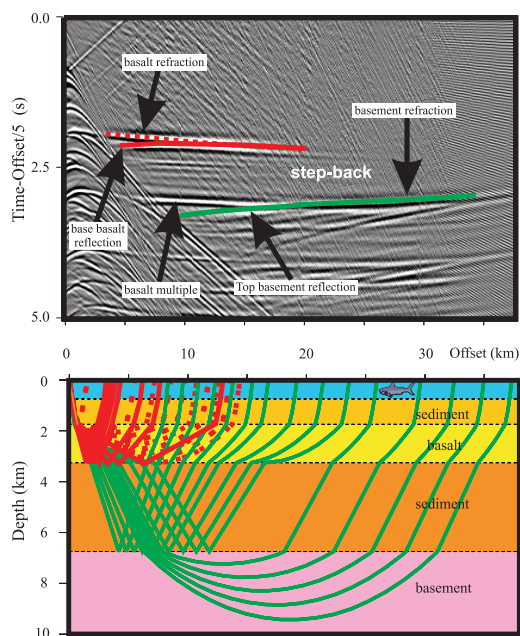


**Figure 5.** Synthetic seismogram calculated using the full waveform reflectivity response (Fuchs and Müller, 1971), showing the main arrivals and corresponding raypaths that constrain the thickness and velocity of the basalt and of the sub-basalt sediment, modified from White *et al.* (2003). Broken red rays are diving waves through the basalts and solid red rays are reflections off the base of the basalts. Green rays are diving waves through the basement and reflections off the top of the basement. Note the step-back of about 1 s in first arrivals visible at an offset of about 20 km, caused by the low-velocity sediments lying beneath the high-velocity basalt flows. Travel times are reduced with a linear moveout of 5 km/s.

resolution from the near-offset data, having confidence that they are not multiples.

### Travel time tomography

From the travel times alone, the gross structure can be derived by ray-tracing through a model of the velocity field and iterating the model until there is a satisfactory fit between the calculated and observed travel times. There are several forward modelling and inverse ray-tracing programs that can be used for this, some of which use only first arrivals and others of which also accommodate second arrivals and reflections. This is generally a labour-intensive technique, because it depends on identifying and picking arrivals from coherent phases. There is always the possibility of a trade-off between vertical and lateral variations in ve-

locity structure. Therefore the velocity model is constrained best where there are multiple crossing ray-paths. An example of this is shown in Figure 6, from the FLARE-1 profile (location shown in Figure 1). These data were from multi-pass, two-ship profiles, with maximum offsets of 38 km (White *et al.*, 1999), and provide a first look at the structure beneath the basalts that flowed east from the rift zone near the present location of the Faroe Islands toward the Faroe-Shetland Trough. The crossing ray-paths constrain the structure down to the top of the acoustic basement rocks (probably here of Cretaceous age by analogy with rocks drilled on the eastern flank of the Faroe-Shetland Trough) beneath the basalts. This does not provide detailed structural information on the sub-basalt sediments, but it is sufficient to demonstrate their presence and approximate thickness. It also provides velocity information that can be used for pre-stack depth migration of seismic profile data along the same line.

Another aspect of long-offset data is that the depth of good resolution is limited by the maximum offsets to which data are recorded, as illustrated in Figure 6a. In the particular profile shown in Figure 6, we also deployed 3-component land stations on the Faroese island of Suðuroy, straddling the Lopra borehole and crossing the island (Richardson *et al.*, 1999). The longer-offset arrivals recorded by these fixed stations detected Moho reflections at large range, which allow the depth of the Moho to be constrained, at least at the reflection points.

### Integration of seismic and other data

Although seismic surveying remains the technique of choice for imaging the sub-surface, regional extrapolation is possible using other potential field measurements such as gravity, magnetic field and electromagnetic sounding. For example, the Moho has been extrapolated along the profile in Figure 6 using gravity data and the local constraint from the land recording of a wide-angle Moho reflection over a short length of the profile. Magnetic anomaly measurements are also useful for mapping the basaltic and top basement layers (Smallwood *et al.*, 2001), and direct measurement of gravity gradients may also yield high-resolution information on the sub-basalt structure (Murphy *et al.*, 2002). Other more experimental techniques that may

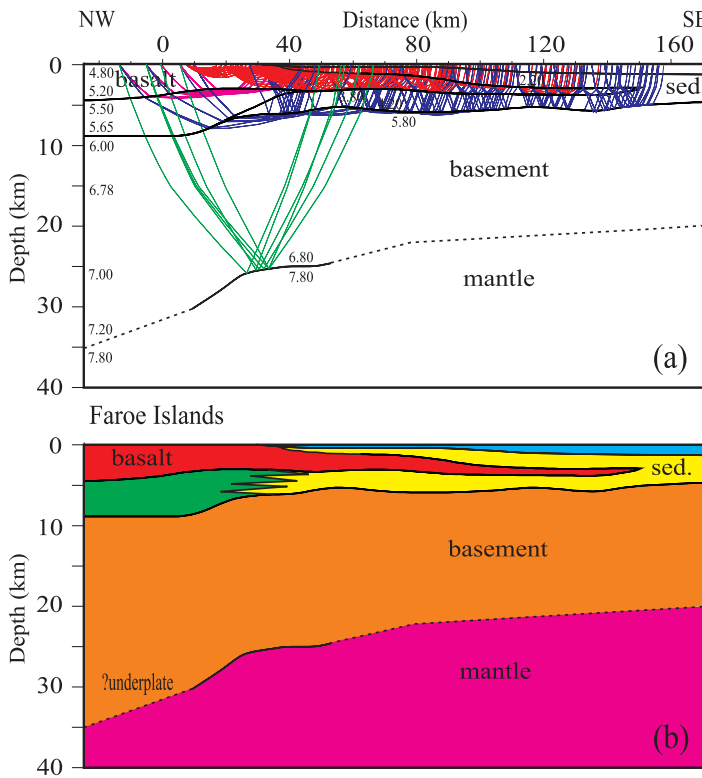


**Figure 6.** (a) Representative wide-angle ray-paths from travel-time tomography through the crustal velocity model along the FLARE-1 profile, including both offshore two-ship data (38 km maximum offset), and onshore land station recording on Suðuroy, which also recorded Moho reflections (for location of FLARE-1 see Figure 1). 0 km is at the projected position of the Lopra well (Figure 1) onto the profile. Red rays are those turned in the basalt layers, or reflected off their bottom. Blue rays are reflected off the top of the basement which marks the base of the sub-basalt sediments, or returned as diving rays through the top of the basement. Green rays are reflections off the Moho. Only every tenth ray is shown for clarity. Selected velocities shown in km/s. (b) Interpreted cross-section from the seismic data above, with the extension of the base of the crust across the Faroes shelf extrapolated by gravity modelling from the region where it is constrained by seismic data. Figures modified from Richardson *et al.* (1999).

help show the presence of sub-basalt sediments include controlled source electromagnetic measurements (MacGregor, 2003), seabed compliance measurements (Crawford *et al.*, this volume), and joint inversion of data from different sources such as gravity, MT and seismic (Jegen-Kulcsar and Hobbs, this volume).

### Imaging with wide-angle data

Although, as shown in Figure 6, a certain amount of geological interpretation can be obtained from just the 2D velocity field in the subsurface (and this is enhanced if the shear wave velocities and hence the Poisson's ratios of the layers can be determined, because then the rock types are constrained better), an important objective of exploring the geology beneath basalts is to make an image of the sub-basalt region. The recognition of tilted fault blocks, of sills or of structures likely to be of interest as hydrocarbon reservoirs requires knowledge of the shape of reflectors and of the structure of the subsurface. Such images are still obtained most effectively from the nearer-offset reflection data conventionally used for seismic profiling. Unfortunately, even if the energy does

penetrate below the basalts, the near-offset images are plagued by the presence of many interbed multiples. Therefore, it is often difficult to know which deep arrivals are primary and which are multiples.

However, the wide-angle data can also be migrated back to normal incidence using pre-stack migration techniques, provided the velocity field is well known (for example from travel-time tomography). If the portion of the wide-angle wavefield outside the water-wave cone that is known to come from the base-basalt reflection is isolated and then is migrated back to normal incidence, this will give a low-resolution image of the shape of the base-basalt reflection (Flidner and White, 2003). The fact that reflection amplitudes generally increase as the critical angle is approached means that the wide-angle reflections are often very strong, which improves their usefulness for imaging. These migrated wide-angle reflections can then be used to 'tag' which of the many candidate reflections on the profile constructed from the near-offset data is in fact the base-basalt reflection. An example of this is shown in Figure 7, from FLARE profile 2 (see Figure 1 for location). The upper panel (Figure 7a) shows the entire pre-stack depth migrated

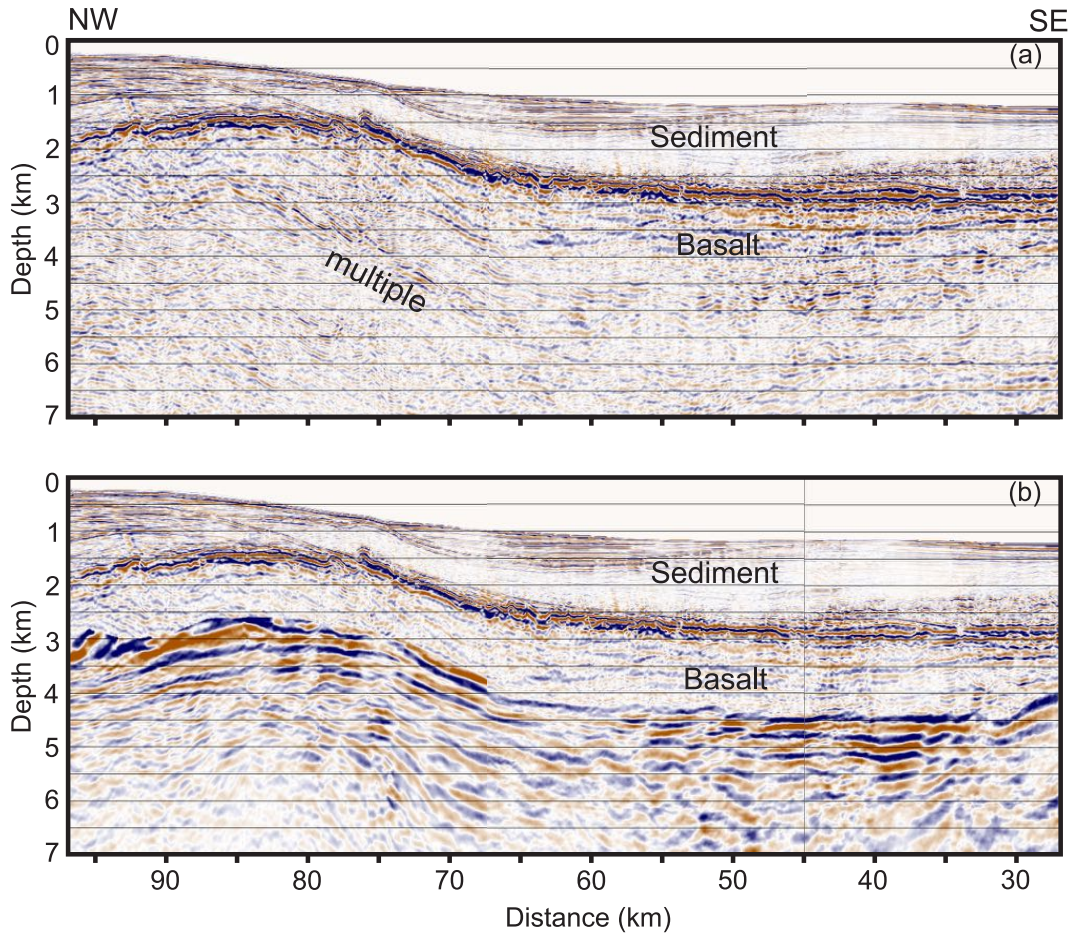


**Figure 7.** Enlargement of part of FLARE 2 profile (from White *et al.*, 2003), showing (a) pre-stack depth migration of the entire seismic dataset, and (b) composite image produced by combination of the shallow sediment and top-basalt section with the migrated wide-angle base-basalt arrival. Note the better resolution of the upper panel, but the usefulness of the wide-angle data in the lower panel for identifying which of the candidate reflections in the upper panel is indeed the base-basalt reflector – others are likely to be caused by multiples. See Figure 1 for location.

dataset, complete with many multiples, while the lower panel (Figure 7b) has migrated wide-angle data superimposed. From this it is clear which reflector is from the base-basalt, therefore facilitating interpretation. The technique can be extended to other prominent wide-angle reflections, such as the basement reflector that forms the base to the sub-basalt sediments (Flüedner and White, 2001b), or the prominent wide-angle reflections off the base of the crust (as shown in Figure 4).

#### **Amplitude modelling and waveform inversion**

The amplitudes of seismic reflections and refractions contain much more information on the velocity structure than do the travel times alone. In

general, the amplitudes are controlled by more local structure than the travel times, because the amplitude of a reflection is affected strongly by the impedance contrast across the reflecting interface, whereas the travel time is the integrated effect of travel along a long path through the entire structure between the source and the receiver. Flüedner and White (2001a) have shown how synthetic seismogram modelling can be used to infer details from wide-angle data of the velocity structure of offshore basalt flows in the Faroes region. Around boreholes, the matching of well log information with surface seismic data is a well-known technique (e.g., for Lopra well, see Christie *et al.*, in press): the frequent observation from such studies



is that while massive single flows can occasionally be identified, the reflectors imaged within basalt sequences are an integrated interference effect of flows on a much finer scale than the seismic wavelength (e.g., Smallwood *et al.*, 1998).

Waveform inversion of the full wide-angle dataset is the obvious next step in constraining the seismic velocity structure along a profile. At present waveform inversion is limited partly by the quality of available data, and partly by the huge computer resources required. In all cases, it is desirable to use a travel-time tomographic method first to find the large-scale velocity structure, and then to use waveform inversion to refine this model. By making simplifying assumptions such as restricting model construction to the acoustic case and ignoring converted energy, or by inverting using a limited number of frequencies in the spectral domain, an inversion scheme can be implemented in a reasonable time using current computer technology (e.g., Pratt, 1999). The ultimate goal remains use of a full elastic model in the waveform inversion (e.g., Shipp and Singh, 2002).

## Methods of recording long offsets

### *Use long streamers*

The simplest way to record to longer offsets is to tow a longer streamer. Streamer lengths have increased from a typical 2,400 m in the 1970s to a routine 6,000 m and up to 12,000 m for specialist profiles by the end of the 1990s. In the iSIMM survey three streamers were deployed, with a 12,000 m streamer in the centre, and two 4,000 m streamers towed 150 m to either side. This gives a measure of 3D control, particularly on the shallow subsurface structure and on returns scattered from rough surfaces. Relative positioning between the streamers was recorded by acoustic cross-bracing, which allows the three hydrophone streamers to be used to estimate directions of wavefronts moving across the streamer antennae. The fidelity of the detectors within the streamers has also improved over the years, moving from analogue to digital streamers, and in the case of the WesternGeco Q-streamer used for the iSIMM acquisition, to closely spaced (3.125 m) single sensor recording. The 12-km long streamer used for the iSIMM profiles contained 4,000 separately recorded sensors. The

advantage of single-sensor recording is that it is possible to use data or noise-adaptive spatial filtering in post-processing after the acquisition to form traces at conventional group intervals (typically 12.5 m or 25 m) with high signal-to-noise ratios for further processing.

With such long streamers it becomes important to know the geometric shape and location of the streamer, which may be pushed sideways behind the ship by the effects of currents and wind. The shape of the streamer behind the ship may be determined by Global Positioning Satellite (GPS) measurements of the locations of buoys at the head and tail of the streamer, together with acoustic cross-bracing and/or magnetic compasses positioned along the streamer.

### *Use two ships*

If two seismic vessels are sailed in line astern, a much longer streamer can be synthesised than that towed by a single ship. In the simplest form of this, the trailing ship steams just behind, or alongside the tail buoy of the lead ship, so that the maximum offset is the sum of the two streamers. This has the advantage of there being just one airgun source array, so there is no variation in source along the synthesised streamer, and the shooting ('pop') interval can be as small as in a conventional streamer profile – typically 50 m.

An interesting development of this is to fire airguns alternately from the two ships in a flip-flop firing pattern, in a method first described by Stoffa and Buhl (1979), and by Buhl *et al.* (1982). If the streamers on each ship are the same length, and the trailing ship is two streamer lengths behind the lead ship, then all offsets from zero to three times the streamer length are recorded by this arrangement: so with 6,000 m long streamers, the two ships together can record a profile with offsets up to 18,000 m in a single pass. If multiple passes are made with different ship separations, it is possible to synthesise arbitrarily long streamers. Using this method, the FLARE profiles on the Faroes Shelf acquired data with three passes of two ships to record offsets up to 38,000 m (White *et al.*, 1999).

There are, however, some drawbacks to using two ships to acquire long-offset data. First, the flip-flop shooting means that the fold of coverage is halved compared to single ship firing and

the shot interval is doubled (typically to 100 m). Second, the fact that two different sources and streamers must be used is in itself a disadvantage, since however much care is used in matching the sources and receivers, in practice there will always be some differences which will cause the waveform to vary as different combinations of shots and receivers are used at different offsets. Lastly, because each streamer is liable to feather independently, the assumption of locally 2D structure (i.e. that the structure is invariant perpendicular to the profile) has to be made in the processing. Although such an assumption is inherent in any 2D processing, deviations in the geology from this assumption may lead to discontinuities in the shot gathers calculated from two-ship data which cause worse artefacts in the processing than do the smoothly varying deviations that the same deviations from 2D structure would produce in single-ship data.

#### *Use ocean bed receivers*

Offsets to any arbitrary distance, limited only by the power of the seismic source, can be achieved by using fixed seafloor receivers, either in the form of ocean bed cables where the data are fed back to a conventional recording system on a surface ship, or by using autonomous ocean bottom seismometers (OBS). We have already discussed the improved low-frequency bandwidth that is available from ocean bottom receivers (Figure 3c). There is

a further considerable advantage of seafloor receivers, which is that 3-component seismometers may be deployed in addition to hydrophones. This enables the direct recording of shear waves, the separation of upgoing and downgoing wavefields by PZ summation (useful for water multiple suppression), and direct measurement of particle motions which may help invert for anisotropy in the subsurface. The disadvantage of seabed recorded data is the spatial inflexibility and relative scarcity of autonomous OBS, and the extra cost of cable-mounted seafloor receivers, which require a second ship.

Along the iSIMM profile, good wide-angle seismic arrivals were recorded by 85 OBS from the entire crust and into the upper mantle out to ranges beyond 130 km (e.g., Figure 4). In the iSIMM project the advantages of long-offset streamer data with their high spatial sampling and fixed OBS data which give better control on the deep structure and on converted waves were combined by recording both types of data along the same profile.

#### Examples of sub-basalt imaging in Faroes region using wide-angle profiles

##### **FLARE example from two-ship data**

In Figure 8 we show a crooked-line profile which

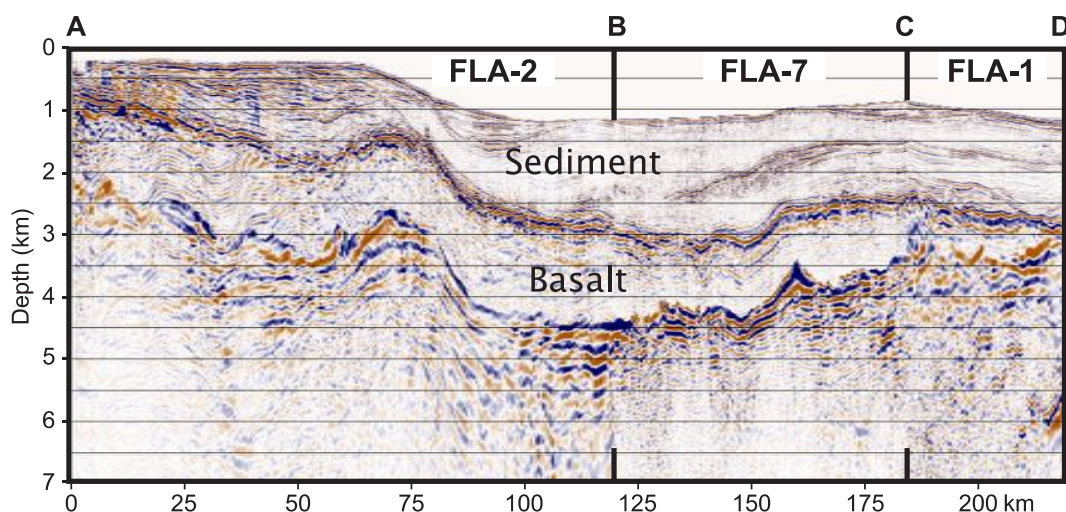


**Figure 8.** Unfolded seismic section, highlighting the top and base of the basalt flows from FLARE lines 1, 2 and 7 along a transect (shown by red dashes on map in Figure 1, with intersections marked by letters A–D), extending from thick basalts near the Faroe Islands to the feather edge of the sub-surface basalt flows beneath the Faroe-Shetland Trough (from White *et al.*, 2003).

combines sections of FLARE lines 1, 2, and 7 extending from the region of thick basalts near the Faroe Islands to the feather edge of the basalts in the southeast (for location see broken red line on Figure 1). The shallow sedimentary section and the top of the basalt is imaged best using conventional near-offset data. For the deeper section, we have migrated the base-basalt wide-angle reflection and merged it with a pre-stack depth migration of the sediments and top-basalt reflection, as described earlier. It shows good ties at the line intersection points, which gives confidence in the velocity models which were derived independently along each 2D FLARE profile. Note that on the image in Figure 8, the amplitudes of the base-basalt reflection are not directly comparable to those in the shallower section, because we have taken advantage of the high amplitudes of the wide-angle reflections to produce a strong base-basalt image.

The image is often poor where the basalts are thin, because the wide-angle seismic data contain only short segments of reflections from the base of the basalt across a limited range of offsets. Furthermore, diving waves through the basalt are close in travel time to the wide-angle reflections, so they are not easily separated (see Figure 5). Fortunately, in areas of thin basalt, conventional seismic reflection profiles with 6,000 m streamers provide adequate penetration in any case, so the pre-stack depth migration of the long-offset arrivals used in producing our composite image is less important for interpretation where the basalts are thin. By using a mixture of long-offset and conventional seismic profile data, we have been able to map the thickness of the basalts across the Faroes Shelf (Figure 9). Using the same method of migrating the wide-angle reflection at long offsets, but this time choosing the basement arrival (of presumed Cretaceous age), the thickness of the underlying sediment above basement has also been mapped (White *et al.*, 2003).

### iSIMM examples from 12-km streamer data

The 400 km long iSIMM seismic profile was acquired using a deep-towed airgun source tuned on the bubble for good low-frequency response (Figure 3d), with a 12-km long streamer. The iSIMM profile extends from the edge of the continental Shetland platform in the southeast to the oceanic crust underlying the Norwegian Sea in the north-

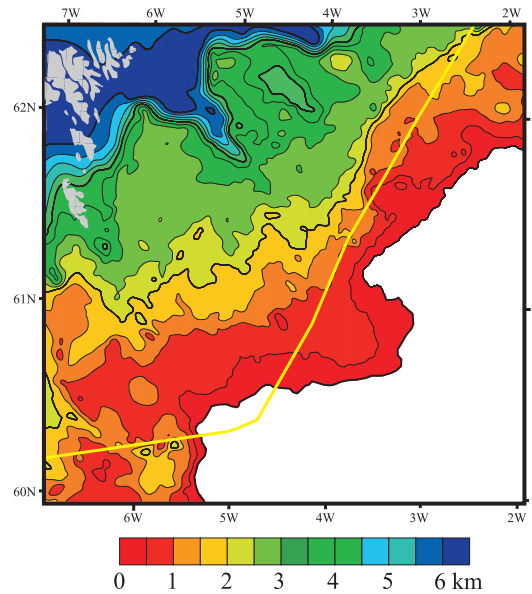


**Figure 9.** Map of basalt thickness on the Faroes Shelf, using as control the results from FLARE profiles and a large grid of conventional 6-km streamer seismic profiles in the region. The white region in the southeast corner marks the area beyond the feather edge of basalt flows. Map is smoothed, with a contour interval of 500 m. Yellow line marks boundary between UK and Faroese waters. Adapted from White *et al.* (2003).

west (Figure 10). The profile traverses several distinct provinces, including the stretched continental crust of the Mesozoic Faroe-Shetland Trough, the shallow Fugloy Ridge in the central part of the profile, where basalt flows lie just beneath the seafloor, the volcanic continent-ocean transition created during early Tertiary continental breakup and fully oceanic crust in the northwest. In the Faroe-Shetland Trough, large tilted fault blocks are visible in the basement and extensive igneous sills intrude the sediments. Elsewhere, basalt flows are ubiquitous.

Two extracts of the long iSIMM regional profile are shown in Figures 11 and 12, and discussed below in more detail. They exemplify the different nature of the extrusive volcanism on the continent-ocean margin and on the flank of the Faroes-Shetland Trough. The extract across the continent-ocean transition also demonstrates the seismic response of the lower crustal intrusions and the Moho across the continental margin.

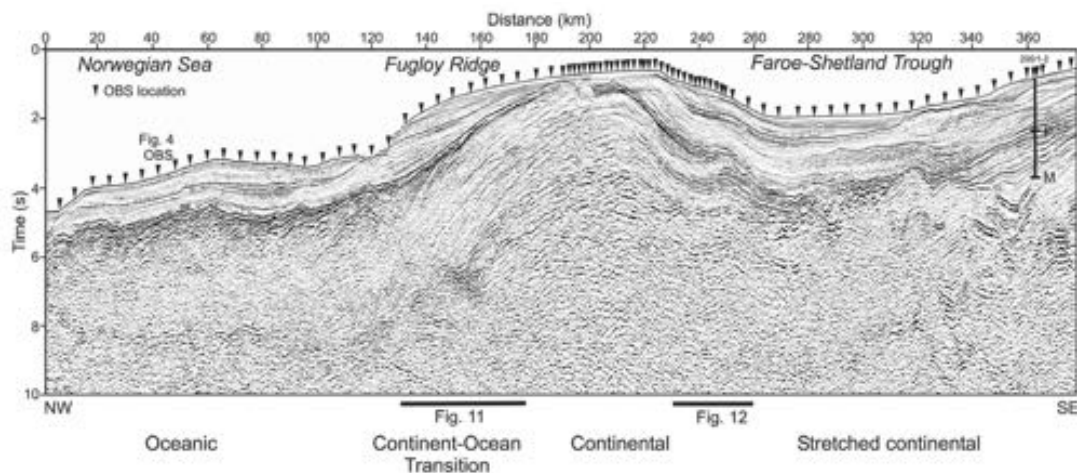


**Figure 10.** Squash-plot of entire 375 km long iSIMM profile (see Figure 1 for location), after source signature, multiple suppression, and time migration, showing location of hole 206/1-2, which terminates in the Maastrichtian, and of OBS (triangles). P and M mark the tops of the Paleocene and Maastrichtian layers. Data are shown with permission of WesternGeco.

### *Continent-ocean transition*

The most prominent feature of the volcanic rocks on the continental margin are the convex-upward, seaward dipping reflectors (SDRs) illustrated in Figure 11. The SDRs are formed by the massive and rapid extrusion of basalts which accompanied continental breakup in the early Tertiary, as a result of interaction between rifting and the thermal anomaly caused by an underlying mantle plume which now lies beneath Iceland (White and McKenzie, 1989). They extend more than 2,500 km along the rifted continental margins in the northern North Atlantic on both the European and Greenland sides. The Faroes region was close to the centre of the mantle plume at the time of breakup, so the melt production here was highest (White and McKenzie, 1989). Hinz (1989) showed that the SDRs were formed by lavas from fissures at the presently down-dip end of the reflectors, which at the time of lava production were elevated by the underlying mantle plume. The lavas originally flowed downhill away from these vents toward the continental hinterland (i.e. toward the right on Figure 11). From borehole sampling of analogous SDRs on the Vøring, Hatton and Edoras Bank margins, they were probably emplaced near sea level (Barton and White, 1997b). The present seaward-dipping, arcuate shape is due to the continued extension of the crust and the loading of the extruded lavas as continental breakup proceeded.

Individual reflectors are coherent over lateral

distances of 20 km or more and the entire package of SDRs attains a maximum thickness of 4 km adjacent to the oldest oceanic crust, thickening rapidly from the continental (southeastern) to the oceanic (northwestern) part of the continent-ocean transition. The lateral continuity of the SDRs suggests that the lavas flowed across a flat surface with little topography to impede or channel the flow.

It is probable that the crust in the transition region between continent and ocean was so heavily intruded by the time the SDRs were being formed that it had become hot and ductile, and responded to the ongoing stretching primarily by ductile thinning. The transition region from continent to ocean is very narrow (only a few tens of kilometres wide), which is in marked contrast to non-volcanic margins, where the continental stretching can extend over 250 km width: again this is probably due to the extensive igneous intrusion which so weakened the crust that it focussed further stretching into this narrow, weak region.

The lower part of the continental crust below the SDRs, some 15 km thick, is marked by extensive, strong sub-horizontal reflectivity (Figure 11), with a seismically transparent region between the bottom of the SDRs and the top of the lower-crustal layering. The region of the lower crust with strong layering coincides with abnormally high seismic velocities (above 7.2 km/s) found from the wide-angle OBS analysis. These seismic velocities are markedly higher than the velocities found



in the equivalent portion of lower crust under the adjacent British mainland, and are interpreted as due to the intrusion of mantle-derived magmas during continental breakup (White and McKenzie, 1989). Primitive picritic magmas intruded into the lower crust, rich in iron and magnesium, are likely to have differentiated to produce the less dense, and so more buoyant tholeiitic basalt lavas that were extruded to form the SDRs, leaving behind the denser (and higher seismic velocity) residual in the lower crust. Petrological models suggest that the volume of residual melt left in the lower crust is likely to be two or three times the extruded volume. This is consistent with the relative thicknesses of the lower crust over which prominent layering is seen (interpreted as igneous intrusions), and the thickness of SDRs (interpreted as extruded basalts) (Figure 11), although further detailed seismic analysis is underway to attempt to refine constraints on the percentage of intruded rock in the lower crust.

The lower crustal layering decreases greatly in intensity from the continent-ocean transition to the adjacent oceanic crust to the northwest. This is consistent with the decrease in contrast between physical properties that occur in the lower section

of the oceanic crust, where new melt intrudes a mafic crust of similar composition. By contrast, where mafic melts intrude continental crust, there may be a much larger difference in physical properties, and therefore in impedance between the new melts and the pre-existing crust (probably here granitic Lewisian crust), which produces much stronger reflectivity. This probably explains the marked lower crustal reflectivity in the region under the SDRs.

A strong, well-defined reflector at the base of the crust shallows steeply from the continental to the oceanic crust (Figures 10, 11). This reflector is interpreted as marking the Moho discontinuity, based on the strong wide-angle PmP reflections it produces on the OBS (e.g., Figure 4), and the velocities derived from analysis of the OBS arrivals. The 15 km thick oceanic crust adjacent to the continent-ocean transition is considerably thicker than the crust formed above normal oceanic spreading centres away from mantle plumes, but it is consistent with the thickness of the oldest oceanic crust elsewhere on the northern North Atlantic margins (e.g., Barton and White, 1997a; Korenaga *et al.*, 2000; Holbrook *et al.*, 2001), and is thus indicative of raised mantle temperatures caused by the mantle plume at the time of continental breakup.

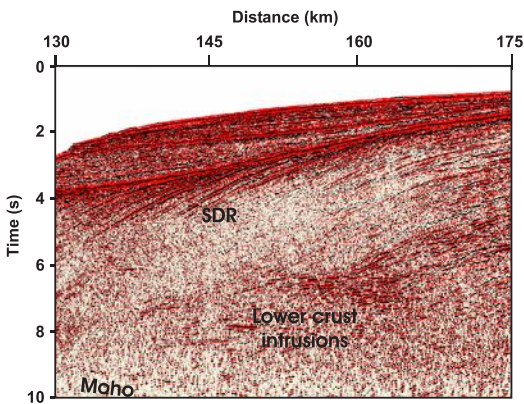


**Figure 11.** Section of seismic profile crossing the seaward dipping reflector sequence on the continent-ocean boundary (see Figure 10 for location of this 45 km-long extract). Processing includes source designation, multiple suppression and post-stack time migration. Note the superbly imaged SDRs, interpreted as lava flows extruded near sea level from the developing Atlantic rift and flowing landward over the hinterland; the strong lower-crustal layering coincident with high-velocities, presumed to represent lower-crustal intrusions; and the sharp Moho reflection which shallows markedly from continental (southeast) to oceanic (northwest) crust. Data shown with permission of WesternGeco.

#### *Flank of the Faroes-Shetland Trough*

The style of extrusive Paleocene volcanic rocks which flowed toward the continental hinterland (which experienced little or no stretching during the Tertiary continental breakup), is quite different from that found at the continent-ocean transition. Figure 12 shows a 30 km extract from the iSIMM seismic profile to illustrate this. The lavas, produced in the volcanically active Atlantic rift to the northwest of this location, flowed up to 150 km landward across a pre-existing and partly sediment-filled landscape toward the Faroe-Shetland Trough, thinning as they flowed (Figure 9). Where they reached the paleo-shoreline, they produced strong, southeastward dipping, sigmoidal reflectors within the basalt sequence. The sigmoidal reflections move upward and southeastward across the section as the lavas progressively built outward, pushing the coastline eastward (Kjørboe, 1999). Strong sub-horizontal layering below the sigmoidal reflectors probably represents early hyaloclastites and lava flows from the first phase of volcanic activity in the Faroes region, while the

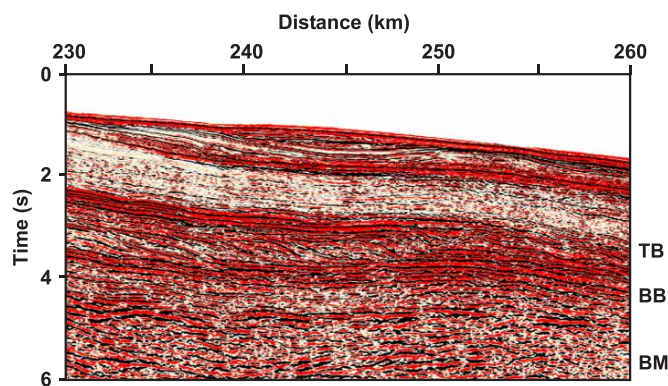


**Figure 12.** Section of migrated seismic profile crossing the basalt escarpment on the northwestern flank of the Faroe-Shetland Trough (see Figure 10 for location of this 30 km-long extract). Processing includes source designature, multiple suppression and post-stack time migration. Strong sigmoidal foresets are well imaged within the basalt sequence between 3–4 s two-way travel time: these are interpreted as the paleo-coastline in this region when the lavas were extruded. TB – top basalt; BB – base basalt; BM – basement. Data shown with permission of WesternGeco.

equally strong layering above the top of the sigmoidal reflectors is interpreted as due to late lava flows crossing the entire region, capped by lower to middle Eocene and younger sediments. Beneath the bottom of the basalt sequence, lowered velocities measured from the long-offset wide-angle data show the presence of sediments over which the early basalts flowed (Spitzer *et al.*, 2004), with faulted acoustic basement rocks of presumed Cretaceous age beneath them.

## Conclusions

Significant improvements to intra- and sub-basalt seismic imaging can be made by careful attention to tuning the source and receiver characteristics so as to optimise the low-frequency response. In the Faroes area, this is shown by the high-quality iSIMM profiles in Figures 10–12. The recording of long-offset data can also provide significant new data, because it is then possible to use the refracted and wide-angle reflected energy outside the water-wave cone both to constrain the velocity distribution in the sub-surface for better pre-stack depth migration, and also for direct imaging using the high-amplitude wide-angle reflections as demonstrated with the FLARE data in Figures 7 and 8. Although the migrated wide-angle reflections are of great value in showing which arrivals are from the base of the basalt, and from deeper in the section, their low frequency content and the large angles at which reflections occur (and therefore the large size of the Fresnel zones), means that they have much poorer resolution than do reflections from closer to normal incidence. So for interpretation purposes it is best to use both a conventional migrated image, together with the composite im-

age that contains the separately identified and migrated high-amplitude wide-angle arrivals which allows us to identify which arrivals are from the deep horizons of interest.

## Acknowledgements

The FLARE profiles were shot by Amerada Hess Limited and its partners LASMO (ULX) Limited, Norsk Hydro ASA., DOPAS and Atlantic Petroleum. The iSIMM project is supported by Liverpool and Cambridge Universities, Schlumberger Cambridge Research, Badley Technology Limited, WesternGeco, Amerada Hess, Anadarko, BP, ConocoPhillips, ENI-UK, Statoil, Shell, the Natural Environment Research Council and the Department of Trade and Industry. We thank the Masters and crews of both the *RRS Discovery* and the *M/V Geco Topaz* for their expertise in acquiring high quality datasets for iSIMM. P. Sabel, J-F Hopperstad, A. Harber, A. Langridge and J. Bacon of WesternGeco are thanked for support during the pre-survey modelling and processing of the iSIMM Q-data. We are grateful to M. Flidner, J. Fruehn and J. Smallwood for their contributions to understanding the FLARE data. University of Cambridge contribution number ES7903.

## References

- Avedik, F., Renard, V., Allenou, J.P. and Morvan, B. 1993. Single bubble air-gun array for deep exploration. *Geophysics* 58: 366–382.
- Barton, P.J. and White, R.S. 1997a. Crustal structure of the Edoras Bank continental margin and mantle thermal anomalies beneath the North Atlantic. *Journal of Geophysical Research* 102: 3109–3129.
- Barton, P.J. and White, R.S. 1997b. Volcanism on the Rockall continental margin. *Journal of the Geological Society, London* 154: 531–536.
- Boldreel, L.O. and Andersen, M.S. 1993. Late Paleocene to Miocene compression in the Faeroe-Rockall area. In: Parker, J.R. (ed.) *Petroleum Geology of Northwest Europe: Proceedings of the 4<sup>th</sup> Conference*. Geological Society, London: 1025–1034.

- Buhl, P., Diebold, J.B. and Stoffa, P.L. 1982. Array length magnification through the use of multiple sources and receiving arrays. *Geophysics* 47: 311–315.
- Christie, P.A.F., Gollifer, I., and Cowper, D. 2002. Borehole seismic results from the Lopra Deepening Project. *Journal of Conference Abstracts* 7(2): 138–139.
- Christie, P.A.F., Gollifer, I. and Cowper, D. in press. Borehole seismic studies of a volcanic succession from the Lopra 1/1A borehole in the Faroe Islands, NE Atlantic. *Geology of Denmark Survey Bulletin*.
- Crawford, W.C., Singh, S.C., Hulme, T. and Smallwood, J.R. this volume. Applications of seafloor compliance measurements in the Faroes-Shetland Basin. In: Ziska, H., Varming, T. and Bloch, D. (eds.) *Faroe Islands Exploration Conference: Proceedings of the 1<sup>st</sup> Conference, Annales Societatis Scientiarum Faeroensis*, Supplementum 43, Tórshavn.
- Doré, A.G., Cartwright, J.A., Stoker, M.S., Turner, J.P. and White, N.J. (eds.) 2002. Exhumation of the North Atlantic Margin: Timing, Mechanisms and Implications for Petroleum Exploration. Geological Society, London, Special Publications 196.
- Ebdon, C.C., Granger, P.J., Johnson, H.D. and Evans, A.M. 1995. Early Tertiary evolution and sequence stratigraphy of the Faeroe-Shetland Basin: implications for hydrocarbon prospectivity. In: Scrutton, R.A., Stoker, M.S., Shimmield, G.B. and Tudhope, A.W. (eds.) *The Tectonics, Sedimentation and Palaeoceanography of the North Atlantic Region*. Geological Society, London, Special Publications 90: 51–69.
- Eldholm, O. and Grue, K. 1994. North Atlantic volcanic margins: dimensions and production rates. *Journal of Geophysical Research* 99: 2955–2988.
- Fliedner, M.M. and White, R.S. 2001a. Seismic structure of basalt flows from surface seismic data, borehole measurements and synthetic seismogram modeling. *Geophysics* 66: 1925–1936.
- Fliedner, M.M. and White, R.S. 2001b. Sub-basalt imaging in the Faeroe-Shetland Basin with large-offset data. *First Break* 19: 247–252.
- Fliedner, M.M. and White, R.S. 2003. Depth imaging basalt flows in the Faeroe-Shetland Basin. *Geophysical Journal International* 152: 353–371.
- Fuchs, K. and Müller, G. 1971. Computation of synthetic seismograms with the reflectivity method and comparison with observations. *Geophysical Journal of the Royal Astronomical Society* 23: 417–413.
- Hinz, K. 1981. A hypothesis on terrestrial catastrophes: wedges of very thick oceanward dipping layers beneath passive margins – their origin and paleoenvironmental significance. *Geologisches Jahrbuch Reihe E* 22: 2–28.
- Hoare N., Schearer, P., Langridge, A., Saragoussi, E., Christie, P. and iSIMM Team. this volume. Imaging sub-basalt with deep towed streamer: a case study from the Faroe Islands. In: Ziska, H., Varming, T. and Bloch, D. (eds.) *Faroe Islands Exploration Conference: Proceedings of the 1<sup>st</sup> Conference, Annales Societatis Scientiarum Faeroensis*, Supplementum 43, Tórshavn.
- Hobbs, R. and Jakubowicz, H. 2000. Marine source signature measurement using a reference seismic source. *Eur. Assn. Geosci. Eng., 62<sup>nd</sup> Meeting*, Session L0013.
- Holbrook, W.S., Larsen, H.C., Korenaga, J., Dahl-Jensen, T., Reid, I.D., Kelemen, P.B., Hopper, J.R., Kent, G.M., Lizarralde, D., Bernstein, S. and Detrick, R.S. 2001. Mantle thermal structure and active upwelling during continental breakup in the North Atlantic. *Earth and Planetary Science Letters* 190: 251–266.
- Jacobson, R.S. and Lewis, B.T.R., 1990. The first direct measurements of upper oceanic crustal compressional wave attenuation. *Journal Geophysical Research* 95: 17417–17429.
- Japsen, P., Andersen, C., Andersen, H.L., Andersen, M.S., Boldreel, L.O., Mavko, G., Mohammed, N.G., Pedersen, J.M., Petersen, U.K., Rasmussen, R., Shaw, F., Springer, N., Waagstein, R., White, R.S. and Worthington, M. 2005. Sub-basalt imaging – new insight from investigations of petrophysical and seismic properties of Faroes basalts (SeiFaBa project). In: Doré, A.G. and Vining, B. (eds.) *Petroleum Geology: North-West Europe and Global Perspectives – Proceedings of the 6<sup>th</sup> Petroleum Geology Conference*. Geological Society, London.
- Jegen-Kulcsar, M. and Hobbs, R. this volume. Outline of a joint inversion of gravity, MT and seismic data. In: Ziska, H., Varming, T. and Bloch, D. (eds.) *Faroe Islands Exploration Conference: Proceedings of the 1<sup>st</sup> Conference, Annales Societatis Scientiarum Faeroensis*, Supplementum 43, Tórshavn.
- Lunnon, Z.C., Christie, P.A.F. and White, R.S. 2003. An evaluation of peak and bubble tuning in sub-basalt seismology: modelling and results. *First Break* 21: 51–56.
- Kjørboe, L. 1999. Stratigraphic relationships of the Lower Tertiary of the Faeroe basalt plateau and the Faeroe-Shetland Basin. In: Fleet, A.J. and Boldy, S.A.R. (eds.) *Petroleum Geology of Northwest Europe: Proceedings of the 5<sup>th</sup> Conference*. Geological Society, London: 559–572.
- Korenaga, J., Holbrook, W.S., Kent, G.M., Kelemen, P.B., Detrick, R.S., Larsen, H.C., Hopper, J.R. and Dahl-Jensen, T. 2000. Crustal structure of the southeast Greenland margin from joint refraction and reflection seismic tomography. *Journal of Geophysical Research* 105: 21,591–21,614.
- MacGregor, L.M. 2003. Joint analysis of marine active and passive source EM data for sub-salt or sub-basalt imaging. *65<sup>th</sup> Meeting of the European Association of Geoscientists and Engineers, Expanded Abstract*: F18.
- Maresh, J., Hobbs, R.W., White, R.S. and Smallwood, J.R. 2003. Attenuation of Atlantic margin basalts using downhole VSP (extended abstract). *73<sup>rd</sup> Ann. International Meeting: Society of Exploration Geophysicists*, Dallas: 1310–1313.
- McBride, J.H., Henstock, T.J., White, R.S. and Hobbs, R.W. 1994. Seismic reflection profiling in deep water: avoiding spurious reflectivity at lower-crustal and upper-mantle traveltimes. *Tectonophysics* 232: 425–435.
- Murphy, C.A., Mumaw, G.R. and Stalin, F. 2002. Resolving basalt and sub-basalt geology with high precision, high resolution gravity gradient data. *Journal of Conference Abstracts*, 7(2): 178.

- Nadin, P., Kusznir, N.J. and Cheadle M.J. 1997. Early Tertiary plume uplift in the North Sea and Faeroe-Shetland Basin. *Earth and Planetary Science Letters* 148: 109–127.
- Naylor, P.H., Bell, B.R., Jolley, D.W., Durnall, P. and Fredsted, R. 1999. Palaeogene magmatism in the Faeroe-Shetland Basin: influences on uplift history and sedimentation. In: Fleet, A.J. and Boldy, S.A.R. (eds.) *Petroleum Geology of Northwest Europe: Proceedings of the 5<sup>th</sup> Conference*. Geological Society, London: 545–558.
- Planke, S., 1994. Geophysical response of flood basalts from analysis of wire line logs: Ocean Drilling Program Site 642, Vøring volcanic margin. *Journal of Geophysical Research* 99: 9279–9296.
- Pratt, R.G. 1999. Seismic waveform inversion in the frequency domain, Part 1: Theory and verification in a physical scale model. *Geophysics* 64: 888–901.
- Pujol, J. and Smithson, S. 1991. Seismic wave attenuation in volcanic rocks from VSP experiments. *Geophysics* 56: 1441–1455.
- Richardson, K.R., White, R.S., England, R.W. and Fruehn, J. 1999. Crustal structure east of the Faeroe Islands. *Petroleum Geoscience* 5: 161–172.
- Roberts, A.W., White, R.S., Lunnon, Z. C., Christie, P. A. F., Spitzer, R. and iSIMM Team. in press. Imaging magmatic rocks on the Faroes margin. In: Doré, A.G. and Vining, B. (eds.) *Petroleum Geology: North-West Europe and Global Perspectives - Proceedings of the 6<sup>th</sup> Petroleum Geology Conference*. Geological Society, London.
- Rutledge, J.T. and Winkler, H. 1987. Attenuation measurements in basalt using vertical seismic profile data from the eastern Norwegian Sea. *57<sup>th</sup> SEG Annual Meeting, New Orleans, USA, Expanded Abstracts* 87: 711–713.
- Safar, M.H. 1980. An efficient method of operating the air-gun. *Geophysical Prospecting* 28: 85–94.
- Shaw, F., Worthington, M.H., Andersen, M.S. and Petersen, U.K. 2004. A study of seismic attenuation in basalt using VSP data from a Faeroe Islands borehole (expanded abstract P015). *66<sup>th</sup> Meeting: European Association of Geoscientists and Engineers*, Paris.
- Shipp, R.M. and Singh, S.C. 2002. Two-dimensional full wavefield inversion of wide-aperture marine seismic streamer data. *Geophysical Journal International* 151: 325–344.
- Smallwood, J.R., White, R.S. and Staples, R.K. 1998. Deep crustal reflectors under Reydarfjörður, eastern Iceland: Crustal accretion above the Iceland mantle plume. *Geophysical Journal International* 134: 277–290.
- Smallwood, J.R., Staples, R.K., Richardson, K.R., White, R.S. and FIRE Working Group. 1999. Crust generated above the Iceland mantle plume: from continental rift to oceanic spreading center. *Journal of Geophysical Research* 104: 22,885–22,902.
- Smallwood, J.R., Towns, M.J. and White, R.S. 2001. The structure of the Faeroe-Shetland Trough from integrated deep seismic and potential field modelling. *Journal of the Geological Society, London* 158: 409–412.
- Smallwood, J.R. and Maresch, J. 2002. The properties, morphology and distribution of igneous sills: Modelling, borehole data and 3D seismic from the Faeroe-Shetland area. In: Jolley, D.W. and Bell, B.R. (eds.) *The North Atlantic Igneous Province: stratigraphy, tectonic, volcanic and magmatic processes*. Geological Society, London, Special Publications 197: 271–306.
- Sørensen, A.B. 2003. Cenozoic basin development and stratigraphy of the Faroes area. *Petroleum Geoscience* 9: 189–207.
- Spitzer, R., White, R.S., Christie, P.A.F. and iSIMM Group 2004. Sub-basalt imaging along the iSIMM profile – integration of surface and ocean bottom seismic data (expanded abstract D042). *66<sup>th</sup> Meeting: European Association of Geoscientists and Engineers*, Paris.
- Staples, R.K., Hobbs, R.W. and White, R.S. 1999. A comparison between airguns and explosives as wide-angle seismic sources. *Geophysical Prospecting* 47: 313–339.
- Stoffa, P.L. and Buhl, P. 1979. Two-ship multichannel seismic experiments for deep crustal studies: Expanding spread and constant offset profiles. *Journal of Geophysical Research* 84: 7645–7660.
- Toksöz, M.N., Johnston, D.H. and Timur, A. 1979. Attenuation of seismic waves in dry and saturated rocks: I. Laboratory measurements. *Geophysics* 44: 681–690.
- Waagstein, R. 1988. Structure, composition and age of the Faeroe basalt plateau. In: Morton, A.C. and Parson, L.M. (eds.) *Early Tertiary Volcanism and the Opening of the NE Atlantic*. Geological Society, London, Special Publications 39: 225–238.
- White, N.J. and Lovell, B. 1997. Measuring the pulse of a plume with the sedimentary record. *Nature* 387: 888–891.
- White, R. and McKenzie, D. 1989. Magmatism at rift zones: The generation of volcanic continental margins and flood basalts. *Journal of Geophysical Research* 94: 7685–7729.
- White, R.S., McBride, J.H., Maguire, P.K.H., Brandsdóttir, B., Menke, W.H., Minshall, T.A., Richardson, K.R., Smallwood, J.R., Staples, R.K. and the FIRE Working Group. 1996. Seismic images of crust beneath Iceland contribute to long-standing debate. *EOS* 77: 197 and 200–201.
- White, R.S., Fruehn, J., Richardson, K.R., Cullen, E., Kirk, W., Smallwood, J.R. and Latkiewicz, C. 1999. Faroes Large Aperture Research Experiment (FLARE): Imaging through basalts, in Fleet, A.J. and Boldy, S.A.R. (eds.) *Petroleum Geology of Northwest Europe: Proceedings of the 5<sup>th</sup> Conference*. Geological Society, London: 1243–1252.
- White, R.S., Christie, P.A.F., Kusznir, N.J., Roberts, A., Hurst, N., Lunnon, Z., Parkin, C.J., Roberts, A.W., Smith, L.K., Spitzer, R., Surendra, A. and Tymms, V. 2002. iSIMM pushes frontiers of marine seismic acquisition. *First Break* 20: 782–786.
- White, R.S., Smallwood, J.R., Fliedner, M.M., Boslaugh, B., Maresch, J. and Fruehn, J. 2003. Imaging and regional distribution of basalt flows in the Faeroe-Shetland Basin. *Geophysical Prospecting* 51: 215–231.
- Ziolkowski, A., Parkes, G., Hutton, L. and Haugland, T.

1982. The signature of an air-gun array – Computation from near-field measurements including interactions. *Geophysics* 47: 1413–1421.
- Ziolkowski, A., Hanssen, P., Gatliff, R., Jakubowicz, H., Dobson, A., Hampson, G., Li, X.-Y. and Liu, E. 2003. Use of low frequencies for sub-basalt imaging. *Geophysical Prospecting* 51: 169–182.



# Applications of Seafloor Compliance Measurements in the Faroes-Shetland Basin

WAYNE C. CRAWFORD<sup>1\*</sup>, SATISH C. SINGH<sup>1</sup>, THOMAS HULME<sup>1</sup> AND JOHN R. SMALLWOOD<sup>2</sup>

1: Laboratoire de Géosciences Marines, IPGP Case 89, Tour 14-15,  
Seme etage, 4 Place Jussieu, 75252 Paris Cedex 05, France.

\* E-mail: crawford@ipgp.jussieu.fr; Tel: +33 (0)1 4427 2821; Fax: +33 (0)1 4427 9969

2: Amerada Hess Ltd., 33 Grosvenor Place, London, SW1X 7HY, UK.

## Abstract

Seafloor compliance is a geophysical prospecting method that uses the seafloor motion under ocean waves to determine the shear modulus structure of the subsurface. Seafloor compliance measurements are of interest to petroleum exploration because they are sensitive to fluid-filled regions and because their source is always “on”, which should permit continuous monitoring of regions of interest during exploitation. We review the seafloor compliance method and previous studies made using the method, and then calculate the sensitivity of seafloor compliance measurements to sub-surface features of interest in the Faroes-Shetland Basin, particularly to sub-basalt sediments. We find that seafloor compliance measurements will be sensitive to shear velocity structure from 50 meters to as much as 6 km beneath the seafloor. They will be sensitive to sub-basalt sediments almost everywhere where the water depth is greater than 0.9 km and in some shallower areas directly south of the Faroe Islands. Assuming sub-basalt sediments start 3.5 km beneath the seafloor, compliance measurements will constrain their depth and thickness to within 0.1-0.2 km if the water depth is 1 km or more. For the same water depths, if the depth limits of the sub-basalt sediments are already well constrained, seafloor compliance measurements will constrain their shear velocities to within approximately 0.1 km/s. For water depths greater than 0.05 km, seafloor compliance measurements should constrain the average shear wave velocity in sediments above the basalt flows to within 0.01 km/s.

## Introduction

Fluid-rich zones are an important but often difficult to locate target in petroleum exploration. The Faroes region is a prime example, with potential petroleum reservoirs lying undetected in fluid-rich sediments beneath basalt flows or in trapped unconsolidated sediment layers (Mack, 1997). Fluids are defined by their inability to support shear without deformation, but most geophysical methods are insensitive or secondarily sensitive to low shear modulus/velocity regions and some are even hindered by them. The seismic method is one of the best tools for detecting and monitoring petroleum reservoirs, but it is mostly sensitive to compressional-wave velocities and the acoustic impedance. In addition, the well-known difficulties of seismic imaging beneath stratified basalt flows hinder seismic imaging of sub-basalt sediments in the Faroes region. Much work has been done to overcome these difficulties (Fruehn *et al.*, 1999;

White *et al.*, 1999; Barzahi *et al.*, 2001; Fliedner and White, 2001; Fruehn *et al.*, 2001; Martini and Bean, 2001; Hobbs, 2002; Fliedner and White, 2003; White *et al.*, 2003; Ziolkowski *et al.*, 2003), but the problem remains difficult.

Seafloor compliance measurements should help to locate and study fluid-rich zones. Seafloor compliance is the displacement of the seafloor under pressure forcing from slowly propagating ocean surface waves. Seafloor compliance measurements are most sensitive to the sub-surface shear modulus and compliance values are largest over low shear modulus zones, making compliance measurements a perfect complement to seismic data. Seafloor compliance measurements have been used to study shallow sediment properties (Yamamoto and Torii, 1986; Trevorrow and Yamamoto, 1991), gas hydrates (Willoughby and Edwards, 1997; 2000) and the melt structure between mid-ocean ridges (Crawford *et al.*, 1994; Crawford *et al.*, 1999; Crawford and Webb, 2002), and have proven par-

ticularly sensitive to fluid-rich targets at depth. Much progress has been made recently in modeling seafloor compliance and in understanding its properties (Crawford *et al.*, 1998; Latychev and Edwards, 2003; Hulme *et al.*, 2004). The method has its limitations, in particular a relatively low vertical resolution, but these can be overcome by combining with seismic data (Hulme *et al.*, 2004; Roberts, 2004).

In this paper, we review the state of the art in seafloor compliance measurements, modeling, and data inversion, and investigate what compliance measurements can contribute to studies of the Faroes-Shetland Basin. We first review the seafloor compliance method describe what it is sensitive to and how it is modeled. We then present the data inversion technique we use to calculate subsurface structure from seafloor compliance data. We estimate the sensitivity of seafloor compliance measurements to subsurface features of interest in the Faroes region by applying our data inversion to synthetic Faroes-area compliance data. We calculate the depths to which compliance will be sensitive throughout the Faroes region and identify where compliance measurements can be used to study sub-basalt sediments.

## Seafloor Compliance

Seafloor compliance is the transfer function between pressure forcing from linear ocean surface gravity (LOSG) waves and the seafloor displacement beneath them. It is measured using a seafloor broadband seismometer and pressure gauge (Figure 1). Both the seafloor compliance and seismic methods are based on elastic motions, but the compliance method uses the quasi-static subsurface deformation under shear stress rather than wave propagation, which gives it quite different properties than active seismic methods. The applied stress is mostly shear because the pressure highs and lows act normal to the seafloor and are separated horizontally.

We use LOSG waves because we can calculate their wavelength,  $L(\omega)$ , from the water depth,  $H$ , and the angular frequency,  $(\omega)$ , using the LOSG wave dispersion relation:

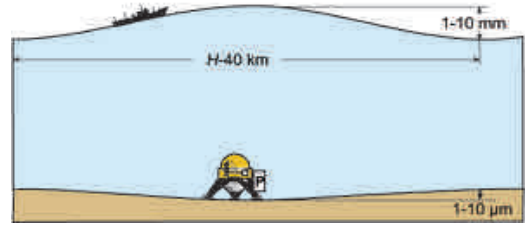


**Figure 1.** Cartoon representation of the compliance wave source and the compliance measurement using a broadband seismometer and differential pressure gauge (P) deployed to the seafloor. The typical ocean wave and the seafloor signal amplitudes are shown.  $H$  is the water depth.

$$\omega^2 = gk(\omega)\tanh(k(\omega)H) \quad (1)$$

where  $k(\omega) \equiv 2\pi/L(\omega)$  is the wavenumber and  $g$  is the gravitational acceleration (Apel, 1987). In general, LOSG waves only generate a measurable seafloor pressure signal if  $L > H$ , because the pressure signal decays exponentially with depth (Apel, 1987). The upper frequency bound,  $f_{\max}$ , for compliance measurements is the frequency where both the seafloor pressure signal and the seafloor motion underneath it are significantly above background noise levels, which corresponds approximately to  $L = 1.1H$ . Using this observation and equation (1), we can calculate  $f_{\max}$  as a function of water depth: for example,  $f_{\max} \approx 0.119$  Hz for  $H = 100$  meters and 0.038 Hz for  $H = 1000$  meters. Ocean surface waves that are visible to the naked eye are generally less than 100 meters long, so most of the seafloor signal at water depths greater than 100 meters comes from very small (0.001-0.01 meter tall), low frequency LOSG waves known as *free infragravity* waves (Webb *et al.*, 1991).

Figure 2 shows seafloor acceleration and pressure spectra measured at 345, 900, and 2600 meter water depths. The free infragravity waves are the high energy in the pressure signal between 0.001 and 0.1 Hz (Figure 2a). At the shallowest site, wind waves generate a small pressure peak at 0.05 Hz ( $L \approx 500$  meters) (these waves are also LOSG waves, and so their signal and effects can be used for compliance studies). The compliance motion under free infragravity waves generates a broad peak in the acceleration signal between 0.0035 and 0.1 Hz (Figure 2c). By plotting the spectra as a function of the wavelength calculated using

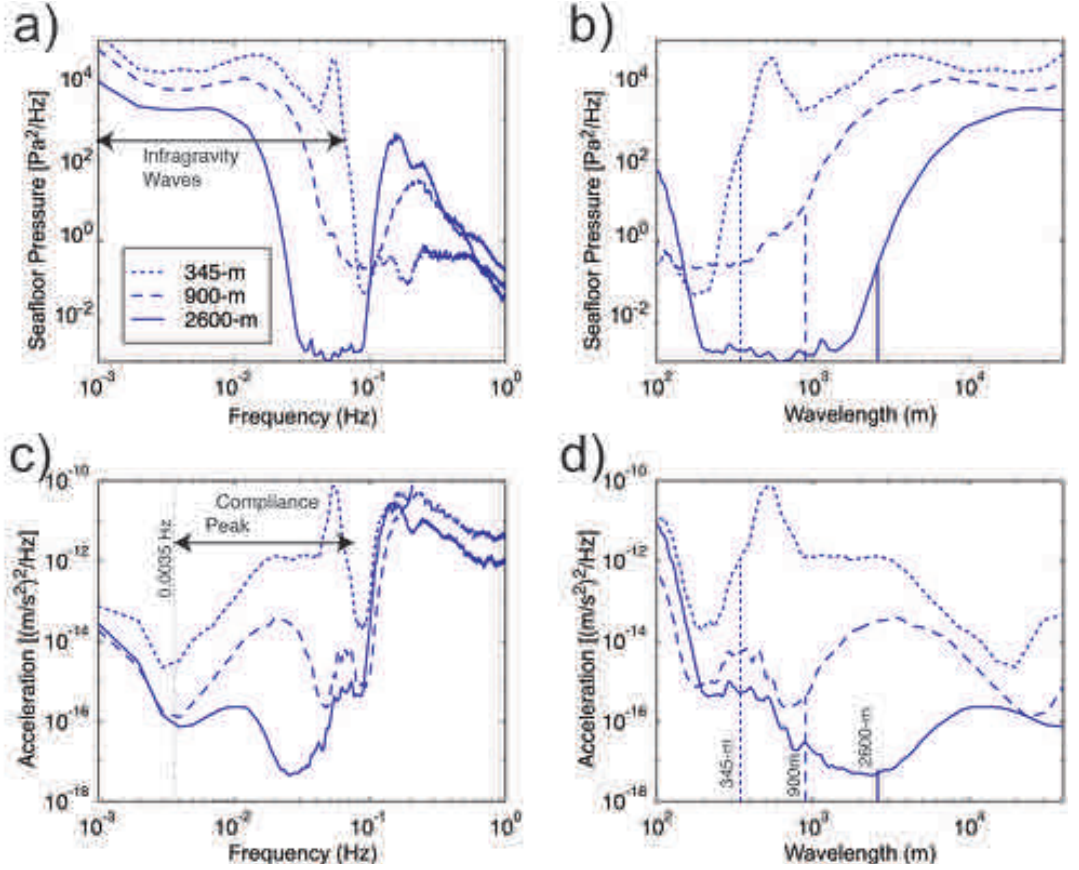


**Figure 2.** Seafloor pressure and acceleration power spectral densities (PSD) in the compliance frequency-wavelength band, measured at 345-m, 900-m and 2600-m water depths. In the right column, a vertical line marks the wavelength equal to the water depth for each measurement. (a) Pressure PSD as a function of frequency. (b) Pressure PSD as a function of wavelength. (c) Acceleration PSD as a function of frequency. (d) Acceleration PSD as a function of wavelength.

equation (1), it is clear that most of the compliance signal is at wavelengths longer than the ocean depth (Figure 2b, d). The seafloor compliance is the transfer function between the acceleration and pressure in this band.

Compliance is governed by the same equations of motion that describe elastic wave motion:

$$\rho(\mathbf{x})\ddot{u}_i(\omega, \mathbf{x}) = \tau_{ij,j}(\omega, \mathbf{x}) \quad (2)$$

where  $\rho$  is the material density,  $u_i$  is the motion in the  $i$ th direction and  $\tau_{ij}$  is the stress acting in the  $j$ th direction across the plane normal to the  $i$ -axis ( $i, j=1,2,3$ ). We define seafloor compliance as

$$\eta(\omega) = k(\omega) \frac{\mathbf{u}(\omega)}{\tau_{zz}(\omega)} \Big|_{z=0} \quad (3)$$

The seafloor compliance has been calculated for

an isotropic uniform half-space and slow wave forcing:

$$\eta(\omega) = \frac{-1}{2(\lambda + \mu)} i \hat{x} + \frac{(\lambda + 2\mu)}{2\mu(\lambda + \mu)} \hat{z}, \quad (4)$$

where  $\lambda$  is the dilatation modulus,  $\mu$  is the shear modulus and  $\hat{x}$  and  $\hat{z}$  are unit vectors (Crawford, 2004). The horizontal compliance motion is very hard to measure at the seafloor, so we concentrate here on the vertical compliance motion ( $\hat{z}$  term). This motion is at least 5 times more sensitive to  $\mu$  than to  $\lambda$  and is inversely proportional to  $\mu$  if  $\mu = \lambda$ . It is this sensitivity to  $\mu$ , especially where  $\mu$  is small, that makes compliance useful for studying fluid-rich regions within the sub-surface. A fluid-rich region within the subsurface generates a peak in the compliance (Figure 3) whose center frequency depends on the region's depth: the deeper



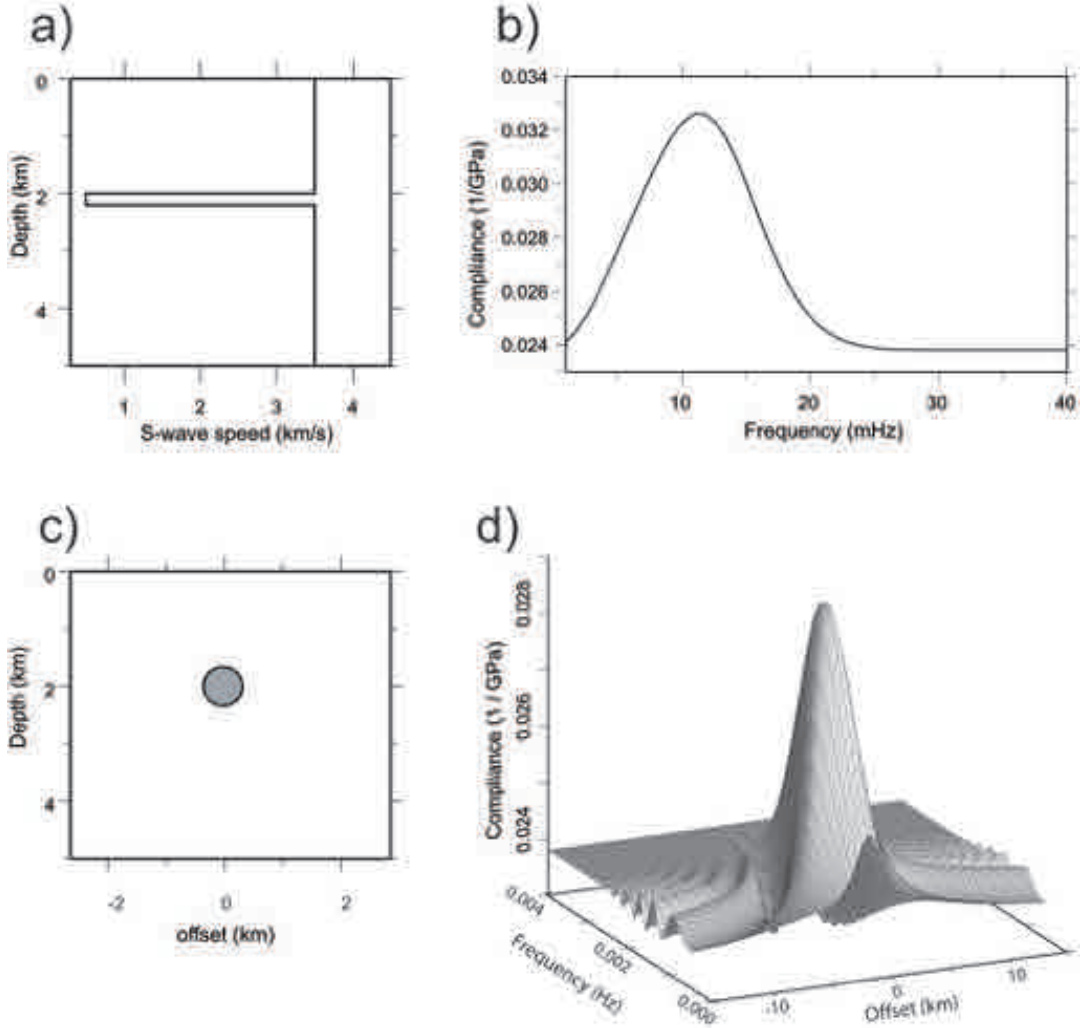


**Figure 3.** The effect of a low velocity zone on seafloor compliance, calculated using 1D and 2D models. In both cases the LVZ is 2 km beneath the seafloor. (a) 1D shear velocity model. (b) 1D compliance. (c) 2D velocity model, the low velocity zone is modeled as a cylinder (Hulme *et al.*, 2004). (d) Compliance of the 2D model as a function of frequency and offset.

the region is, the lower is the peak frequency. If the fluid-rich region is bounded horizontally, the peak is largest directly over the region and decays to one-half its maximum height at a distance away from the region equal to 1.7 times the region's depth (Crawford *et al.*, 1998; Latychev and Edwards, 2003; Hulme *et al.*, 2004). A large number of compliance measurements can be made with a few instruments because each instrument can be deployed multiple times and there is no need to make the measurements concurrently. Typically, we recover and redeploy each compliance instrument every two days.

The depth,  $D_{sens}$ , beneath the surface to which compliance is sensitive is between  $L(\omega)/6$  and  $L(\omega)/4$  (Crawford *et al.*, 1991; Crawford *et al.*, 1998). The shortest wavelength is approximately  $1.1H$  and the longest, from equation (1), is  $\sqrt{gH} / f_{min}$ , where  $f_{min}$  is the minimum measured frequency (typically 0.0035 to 0.004 Hz). If we assume  $D_{sens} = L/5$  and  $f_{min} = 0.0035$  Hz, the minimum sensitive depth is approximately  $H/5.5$  and the maximum sensitive depth,  $D_{max}$ , is approximately  $180\sqrt{H}$  (Figure 4). Compliance measurements can be used to calculate the average velocity above and just below these bounds, but

they can only distinguish velocity structure within these bounds.

The sensitivity of compliance to a given feature depends on the feature's size and shear modulus: small but very low shear modulus features can generate a stronger signal than larger features with more subtle shear modulus variations (e.g. Crawford *et al.*, 1991; Crawford *et al.*, 1999; Latychev and Edwards, 2003; Hulme *et al.*, 2004). To date, compliance measurements have been used to study shallow sediment shear moduli at shallow water sites (Yamamoto and Torii, 1986; Trevorrow and Yamamoto, 1991), magma chambers beneath volcanic seamounts (Crawford *et al.*, 1991), gas hydrates (Willoughby and Edwards, 2000) and lower crustal partial melting beneath oceanic ridges (Crawford *et al.*, 1994; Crawford *et al.*, 1999; Crawford and Webb, 2002). In November 2004, seafloor compliance was measured in the Faroe-Shetland Basin to study sub-basalt sediments.

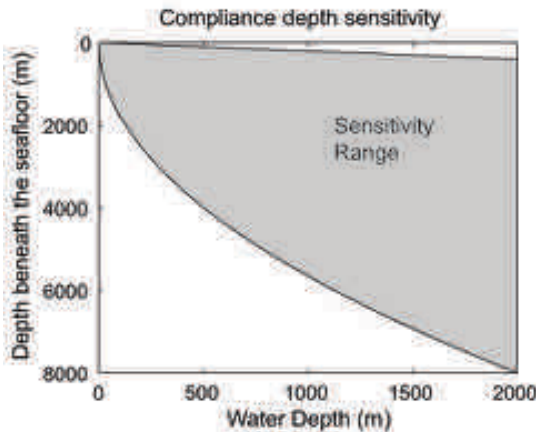


**Figure 4.** Depth sensitivity of compliance. For a given water depth (x-axis), compliance is sensitive to structure at the shaded sub-surface depths. The calculations assume a minimum sensitive frequency of 0.0035 Hz.

If shear velocities are available from seismic data, these values can be combined with compliance-estimated shear velocities to calculate the shear wave attenuation. The compliance frequency band is several orders of magnitude lower than the active seismic frequency range and the shear wave velocity may be significantly lower in the compliance frequency band if attenuation is important between

the two bands (Figure 5). This was the case at a site on the East Pacific Rise, where converted S-wave phases recorded using a shot-streamer configuration indicated much higher upper crustal shear velocities than did seafloor compliance data. Hulme *et al.* (2003) found that transverse anisotropy could explain up to a 5% variation between shear wave velocities measured by seismic and compliance methods and that anelasticity could cause up to a 40% decrease in seismic velocities between the seismic and seafloor compliance frequency bands (Figure 5). If there is significant anelasticity, compliance-derived shear velocities should better indicate a region's permeability to fluid flow, since this flow generally occurs over time scales closer to seafloor compliance frequencies than to seismic frequencies.

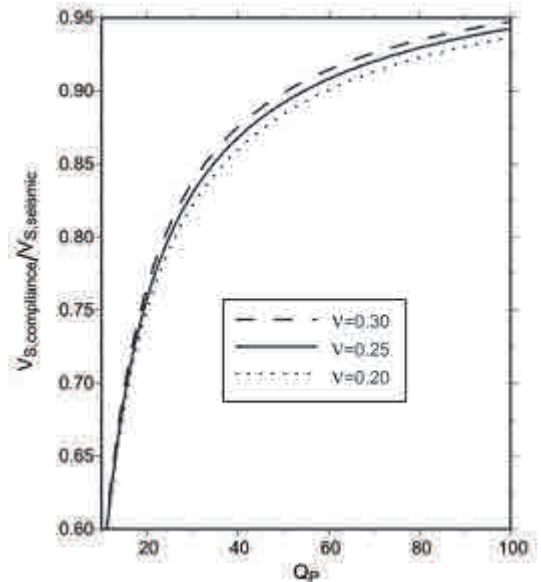


**Figure 5.** The ratio of shear wave speed values measured by compliance versus active seismic data as a function of quality factor  $Q_p$ . The different curves show values for different Poisson's ratios (0.2 to 0.3) (from Hulme *et al.*, 2003).

## Compliance measurements, modeling and data inversion

Compliance is measured using a seafloor seismometer and pressure gauge (Figure 1). If the wa-

ter is more than 100 meters deep, these instruments should be sensitive out to at least 300 seconds period. We use a broadband seismometer (Streckeisen STS-2 or Guralp CMG3-T) and a differential pressure gauge (Cox *et al.*, 1984). To reduce uncertainty, we stack 100 or more data windows during which there are no extraneous signals from instrument settling, earthquakes, ships, and etcetera. We generally deploy each seafloor compliance sensor every two days to obtain one hundred or more good 1024-second windows (28.5 hours), while allowing for the time required to recover and redeploy the instruments (6-8 hours), for them to thermally and mechanically settle at the seafloor (5-10 hours) and for events such as earthquakes that mask the compliance signal (0-5 hours).

We calculate the subsurface shear modulus from the compliance data using geophysical inversions in which the model constraint is either minimum structure or *a priori* values (Crawford, 2004). Using the minimum structure constraint, the results are independent of the starting model, but we cannot use prior data and a large model parameter space is required, making the inversion slow for all but 1-D models. Using an *a priori* constraint takes advantage of prior data and gives quicker inversions for 2D and 3D models.

## Some compliance applications in the Faroes region

We begin our investigation of compliance applications in the Faroes region by calculating the depth range of compliance sensitivity around the islands (Figure 6), and comparing these ranges to the estimated depths of sub-surface features of interest. We focus on the area where most of the seismic lines have been shot in Faroes waters (blue polygon, Figure 6a) and a sub-region of this area in which seismic coverage is particularly dense (red polygon). We refer to these areas as the “exploration area” and the “densest seismic area”, respectively. Within the exploration area, water depths are concentrated at 200 and 900 meters (Figure 6b), corresponding to maximum sensitive depths of 2500 and 5500 meters beneath the seafloor, respectively (Figure 6d). Within the densest seismic area the depths are clustered at 300 and 1100 meters, cor-

responding to maximum sensitive depths of 3000 and 6000 meters. Compliance measurements are sensitive to subsurface structures starting about 50 meters beneath the seafloor in the shallower zones and about 200 meters beneath the seafloor in the deeper waters (Figure 6c).

To determine the sensitivity of compliance to sub-basalt sediments and surface sediments, we ran geophysical inversions on synthetic compliance data calculated for the range of water depths and subsurface structures expected in the Faroes region. The synthetic compliance data includes uncertainties calculated using typical seafloor noise levels and assuming 28.5 hours of good data (Crawford, 2004).

### Shallow sediment properties

Compliance is very sensitive to shallow sediments, especially if they have low shear moduli (unconsolidated sediments, for example). Crawford *et al.* (2004) ran inversions on synthetic data for a model with a 50 meters thick, 200 m/s shear velocity sediments overlying 1500 meters thick sediments with 700 m/s shear velocity layer, for a water depth of 1300 meters. They recovered the surface sediment layer thickness to within 10 meters and its shear velocity to within 30 m/s, and the underlying layer thickness to within 10 meters and its shear velocity to within 1 m/s. Inversion uncertainties will be greater for real data because of lateral inhomogeneities and depth variations in velocity within each layer, but the results underline the sensitivity of compliance measurements to low shear velocity regions. When compliance measurements are combined with active seismic data that provide accurate information about horizon depths and lateral variations, one may obtain inversion accuracies approaching these ideal values.

### Sub-basalt sediments

Compliance should be sensitive to sub-basalt sediments if  $D_{\max}$  is more than 1000 meters beneath the bottom of the basalts. A typical case for Faroes Basin is  $H=1000$  meters and the bottom of the basalts is 3500 meters beneath the seafloor (White *et al.*, 2003). For this case, a minimum structure inversion detects the sub-basalt sediments (Figure 7a) and a Bayesian inversion constrains the depth to their top to within 200 meters. If the sediments

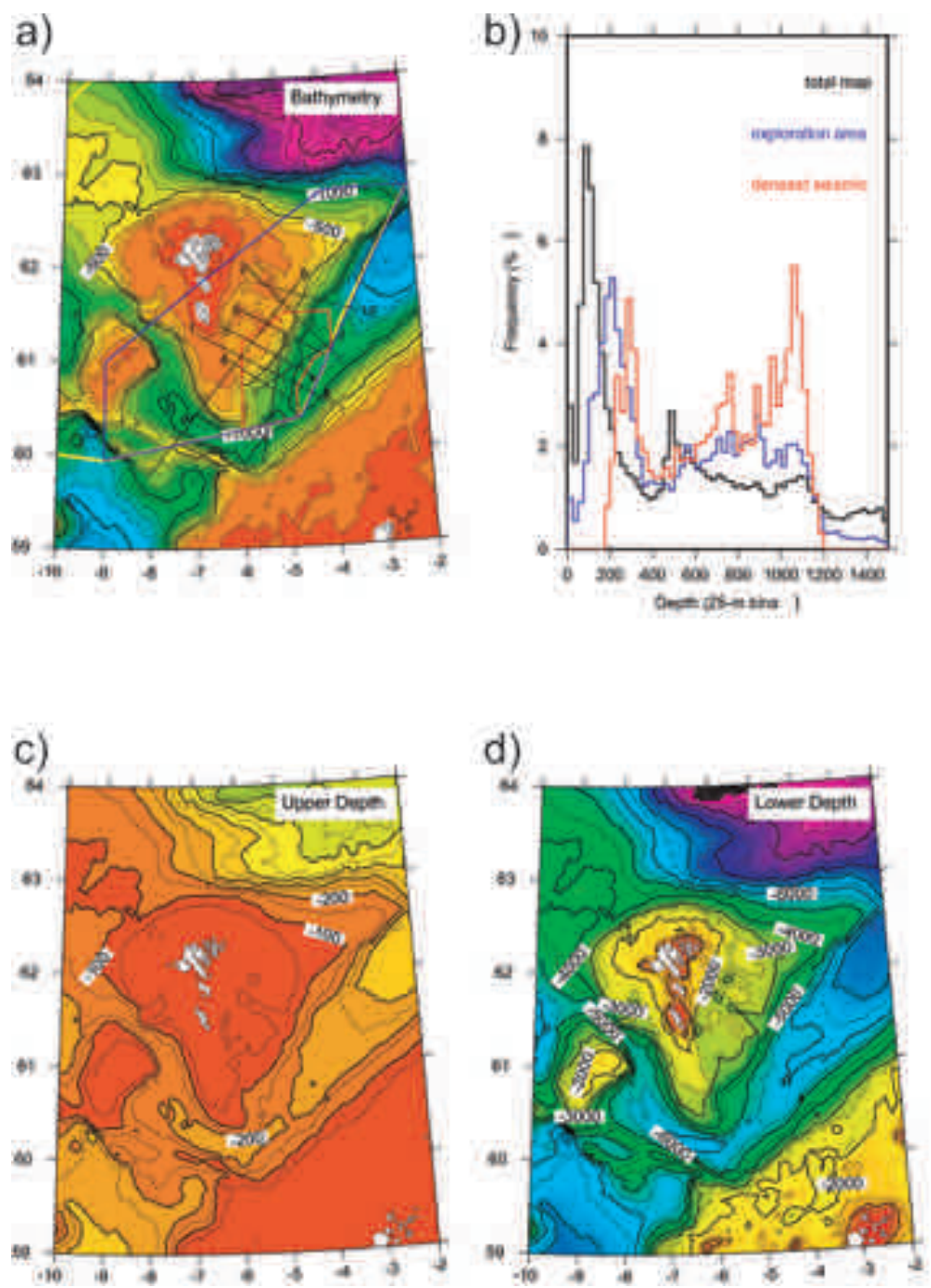


**Figure 6.** Bathymetry and compliance depth sensitivity around the Faroe Islands. (a) Bathymetry. The blue polygon contains the region of principal seismic exploration within the Faroes economic zone. The red polygon contains the densest region of seismic studies (from the SINDRI web site: [http://www.sindri.fo/data/surveys/geophys\\_data.html](http://www.sindri.fo/data/surveys/geophys_data.html)). The numbered black lines mark wide-angle seismic lines from the FLARE experiment (Fruehn *et al.*, 1999; White *et al.*, 1999; Fruehn *et al.*, 2001; Flidner and White, 2003). The yellow line marks the boundary between Faroes and United Kingdom waters. (b) The distribution of water depths within the entire map (black line) and the two polygons. (c) The upper (shallow) limit of compliance sensitivity to structural variations in the subsurface. (d) The lower (deep) limit of compliance sensitivity to structural variations in the subsurface.



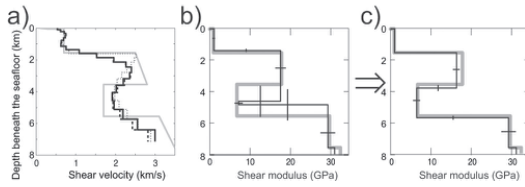


**Figure 7.** Minimum structure and Bayesian inversion results for a model with sub-basalt sediments starting 3500 meters beneath the seafloor. (a) Minimum structure inversion (the starting model contains no low-velocity zone). Grey line = true model. Thick black lines: inversion results with no *a priori* information. Thin dashed line: inversion results if the depth to the top of the basalts is known. (b) One *a priori* model (black line) and uncertainties. Grey line = true model. (c) Bayesian inversion result (black line) and uncertainty calculated from the *a priori* model and synthetic compliance data as discussed in the text.

are 2000 meters thick, the depth to their bottom is also constrained to within 200 meters. Without *a priori* constraints, a sub-basalt sediment layer more than 600 meters thick should be detected by compliance data (Crawford, 2004).

To determine where in the Faroes region seafloor compliance measurements will be sensitive to sub-basalt sediments, we subtracted the depth to the bottom of the basalts (White *et al.*, 2003) from  $D_{\max}$  in the Faroes area (Figure 8). North of  $\sim 61^\circ\text{N}$ , this region is limited to water depths greater than 900 meters, whereas south of  $61^\circ\text{N}$ , where the sub-basalt sediments are shallower, the region spans most of the Faroes waters. The region of sensitivity includes about 75% of the densest seismic area.

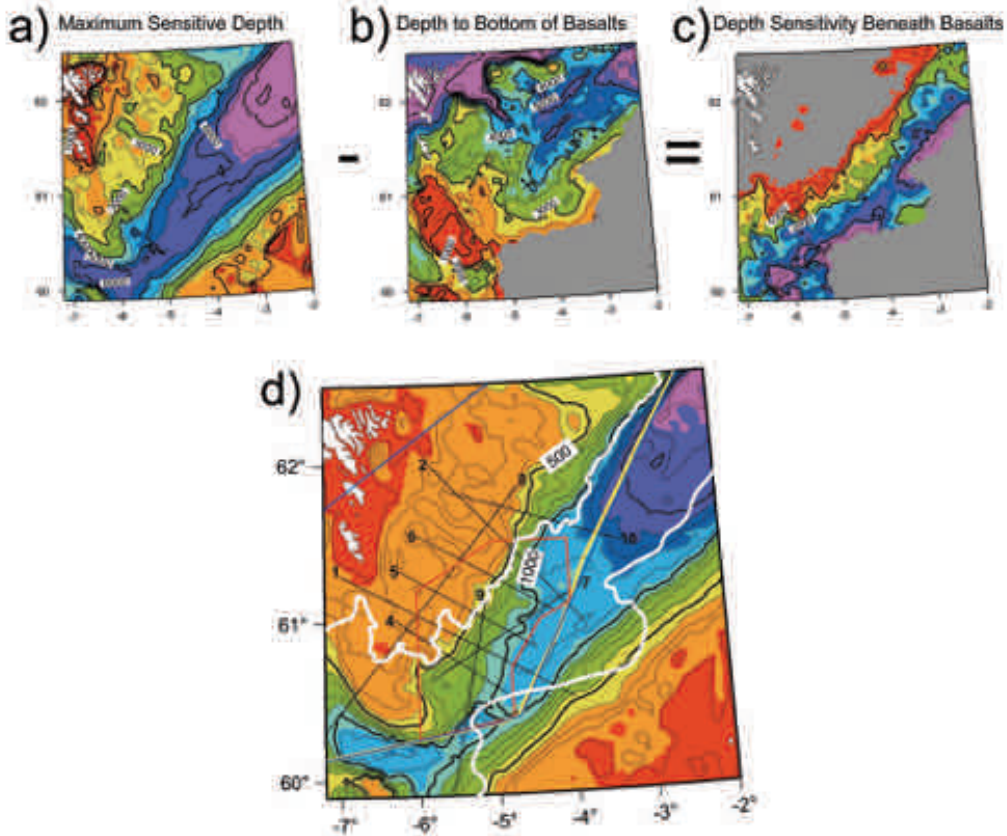


**Figure 8.** Estimates of where compliance measurements can be used to study sub-basalt sediments in the Faroes region (white colour, subplot (d)). (a) Maximum sensitive depth of compliance. (b) Depth to the bottom of the basalt layer (calculated using a compilation of seismic lines in the region and first published in White *et al.*, 2003). (c) Compliance depth sensitivity beneath the basalts, obtained by subtracting (b) from (a). (d) Faroes bathymetry, with the “good compliance” zone (wherever compliance is sensitive to more than 1000 meters beneath the basalts) within the white outline. The eastern bound of this zone is the limit of the basalt flows. Depth contours and lines indicating other boundaries are the same as in Figure 6a.

Figure 9 compares the compliance depth sensitivity to subsurface cross-sections from the two-ship active seismic FLARE experiment (White *et al.*, 1999; Flidner and White, 2003; White *et al.*, 2003).

We identified two end member structures, a “Faroes Deep” (FD) profile with sub-basalt sediments starting 3500 meters beneath the seafloor and a “Faroes Shallow” (FS) profile with sub-basalt sediments starting 2500 meters beneath the

seafloor. We used these models as references to calculate the seafloor compliance sensitivity to surface and sub-basalt sediments. We assumed the basalt layer was 1000 meters thick in the FS model and 2000 meters thick in the FD model. The FD model is the same as that used by (Crawford, 2004) to investigate sub-basalt compliance sensitivity, except we decreased the water depth from 1300 to 1000 meters to more accurately represent the Faroes region. We use realistic infragravity wave

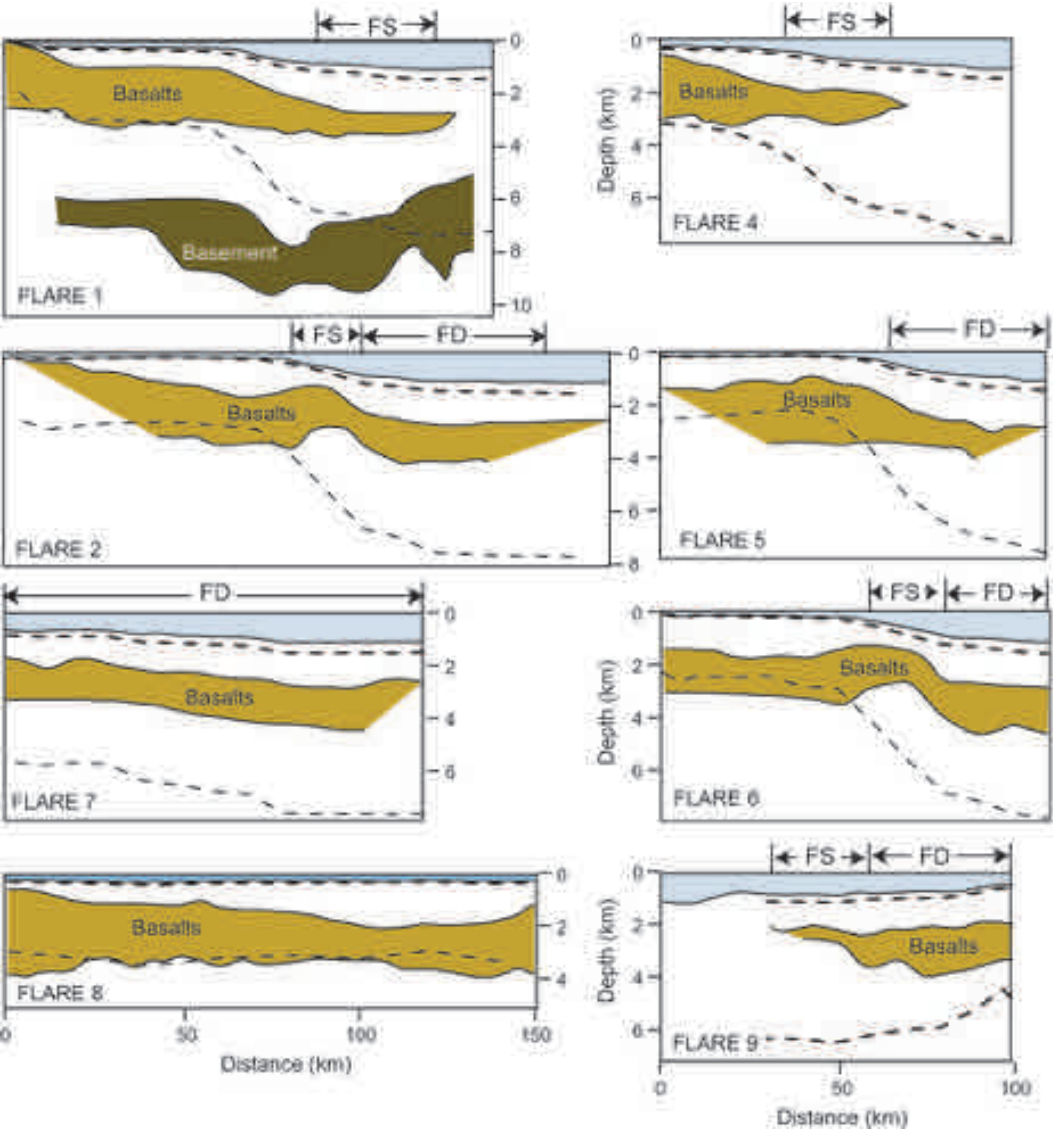


**Figure 9.** Cross-sections of sub-surface structure obtained from the FLARE experiment (Flidner and White, 2003; White *et al.*, 2003), compared to the compliance depth sensitivity limits (dashed lines). The top shaded area is water. The sections “FS” and “FD” indicate the models we ran that are most similar to these sections (Figures 7 and 10).

Parameter	FS model			FD model		
	Value	Uncertainty		Value	Uncertainty	
		<i>a priori</i>	After inversion		<i>a priori</i>	After inversion
Depth to top of middle sediments (meters)	50	20	3	50	20	3
Depth to top of basalts (meters)	1500	100	5	1500	100	4
Depth to top of sub-basalt seds (meters)	2500	1000	100	3500	1000	200
Depth to bottom of sub-basalt seds (meters)	5500	1000	200	5500	1000	200
Shear velocity of top sediments (m/s)	200	50	3	200	50	3
Shear velocity of middle sediments (m/s)	700	100	1	700	100	1

**Table 1:** Compliance sensitivity to features of two Faroes Basin sub-surface models.

source levels and random seismic noise based on observed seafloor noise levels to calculate hundreds of synthetic seafloor compliance data for each model. We ran inversions on all the data and statistically analyzed the results to determine the compliance sensitivity to each model layer (Crawford, 2004). Table 1 lists the *a priori* and final parameter uncertainties for both models and Figure 10 shows the uncertainties for the FS model.

The only significant difference in the compliance sensitivity to the FS and FD models is to the depth of the top of the sub-basalt sediments. Compliance measurements constrain this depth to within 100 meters in the FS model and to within 200 meters in the FD model. Both are significant improvements over the *a priori* uncertainty of 1000 meters. The depth of the sub-basalt sediments controls the compliance sensitivity, not the thickness of the overlying basalts (Crawford, 2004).

Discussion and Conclusions

Seafloor compliance measurements may be used to detect and study low shear modulus zones associated with unconsolidated sediments and sub-basalt sediments. They should be sensitive to unconsolidated sediments up to several km beneath the seafloor throughout the Faroes region and useful for studying sub-basalt sediments in the deeper waters (greater than 500 meters water depth to the south of the Faroe Islands and greater than 900 meters water depth to the east). The shallower the sub-basalt sediments are, the more sensitive the compliance measurements will be to them.

The greatest uncertainty in this analysis is the pressure levels of the source infragravity waves. We assumed that the pressure level was  $10^4 \text{ Pa}^2/\text{Hz}$ , which is a typical value worldwide, but the levels in the Faroes region could be higher or lower because of local effects. The only way to know these levels are to measure them directly at the seafloor over a period long enough to cover any seasonal

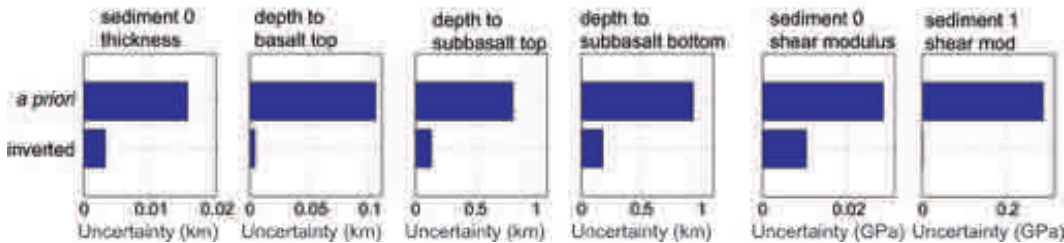


**Figure 10.** Uncertainties in Faroes FS model parameters before and after inversions using synthetic compliance data. The data are generated assuming a 1000 meters water depth, infragravity wave power spectral density of  $10^4 \text{ Pa}^2/\text{Hz}$  and 100 data windows of 1024 seconds each (see Crawford (2004) for details).

variations. The ideal solution would be year-long pressure measurements at a site in shallow water near the Faroe Islands and at a second site at 1000 meters water depth in the Faroes Basin.

Compliance inversions can be considerably improved by using *a priori* data, and the structure should be even better constrained using joint inversions with seismic and electromagnetic data. An experiment is scheduled to measure compliance over the FLARE-1 and FLARE-10 seismic lines in the Faroes Basin. The FLARE 10 line was the site of recent electromagnetic measurements (Jegen-Kulcsar and Hobbs, this issue): compliance measurements on this line should provide a good opportunity to investigate the relative strengths of active seismics, EM and compliance for studying unconsolidated and sub-basalt sediments and will provide a test bed to study the usefulness of joint seismic-compliance-EM inversions.

## Acknowledgements

We are grateful to the SINDRI consortium for their support in this research and the Faroese Geological Survey for organizing the 2004 Faroe Islands Exploration Conference and this publication. We thank Professor Robert White and an anonymous reviewer for their constructive reviews and thoughtful suggestions.

## References

- Apel, J.R. 1987. Principles of ocean physics, Academic Press, London.
- Barzahi, I., Calacagni, D., Passolunghi, M. and Sandroni, S. 2001. Faeroe Sub-basalt seismic imaging - a new iterative time processing approach. *EAGE 63rd Conference and Technical Exhibition*: O-20.
- Cox, C.S., Deaton, T. and Webb, S.C. 1984. A deep sea differential pressure gauge. *J. Atmos. Oceanic Technol.* 1: 237-246.
- Crawford, W.C. 2004. The sensitivity of seafloor compliance measurements to sub-basalt sediments, *Geophys. J. Int.* 157: 1130-1145.
- Crawford, W.C. and Webb, S.C. 2002. Variations in the distribution of magma in the lower crust and at the Moho beneath the East Pacific Rise at 9–10°N. *Earth Plan. Sci. Lett.* 203(1): 117-130.
- Crawford, W.C., Webb, S.C. and Hildebrand, J.A. 1991. Seafloor compliance observed by long-period pressure and displacement measurements. *J. Geophys. Res.* 96(10): 16151-16160.
- Crawford, W.C., Webb, S.C. and Hildebrand, J.A. 1998. Estimating shear velocities in the oceanic crust from compliance measurements by two-dimensional finite difference modeling. *J. Geophys. Res.* 103(5): 9895-9916.
- Crawford, W.C., Webb, S.C. and Hildebrand, J.A. 1999. Constraints on melt in the lower crust and Moho at the East Pacific Rise, 9°48'N, using seafloor compliance measurements. *J. Geophys. Res.* 104(2): 2923-2939.
- Crawford, W.C., Webb, S.C. and Hildebrand, J.A. 1994. The Coaxial segment crustal magma source. *EOS, Transactions, Amer. Geophys. Union* 75(44): 617.
- Flidner, M.M. and White, R.S. 2001. Sub-basalt imaging in the Faeroe-Shetland Basin with large-offset data. *First Break* 19: 247-252.
- Flidner, M.M. and White, R.S. 2003. Depth imaging of basalt flows in the Faeroe-Shetland Basin. *Geophys. J. Int.* 152: 353-371.
- Fruehn, J., Flidner, M.M. and White, R.S. 2001. Integrated wide-angle and near-vertical subbasalt study using large-aperture seismic data from the Faeroe-Shetland region. *Geophysics* 66(5): 1340-1348.
- Fruehn, J., White, R.S., Flidner, M.M., Richardson, K.R., Cullen, E., Latkiewicz, C., Kirk, W. and Smallwood, J.R. 1999. Large-aperture seismic: Imaging beneath high-velocity strata. *World Oil*: 109-112.
- Hobbs, R. 2002. Sub-basalt imaging using low frequencies. *Journal of Conference Abstracts* 7(2): 152-153.
- Hulme, T., Crawford, W.C. and Singh, S.C. 2004. Calculation and inversion of two-dimensional compliance data. *Geophys. J. Int.*, submitted.
- Hulme, T., Ricolleau, A., Bazin, S., Crawford, W.C. and Singh, S.C. 2003. Shear wave structure from joint analysis of seismic and seafloor compliance data. *Geophys. J. Int.* 155: 514-520.
- Jegen-Kulcsar, M. and Hobbs, R. this volume. Outline of a joint inversion of Gravity, MT and Seismic Data. In: Ziska, H., Varming, T. and Bloch, D. (eds.) *Faroe Islands Exploration Conference: Proceedings of the 1st Conference, Annales Societatis Scientiarum Faeroensis*, Supplementum 43, Tórshavn.
- Latychev, K. and Edwards, R.N. 2003. On the compliance method and the assessment of three dimensional sea floor gas hydrate deposits. *Geophys. J. Int.* 155(3): 923-952.
- Mack, H. 1997. Seismic response of Tertiary basalt flows in Northeast Atlantic – a modelling study. In: EAGE 59th Conference and Technical Exhibition, Paper B017, EAGE, Geneva, Switzerland.
- Martini, F. and Bean, C.J. 2001. Application of pre-stack wave equation datuming to remove interface scattering in sub-basalt imaging. *EAGE 63rd Conference and Technical Exhibition*: O-17.
- Roberts, M. 2004. Joint inversion of seismic and compliance data. *Lithos Science Report* 6, in press.
- Trevorrow, M.V. and Yamamoto, T. 1991. Summary of marine sedimentary shear modulus and acoustic speed



- profile results using a gravity wave inversion technique. *J. Acoust. Soc. Am.* 90 (1): 441-456.
- Webb, S.C., Zhang, X. and Crawford, W.C. 1991. Infra-gravity waves in the deep ocean. *Journ. Geophys. Res.* 96(C2): 2723-2736.
- White, R.S., Fruehn, J., Richardson, K.R., Cullen, E., Kirk, W., Smallwood, J.R. and Latkiewicz, C. 1999. Faeroes large aperture research experiment (FLARE): imaging through basalt. In: Fleet, A.J. and Boldy, S.A.R. (eds.) *Petroleum Geology of Northwest Europe: Proceedings of the 5<sup>th</sup> Conference*. Geological Society, London: 1243-1252.
- White, R.S., Smallwood, J.R., Flidner, M.M., Boslaugh, B., Maresh, J. and Fruehn, J. 2003. Imaging and regional distribution of basalt flows in the Faeroe-Shetland Basin. *Geophysical Prospecting* 51: 215-231.
- Willoughby, E.C. and Edwards, R.N. 1997. On the resource evaluation of marine gas-hydrate deposits using seafloor compliance methods. *Geophys. J. Int.* 131(3): 751-766.
- Willoughby, E.C. and Edwards, R.N. 2000. Shear velocities in Cascadia from seafloor compliance measurements. *Geophys. Res. Lett.* 27(7): 1021-1024.
- Yamamoto, T. and Torii, T. 1986. Seabed shear modulus profile inversion using surface gravity (water) wave-induced bottom motion. *Geophys. J. R. Astr. Soc.* 85: 413-431.
- Ziolkowski, A., Hanssen, P., Gatliff, R., Jakubowicz, H., Dobson, A., Hampson, G., Li, X.-Y. and Liu, E. 2003. Use of low frequencies for sub-basalt imaging. *Geophysical Prospecting* 51: 169-182.

# Effects of Tertiary Volcanism and later Events upon the Faroese Hydrocarbon System

STEPHEN LINNARD<sup>1\*</sup> AND ROB NELSON<sup>1</sup>

1: Anadarko Algeria Company LLC,

P.O. BOX 576, The Atrium, 1 Harefield Road, Uxbridge, Middlesex, UB8 1YH, UK.

\* E-mail: stephen\_linnard@anadarko.com; Tel: +44 (0)1895 209526; Fax +44 (0)1895 209670

## Abstract

The Faroes-Shetland continental margin has long been a tectonically active area. It is only with a regional geological understanding that goes beyond the Faroes that the hydrocarbon potential of that region can be properly assessed. Information has been gathered from numerous sources in order to build a picture of the evolution of the area. This is a massive undertaking and must consider analyses, observations and conclusions of co-workers from both industry and research. Ideas are offered on how just one part of the geological jigsaw, the early Tertiary volcanic phase, may have fundamentally affected the development of the hydrocarbon system of the Faroese continental area as a result of rapid transient and then permanent uplift, particularly in the area of the present day Munkagrinnur Ridge. This paper discusses the major impact of volcanic events at this time on trapping, source, reservoir seal and charge. In addition, geological activity after the Palaeocene-early Eocene volcanic events have also significantly affected the Faroese hydrocarbon system and should be given due consideration.

This paper is intended primarily to provoke a thought process amongst explorers, and it is in this spirit that it is offered.

## Introduction

When Anadarko applied for Licences 007 and 006 in 2000 (Figure 1), it was understood that the nature and age of the basalts that covered the region would be of key importance in determining the prospectivity of the underlying sediments. Anadarko's model at that time was for the Faroes flood basalts, or their equivalents, erupting somewhere to the north and west of the Faroes Islands from the earliest Palaeocene until earliest Eocene.

Discussions in this paper have been subdivided into the following five sub-sections:

1. Regional Palaeocene igneous activity;
2. Impact of thermal uplift in the Faroes-Shetland Basin;
3. Impact of igneous related activity on the Faroes-Shetland hydrocarbon system;

4. Model for the origin for the Munkagrinnur Ridge;
5. Impact of Post-Igneous Events on the Faroes Hydrocarbon System.

Formation names referred to in this paper are shown in Figure 2 and linked to the BP/Shell 'T' sequence naming convention, as described by Lamers and Carmichael (1999).

## 1. Regional Palaeocene igneous activity

A key question for Palaeocene prospectivity which arose from our model was how quickly could clean Palaeocene sands from the west, or from elsewhere for that matter, be deposited in the area before the advancing basalts and their preceding detritus, contaminated siliclastic deposition. The work of Jolley

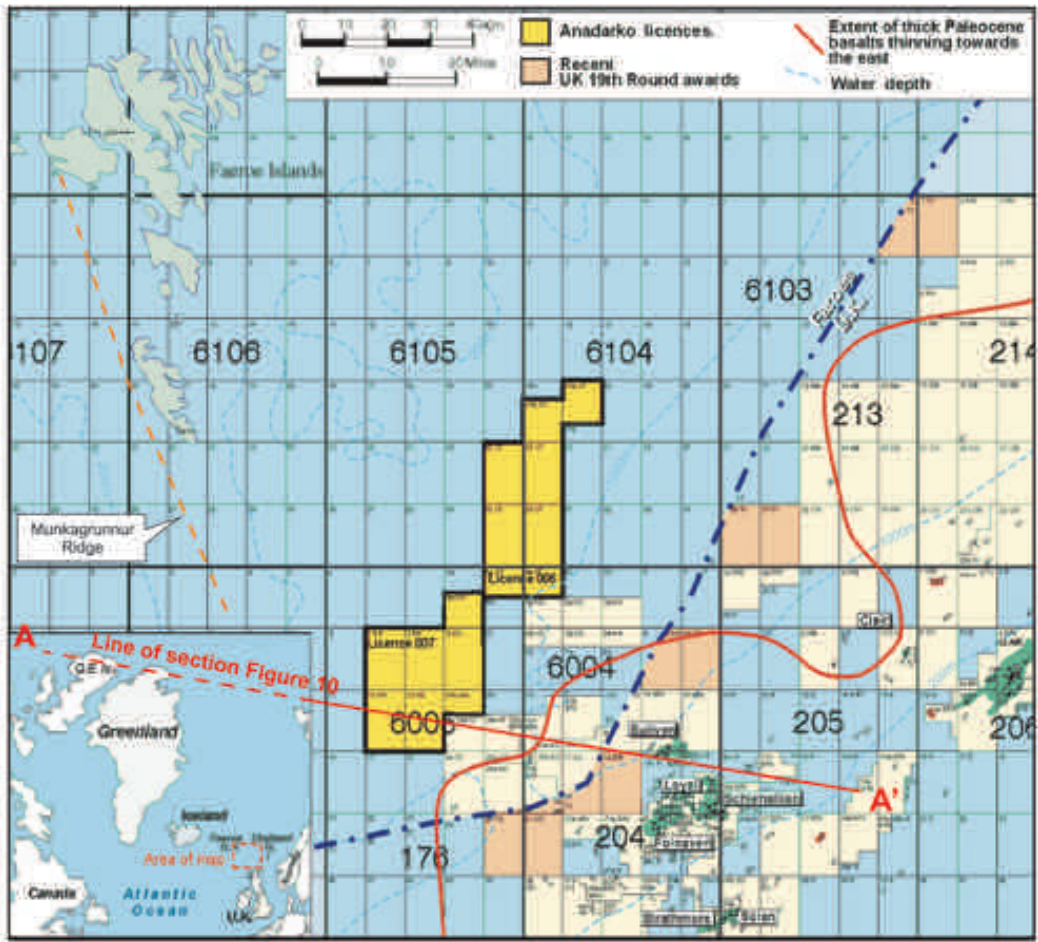


**Figure 1.** Regional location map: Anadarko Licence 007.

and Bell (2002) in particular however, but also the fieldwork and conclusions of researchers from the Cambridge Arctic Shelf Programme (CASP) and the Geological Survey of Denmark and Greenland (GEUS) in the Kangerlussuaq area of south east Greenland, along with Anadarko's own interpretation of the age of the Lopra well basalts (drilled on the southernmost Faroese Island of Suderoy in 1981 and deepened in 1996), has demonstrated to our satisfaction that the Faroes basalts are of latest Palaeocene to earliest Eocene Flett age and are therefore age equivalent to Flett Formation present within the Faroe-Shetland Basin.

The time chart shown in Figure 2 illustrates our current understanding of the timing of early-Tertiary regional volcanic activity (after Jolley and Bell, 2002).

Therefore whilst concerns over the impact of the Faroes basalts on the prospectivity of Licence 007

and 006 areas were abated, there was little doubt that other regional igneous activity had occurred in pre-Flett (pre-T40) time, as shown in Figure 3, even though the absolute age of each individual event remains unresolved:

- 1) Lundy Island granite off SW England (Ritchie *et al.*, 1999);
- 2) Antrim basalts in Northern Ireland (Ritchie *et al.*, 1999);
- 3) Igneous complexes of Rum and Skye (Jolley and Bell, 2002);
- 4) Basaltic sands in West of Shetlands well 205/9-1 and the Kettla Tuff, of Vaila or similar age;
- 5) Sills interpreted from WOS-Faroes 3D seismic data which appear to have been intruded into the near surface at Late Vaila time;
- 6) Offshore complexes to the south-west of the study area in the Rockall/N. E. Rockall Basins

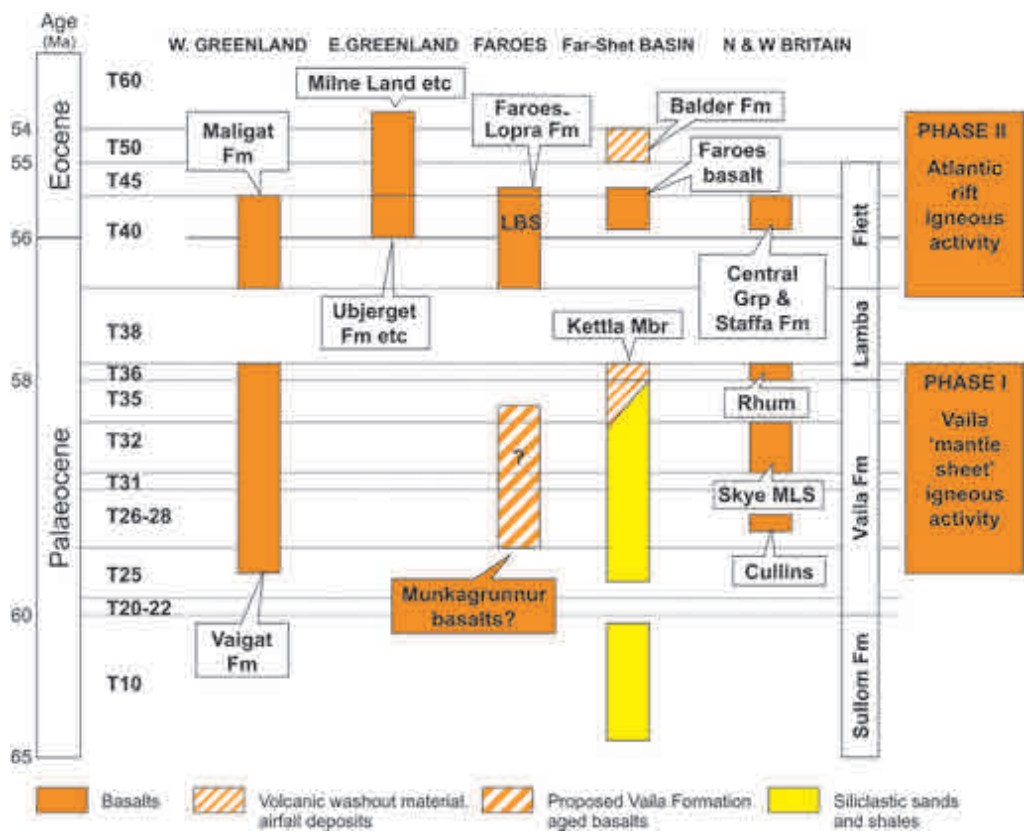


Figure 2. Timing of early-Tertiary regional volcanic activity (after Jolley and Bell, 2002).

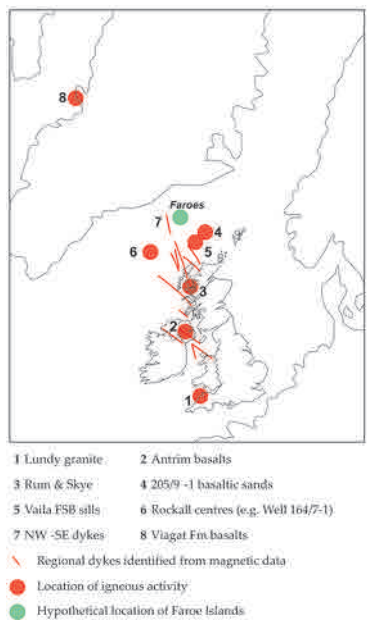


Figure 3. Spatial distribution of (pre-Flett Fm) mid-Tertiary 'Vaila' regional volcanic activity using palaeogeographic reconstruction at Vaila Formation time.

- that are reported as being older than Flett age (Ritchie *et al.*, 1999).
- 7) Large NW-SE trending dyke swarms seen on regional magnetic data to extend from the North of England through the west coast of Scotland and northward to the Faroes via the Munkagrinnur Ridge, which, it is suggested may be related to these events (Figure 4);
  - 8) Basalts of the Viagat Formation of West Greenland of around Vaila age (Dam *et al.*, 1998).

During the same Palaeocene period (~60-58 Ma) sedimentation patterns provide evidence of crustal uplift which may be related to the influence of thermal and igneous activity, based on the following evidence (Figure 5):

- A) Major regional uplift of up to 2-3 km centred in the Irish Sea and Western Britain, responsible for the most extensive of the Palaeocene turbidite systems in the North Sea, namely the Andrew Formation (White and Lovell, 1997);



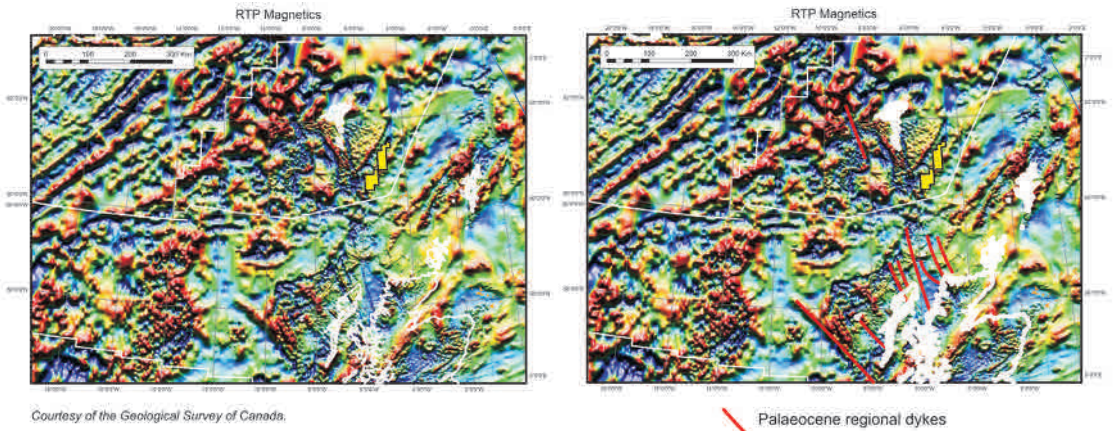


**Figure 4.** NW-SE trending dyke swarms observed on regional magnetic data extend from the North of England through the west coast of Scotland and northward into the Munkagrunnur Ridge (courtesy of *Geological Survey of Canada & British Geological Survey*; Verhoef *et al.*, 1996).

- B) Onlap of the West Shetland basin margins and marginal highs by Lamba shales onto a major unconformity. The Judd High is one such area, where Lamba shales unconformably onlap Lower Cretaceous mudstones.
- C) Simultaneous with the North Sea Andrew Fm deposition, catastrophic deposition of ~2 km of Vaila sediment, predominantly sands, occurs in the Faroe-Shetland basin.
- D) An end Danian uplift is recorded in the N. E. Rockall Basin from well penetrations (Waddams and Cordingley, 1999);
- E) An absence of Palaeocene deposition in S.E. Greenland. Eocene sediments overlie Upper Cretaceous units, suggesting a major unconformity, presumably due to uplift (the Kangerlussuaq Dome). Vitrinite reflectance data in East Greenland supports this, with values increasing southward towards Kangerlussuaq. This is in line with an interpretation of major exhumation occurring at some point in time in that area. That point in time may be early Vaila.
- F) Incision and 'valley fill' sediments of the Atanikerdluk Formation are described in West Greenland, where as much as 1.3 km erosion is estimated (Dam *et al.*, 1998);
- G) Clift (1999) calculated areas of predicted thicker crust due to underplating from offshore well data which, in conjunction with the work of White and Lovell (1997) shows an overall pattern of uplift in the Faroes-West of Britain area. Underplating is the process by which continental crust is thickened, primarily by intrusion at

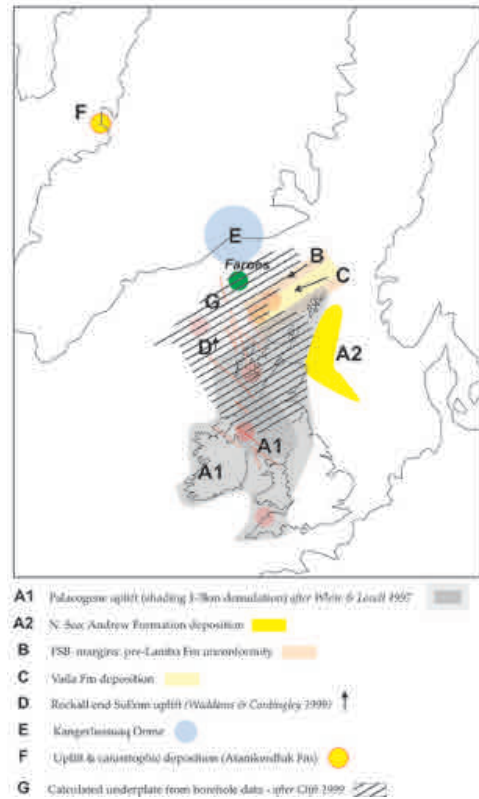


**Figure 5.** Mid-Palaeocene (Vaila Formation: 60-58 Ma) sedimentation patterns provide evidence of crustal uplift which relates to influence of thermal and igneous activity.

its base, due to accretion of underlying mantle melt (White and McKenzie, 1989).



## 2. Impact of thermal uplift in the Faroes-Shetland Basin

Underplating has been interpreted from deep seismic data from the marginal highs of Norway to the Faroes by many authors. Underplate suggests permanent regional uplift and may reflect the shape of the 'plume'. This permanent uplift is the result of increased buoyancy of the continental crust due to the accretion of the relatively lower density fractional melt of the mantle, since although higher in density than the overlying continental crust, this accreted fractionated layer is lower in density than that of the mantle itself (White and McKenzie, 1989). Based on the information cited, the postulated location of this early Vaila aged plume belt is shown in Figure 6. Its shape is also described by Smallwood and White (2002).

It is suspected, however, that an initial rapid, re-

gional 'transient' thermal uplift event was responsible for the short-lived (1-2 Ma) but extreme vertical movement, which gave rise not only to the major Andrew (North Sea) and time equivalent Vaila (Faroes-West of Shetland) clastic pulses, but also to the dramatic incision and catastrophic 'valley fill' sedimentation observed in West Greenland. This rapid uplift would have occurred in earliest Vaila time, whilst its decline is reflected in the later basin-wide Lamba aged marine shale transgression.

As an illustration of the amount of vertical uplift that may have occurred, ConocoPhillips N. E. Rockall well 164/7-1 on the eastern flank of the Darwin centre is reported (Archer *et al.*, 2002) to have undergone 2.5 km uplift and erosion *prior* to initial extrusion of Flett age marine hyaloclastites. Such uplift would have been due in part to the 70 intrusive bodies encountered, ranging from <3 m to >150 m thick, dated at ~63 Ma, and also the large plutonic body interpreted to exist below the well. Such intrusive bodies form part of the underplating process, since not all mantle melt is accreted to the base of the crust, instead a portion would be intruded into the crust, whilst a smaller fraction still will be extruded at the surface.

Thus the idea of Smallwood and White (2002) and others of a rising sheet of hot mantle causing early Palaeocene igneous activity has considerable supporting evidence, and provides a mechanism for both temporary and permanent regional uplift to occur.

## 3. Impact of igneous related activity on the Faroes-Shetland hydrocarbon system

But what does this mean for hydrocarbon exploration in the Faroes? The impact of such major but sudden uplift and subsidence events needs to be factored into the input for hydrocarbon basin modelling to account at any point in time for:

- 1) Palaeo-basin shape and structure;
- 2) The environment and areas of sedimentation (or erosion);
- 3) Deposition patterns for prediction of sand thickness and quality;
- 4) Impact of uplift and burial on the source rock;
- 5) Deposition of reservoir seal rocks.

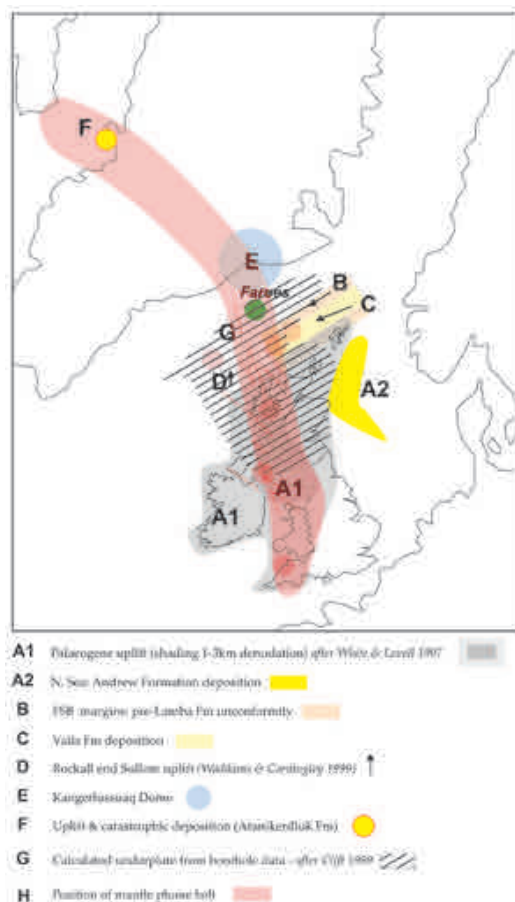


**Figure 6.** Proposed regional location of the 'Vaila plume belt'.

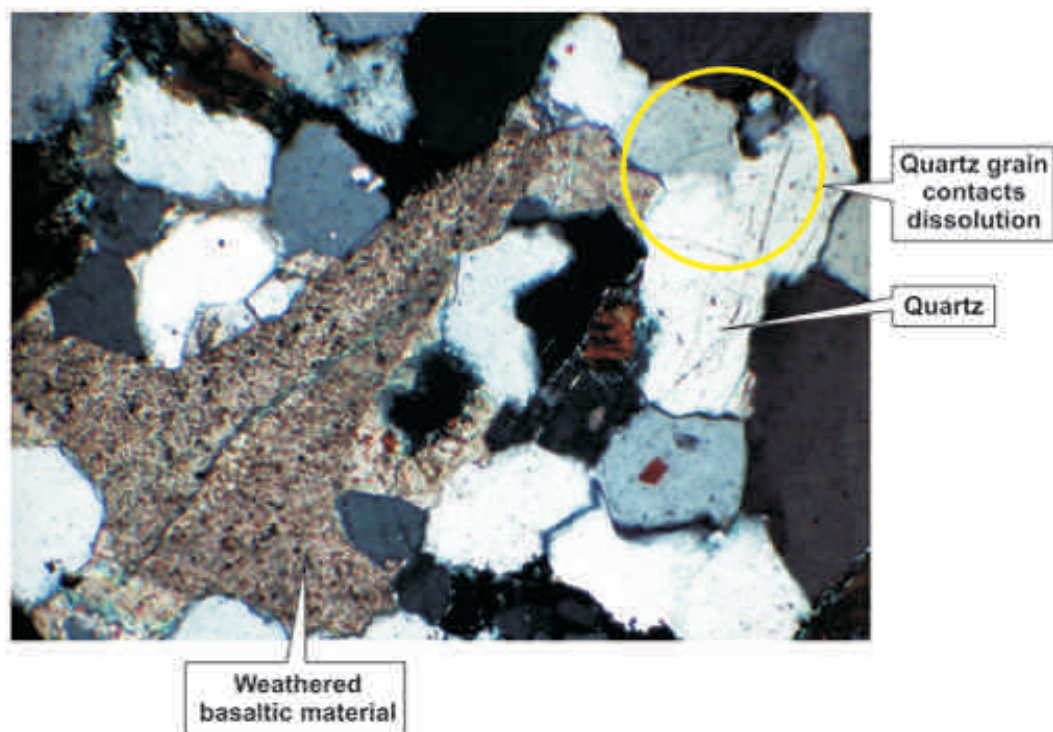


**Figure 7.** Low grade burial metamorphism of Sullom Formation sands is demonstrated in thin section (polarised light) by quartz grain dissolution. Sample is taken from a well within the Faroes-Shetland Basin.

Subtle evidence from well data can be observed that hints at dramatic uplift, erosion and burial. A well from an Anadarko proprietary study within the Faroes-Shetland Basin has observed pressure solution of quartz grains, indicating low grade burial metamorphism in Sullom Formation sands. These sands are overlain directly by Vaila Formation sands, where no such burial metamorphism indications are observed (Figure 7).

This suggests that earliest Vaila uplift and erosion has occurred within the basin, not only at the margins.

Based on other in-house well studies, a western “Greenlandic” sediment source is also predicted, based on palynological evidence in sediments from the lower to mid-Vaila interval, whilst increasing levels of basalt contamination occur in the middle to upper Vaila, suggesting an uplifted western hinterland which was rapidly being denuded, and whose provenance areas were increasingly being affected by drainage from sub-aerial basalt lava fields. Basinal Vaila clastics encountered appear to be composed of sand, rather than coarser conglomeratic material, and therefore it is likely that

these sediments are either being sourced from intermediate shelf ‘holding’ areas, or have not been lithified prior to reworking.

The Kettla Tuff overlies the Vaila Formation. Based on in-house petrographic analyses, it is not an air-fall deposit however, as the name suggests, but is the last major influx of basaltic washout material prior to subsidence and the onset of fully marine conditions in the overlying Lamba Formation. There is a conspicuous absence of any further Greenlandic sediment source signature in the overlying Lamba shales. It is proposed that the marine transgression that began during the early Lamba period would have rapidly encroached on a flat lying lava field (analogous perhaps to the Eldjga and Laki lava fields in S.E. Iceland today), washing away sub-aerially eroded basalt detritus and being responsible for the northward deposition of the Kettla Tuff in a “one off” event. Once these lava fields had subsided below sea level, no further basaltic material would have been deposited in the basin. From then, based on palynological evidence, the eastern sediment source predominates. A point of interest to us is how channel geometries seen on

end Vaila/early Lamba (T36, Figure 2) amplitude extraction maps from 3D seismic show brightening within the channels, suggesting that the channels themselves contain higher velocity basaltic wash-out material.

#### 4. Model for the origin for the Munkagrunnur Ridge

The Munkagrunnur Ridge dominates much of the Faroese continental shelf and is deserving of separate consideration.

It is suggested that the Munkagrunnur Ridge itself may have formed the main relief of this western “Greenland” continental hinterland, having been preferentially uplifted by the plume, then underplated and intruded. The alignment of the regional dyke swarms (magnetic data) from the south with the Munkagrunnur Ridge (section 1), together with deep and conventional seismic studies and also other potential fields (gravity) modelling support the model of thicker continental crust in the Faroes area. It was this accretion event which may have formed the core, and consequent focus for *later inversion* of this structure, as well as sedimentary basins adjacent to it. It may be that the geographical distribution of the later (Flett) Faroes coals was also influenced by this ridge.

The Munkagrunnur Ridge fits well with the regional NW-SE trend identified, and that of the location of an early Vaila age plume event. However it may be considered anomalous in terms of its orientation and size when compared with later (post-Early Eocene) major structures along the N. E. Atlantic margin, which clearly have a purely inversion origin. Other authors have however provided explanations as to the formation of the Munkagrunnur Ridge (Boldreel and Andersen, 1993; Tate *et al.*, 1999). There is no doubt that later inversion has occurred along the Munkagrunnur Ridge, but it is suggested that this has been in response to the *pre-existing* Vaila aged structure, just as structures along the East Faroes High, which form the western margin of the Cretaceous rift (with Caledonian trend) have also been reactivated by such compressional events.

Indirect support for an emergent area in the vicinity of the Wyville-Thomson Ridge even as late as Flett time is indicated by the southward progradation of later Faroes aged hyaloclastites into the

North-East Rockall Basin (Waddams and Cordiner, 1999).

After this initial dramatic but short lived early-Vaila transient thermal uplift, there followed its equally rapid demise due to cooling of this intruded mantle ‘plume’ material. Thus, the Lamba Formation, which overlies the Vaila Formation in the Faroes-Shetland Basin, comprises on-lapping marine shales, forming part of a widespread regional marine transgression leading to the consequent return to marine sedimentation.

Later on during early Flett time there was a second major (Sele) uplift. Faroes fissure basalts were erupted mainly from the north and west of the Faroes and the resulting lava fields encroached over the entire Faroes area, including the Munkagrunnur Ridge. These basalts are recognised today as the Faroes Basalt Formations from which the Faroe Islands are composed, which also subcrop at seabed offshore, such as on the Munkagrunnur Ridge itself, or underlie younger sediments on the entire Faroes shelf area. It is suggested that the Faroes volcanism reflects the intersection and capture of the earlier, but now *declining* NW-SE Vaila aged plume belt by the northward advancing

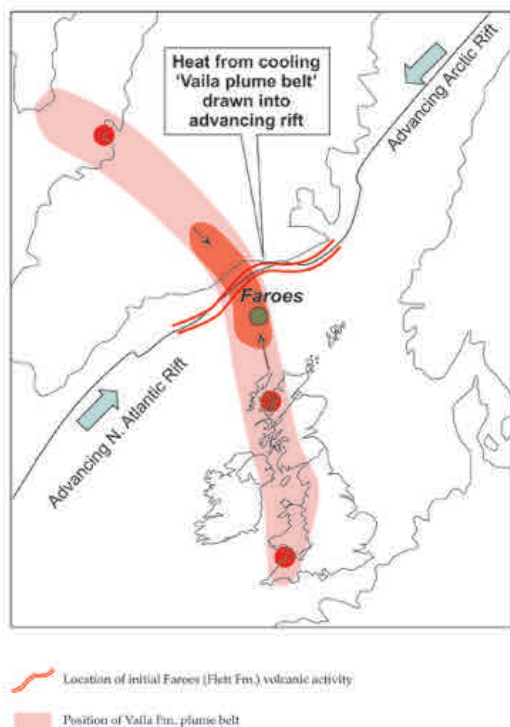


**Figure 8.** Sketch map showing the capture of the ‘Vaila plume belt’ by the advancing Atlantic rift.

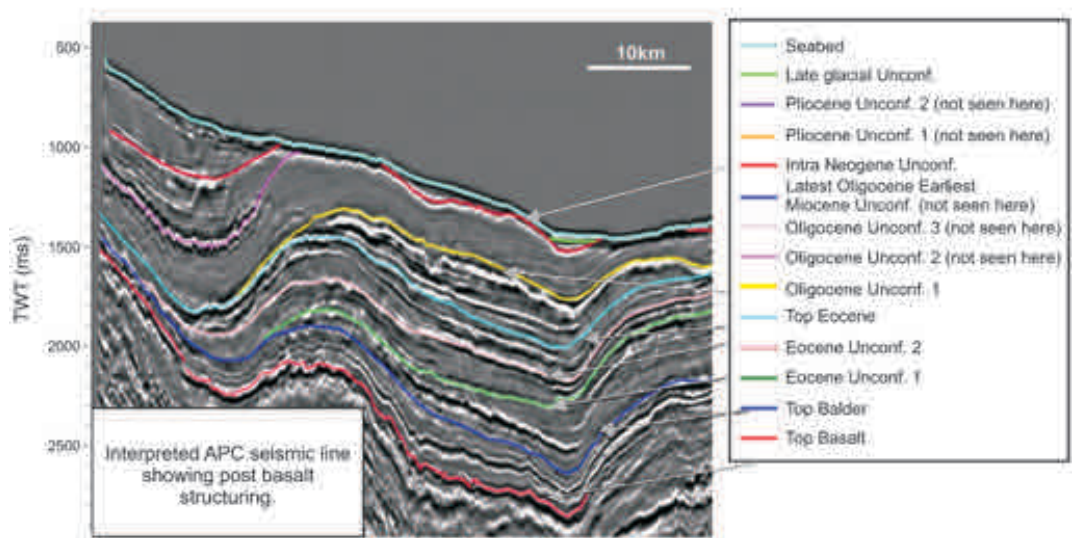


Figure 9. Proprietary Anadarko seismic profile with post basalt interpretation.

Atlantic rift, and southward propagating Arctic rift (Figure 8).

5. Impact of post-igneous events on the Faroes hydrocarbon system

Detailed mapping and modelling of the post-basalt sequence (shown in Figures 9 and 10) may

be just as important in understanding present day hydrocarbon distribution as the earlier Palaeocene events.

A number of key tectonic events have occurred since the extrusion of the basalts, which ended in Early Eocene time in this area, in particular:

- 1) Latest Oligocene-Early Miocene (LOEMU)

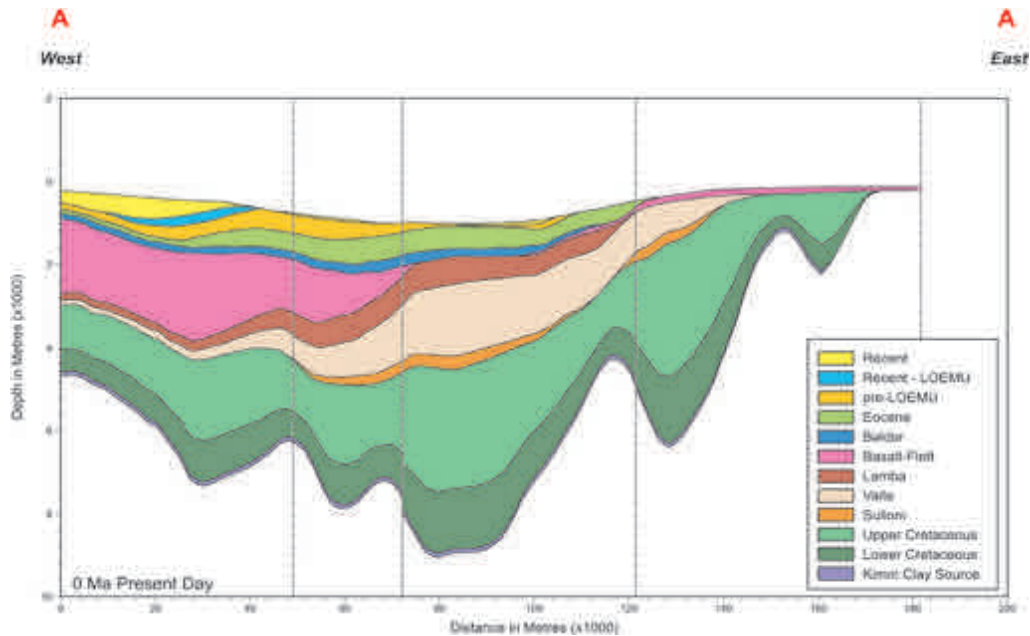


Figure 10. Regional west-east modelled section across the Faroes-Shetland basin showing the significance of post basalt structuration. Line of section shown in Figure1.



- and Intra Neogene (INU) unconformities;
- 2) Pliocene uplift of the continental margins;
- 3) Glacial rebound and tilting.

It is noted, for example, that the original Oligocene depositional thickness prior to the Latest Oligocene-Early Miocene Unconformity (LO-EMU) could have a tremendous impact upon the burial and generation potential of source rocks along the basin margins. If there had been a substantial thickness of Oligocene burial prior to the LOEMU uplift, then Jurassic source rock generation might have ended at 30 Ma, never to resume. This is shown on the modelled source rock burial plot (Figure 11). By reducing the original pre-LO-EMU burial thickness however, and hydrocarbons will return into the generation window and continue to be generated to present day. This is particularly important for gas generation from a Jurassic source rock but is also just as relevant were an Upper Cretaceous source rock to be modelled, which has been postulated to exist, on account of the presence of oil deep in the southern part of the Faroes-Shetland Basin.

## Conclusions

The ideas proposed have required the integration of all manner of geological and geophysical data, from large scale satellite surveys to thin section petrography. It is by utilising all these data to offset the poor quality of the seismic in the sub-basalt (seismic data being the usual front line exploration tool) that the following conclusions are proposed:

1. A major, but short lived regional uplift in earliest Vaila time may have been responsible for the high deposition rates during the Vaila period in the Faroes Basin. Sediment was derived from all sides of the basin, but particularly from areas directly above the maximum thermal uplift, which, based on the ideas outlined here, could have been in the area of the present day Munka-grunnur Ridge.
2. Based on regional observations of timing and trends, this proposed early Vaila uplift may be attributed to a transient thermal uplift associated with rising mantle sheets, which affected an area as far afield as south west England to West Greenland.

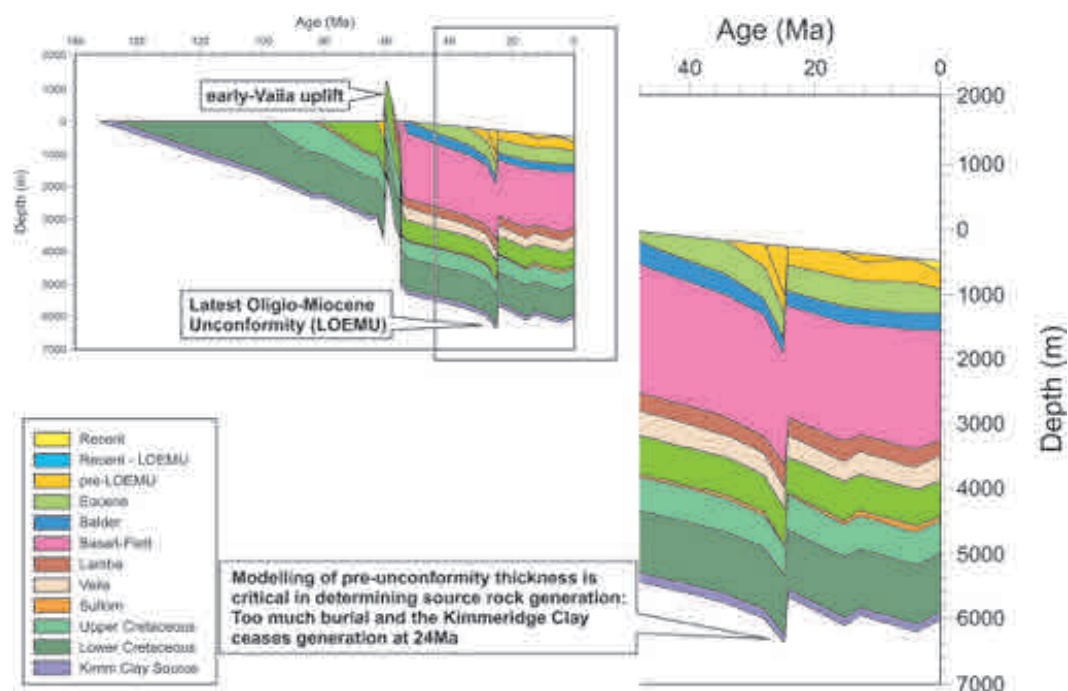


**Figure 11.** Upper Jurassic source rock burial versus time plot. Modelling the eroded thickness of pre-LOEMU sediments may be critical in predicting late hydrocarbon generation. Location: Faroes Basin.



3. The origins of the Munkagrannur Ridge may lie in the transient Vaila thermal uplift. The Ridge would have been sustained thereafter by underplating and intrusion of molten igneous material, resulting in permanent uplift. Later inversion along the Munkagrannur structure has clearly occurred, but it is suggested that inversion may not be the primary cause of this feature.
4. Any impact of the Faroes volcanism on Palaeocene oil and gas prospectivity is likely to be due to intrusive rather than extrusive events, such that the presence of intrusive material may degrade seismic imaging, therefore increasing uncertainty in interpretation, and also pose problems during drilling.
5. Sensitivity modelling of missing section prior to events such as the Latest Oligocene Earliest Miocene (LOEMU) and intra-Miocene (INU) unconformities and Pliocene uplift may be of major importance in predicting generation, migration and charge throughout the area.

## Acknowledgements

Thanks are given to Anadarko Petroleum Corporation for permission to publish this paper, and in particular to the following individuals and groups:

Steven Crews and Euan Shand (Anadarko Petroleum Corporation) for their basin modelling work;  
 Brian Bell (University of Glasgow) and David Jolley (University of Sheffield) for their work both for Anadarko and that published;  
 Peter Gibbs (Wealden Exploration);  
 The British Geological Survey (BGS) for their permission to reproduce the regional magnetics map and for their general support in our work;  
 Andrew Whitham and Robert Scott from the Cambridge Arctic Shelf Project (CASP);  
 The Faroes Geological Survey (JFS) and the Faroes Petroleum Administration (Ministry of Trade & Industry)  
*Also the very many workers, too numerous to mention, without whose research and ideas this paper would not have been possible.*

## References

- Archer, S., Bergman, S., Iliffe, J., Murphy, C. and Thornton, M. 2002. The thermal history of well 164/07-1, and implications for the hydrocarbon prospectivity of the Northeast Rockall Trough. *Abstract and presentation at "Frontier Exploration of Volcanic Margins" (Conference)*, Geological Society of London.
- Boldreel, L.O. and Andersen, M.S. 1993. Late Paleocene to Miocene compression in the Faroe-Rockall area. *In: Parker, J.R. (ed.) Petroleum Geology of Northwest Europe: Proceedings of the 4<sup>th</sup> Conference*. Geological Society, London: 1025-1034.
- Clift, P.D. 1999. The thermal impact of Paleocene magmatic underplating in the Faeroe-Shetland-Rockall region. *In: Fleet A.J. and Boldy S.A.R. (eds.) Petroleum Geology of Northwest Europe: Proceedings of the 5<sup>th</sup> Conference*. Geological Society, London: 585-594.
- Dam, G., Larsen, M. and S nderholm, M. 1998. Sedimentary response to mantle plumes: Implications from Palaeocene onshore succession, West and East Greenland. *Geology* 26(3): 207-210
- Jolley, D.W. and Bell, B.R. 2002. The evolution of the North Atlantic Igneous Province and the opening of the NE Atlantic Rift. *In: Jolley, D.W. and Bell, B.R. (eds.) The North Atlantic Igneous Province: stratigraphy, tectonic, volcanic and magmatic processes*. Geological Society, London, Special Publications 197: 1-13.
- Lamers, E. and Carmichael, S. 1999. The Paleocene deep-water sandstone play West of Shetland. *In: Fleet, A.J. and Boldy, S.A.R. (eds.) Petroleum Geology of Northwest Europe: Proceedings of the 5<sup>th</sup> Conference*. Geological Society, London: 645-659.
- Ritchie, J.D., Gatiloff, R.W. and Richards, P.C. 1999. Early Tertiary magmatism in the offshore NW UK margin and surrounds. *In: Fleet, A.J. and Boldy, S.A.R. (eds.) Petroleum Geology of Northwest Europe: Proceedings of the 5<sup>th</sup> Conference*. Geological Society, London: 573-584.
- Smallwood, J.R. and White, R.S. 2002. Ridge-plume interaction in the North Atlantic and its influence on continental breakup and seafloor spreading. *In: Jolley, D.W. and Bell, B.R. (eds.) The North Atlantic Igneous Province: Stratigraphy, Tectonic, Volcanic and Magmatic Processes*. Geological Society, London, Special Publications 197: 15-37
- Tate, M.P., Dodd, C.D. and Grant N.T. 1999. The Northeast Rockall Basin and its significance in the evolution of the Rockall-Faeroes/East Greenland rift system. *In: Fleet, A.J. and Boldy S.A.R. (eds.) Petroleum Geology of Northwest Europe: Proceedings of the 5<sup>th</sup> Conference*. Geological Society, London: 391-406.
- Verhoef, J., Roest, W.R., MacNab, R., Arkani-Hamed, J., et al. 1996. Magnetic anomalies of the Arctic and North Atlantic Oceans and adjacent land areas. *Geological Survey of Canada Open File Report* 3125a. Geological Survey of Canada, Dartmouth.
- Waddams, P. and Cordingley, T. 1999. The regional geology and exploration potential of the NE Rockall Basin. *In: Fleet, A.J. and Boldy, S.A.R. (eds.) Petroleum Geology of Northwest Europe: Proceedings of the 5<sup>th</sup> Conference*. Geological Society, London: 379-390.
- White, N. and Lovell, B. 1997. Measuring the pulse of a plume with the sedimentary record. *Nature* 387: 888-891.
- White, R. and McKenzie, D. 1989. Magmatism at Rift Zones: The Generation of Volcanic Continental Margins and Flood Basalts. *Journal of Geophysical Research* 94(B6): 7685-7729.

# Elastic Impedance Inversion to aid Lithology Prediction in the Palaeocene of the Judd Sub-Basin

MARK WOODFIN<sup>1\*</sup>, JON SEEDHOUSE<sup>2</sup>, GIACOMO SPADINI<sup>3,4</sup> AND MAURIZIO CARDAMONE<sup>3</sup>

1: (From July 2005) Reservoir Management Limited, 7 Bon Accord Square, Aberdeen AB 11 6DJ.

\*E-mail: mark.woodfin@eniuk.com

2: Talisman Energy (UK) Limited, Talisman House, 163 Holburn Street, Aberdeen AB10 6BZ

3: ENI - E&P Division, Via Emilia 1, San Donato Milanese, 20097, Italy.

4: Present address. ENI Petroleum, 1201 Louisiana #3500, Houston, TX 77002, USA.

## Abstract

Prior to drilling in Faroe Islands Licence 002, the presence of seals and trapping geometries were highlighted as the highest risk elements of the petroleum system. This paper outlines how elastic impedance inversion was used to aid prospect definition within the sand-prone Palaeocene sediments of Judd sub-basin.

Two discrete stratigraphic traps were defined and matured using 3D inversion volumes generated with calibration to a single offset well. A second well was made available prior to drilling and an interim inversion exercise, using the data from two offset wells, was undertaken prior to the drilling of the 6004/17-1 well. 3D data volumes for P impedance, S impedance, and Poisson's Ratio, along with lithology indicator volumes were generated for discrete zones of interest and used to describe and refine new and previously identified prospects within Licence 002. Good lithology prediction was achieved in the 6004/17-1 well, despite the limited well control.

Knowledge of P impedance, S impedance and Poisson's Ratio sheds light on the subtle lithological variations responsible for the stratigraphic traps and the presence and quality of reservoirs. The integration of elastic impedance data from well analysis and fluid-replacement modelling was the key ingredient for lithology prognosis and definition of stratigraphic traps.

Key issues arising from the well results involve the prediction of tuffaceous sandstones and the vertical resolution of the inversion volumes. The shale intervals encountered in the 6004/17-1 well are at the very limit of the resolution of this technique.

## Introduction

Licence 002 in the Faroe Islands (Figure 1) is located between the Judd and Westray transfer zones within the Faroe Shetland Basin (Lamers and Carmichael, 1999). A series of prospects were identified in this area prior to the award of exploration licences in 2000. These prospects relied mostly on stratigraphic trapping mechanisms and were based upon a series of seismic anomalies within the Palaeocene sediments. In 2001 the AFI2001 3D seismic dataset (Figure 1) was acquired over the licence area while drilling by other companies in the region provided a series of mixed and sur-

prising results. During late 2001 and 2002 a series of well trades allowed the offset well data (Figure 1) to be reviewed alongside the newly acquired 3D seismic data. The models on which the licence application prospects had been defined were subsequently revised prior to selecting a prospect and location for drilling the 6004/17-1 well in the summer of 2003.

The high net sand to gross interval thickness ratio encountered in the offset wells in the area, combined with the unexpected causes of seismic amplitude anomalies in the Palaeocene section, forced a revision of perceived risks associated with the prospects. In order to better understand these

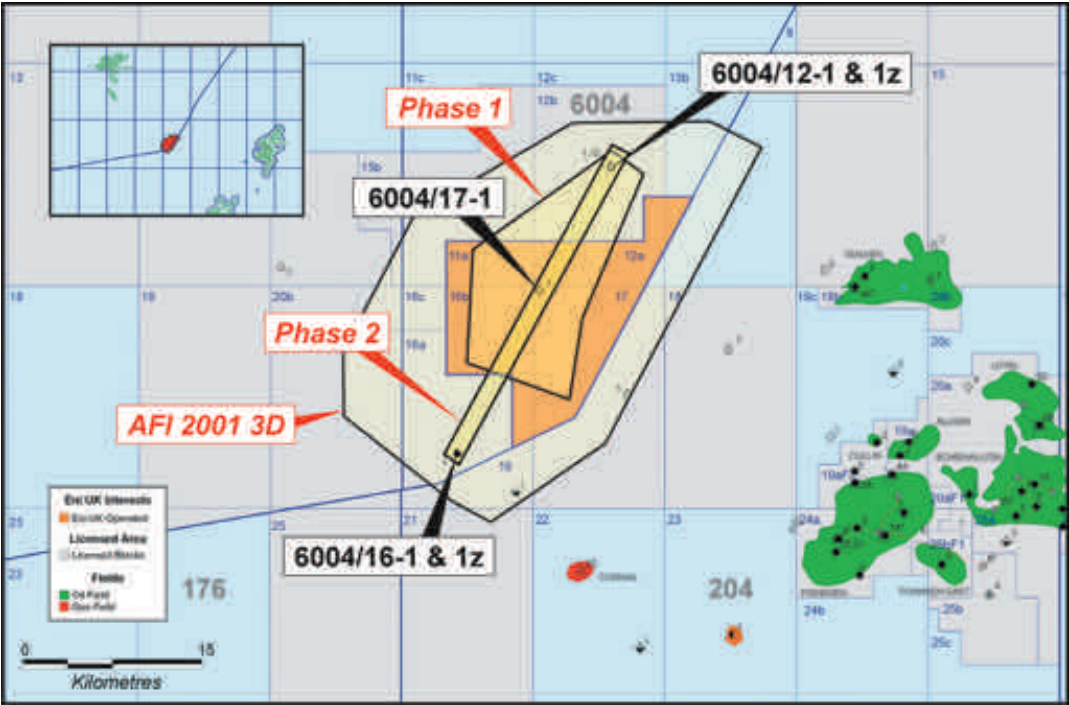


**Figure 1.** Map showing the location of Faroe Islands Licence 002, the well 6004/17-1, offset traded wells 6004/12-1, -1z and 6004/16-1, -1z, the area covered by the AFI2001 3D seismic survey, and the areas of data used for the seismic inversion exercise.

risks prior to the final choice of drilling location an elastic impedance inversion study was carried out as part of a comprehensive work programme. A

further reason for the study was to investigate the possible amplitude versus offset effect of potential hydrocarbon accumulations.

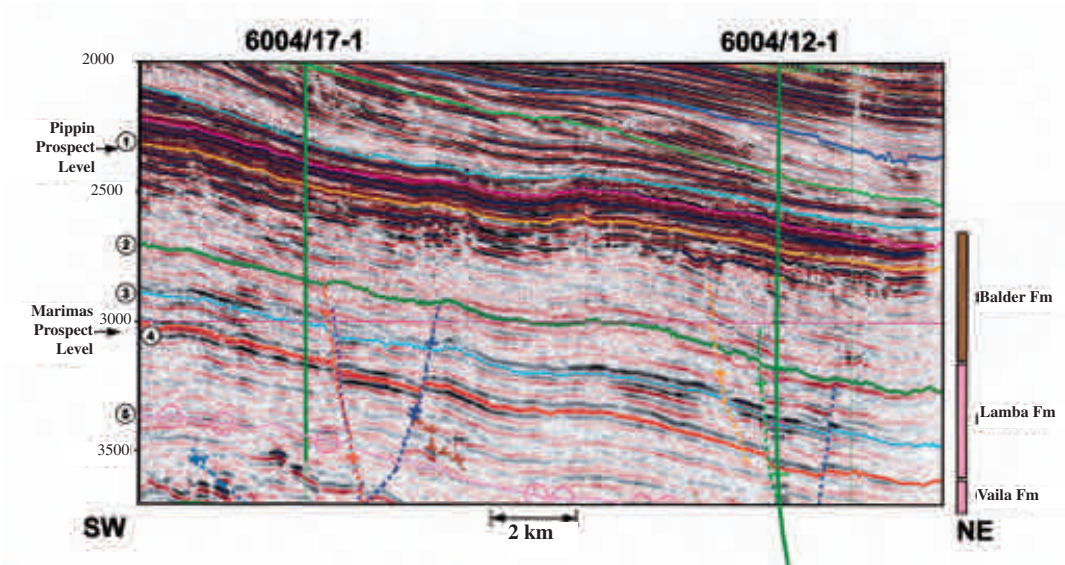


**Figure 2.** A seismic line from the pre-stack time migration data between wells 6004/17-1 and 6004/12-1, -1z showing the strong lateral continuity of seismic reflectors in the Vaila Formation. These reflectors represent basinal, sand-rich turbidite systems with tabular geometries.

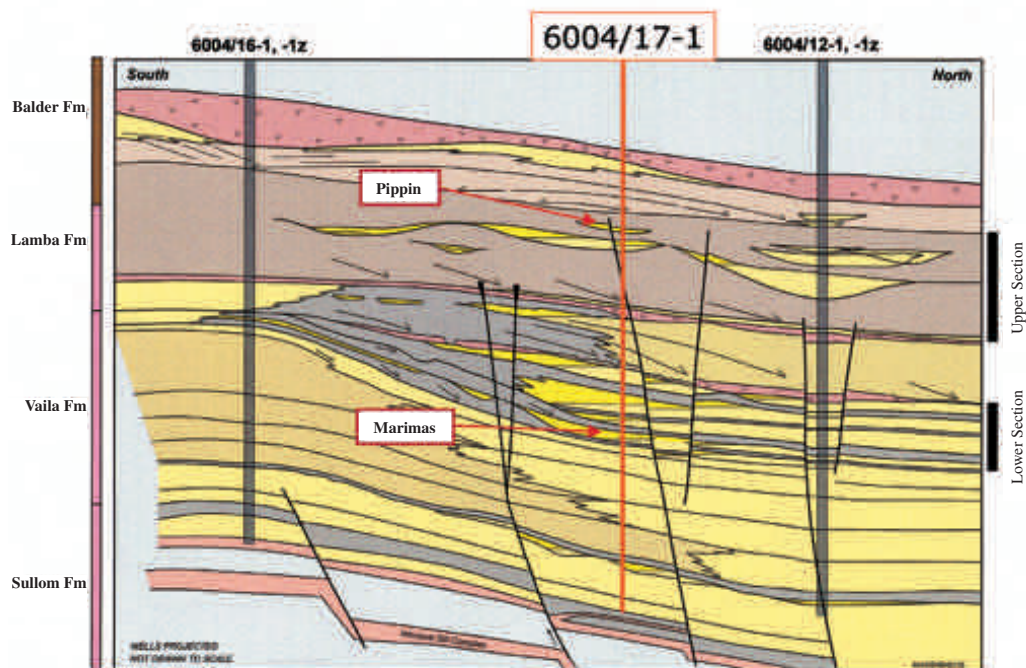


**Figure 3.** Schematic geoseismic section through the Faroe Islands Licence 002 area of the Judd sub-basin. This shows the prognosed, pre-drill geological setting of the Marimas and Pippin targets in relation to the two traded offset wells (6004/12-1, -1z and 6004/16-1, -1z).

Well results indicate that the main reservoir rocks in the Palaeocene Vaila Formation near Licence 002 are sand-rich turbidite systems characterised by very high sand/shale ratio and overall tabular geometries extending for tens of kilometres (Figure 2).

The potential seal rocks consist of thin mudstone drapes in the basinal areas. These may merge with mud-prone slope sediments towards the basin margins. The stratigraphic play in the Vaila Formation is therefore linked closely to the marine onlap of basin floor turbidites against the slope system. This is the inferred trapping mechanism for the Marimas prospect (Figure 3), which was the main prospect in Licence 002 and the primary target of the 6004/17-1 well. The interval containing the Marimas prospect was inferred to pinch-out between the wells 6004/12-1z and 6004/16-1z but the pinch-out could not be mapped from the conventional seismic data.

Other play concepts in Upper Lamba/Lower Balder are related to shallow marine, shelfal and pro-delta gravity flow bodies deposited basinward of prograding deltas. The Pippin prospect (Figure

3), a secondary target of the 6004/17-1 well, was identified in this setting using the inversion volumes.

Well 6004/17-1 was drilled in the summer of 2003. Due to the stacked nature of the prospects identified in Licence 002 both the Marimas and Pippin prospects were targeted with a single vertical well (Figure 3).

## Objectives

The main objective of the elastic impedance inversion study was to assist lithology prediction within the Upper Palaeocene sediments in the Licence 002 area, in order to discriminate sandstones from shales and tuffaceous sandstones, and to investigate any amplitude versus offset effect of hydrocarbon accumulations. A further objective was to extrapolate this knowledge away from well control by elastic impedance inversion of the seismic data and the generation of calibrated inversion volumes. Due to the lack of shale in the sedimentary section, as indicated in the offset wells (Smallwood *et al.*, 2004. Poulsen *et al.*,



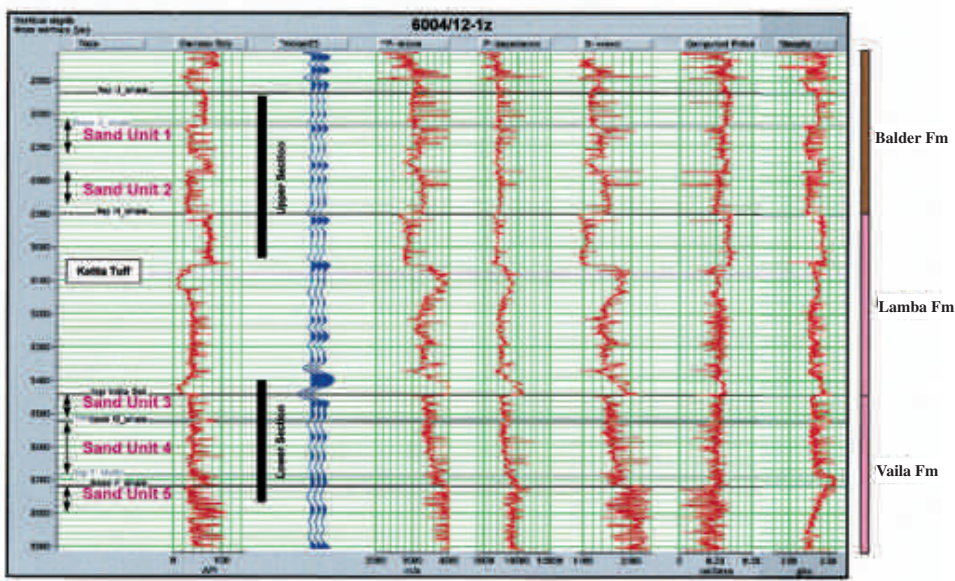


**Figure 4.** Acoustic and elastic impedance logs from the interval between 2460 and 3900 m tvdss in the 6004/12-1 well, showing zones of interest (“Upper Section” and “Lower Section”) described in this study. Individual Sand Units 1 to 5 are also labelled. Synthetic trace; reverse polarity, wavelet Ricker 25 Hz zero phase.

2004), a key objective was to produce a dataset which would allow potential sealing intervals to be identified and tracked in order to define their lateral extent.

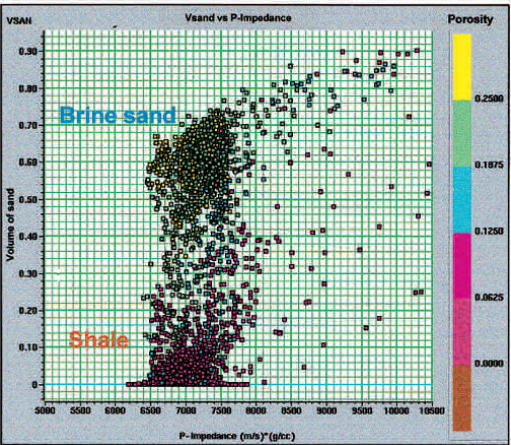
Method

Introduction

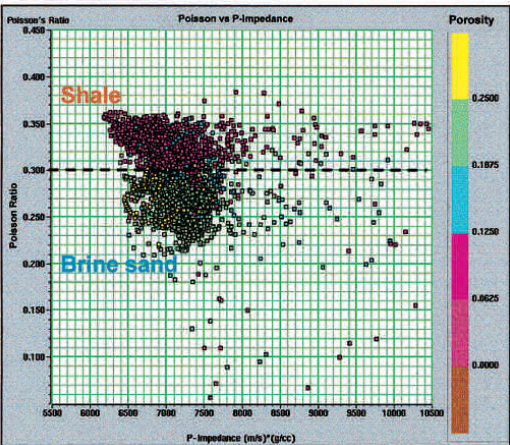
The study is made up of four parts which are described in this section. These are; (1) zone defini-

tion, (2) petro-acoustic characterisation and well calibration, (3) fluid replacement and AVO modelling, and (4) elastic impedance inversion and lithologic characterization

The pre-stack time migration data of the proprietary AFI2001 3D seismic survey (Figure 1) were used as the source for the elastic impedance inversion. Angle stacks for nears, fars and ultra-far ranges were available for the elastic inversion, which was carried out using the proprietary Jason



a)



b)

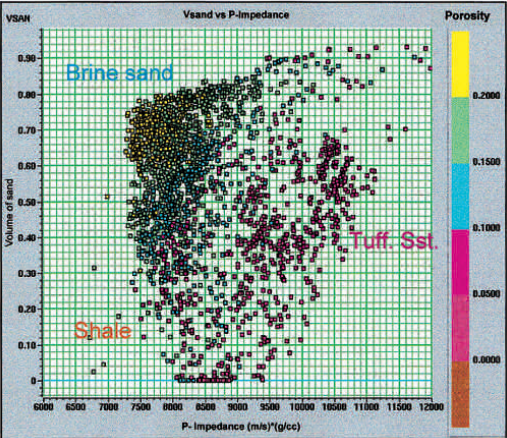
**Figure 5.** Plots of petro-acoustic properties of the Upper Section (Sand Units 1 and 2) from the 6004/12-1 well, showing P impedance plotted against fraction of sand (a), and P impedance plotted against Poisson's Ratio (b). A Poisson's Ratio value of 0.3 (indicated by the dashed line) can be used to separate sandstones and shales in this section.



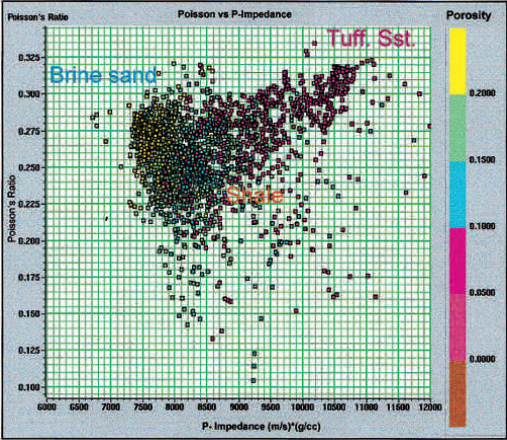
Geosystems sparse spike method (Pendrel and Van Riel, 1997). The inversion was performed in two phases due to the timing of availability of the calibration wells 6004/12-1, -1z and 6004/16-1, -1z. The first phase was carried out on a 170 km<sup>2</sup> subset of the AFI2001 3D covering the Marimas prospect and tied to the 6004/12-1, 1z well (Figure 1). Because this well lies at the extreme downdip extent of the subvolume there was a risk that the calibration would be progressively less valid for the updip portions of the Marimas body. When the 6004/16-1, -1z well was traded a narrow strip (Figure 1) of data that covered both wells and the proposed 6004/17-1 well location was inverted again, using both wells for calibration. The result of this second

phase of inversion was to prove that the original model was substantially correct and that geobodies/objects detected in the first phase were valid.

The following inversion volumes were generated during the project; P impedance, S impedance, Poisson's Ratio, Sand Indicator (2 calibrated volumes defined from cross-plot analysis of S impedance against Poisson's Ratio, and S impedance against P impedance). Lithology classification from elastic impedance inversion relies on an analysis of the petro-acoustic character of the drilled sequences. At the same time, fluid replacement modelling, of different hydrocarbon saturation conditions, allowed possible hydrocarbon indicators to be derived from the inversion volumes.

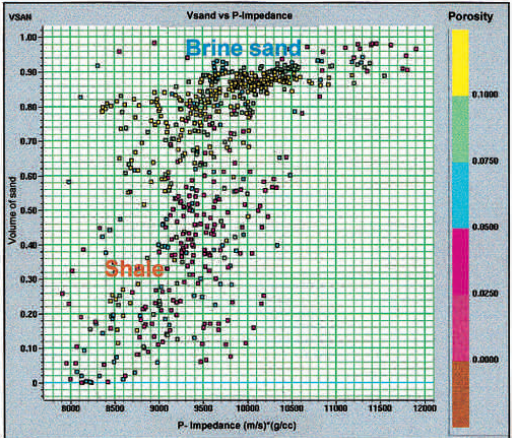


a)

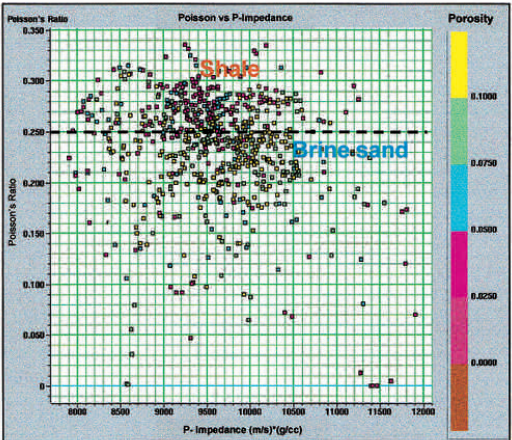


b)

**Figure 6.** Plots of petro-acoustic properties of the Lower Section (Sand Units 3 and 4) from the 6004/12-1 well, showing P impedance plotted against fraction of sand (a), and P impedance plotted against Poisson's Ratio (b). Simple lithology cut-offs can not be applied in this Lower Section.



a)



b)

**Figure 7.** Plots of petro-acoustic properties of the Lower Section (Sand Unit 5) from the 6004/12-1 well, showing P impedance plotted against fraction of sand (a), and P impedance plotted against Poisson's Ratio (b). A Poisson's Ratio value of 0.25 (indicated by the dashed line) can be used to separate sands and shales in this interval.



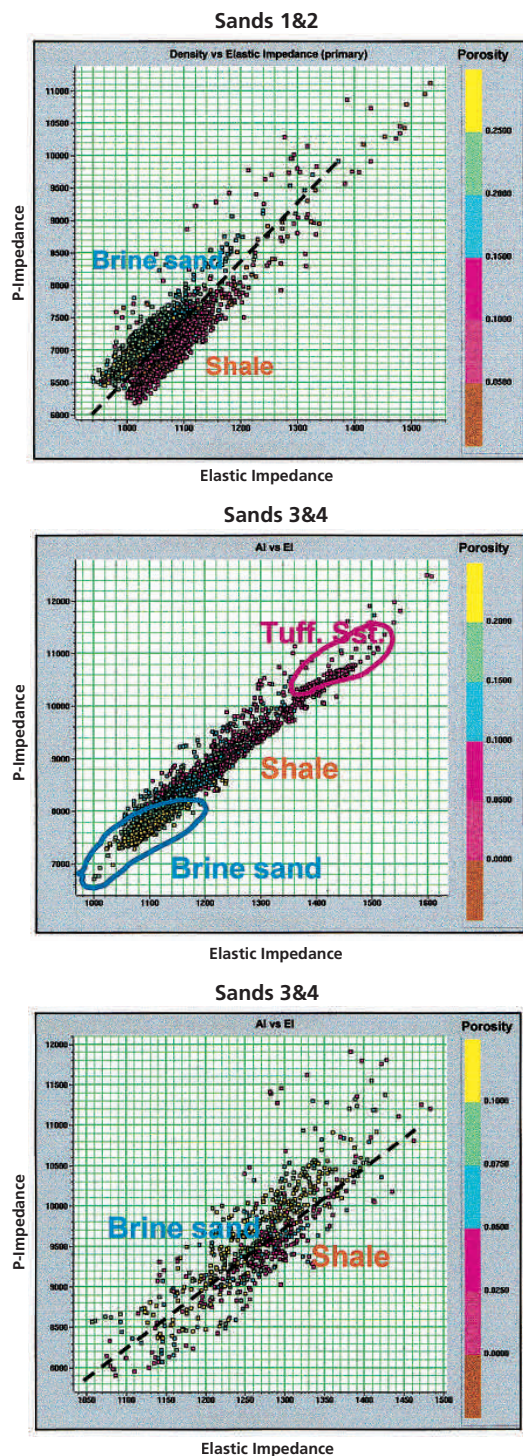


**Figure 8.** Plots of acoustic impedance versus elastic impedance at 30 degrees offset for Sand Units 1 and 2, 3 and 4, and 5. These plots illustrate that neither AI nor EI alone are good lithology discriminators but in combination with one another, sands and shales can be distinguished in AI-EI space.

### Zone definition

Following examination of the 6004/12-1 well data, zones for detailed analysis were defined on the basis of distinct log characteristics (relationships between density and acoustic properties in sands and shales within the well). The stratigraphic intervals in which prospects had previously been defined were also taken into consideration. Two zones are described in this paper; the Lower Balder and Upper Lamba Formations ("Upper Section"), and the Uppermost Vaila Formation ("Lower Section") (Figures 3 and 4). In total these two zones cover five discrete sandstones with interbedded shales and tuffaceous sandstones, which were chosen for petro-acoustic analysis.

In the Upper Section (Figure 4) the sand units (Sand Units 1 and 2) have very little P impedance contrast at their interfaces. Sandstones in the Upper Section have blocky log signatures, with very thin intercalated shale layers. S-wave velocity in Sand Units 1 and 2 is higher than that of the surrounding shales but the density is lower. The result is that these sandstones cannot be clearly recognised on either conventional seismic data or by using P impedance but are best distinguished from the surrounding using Poisson's Ratio (Figures 4 and 5).

The Lower Section (Figure 4) comprises sand units (Sand Units 3, 4 and 5) found below an Upper Paleocene tuffaceous sandstone. Sand Unit 3 is in contact with the lower high impedance tuffaceous sandstones (above). A thin shale between Sand Units 3 and 4 is also a high impedance unit.

The last sand prone layer examined in the Lower Section (Sand Unit 5) lies below a high impedance shale. Sand Unit 5 is quite different from Sand Units 3 and 4 in the Lower Section. The density of Sand Unit 5 is high but slightly less than the overlying shale. P-wave and S-wave velocities are lower in the overlying shale. The result is an increase in acoustic impedance at the top of Sand Unit 5.

Sand Units 1 and 2 typically have a class 2 (Castagna, 1993) acoustic response. Sand Units 3 and 4 have a class 3 (Castagna, 1993) response and Sand Unit 5 has a class 1 response (Castagna, 1993).

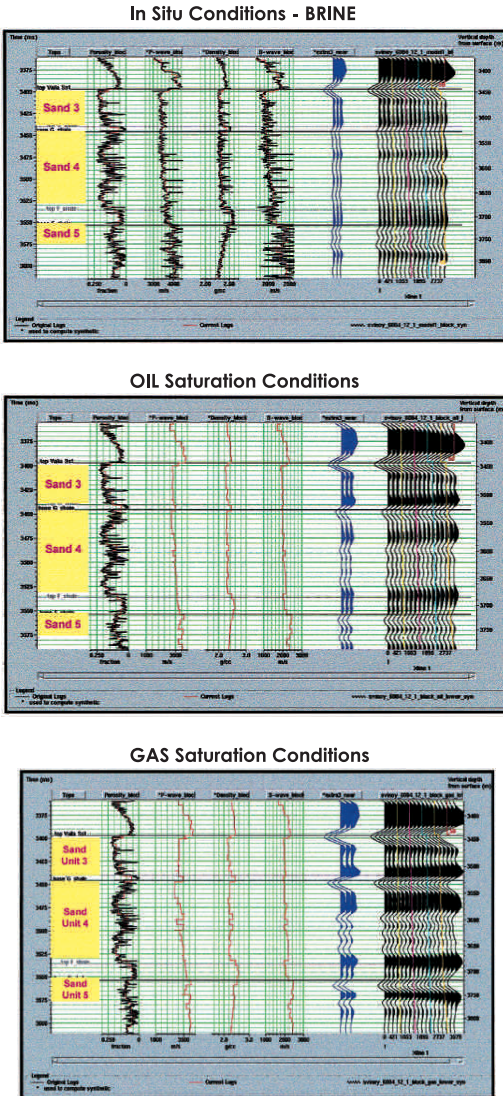


**Figure 9.** Fluid replacement modelling results in the Lower Section. The presence of oil is not expected to give rise to changes in amplitude with offset or stacked amplitude anomalies large enough to be separated from background lithological effects. Gas produces brightening across all offsets and should be visible in stacked seismic data.

**Petro-acoustic characterisation and well calibration**

Petro-acoustic properties of the Upper and Lower Units were investigated by cross-plotting key parameters. This highlighted the relationships between lithological and acoustic properties as a necessary step in understanding seismically derived acoustic and elastic parameters as indicators for lithology and fluid presence.

Figures 5, 6, and 7 illustrate the petro-acoustic properties of Sand Units 1 and 2, 3 and 4, and 5 respectively. In the Upper Section (Figure 5), when the P impedance is plotted against a lithology indicator (volume of sand with porosity in colour code) it shows an overlap between values related to sand units and those of shales. Thus P impedance cannot be effectively used to separate sand from shale. On the other hand, Poisson's Ratio values for the same interval distinguish between lithologies. In the Poisson's Ratio domain a threshold at around 0.3 was defined to separate the shales and the sandstones.

For the Lower Section (Figure 6) Sand Units 3 and 4 have lower impedance values compared to the shale, but large areas of overlap exist. The highest impedance values are recorded from the low porosity tuffaceous sandstones. For Sand Units 3 and 4 Poisson's Ratio is not a useful lithology discrimination parameter, although an area can be seen in the Poisson's Ratio–P impedance space, where the clean brine sands are concentrated.

Sand Unit 5 of the Lower Section (Figure 7) shows different acoustic properties. The impedance values of brine sands overlap and exceed the values of the shale units, consistent with the class 1 behaviour (dimming of amplitude with offset, Rutherford and Williams, 1989). For this sand a cut off value of 0.25 Poisson's Ratio discriminates brine sand from shales. This cutoff was used as a guide in the interpretation of the Marimas sand body and to evaluate the continuity of the overlying shale. Phase 2 of the study (including the 6004/16-1, -1z well) confirmed that there was a depth dependant dimension to this relationship and that instead of a simple cutoff value, a more complex method of discrimination was needed.

The partial effectiveness of Poisson's Ratio as a lithology discriminator suggested that lithological information could be extracted from the seismic data by looking at angle dependant amplitude variations (Anderson and Bogaards, 2000). To test this concept, the use of angle dependant properties was investigated by cross-plotting acoustic and elastic impedance values. Plots (Figure 8) of P impedance versus elastic impedance calculated at 30° offset indicates that neither parameter alone is a particularly good separator but when combined together these can be effectively used to discriminate lithology.



**Fluid replacement and AVO modelling**

The AVO study carried out for this project was aimed at predicting the pre-stack amplitude behaviour of the target lithologies and to test the capability of the AVO method to discriminate different fluid content in the specific rock types (Hampson, 1991; Castagna, 1993; Ostrander, 1984; Anderson and Bogaards, 2000). This was considered essential since the application of AVO had been called into question by a series of unexpected drilling results in the region.

The AVO modelling was performed using elastic parameters of sand prone and shale prone layers, computed from log data of the 6004/12-1 well in a depth range between 2500 and 3800 meters (TVDSS). Figure 9 shows the acoustic model used

as starting point for the calculation of the pre-stack behaviour of the relevant interfaces for the Lower Section. Brine was replaced by hydrocarbons in all Sand Units in order to calculate the corresponding elastic parameters using the Biot-Gassman model (Gassmann, 1951).

The fluid replacement modelling indicates that the presence of oil is not expected to give rise to changes in P impedance large enough to produce brightening (or dimming) of the post stack seismic amplitudes that could be easily separated from background lithological effects (Figure 9). On the other hand, modelling suggests that the presence of gas produces brightening of amplitudes at all angles for most of the sand-shale interfaces (Figure 9). Gas should therefore be visible, where

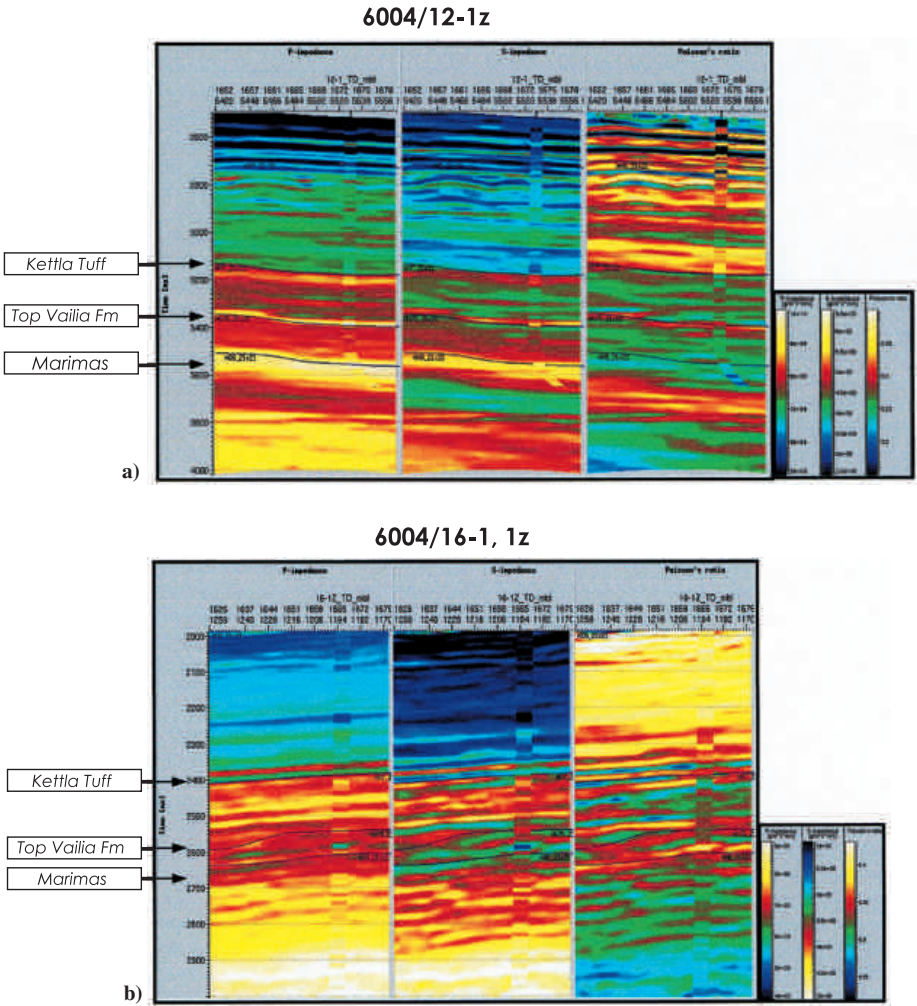


**Figure 10.** Illustration of products (P impedance, S impedance and Poisson's Ratio) from AVA simultaneous inversion for wells 6004/12-1, -1z (a) and 6004/16-1, -1z (b).

6004/12-1. Upper Section  
P-Impedance vs S-Impedance. Derivation of Sand Indicator Volume

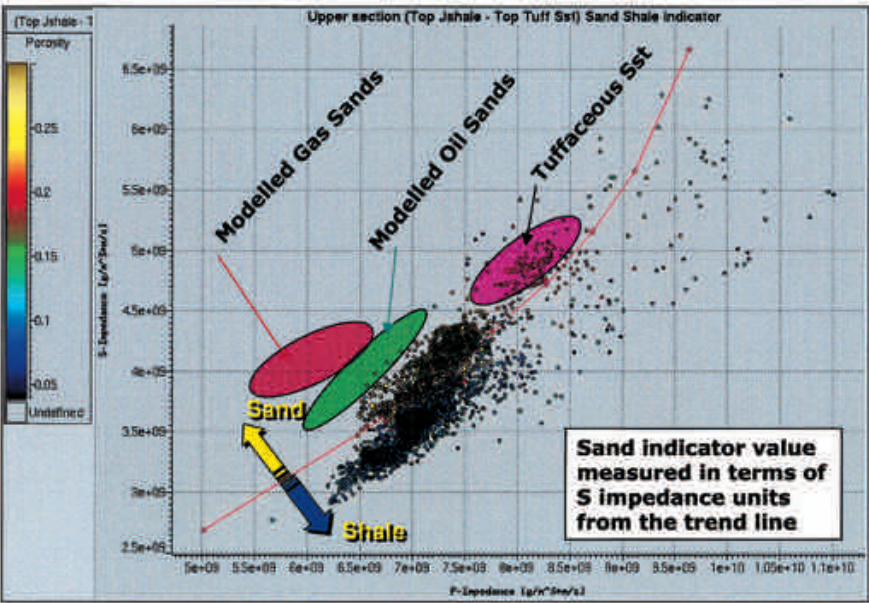


**Figure 11.** Plot of P impedance versus S impedance for the Upper Section of well 6004/12-1. These data were used to calculate Sand Indicator values for this section by measuring the distance (in S impedance units) of points from the calculated trend line. Anticipated areas for oil and gas bearing sands are plotted as polygons generated by fluid replacement modelling.

present, as a bright seismic anomaly. It should be remembered that this will be difficult to distinguish from the amplitude anomalies produced by lithology changes. The AVO modelling indicates that the classical analysis of amplitude variation with offset is inefficient in detecting possible hydrocarbons accumulations in this dataset. The generation of prospects in Licence 002 did not rely on amplitude or AVO effects.

An important outcome of the fluid replacement modelling was the calculation of the P-wave, S-wave velocities and density for different saturation conditions of the target layers. This allowed the possibility of separating sandstone and hydrocarbon-bearing zones from non-reservoir layers in a P impedance - S impedance domain to be explored.

**Elastic impedance inversion and lithologic characterization**

The amplitude versus angle (AVA) inversion was designed to provide information on the elastic parameters of the section and therefore on the sand-shale distribution. An angle dependent sparse spike inversion technique was used (Pendrel and

Van Riel, 1997). This allowed estimation of a consistent set of elastic parameters using simultaneous inversion of angle stacks.

AVA constrained sparse spike inversion technology was chosen in preference to conventional reflectivity data or other conventional AVA analyses for several reasons including handling of phase and polarity-related issues in the input seismic and the possibility of deriving absolute quantities that maximize the separation of sands and shales. The process also allowed the generation of models of combined parameters to highlight lithology contrasts or possible hydrocarbon presence.

*Well to seismic ties and wavelet estimation*

Well-to-seismic ties were performed by comparison around the well location of synthetic seismograms computed using the conventional 1D vertical convolution model, the offset dependent reflectivity, and an extracted wavelet, with the respective angle stack seismic volumes. Compressional wave sonic, shear wave sonic and density logs were used to compute the offset dependent reflectivity for a range of angles equivalent to that of the three angle



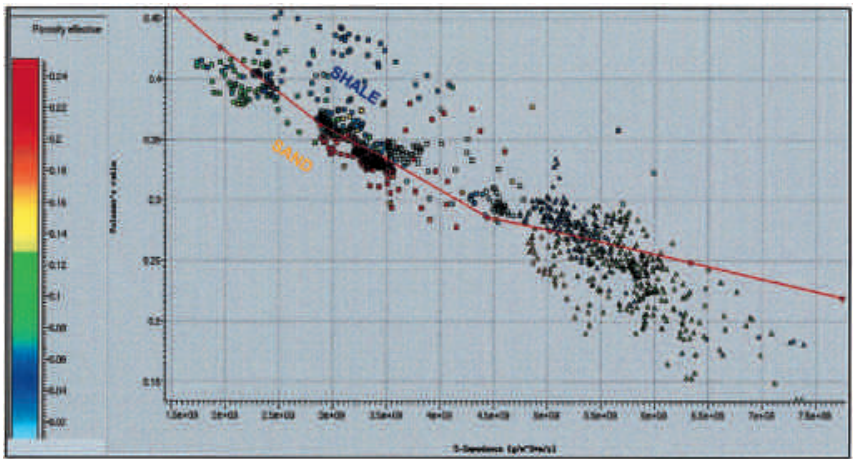


**Figure 12.** Plot of S impedance versus Poisson’s Ratio for the Lower Section. The trend line is used as a sand/shale separator for creating sand/shale volumes. Triangles are from well 6004/12-1, squares are from well 6004/16-1z.

stacks using the Aki-Richards approximation (Aki and Richards, 1980).

*Low frequency model*

Because the reflectivity data that can be obtained from an inversion of the seismic trace contains information only within the available seismic bandwidth additional lower frequency information is needed. To add the information for the lower frequencies a 3D layer earth model was built using the interpreted horizons. Velocity information derived from the stacking velocity was interpolated along layers bounded by interpreted horizons (Numbers 1 to 5 illustrated in Figure 2), to respect

both stratigraphy and structure.

The relationship between the P- velocity and impedance was derived at the well. The resulting correction factors were interpolated to the grid of the velocity file. After the application of the correction the new P impedance, S impedance and density were interpolated to every seismic grid-point. The seismic and well derived models were then merged for the frequencies between 2 and 6 Hz.

*Simultaneous AVA inversion*

The simultaneous angle-dependent seismic inversion method used is a generalized form of the

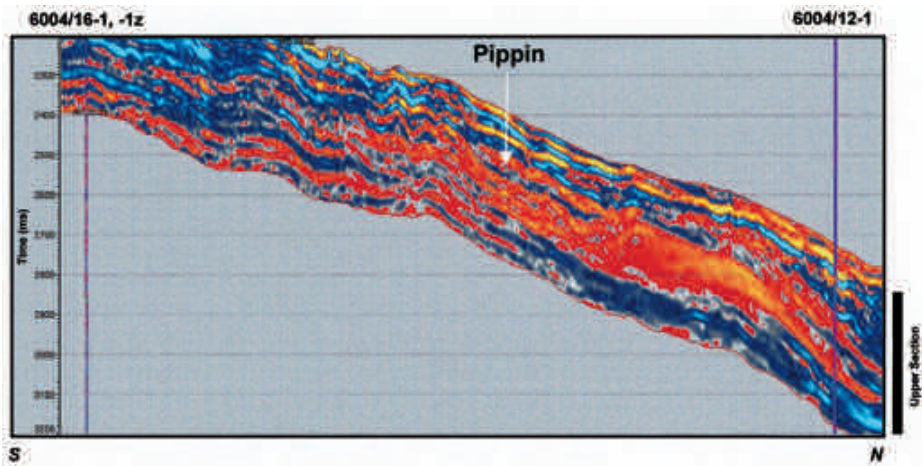


**Figure 13.** Illustrative section through the Upper Section sand indicator volume showing the Pippin prospect. Orange indicate sand prone areas. Blue indicates shale prone areas. Yellow indicates coal bearing sections outwith the calibrated interval.

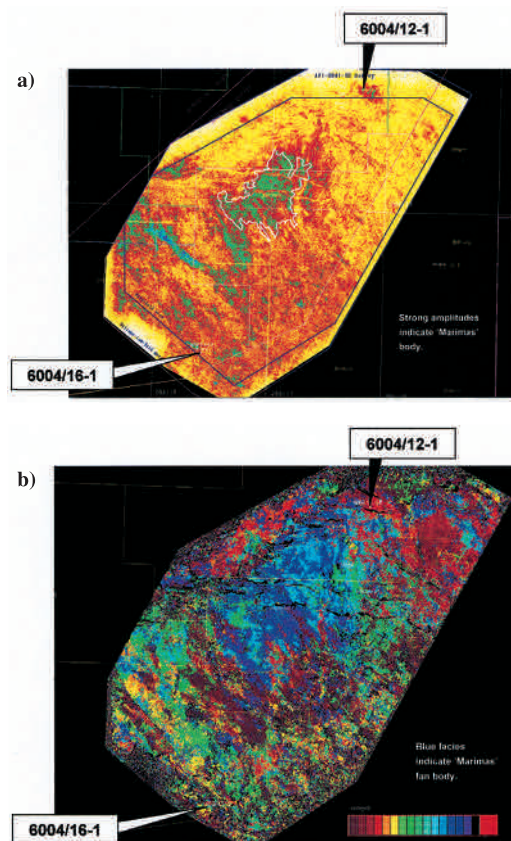


**Figure 14.** The outline of the Marimas prospect as defined by amplitude extractions (this example is taken from a 40 ms window below the seismic marker for the Marimas topsal) from the 3D seismic volume (a), and seismic waveform classification (Paradigm's Stratimagic software) (b).

sparse spike approach in which the objective is to solve for shear impedance and density in addition to acoustic impedance.

The input angle stack data were modelled in the constrained sparse spike algorithm by the simultaneous convolution of the angle dependent wavelets with the corresponding inverted reflection coefficient series. The low frequencies of the density, P and S impedances were constrained to the trend defined by the low frequency model.

The result from the inversion was considered to be good, with the match between the P and S impedance inversion volumes and the same quantities, calculated from well logs, being close (Figure 10). The match for the upper part of the section is better than for the lower part, particularly in the case of the S impedance volume.

The elastic impedance inversion produced three main volumes of data, P impedance, S impedance and Poisson's Ratio (Figure 10). Additionally further "lithology indicator" volumes were derived from these according to the results of the petro-acoustic analysis (cross-plotting) over specific intervals.

#### *Upper Section Sand Indicator volume*

For each point in the seismic volume, the AVA inversion yielded P and S impedance values. A "Sand Indicator" volume was calculated for the Upper Section only, from these pairs. During the petro-acoustic analysis phase, a trend line had been established on a cross-plot of P and S impedance values for the Upper Section that would separate sand from shale (Figure 11). The "Sand Indicator" value was calculated as the vertical distance (in terms of S impedance) of each pair from the separation line defined on the cross-plot.

Using the Upper Section sand indicator volume sand prone intervals could be distinguished very clearly from shale prone intervals. This separation allowed the Pippin prospect to be identified.

Additionally, using the P-sonic, S-sonic and density logs obtained from the fluid replacement modeling, the cross-plotting technique made it possible to highlight two areas in the cross-plot (Figure 11) where oil and gas bearing sandstones would plot. The sand indicator volume also contained regions where the values lay within the oil prone zone. This was significant as these sands, which lay above the regionally extensive Upper Lamba Formation shales, had not previously been considered prospective.

When it became available, the calibration to the 6004/16-1, -1z well confirmed that P and S impedance can effectively discriminate sand from shale in the Upper Section. A re-calculation of the sand indicator volume confirmed the presence of the Pippin prospect.

#### *Lower Section Sand Indicator volume*

After the 6004/16-1, 1z well became available another sand indicator volume was calculated to characterize Sand Units in the Lower Section in a similar manner as the upper section (Figure 12). Poisson's Ratio had been determined earlier (Figure 5) to be the best discriminator of sand and shale at the Marimas level and could be used to detect the

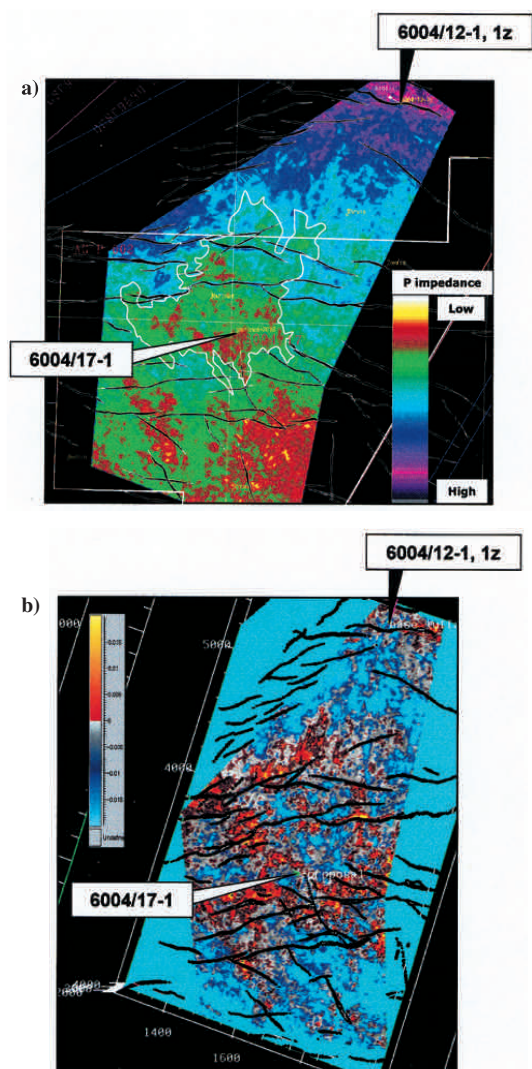


**Figure 15.** The Marimas prospect defined using extractions from P impedance (a) (Lower values – red - of P impedance are caused by increased sand /porosity /or HC charge) and Poisson's Ratio (b) inversion volumes (Lower values – grey and red – indicate best quality sands). The Marimas prospect is outlined in white.

“sweet spots” within the reservoir. The additional calibration provided by 6004/16-1 allowed another sand indicator volume, to be created to separate the Marimas sands from the overlying “topseal” shale and shale sequences beneath. Using a trend line derived from the cross-plot analysis (Figure 12) of Poisson's Ratio versus S impedance, calibrated to lithology at the wells, the sand indicator measure was taken as the distance of each Poisson/S Impedance pair from the line. The sand indicator volume

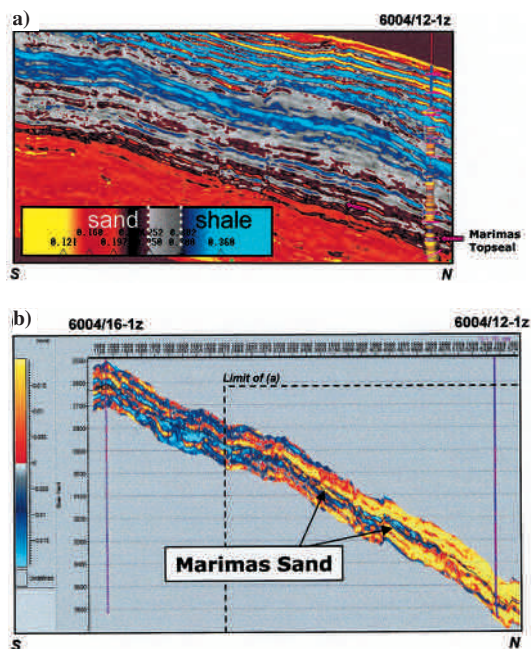


**Figure 16.** Illustrations of the continuity of the Marimas topscale unit. a) Poisson's Ratio used as a sand-shale indicator for the Marimas section on inline 1673 (single well control). The grey to blue colors indicates more shale prone sections. b) Lower Section sand indicator volume. Yellow=sand prone, blue/grey = shale prone.

was produced for an interval greater than that calibrated in the Lower Section. As a result this volume cannot be relied upon for lithology prediction outside the calibrated zone. The discrimination of the sand bodies is less efficient, compared to the Upper Section, but was used to highlight the main sandstone prone sequences and the main non-reservoir intervals (shales and tuffaceous sandstones).

A final note can be added about the detectability of the tuffaceous sandstones. The Sand Indicator model for the Lower Section, the Poisson's Ratio volume, and the P impedance volume are all efficient in identifying tuffaceous layers. These intervals have much higher Poisson's Ratio and P impedance compared to the non-tuffaceous sandstones (Figures 6 and 7).

## Interpretation

### Upper Section

During interpretation of the inversion volumes a new prospect was identified in the Upper Section using the Upper Section sand indicator volume (Figure 13). The Pippin prospect is interpreted as a Lower Balder/Upper Lamba sand-prone interval



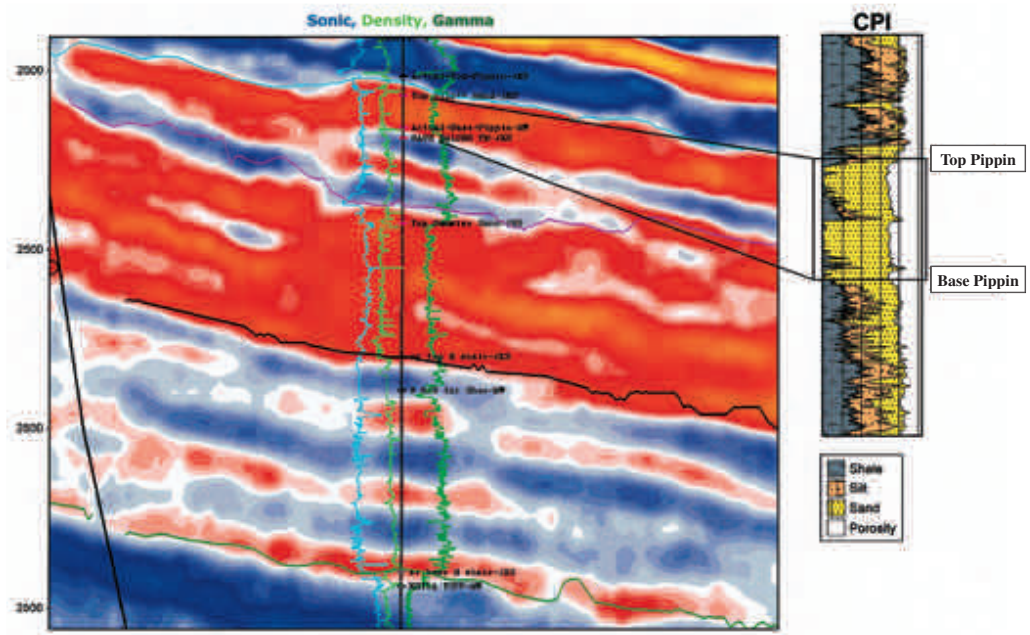


**Figure 17.** Results from the Pippin target interval. Log data are plotted ontop of the Upper Section sand indicator volume, with an expanded petrophysical interpretation posted on the right hand side. Orange = sands. Blue = shales.

deposited as a gravity flow unit in a pro-delta shelfal setting. The Pippin prospect sandstone interval pinches out to a zero edge to the south and south-east and is dip-closed to the north and west. It was noted that hydrocarbon shows have not been seen in the Lower Balder/Upper Lamba sands in either of the offset wells and therefore the main risk associated with the Pippin prospect was thought to be hydrocarbon migration. Some encouragement was seen in the sand indicator volume from the presence of values consistent with the modelled, oil bearing sandstones (Figure 11). The prospect was located above the Lamba regional downlap surface which was considered to be a regional seal. The prospect was, however, located immediately above the shallow extension of a set of east-west faults. These faults run perpendicular to the dip and provided a possible conduit for vertical migration of hydrocarbons into the sands of the Pippin prospect.

**Lower Section**

The Marimas prospect comprised a series of base of slope turbidites within the Upper Vaila Formation (Figure 3). Dip closure was present to the north and northwest, while closure to the south and east relied on pinch-out and facies change where the

base of slope fans onlap a more mud-prone slope. Top and base seals were prognosed to be laterally continuous shales, which are condensed basinal mudstones within a downlapping, prograding slope system. Seal represented the major risk for this prospect. Confidence in the presence of these shales was improved using the inversion volumes.

The Marimas prospect was defined using several measures. Lithological interpretation of the AFI2001 3D volume prior to drilling had been complicated by the apparent seismic polarity reversal at the target interval. Calibration with the VSP and synthetic seismograms post-well confirmed that the data are progressively phase rotated from the Balder interval downwards. Although this was taken into account during the inversion processing it has been a limiting factor in the geophysical interpretation. The Marimas body was nevertheless identified both as a discrete amplitude anomaly and as a distinctive body using seismic waveform classification (Figure 14). Further work using inverted seismic volumes allowed the Marimas prospect to be distinguished using P impedance (to delineate areas of improved porosity or hydrocarbon presence where P impedance is lower) and Poisson's Ratio (to define areas of better sand quality) (Figure 15). The 6004/17-1 well was located to test



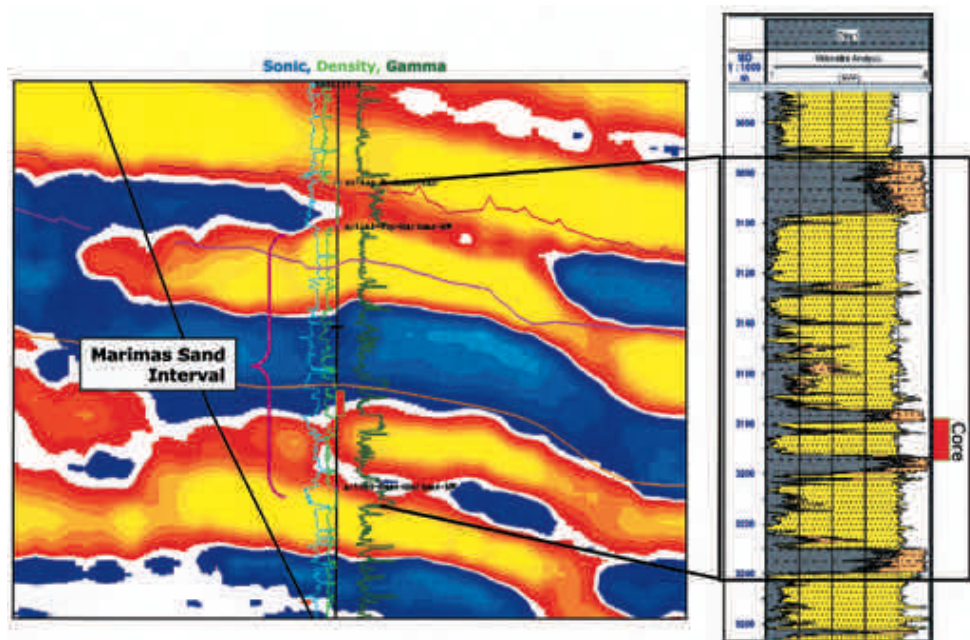


**Figure 18.** Results from the Marimas target interval. Log data are plotted on top of the Lower Section sand indicator volume, with an expanded petrophysical interpretation posted on the right hand side. Yellow = sands. Blue = shales.

both of these measures in an optimal location. The topseal to the Marimas prospect was believed to be provided by a shale horizon which was traced over the prospect using inverted seismic volumes (Figure 16). The top of the Marimas reservoir was defined using a combination of the Lower Section sand indicator, the conventional data and Poisson's Ratio volumes.

—The Marimas prospect sand (Sand Unit 5) was detected as a discrete geobody using P impedance (Figure 15). In the P impedance volume we see a high impedance sand at the 6004/17-1 well location which becomes lower in impedance moving to the south. The Poisson's Ratio, being a function of both P and S waves, is less likely to be affected by the depth/compaction trend. Within the Marimas sand, low values of Poisson's Ratio are interpreted as the better quality sands, possibly with hydrocarbon charge.

The seismic inversion volumes calibrated to 6004/12-1, -1z alone allowed mapping of the extent and the definition of the Marimas prospect away from the well. The second phase of inversion utilising well 6004/16-1, -1z confirmed that the main assumptions of the first phase were valid. Poisson's Ratio was determined to be the best discriminator of sand and shale at the Marimas level

(Figure 7) and could be used to detect the “sweet spots” within the reservoir.

The availability of the 6004/16-1, -1a well allowed a “sand indicator” volume to be produced for this portion of the section, based on Poisson's Ratio and S impedance. This indicator volume, compared to the use of the Poisson's Ratio alone, shows more sand prone units in the area of the 6004/12-1 well, while a strong increase of the shale content is predicted for the updip portions of the sequence, towards the 6004/16-1 well (Figure 16). The 6004/16-1 well information indicated that P impedance alone should not be used for lithology or fluid prediction at the Marimas level since a non-unique relationship was confirmed between P impedance and lithology (or fluid) characteristics.

## 6004/17-1 Well Results and Discussion

### The Upper Section - The Pippin Prospect

The results for the Upper Section were generally in agreement with the lithology prognosis over the calibration interval (Figure 17). The top of the Pippin target was encountered a little below the prognosed depth. The interval representing the Pippin target was judged to be some 37 m thick including 26 m of sand. The sands were of good quality with

a porosity of 29% and a net to gross ratio of 0.7. The target sands were thus successfully predicted as were the shale-prone sections above and below. The thicker sand interval predicted below the Pippin body was likewise successfully encountered.

Lithology predictions for Pippin using the sand indicator volume are good, resulting from the good match between inverted P and S impedances and the log data, and a clear separation of sandstone from shale in the cross-plotting analysis.

The gross prediction of sand and shale in the Upper Section was generally good but the thinner alternating units were not so accurately predicted. The distinction between sand and shale was oversimplified, leading to underestimation of intermediate lithologies (see discussion).

Significant coals were encountered above Pippin, which were not predicted because the relevant calibration section, of the 6004/12-1 well, for the Upper Section did not include coals from within the Balder Formation.

### **The Lower Section - The Marimas Prospect**

The predicted lithology for the Marimas target was sandstone with minor claystone interbeds. The well encountered an interval 134 m thick of which 95 m was sand giving a net to gross ratio of 0.71. The interval was more sand-prone in the upper part, becoming more clay-prone in the lower interval. The average sandstone porosity was 21%. The base of the interval was marked by a 10 m shale layer below which was an alternating series of thin sandstones and shales.

The shale above the Marimas target matched well to the “shalier” response on the Lower Section sand indicator volume (Figure 18). The upper part of the uppermost sand body was successfully predicted but the shale predicted below this was not encountered in the well. This is because the sand-shale indicator is less reliable over the lower half of the interval, a result of being outwith the calibrated interval. The P impedance volume (used with Poisson’s Ratio to predict the better sands) gave a fair correlation of low impedance zones with better sands, although corresponding prediction of thicker shales was not so good. The predicted topseal was encountered in the well although it is only 20 m thick. This is thinner than predicted from inversion volumes and sheds some light on the minimum thickness of shales that we can ex-

pect to detect using this technique in this area. The lateral extent of the topseal remains uncertain.

## **Discussion**

The results of the correlation of the inversion volume to the Upper Section containing the Pippin prospect highlight the fact that thick coal-bearing packages above the Pippin target were not predicted. This was due to the fact that the coal horizons (of the Balder formation) lay closer to the Pippin target in the Marimas well than in either offset well. As a result these coals were not included in the petro-acoustic analysis and the volume was not calibrated for them. Therefore in the upper part of the inversion volume (above the Pippin prospect), coals were not distinguished from very high quality sands. This was not the case in the Pippin prospect itself, where the high quality sands were correctly predicted.

There are a number of reasons for the less than perfect lithology prediction over the whole Marimas interval. One of these reasons is the fact that the petro-acoustic analysis for this interval was done on a limited dataset consisting of wells 6004/12-1, -1z and 6004/16-1, -1z. The interval lies at different depth in both wells and the cross-plot clusters for this interval overlap and are diffuse. Another, more significant, reason is the fact that the inversion volumes, particularly the Lower Section sand indicator volumes, were calibrated only for the interval containing the “topseal” shale and the sand immediately beneath (Sand Unit 5). There seems to be a much greater risk of erroneous lithology predictions if volumes of this type are used outside the calibrated intervals.

In general the volumes of elastic properties (P impedance, S impedance and Poisson’s Ratio) are valid for the whole volume but their lithological significance can vary with facies and depth. The lithological interpretation of these volumes needs to be carefully related to calibrated intervals in nearby wells.

The drive to distinguish sandstone from shale, and to define any sealing intervals, led to an oversimplified lithology prediction, especially in the Upper Section where clear sand-shale boundaries had been seen in the 6004/12-1 well. Because of these clear boundaries, the colour scales of the sand indicator volume seismic displays were optimised to highlight the difference between sand and

shale, with a sharp division between “sand prone” and “shale prone” zones. In reality the gradation between intermediate lithologies are important for trap definition and grade between reservoir and seal and the colour scaling should have allowed recognition of these too. Intermediate (mixed or siltstone prone) lithologies were underestimated in our prognosis.

One effect of this is that the boundaries of the potential “trap” are less well defined than predicted. In future work it would be useful to “quantify” the volume in terms of effective reservoir and particularly the sealing facies to help define traps.

Some of the thinner alternating sand/shale intervals encountered are likely to be below vertical resolution of the original seismic, and hence the inversion method, although the 20 m shale above the Marimas prospect was detected.

## Conclusions

Defining the limits of stratigraphic bodies in this area was always difficult since they were interpreted from seismic attribute anomalies and seismic facies patterns rather than a clear geometric pinch-out, which are easier to map. Nevertheless the main prospect, Marimas, lay within an interval, bounded by shales, that was seen to pinch-out between the downdip well, 6004/12-1, and the updip well, 6004/16-1.

The Marimas play definition was driven by this concept, although it was supported by apparently good geological and geophysical evidence. Prospect definition relied on the results of seismic inversion. In the Upper Section the elastic impedance properties were used to generate the Pippin prospect. This had not been previously recognised on the migrated seismic data (it sits in a stratigraphic interval immediately below the high impedance upper Balder Formation), despite the strong lithology contrasts present in the offset well data. The lithology prediction of seal-reservoir-seal packages was largely proven for Pippin and Marimas at the 6004/17-1 well location, although with limitations due to the vertical resolution and inversion scaling issues described previously. The 6004/17-1 well results prove that despite the limitations described above; the technique is valid for lithology prediction within calibrated intervals, even with a limited well database.

## Acknowledgements

The authors would like to thank Eni and Faroe Petroleum for supporting publication of this work. Many of our colleagues in Aberdeen and Milan have contributed to this project in recent years. Their contributions are all greatly appreciated. BP and Amerada Hess are thanked for permission to use and present data from the traded wells 6004/12-1, 1z and 6004/16-1, -1z respectively. Jason Geosystems carried out the seismic inversion processing and provided several useful suggestions regarding the generation of lithology indicator volumes. Drafting of the figures was carried out by Grant P. Fuller. Reviews by John Smallwood and Thomas B. Espersen have hopefully resulted in an improved version of this manuscript.

## References

- Aki, K. and Richards P.G. 1980. Quantitative Seismology: Theory and methods: W.G. Freeman and Co.
- Anderson, J.W., and Bogaards, M.A. 2000. Quantifying fluid prediction using angle-dependent inversion measured against log fluid substitutions. In: *Society of Exploration Geophysicists annual meeting (Calgary) technical program expanded abstracts*.
- Castagna, J.P. 1993. Petrophysical imaging using AVO. *The Leading Edge* 12(3): 172-178.
- Gassmann, F. 1951. Elasticity of porous media: Über die Elastizität poröser Medien. *Vierteljahrsschrift der Naturforschenden Gesellschaft in Zurich* 96: 1-23.
- Hampson, D. 1991. AVO inversion, theory and practice. *The Leading Edge* 10: 39-42.
- Lamers, E. and Carmichael, S.M.M. 1999. The Paleocene deepwater sandstone play West of Shetland. In: Fleet, A.J. and Boldy, S.A.R. (eds.) *Petroleum Geology of Northwest Europe: Proceedings of the 5<sup>th</sup> Conference*. Geological Society, London: 645-659.
- Ostrander, W. 1984. Plane-wave reflection coefficients for gas sands at non-normal angles of incidence. *Geophysics* 49: 1637-1648.
- Pendrel, J. and Van Riel, P. 1997. Methodology for Seismic Inversion and Modelling: a Western Canadian reef example. *CSEG Recorder* 12.5: 5-15.
- Poulsen, R., Ellis, D., Callagher, J.W., Lundstrøm, R. and Dromgoole, P. 2004. Paleocene development of the Faroes area. *Faroe Islands Exploration Conference 2004*, Abstract.
- Rutherford, S.R. and Williams, R.H. 1989. Amplitude-versus-offset variations in gas sands. *Geophysics* 54: 680-688.
- Smallwood, J.R., Prescott, D. and Kirk, W.J. 2004. Alternatives in Paleocene exploration West of Shetland: A case study. In press for November 2004, *Scottish Journal of Geology*.

# Lithology Prediction from Velocity Data: Paleocene Sediments in the Faroe-Shetland Area

JOHN R. SMALLWOOD

Amerada Hess Ltd., 33 Grosvenor Place, London, SW1X 7HY, UK.  
E-mail: john.smallwood@hess.com; Tel: +44 (0) 207 887 2793

## Abstract

At a position within a basin where the sonic velocity of sandstone and shale is expected to differ, a velocity measurement can be used to predict the lithology. Velocity data from the Paleocene basins between the Faroe Islands and the Shetland Isles are used to illustrate such a method of lithology prediction. Fitting of compiled well-log sonic velocity and density data with an exponential compaction model has established depth trends for these properties for sandstones and for shales. A regional velocity model has then been used together with picked horizons for the top and base of the Paleocene interval to predict sand net-to-gross ratio, porosity and density throughout each of the basins. A dominance of sandstone in the deeper and more distal parts of the Paleocene basins causes sonic velocities to be higher than on the basin margins where the Paleocene deep-water sediments are, on average, finer-grained. The lithology models produced from velocity data can be used to assess relative risks of reservoir presence and seal effectiveness throughout the area. Numerical integration of the three-dimensional N:G, density and porosity parameter fields can also be used to yield total volume and mass estimates of sediment within the basin.

## Introduction

Deep-water elastic sediments of Paleocene age have been an appealing target for hydrocarbon exploration since the discovery of the Foinaven field in the UK West of Shetlands area in 1992 (Fig. 1; Cooper *et al.*, 1999). Wells to date on acreage obtained in the 1<sup>st</sup> Faroes Licensing Round have been drilled to test reservoirs of Paleocene age (Smallwood and Kirk, in press). Lamers and Carmichael (1999) described the principal challenge for Paleocene exploration in the area as the development of effective reservoir sandstones, as several UK wells targeting Paleocene reservoirs failed to encounter good sands at key levels (e.g. Smallwood *et al.*, 2004). However, the wells drilled in the Faroes Sector to date have encountered large quantities of sand within the Paleocene and the challenge of predicting the areal distribution and

vertical extent of shale-prone intervals is therefore also crucial for hydrocarbon exploration. In this paper, a method of using velocity data to model a laterally and vertically varying sand net-to-gross (N:G) ratio throughout a sedimentary basin is presented and applied to the Faroe-Shetland area. The output model includes density and porosity models, in addition to the N:G model, so that sediment mass and volume estimates can also be made. The mass or solid volume of sediment in the basin is of interest for studies seeking to link the denudation from paleo-onshore areas with deposition in surrounding basins (e.g. Jones *et al.*, 2002).

Firstly, wireline log data is compiled from wells drilled in the area to establish depth trends in sonic velocity and density for sands and for shales. Since the sonic velocity of sand and shales differs throughout the depth range, these well-log velocities can be exploited to estimate sand N:G in areas



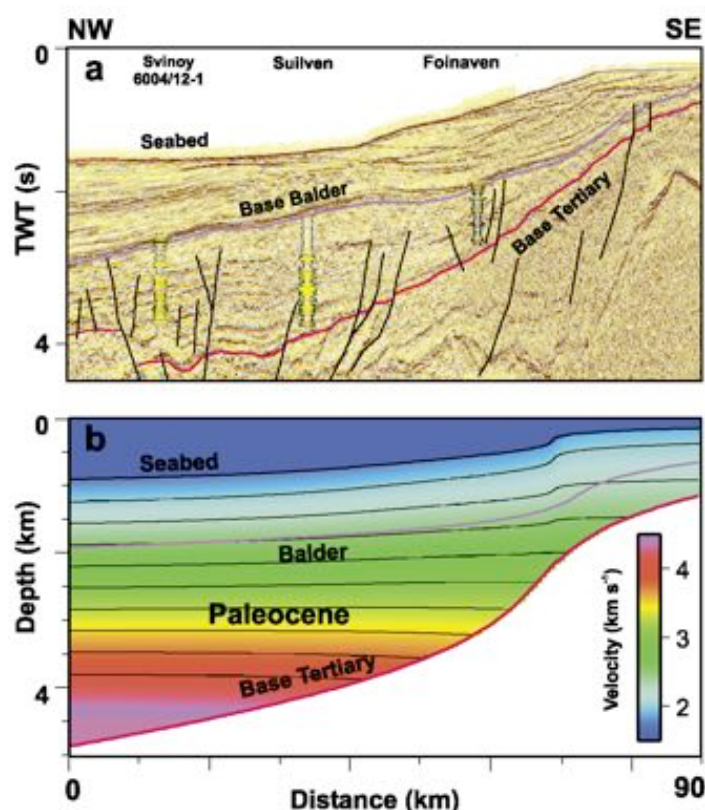


**Figure 1.** (a) Semi-regional NW-SE seismic line (location indicated in Fig. 3a). The two-way time (TWT) interval between the 'Base Balder' seismic reflector (purple) and the 'Base Tertiary' seismic reflector (maroon), taken here to bracket rocks of Paleocene age, thickens into the deeper water areas. Representative well sticks from Hollingsworth (2002) show the increase in sand (yellow) proportion basinward. (b) Regional velocity model for a schematic transect similar to a), based on a compilation of check-shot data (Smallwood, 2002).

away from wells if the average velocity is known by another means. To illustrate the technique a regional velocity model developed from check-shot velocities from a second set of wells has been used. The regional model velocity field for the area is also used to depth convert the surfaces bounding the interval of interest, this case the Top Balder and the Base Tertiary seismic horizons. This interval of interest is then divided into several sub-intervals of equal thickness, in this case seven intermediate surfaces being calculated, to dissect the Paleocene interval into eight layers. For each of the eight depth layers, the areally-varying proportion of sand to shale has been estimated using the well-log based model, which also allows prediction of the porosity of sand and shale fractions.

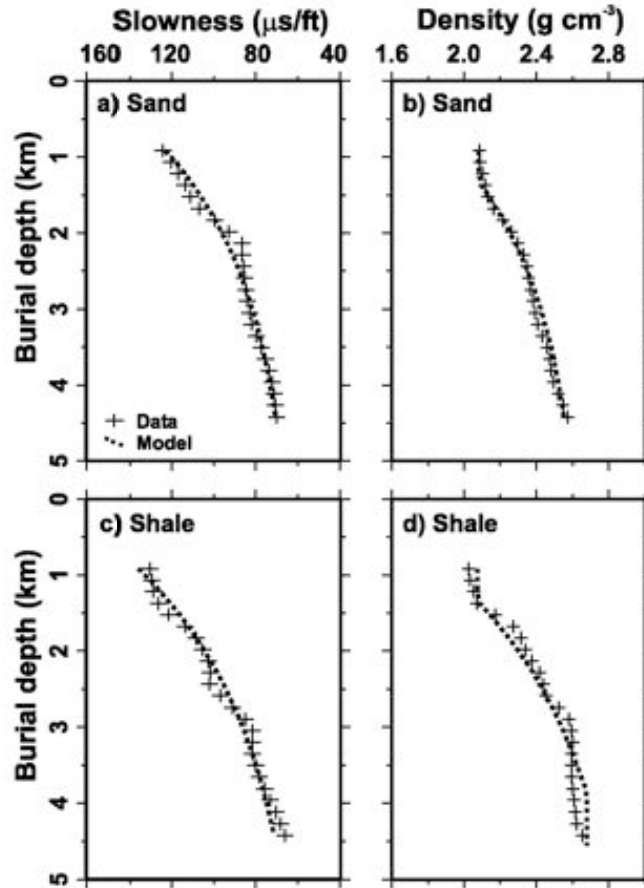
### Well log data depth trends

To describe the variation in physical properties of the Paleocene sediments with depth, a compilation was made of wireline well log data from sands and shales penetrated at a variety of depths within the

basin. Intervals of 'end-member' clean sand and clay-rich shale from which to compile the selected log data were selected using a suite of wireline logs, particularly the Gamma Ray natural radioactivity log, which is often a good sand-shale discriminator in deep-water clastic sediments. Variation in rock properties with depth has implications for many aspects of a basin's hydrocarbon system, including the reservoir quality of sands (e.g. Sullivan *et al.*, 1999), the seal capacity of shales and the seismic response of sand-shale interfaces (Hendrickson, 1999; Smallwood and Kirk, in press).

A smoothed running average of the sand wireline sonic velocity data from twelve wells is shown in Figure 2 (one standard deviation range bars on the data trends are shown in Figures 11 and 14 of Smallwood and Kirk, in press). The trend of the sonic velocity of the Paleocene sands is to increase with depth below the sea floor, a trend shared by the sonic velocity of shales and also the density of both sands and shales (Fig. 2). While several other effects such as constituent mineralogy, overpressure and sedimentological maturity affect the depth trends, the primary increase in sonic veloc-

**Figure 2.** Average wireline well-log data from 12 wells in the area (crosses) and best curve (Equations 1-3) fitted simultaneously to sonic velocity and density data for both sand and shale (dashed lines). Parameters for fitted curves given in Table 1. (a) Sonic velocity for sands. (b) Density for sands. For mass estimation the density has been limited to a value equivalent to 35% porosity. (c) Sonic velocity for shales. (d) Density for shales. For mass estimation the density has been limited to lie between a value equivalent to 45% porosity and  $2.67 \text{ g cm}^{-3}$ .



ity and density with depth observed in the data is caused as vertical effective stress increases and porosity is lost through compaction (e.g. Sclater and Christie, 1980). The compaction trends must be described in order to obtain estimates of sand N:G from velocity measurements made across a range of depths.

Regional uplift could cause rock properties to depart from normal compaction curves, and rock sonic velocities have been used elsewhere to estimate the extent of uplift and erosion (e.g. Japsen, 1993). Areas elevated during transient uplift events may also have anomalously high sonic velocities, due to increased vertical effective stress during initial subaerial exposure, porosity reduction from increased horizontal stress, or local diagenetic effects. However, much of the Faroe-Shetland area was still submarine at the zenith of the regional uplift (Jones and White, 2003), and so compaction trends would not have been greatly perturbed. Furthermore, rapid collapse of the regional uplift, attributed to the confinement of anomalously hot

asthenospheric mantle to the nascent continental rift west of the Faroe Islands, restored deep-water marine conditions to the centre of the basin in the Early Eocene (Smallwood and Gill, 2002). Apart from a few localised areas which have experienced subsequent uplift and erosion (Smallwood, 2004), Paleocene rocks are currently positioned at their maximum burial depth, and so are expected to have compaction trends only weakly affected by the uplift.

The averaged well log data for sands and shales have been fitted with best-fit curves (Figure 2). The sand sonic velocity and density curves were fitted simultaneously with a model based on an exponential decay of a porosity-type parameter,  $\Phi$ , with depth,

$$\Phi^{md} = \Phi_0^{md} e^{-\lambda^{md} z} \quad (\text{Equation 1})$$

where  $\Phi_0$  is the value of the parameter at the sea floor,  $z$  is depth below the sea floor and  $\lambda$  is a decay-type constant describing the rate at which the



porosity-type parameter decreases with increasing depth. The sonic velocity was then modelled as a function of  $\Phi$ , using the time-average equation (Wyllie *et al.*, 1956),

$$dt^{snd} = \Phi^{snd} dt_{\Phi} + (1 - \Phi^{snd}) dt_m^{snd} \quad (\text{Equation 2})$$

where  $dt$  is sonic slowness (the inverse of velocity), and  $dt_m$  and  $dt_{\Phi}$  refer to slowness values of matrix (grains) and porosity fill (water). The sand density,  $\rho^{snd}$ , was modelled with the standard description of a two phase material,

$$\rho^{snd} = \Phi^{snd} \rho_{\Phi} + (1 - \Phi^{snd}) \rho_m^{snd} \quad (\text{Equation 3})$$

using the same decay function for  $\Phi$  as the sonic velocity model. Least-squares fitting with equal weighting given to density and sonic velocity, and simultaneous inversion for the four constant parameters  $\Phi_0$ ,  $\lambda$ ,  $dt_m$  and  $\rho_m$  using a generalised reduced gradient algorithm, gave a more physically robust description of the depth trends than determination of the parameters in isolation. An equivalent determination of four model parameters was made for the shale data points. Values for the constants for this dataset are shown in Table 1.

	$\Phi_0$ (fraction)	$\lambda$ (ft <sup>-1</sup> )	$\rho_m$ (g cm <sup>-3</sup> )	$dt_m$ ( $\mu$ s ft <sup>-1</sup> )
Sand	0.706	$1.6 \times 10^{-4}$	2.67	60.9
Shale	0.827	$1.38 \times 10^{-4}$	2.96	54.7

**Table 1** Parameters for fit to wireline well-log data

It should be noted that the porosity-type parameter is not physically meaningful at shallower depths than those from which the sonic and density data provide constraints. Although alternative empirical functions which describe the data could have been applied, exponential porosity decay and time/density averages were selected since they allowed a simple, simultaneous modelling of sonic velocity and density data, a minimum number of parameters, use of established functions and an approximate estimate of porosity to be made. This model is not intended to imply a particular mechanical compaction behaviour mechanism (e.g. Goult, 2004), but simply to provide a mathematical description of the changes in physical properties with depth.

## Regional velocity model

A regional velocity model was built to use in conjunction with the well log-based trend models to estimate sand distribution across the area. Regional two-way time maps of the 'Base Balder' (purple) and 'Base Tertiary' (maroon) seismic horizons (Figs 1 and 3) were depth converted using functions based on compilation of check-shot data from 17 wells (Fig. 1b; Smallwood, 2002). The basalt lava pile was taken into account during the depth conversion of the 'Base Tertiary' seismic horizon (Fig. 4), using a depth conversion velocity of 4.5 km s<sup>-1</sup>, as measured in well 164/7-1, in which over 1 km of basaltic lavas were penetrated.

These mapped surfaces, interpreted to bracket rocks of Paleocene age, bounded a depth interval that was subdivided into eight layers of equal thickness. An areally-varying parameter with dimensions of velocity was allocated to the mid-point depth of each of the eight depth slices using the water-depth dependent velocity function described in Smallwood (2002). This function describes the instantaneous seismic depth-conversion velocity  $V$  (the tangent to a seismic time-depth curve) as a linear increase in seismic velocity with depth,

$$V = V_0 + K \cdot z \quad (\text{Equation 4})$$

where  $z$  is again depth below the sea floor,  $V_0$  is a parameter representing seismic velocity at the sea floor and  $K$  is the gradient term describing rate of increase of velocity with depth (Slotnick, 1936). Equation 4 integrates to give the time-depth function

$$z = h + \frac{V_0}{K} (e^{Kt} - 1) \quad (\text{Equation 5})$$

where  $h$  is water depth and  $t$  is one-way time to the target at depth  $z$ . In a study using seismic check-shots from seventeen West of Shetland and Faroes wells (Smallwood, 2002), both  $V_0$  and  $K$  were argued to be usefully modelled as linear functions of water depth:

$$V_0 = a \cdot h + b \quad (\text{Equation 6})$$

and

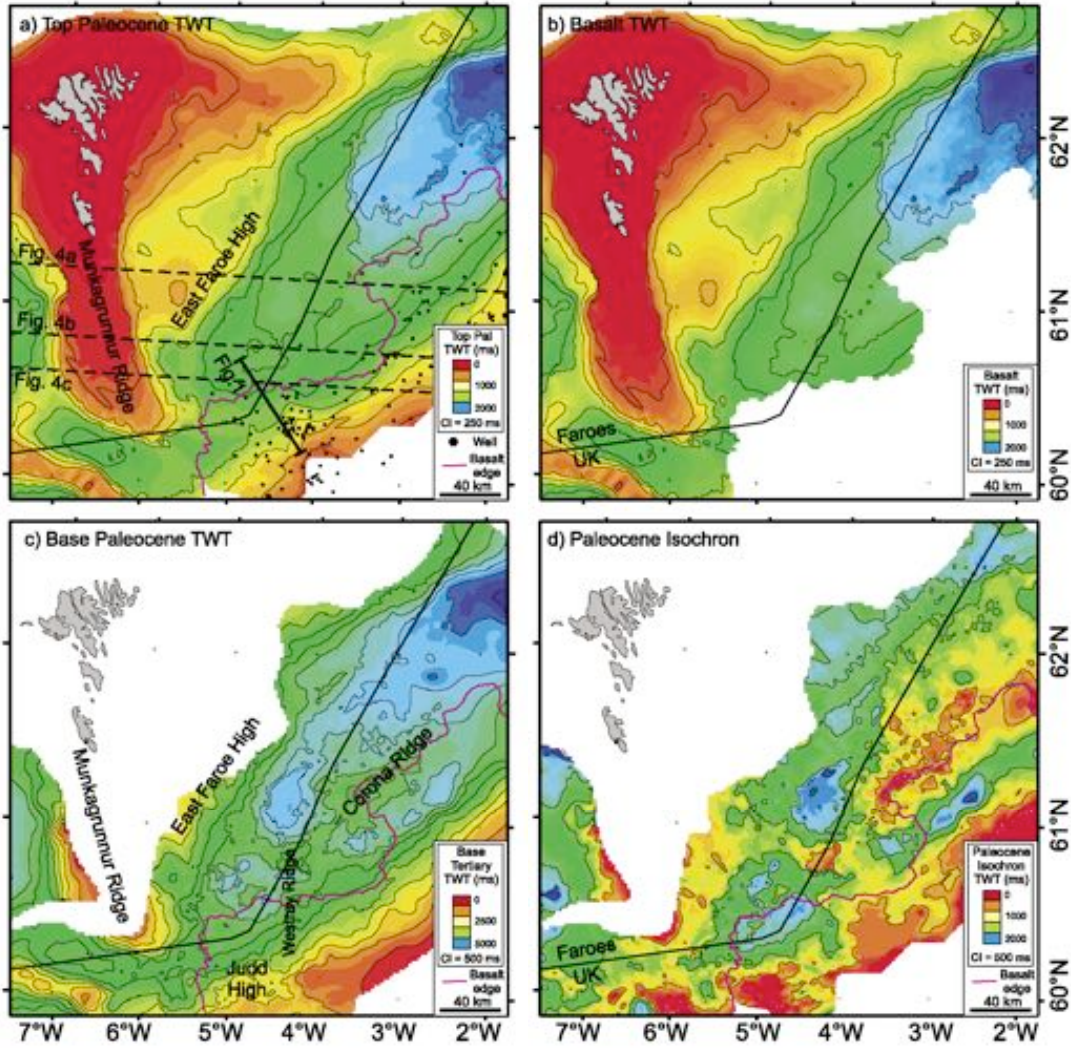


**Figure 3.** (a) Two-way time (TWT) map of 'Top Paleocene' seismic reflection (composite of 'Base Balder', 'Top Basalt' and 'Seabed' seismic reflections; see Fig. 4). The main trough running NE-SW reflects the Cenozoic post-rift thermal subsidence of the basin. Much of the UK sector is beyond the eastern extent of the basalt lava (pink line). Locations of Figs 1 & 4 shown. (b) TWT map of 'Top Basalt' seismic reflection, modified after White *et al.* (2003). (c) TWT map of 'Base Tertiary' seismic reflection, taken to show the lower surface of the Paleocene age rocks in this study. Structural highs marked. (d) Isochron map, showing thickness between maps shown in (b) and (c). Isochronochore thicks define the Paleocene basins.

$$K = c \cdot h + d \quad (\text{Equation 7})$$

where a, b, c, and d are constants. Equations 5-7 combine to give the depth-time relationship

$$z = h + \frac{(ah+b)}{(ch+d)} (e^{(ch+d)t} - 1) \quad (\text{Equation 8}).$$

For this study, values used were  $a = -0.21 \text{ s}^{-1}$ ,  $b = 1.921 \text{ km s}^{-1}$ ,  $c = 0.4228 \text{ km}^{-1} \text{ s}^{-1}$ ,  $d = 0.3972 \text{ s}^{-1}$ . To

avoid extrapolation beyond the water depth range on which the relationships were established,  $V_0$  was limited to a minimum of  $1.711 \text{ km s}^{-1}$  and  $K$  to a maximum of  $0.82 \text{ s}^{-1}$ . This check-shot based regional velocity model was then converted to slowness, and was multiplied by a constant value of 1.1 following comparison of wireline log and check-shot survey rock velocities in the area. Example curves showing variation of sonic slowness with depth in different water depths are shown in Figure



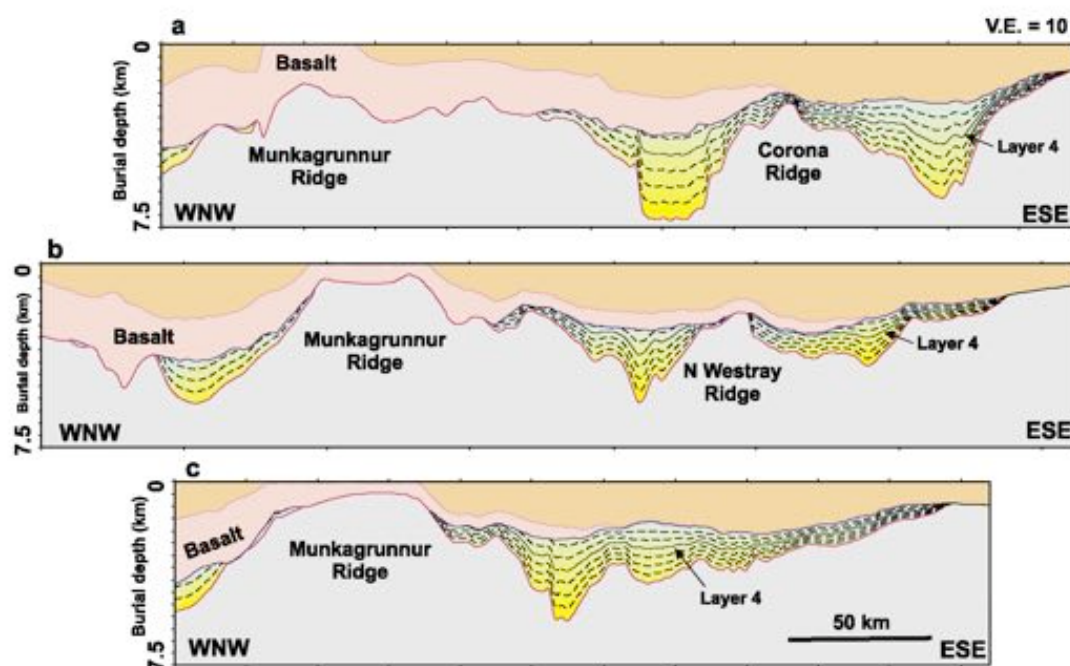


**Figure 4.** Cross-sections through the depth model (faults omitted). Depth conversion was made using functions described in Smallwood (2002) outside the basalt and  $4.5 \text{ km s}^{-1}$  within the basalt lava pile. Line locations shown in Fig. 3a. Main structural highs named. The Top and Base Basalt surfaces and Top and Base Paleocene surfaces are shown as solid lines. The Paleocene sedimentary interval is subdivided into up to eight layers of equal thickness (dashed lines). The dotted line indicates Layer 4, from which some parameters are illustrated in Figs 6 & 7. The basalt generally thickens to the north and west.

5, and velocity on Layer 4 of the model (Fig. 4) is shown in map form in Figure 6.

While the approach described here gives a simple well-based regional velocity model, as an alternative more data-driven approach, seismic stacking velocities could be used to build the regional velocity model. The function-based approach described here is used deliberately, as much to illustrate the method as to provide accurate predictions in areas a long way from well control.

### Modelling sand distribution

The wireline log trends were combined with the regional velocity model to estimate sand and shale distribution across the basin. Figure 5 illustrates the relationship between sand and shale wireline log-based slowness trends and the slownesses in the regional velocity model at three points with different water depths. All three trends show a decrease in sonic slowness (an increase in sonic velocity) with depth. In Paleocene basin margin and slope settings (broadly located in areas with

smaller present-day water depths), the regional velocity model shows a smaller rate of increase with depth than either the sand or shale end member curves (Fig. 5a). This is interpreted to correspond to a decrease in the sand to shale ratio with depth, i.e. a decrease in sand net-to-gross (N:G) ratio, as observed in wells such as 205/8-1 (fig. 4 of Smallwood *et al.*, 2004). In more distal positions in the Paleocene basin (mostly located in areas of larger present-day water depth), the regional velocity model shows overall higher velocities, and a higher rate of increase with depth than either sand or shale end member curves (Figure 5c). This is interpreted to correspond to overall sandier lithologies, and an increase in N:G ratio with depth, as observed in wells such as 205/9-1 (fig. 4 of Smallwood *et al.*, 2004). As noted above, deep-water Faroes' wells 6004/16-1Z and 6004/12-1 encountered higher proportions of sand within the Paleocene interval than most West of Shetlands wells in shallower water. The increase in the velocities of the sand and shale trends from shallow to deep point examples in Figure 5 shows how the modelling process

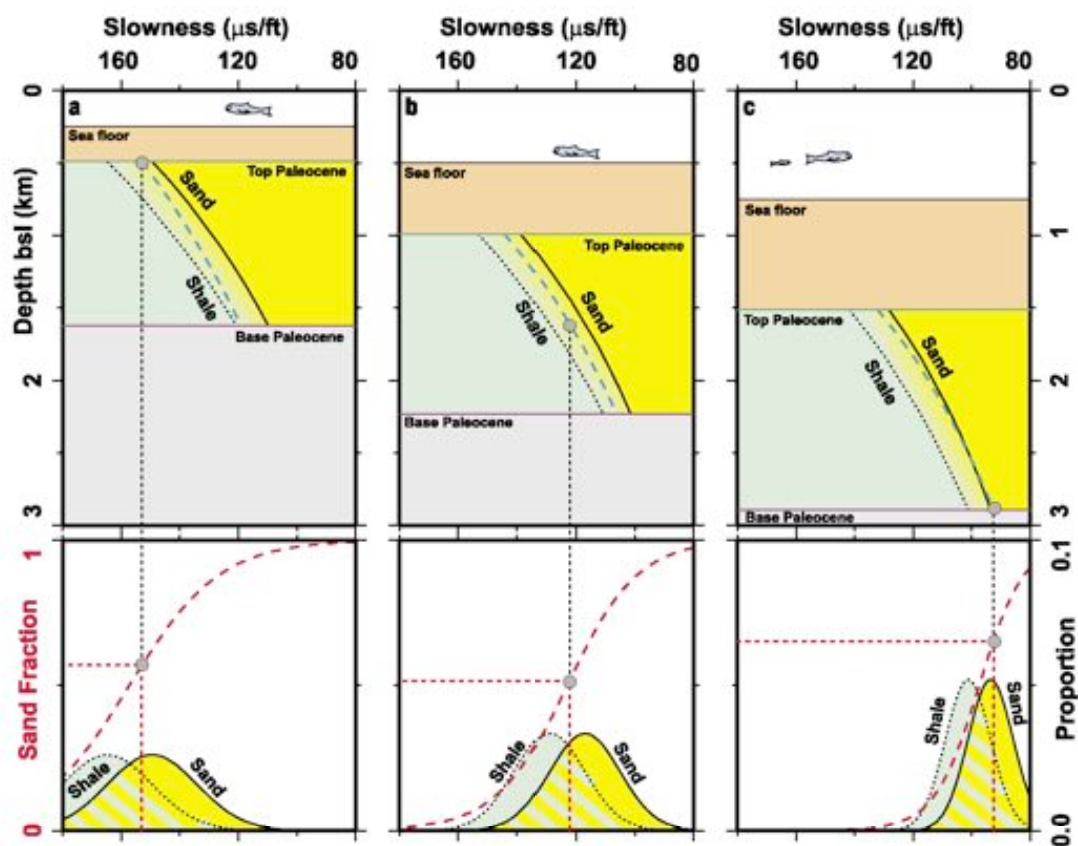


**Figure 5.** Upper panels: Three examples of well-based sand (solid) and shale (dotted) depth trends in sonic velocity data (from Fig. 2) and the regional velocity model (dashed blue line). Lower panels: The model velocity is converted to a sand fraction (Net:Gross) estimate using its position between expected sand and shale slownesses at that depth. The sand and shale slowness probability distribution functions are represented by normal distributions (solid and dotted lines) with means from the mean predicted curves (which decrease with depth; Fig. 2) and standard deviations of the difference between the sand and shale slownesses (which also decrease with depth). The sand fraction is taken from the ratio of probability of sand to shale slowness (dashed red lines). (a) 0.25 km water depth, 0.25 s two-way time (TWT) to Top Paleocene, 1 s TWT to Base Paleocene. Model suggests sand fraction of 0.57 at Top Paleocene (grey circles). (b) 0.5 km water depth, 0.5 s TWT to Top Paleocene, 1 s TWT to Base Paleocene. Model suggests sand fraction of 0.51 at mid-Paleocene (grey circles). (c) 0.75 km water depth, 0.75 s TWT to Top Paleocene, 1 s TWT to Base Paleocene. Model suggests sand fraction of 0.65 at Base Paleocene (grey circles).

includes the compactional velocity effects of the differing overburdens across the basin to allow the lithological effects to be isolated.

The regional 'velocity' model was used to estimate N:G across the area by assuming that the Paleocene interval could be approximated with a bimodal sand-shale system. This assumption is necessary for the technique described here to proceed, but unfortunately glosses over a more complicated reality of lithological variation including marls, tuffs and igneous intrusives as well as ignoring lateral and vertical mineralogical variation other than that captured in the averaging behind the wireline log and regional velocity model. Limi-

tations arising from this assumption are discussed further below.

The velocity-type parameter at each point on each of the eight stacked depth layers was converted to a sand N:G value for that point by assuming that the velocity in the regional model could be decomposed into contributions from a varying proportion of sand and shale with their characteristic sonic velocities at the relevant depth (Figs 5 and 6). Rather than using a linear combination of sand and shale sonic velocities to match each model velocity, a statistical approach was taken in order to allow extrapolation of values outside the well-log model average values for sand and shale. For each



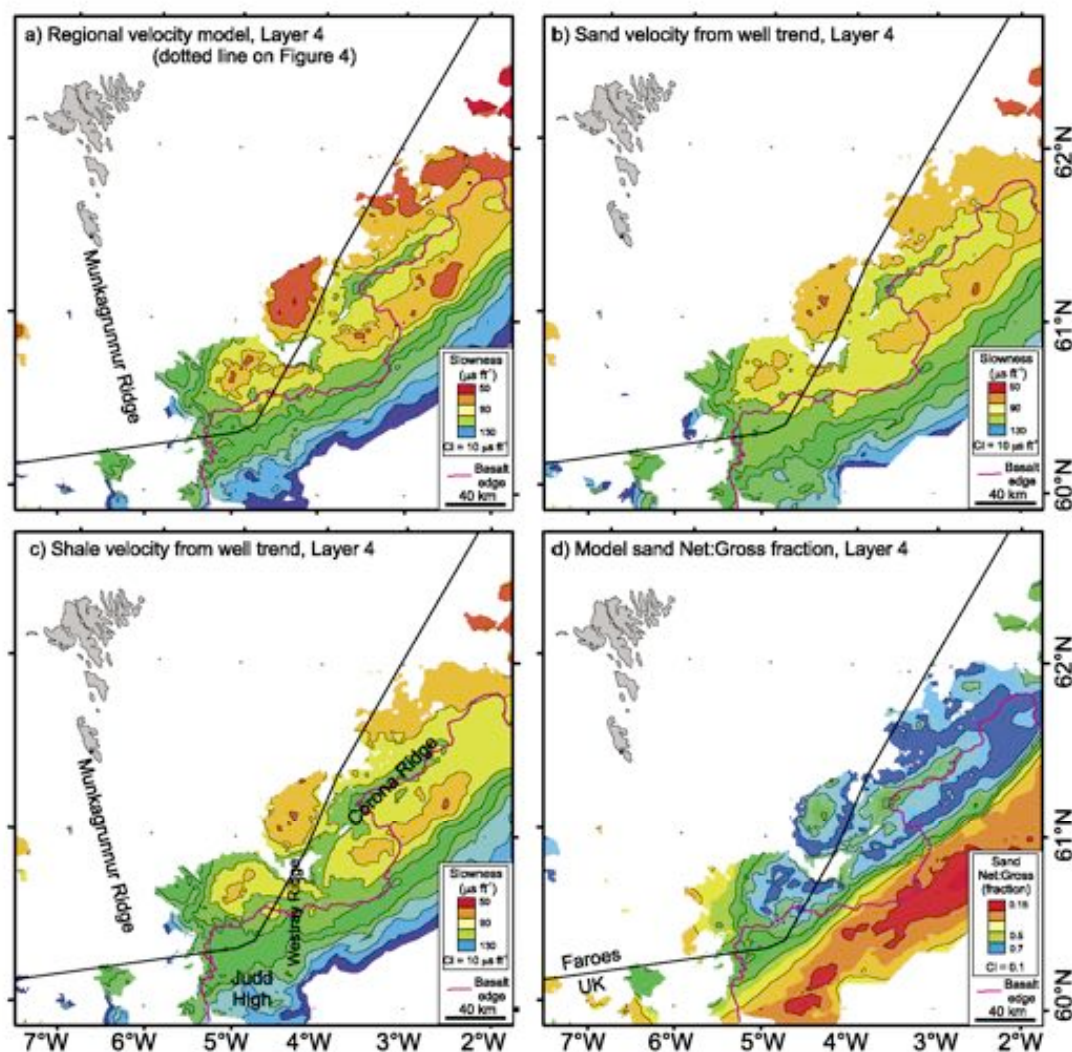


**Figure 6.** Illustrative maps from the fourth layer of the eight-layer Paleocene model. The data does not extend over the full area of the Paleocene basins (Fig. 3c) as the layer is truncated against the basalt (Fig. 4). (a) Slowness from the regional velocity model. (b) Mean model sand velocity from well data. (c) Mean model shale velocity from well data. (d) Model sand fraction (N:G) using velocities in (a)-(c) and method illustrated in Fig. 5. Note that at greater depths the sonic velocity cannot be used to distinguish sand and shale and the algorithm is designed to bring the N:G towards a value of 0.5 (see Fig. 7a for areas where this is relevant).

point a normal probability distribution function of well-log sand and shale sonic velocities was assumed, with a mean of the (average) value and a standard deviation equal to the difference between the sand and shale predicted velocities at that point (bell-curves, Fig. 5, lower panels). The sand N:G was then calculated as the linear ratio of the value of the sand and shale velocity distribution functions at that point (Red dashed curves, Fig. 5 lower panels).

The choice of standard deviations in the sonic velocity distribution for sand and shale to be equal and also to be equal to the difference between the predicted sand and shale sonic velocities at a particular point gives stable sand N:G prediction both where the average velocity is between that of 'pure' average sand and 'pure' average shale and outside that range. At burial depths greater than about 3.75 km though, generally areas of the Paleocene basins below present-day deep water areas,

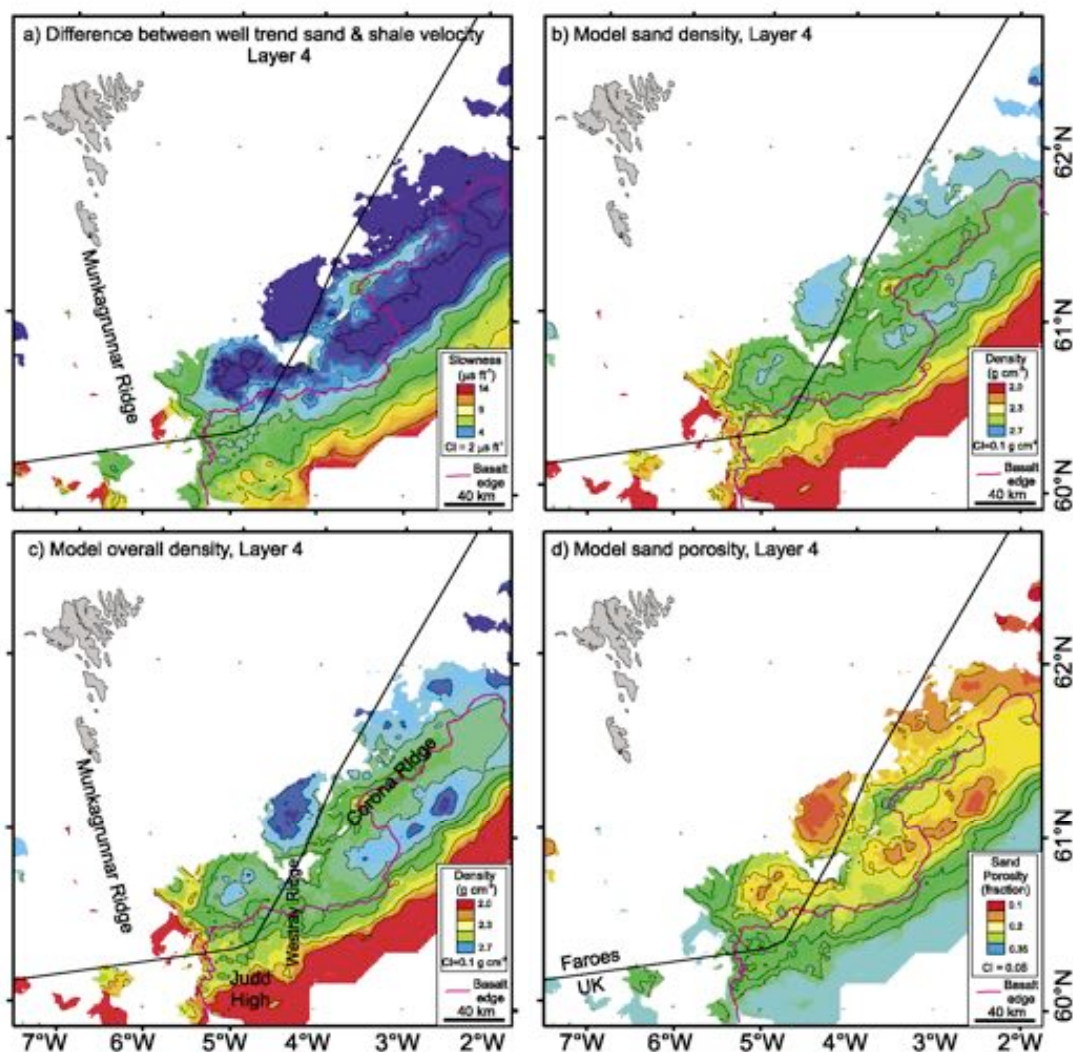


**Figure 7.** Illustrative maps from the fourth layer of the eight-layer Paleocene model. a) Difference between sand and shale model velocities (Fig. 6b & 6c). Where this difference is less than  $4 \mu\text{s ft}^{-1}$ , which occurs at large burial depths, the sonic velocity cannot be used to distinguish sand and shale and the algorithm is designed to bring the N:G towards a value of 0.5 (see Fig. 6d). b) Model sand bulk density. c) Model overall bulk density (shale fraction included). d) Model porosity in the sand fraction.

the wireline data predicts a difference between sand and shale sonic velocities less than  $4 \mu\text{s ft}^{-1}$ , so that the sonic (or seismic) velocity is not a good discriminator between sand and shale. In such intervals the standard deviation was set to a minimum value of  $4 \mu\text{s ft}^{-1}$ , which is consistent with the observed range of well data points (Fig. 7a; Smallwood and Kirk, in press). The effect of imposing this minimum standard deviation to the well-log trends together with a value from the regional velocity model often outside the sand-shale velocity

range is that the N:G tends towards 50%, which here is effectively recognising the lack of discrimination in the velocities. For hydrocarbon exploration this limitation in prediction is not of primary importance, at least for reservoir prediction, as it occurs where porosity is down at a few percent and at water depths and 'target' depths unlikely to be penetrated by drilling in the foreseeable future.

A final step in the production of a N:G model of the basin is the removal of the interval where basalt rather than clastic sediment is interpreted to



be present. The upper surface of the Faroes basalt is easy to interpret on seismic data. The base of the basalt has been mapped using a combination of pre-stack depth migrated wide angle seismic data, well penetrations, potential field modelling and conventional interpretation (Fig. 4; Smallwood *et al.*, 2001; White *et al.*, 2003). The basalt was assumed to contribute to the compaction of underlying sediments in the same way as an overlying sedimentary section. An example map of sand N:G from one of the eight Paleocene depth layers is shown in Figure 6d. The distribution of the sediments within the study area, together with volume and mass estimates and provenance is discussed further in Smallwood (this volume).

## Discussion

The process described here is an attempt to describe geographic and depth variations in sand N:G with a limited set of data. Unfortunately, however, the seismic velocity is a blunt discriminator between sand and shale, as a number of factors are simplified in the process of taking a regional velocity model and decomposing it into a sand-shale two-component system. Assumptions discussed here are those of extrapolation, picking uncertainty, depth conversion uncertainty, additional lithologies and the effects of overpressure. The results of the transformation of velocity data into the N:G value should be regarded with particular caution in areas and intervals beyond those corresponding to the input data range. Extrapolation occurs in several forms within the model discussed here, firstly geographical extrapolation outside areas of well control, secondly extrapolation beyond the depth range covered by wireline log data and thirdly extrapolation of velocities outside the mean sand-shale range at a particular depth.

Extrapolation beyond areas of well control is not a weakness peculiar to this study, as prediction away from wells occupies nearly all the technical effort of the exploration process in one form or another. As with any model, validity must be tested against new data as it is acquired. However, it cannot be expected that the model presented here will provide accurate predictions far from well control into the undrilled sections of the Faroes' area, primarily because the input regional veloc-

ity model used to illustrate the method is only a function-based model and while it may be valid in providing indications of trends, is not based on velocity measured in the undrilled areas. However, exposure to error caused by extrapolation to depths beyond the well-log data range (c. 4500 m sub seafloor) has been limited by clipping the velocity model parameters and densities to physically reasonable values.

Errors in seismic interpretation, or picking uncertainty, are small in the areas of high well density in the UK sector, but likely to increase into less well calibrated areas. Similarly the depth conversion error is low on the southeast side of the study area but larger to the northwest. Overall these two errors give up to a 20% error estimate for Paleocene sediment volumes, but do not influence the lithology prediction technique itself directly.

The limitation of this method in dividing the stratigraphy into a bi-modal system means that the effect of other lithologies is ignored. In particular, mid (silt) grade siliciclastics have effectively been split into the sand and shale end-members, although in the majority of the area deep-water conditions prevailed through much of the lower and mid-Paleocene, and relatively clean sands and high-gamma ray shales predominate. The volume of tuffs inferred from penetrations in UK wells is negligible compared to the volume of sandstones and shales, although volcanic rocks may be more abundant in the Faroes sector (Oljumsáráðid, 2001). The velocity model approach described in this study would be likely to roll the contribution of most volcanic rocks into the faster 'sand' component of the N:G estimate. Igneous sills are widespread throughout the area (fig 1 of Smallwood and Maresh, 2002) and may form a few percent of the volume of the Paleocene section. However, sill volume in the basin is difficult to quantify, as although vertical stacking of sills has been proved by multiple sill penetrations in some wells (e.g. 205/10-2B), seismic imaging is commonly degraded below the uppermost intrusion.

Upper Paleocene and younger sections are commonly normally pressured, while several UK wells encountered overpressure within the Lower Paleocene, particularly beneath the regional seal developed at T35 level in the Flett Basin (Iliffe *et al.*, 1999). The approach taken within this study is to capture the average effects of overpressure on

sonic velocity and density within the depth trend data mathematical descriptions and this may be reflected in the flattening of the shale density trend at depth (Fig. 2). While there may be concern over variable overpressure decreasing the reliability of the quantitative N/G and porosity predictions from this method, without another independent variable overpressure effects cannot be isolated. Offset seismic data can, in principle, give shear-velocity and density estimates, which could provide quantitatively useful additional constraints for lithology prediction.

## Conclusions

The method described uses the laterally and vertically varying seismic velocity within a sedimentary basin together with well-based depth trends in physical parameters of velocity and density to estimate the proportion of sand and shale, porosity and sediment solid volumes. The technique relies on the separation between sand and shale properties and regional velocity model values lying largely between the sand and shale average values. As depth increases, at least in the example of the Faroe-Shetland area, separation between sand and shale properties decreases, and the method becomes unable to discriminate lithology. Since in this example, the (compressional) seismic velocity is the only parameter in the regional model, only two lithological components can be inferred. If an additional parameter, such as shear-wave velocity or conductivity were introduced, then a third lithology may be distinguished. The velocity alone is a relatively blunt instrument for sand-shale discrimination and the results of the model are most appropriately viewed at a regional or sub-basin scale rather than at a prospect level. While the quantitative N/G predictions are subject to a number of assumptions, resulting overall sediment volume estimates are relatively robust to variation in the model parameters and depend more heavily on the accuracy of the mapping of surfaces bounding the Paleocene basin and the lava pile within it.

## Acknowledgements

The regional mapping used in this study was carried out by Amerada Hess Ltd. (AHL) and the original Faroes Partnership: Brian Boslaugh, Wayne Kirk, Arnt Ove Bech, Jan Francois and others. Jacques Leveille and J.C. Wan (AHL) introduced me to the depth trend concept and software. This study benefited from thorough, constructive reviews from Gregers Dam and Mark Woodfin. The seismic data are shown by kind permission of Veritas DGC (Fig. 1). Although the opinions and interpretations expressed herein are not necessarily theirs, thanks are also due to AHL and partner companies for permission to publish.

## References

- Cooper, M.M., Evans, A.C., Lynch, D.J., Neville, G. and Newley, T. 1999. The Foinaven field: managing reservoir development uncertainty prior to start-up. In: Fleet, A.J. and Boldy, S.A.R. (eds.) *Petroleum Geology of Northwest Europe: Proceedings of the 5th Conference*. Geological Society, London: 675-682.
- Goult, N.R. 2004. Mechanical compaction behaviour of natural clays and implications for pore pressure estimation. *Petroleum Geoscience* 10: 73-79.
- Hendrickson, J.S. 1999. Stacked. *Geophysical Prospecting* 47: 663-705.
- Hollingsworth, R. 2002. BP Faroes Licence 004 Status Report, *Offshore Faroes Conference*, Torshavn.
- Iliffe, J.E., Robertson, A.G., Ward, G.H.F., Wynn, C., Peat, S.D.M. and Cameron, N. 1999. The importance of fluid pressures and migration to the hydrocarbon prospectivity of the Faeroe-Shetland White Zone. In: Fleet A.J. and Boldy S.A.R. (eds.) *Petroleum Geology of Northwest Europe: Proceedings of the 5th Conference*. Geological Society, London: 601-611.
- Japsen, P. 1993. Influence of lithology and Neogene uplift on seismic velocities in Denmark: Implications for depth conversion of maps. *American Association of Petroleum Geologists Bulletin* 77: 194-211.
- Jones, S.M. and White, N. 2003. Size and shape of the starting Iceland swell, *Earth and Planetary Science Letters* 216: 271-282.
- Jones, S.M., White, N., Clarke, B.J., Rowley, E. and Gallagher, K. 2002. Present and past influence of the Iceland Plume on sedimentation. In: Doré, A.G., Cartwright, J.A., Stoker, M.S., Turner, J.P. and White, N.J. (eds.) *Exhumation of the North Atlantic Margin: Timing, Mechanisms and Implications for Petroleum Exploration*, Geological Society, London, Special Publications 196: 13-25.
- Lamers, E. and Carmichael, S.M.M. 1999. The Paleocene deepwater sandstone play West of Shetland. In: Fleet A.J. and Boldy S.A.R. (eds.) *Petroleum Geology of Northwest Europe: Proceedings of the 5th Conference*. Geological Society, London: 645-659.
- Oljufáráðgjafi, 2001. Statoil Well 6005/15-1, *Faroe Islands Ministry of Petroleum Press Release* 3rd September.



- Selater, J.G. and Christie, P.A.F. 1980. Continental stretching: an explanation of the post-mid-Cretaceous subsidence of the Central North Sea Basin. *Journal of Geophysical Research* 85: 3711-3739.
- Slotnick, M.M. 1936. On seismic computations, with applications, I. *Geophysics* 1: 9-22.
- Smallwood, J.R. 2002. Use of Vo-K depth conversion from shelf to deep-water: how deep is that brightspot? *First Break* 20: 99-107.
- Smallwood, J.R. 2004. Tertiary inversion in the Faroe-Shetland Channel and the development of major erosional scarps. In: Davies, R.J., Cartwright, J.A., Stewart, S.A., Lappin, M. and Underhill, J.R. (eds.) *3D Seismic Technology: Application to the Exploration of Sedimentary Basins*, Geological Society, London, Memoirs 29:187-198.
- Smallwood, J.R. this volume. Quantity, distribution and provenance of Paleocene sediments in the Faroe-Shetland area. In: Ziska, H., Varming, T. and Bloch, D. (eds.) *Faroe Islands Exploration Conference: Proceedings of the 1<sup>st</sup> Conference*, *Annales Societatis Scientiarum Faeroensis*, Supplementum 43, Tórshavn.
- Smallwood, J.R., Towns, M.J. and White, R.S. 2001. The structure of the Faeroe-Shetland Trough from integrated deep seismic and potential field modelling. *Journal of the Geological Society, London* 158: 409-412.
- Smallwood, J.R. and Gill, C.E. 2002. The rise and fall of the Faroe-Shetland Basin: evidence from seismic mapping of the Balder Formation. *Journal of the Geological Society, London* 159: 627-630.
- Smallwood, J.R. and Maresh, J. 2002. The properties, morphology and distribution of igneous sills: Modelling, borehole data and 3D seismic from the Faroe-Shetland area. In: Jolley, D.W. and Bell, B.R. (eds.) *The North Atlantic Igneous Province: stratigraphy, tectonic, volcanic and magmatic processes*, Geological Society, London, Special Publication 197: 271-306.
- Smallwood J.R. and Kirk, W.J. in press. Exploration in the Faroe-Shetland Channel: Disappointments and Discoveries. In: Doré, A.G. and Vining, B. (eds.) *Petroleum Geology: North-West Europe and Global Perspectives – Proceedings of the 6<sup>th</sup> Petroleum Geology Conference*, Geological Society, London.
- Smallwood, J.R., Prescott, D. and Kirk, W. J. 2004. Alternatives in Paleocene exploration West of Shetland: A case study. *Scottish Journal of Geology* 40 (2): 131-143.
- Sullivan, M., Coombes, T., Imbert, P. and Ahamdach-De-mars, C. 1999. Reservoir quality and petrophysical evaluation of Paleocene sandstones in the West of Shetland area. In: Fleet A.J. and Boldy S.A.R. (eds.) *Petroleum Geology of Northwest Europe: Proceedings of the 5<sup>th</sup> Conference*, Geological Society, London: 627-633.
- White, R.S., Smallwood, J.R., Fliedner, M.M., Boslaugh, B., Maresh, J. and Fruehn, J. 2003. Imaging and regional distribution of basalt flows in the Faroe-Shetland Basin. *Geophysical Prospecting* 51: 215-231.
- Wyllie, M.R.J., Gregory, A.R. and Gardner, L.W. 1956. Elastic wave velocities in heterogeneous and porous media. *Geophysics* 21: 41-70.

# Quantity, Distribution and Provenance of Paleocene Sediments in the Faroe-Shetland Area

JOHN R. SMALLWOOD

Amerada Hess Ltd., 33 Grosvenor Place, London, SW1X 7HY, UK.  
E-mail: john.smallwood@hess.com; Tel : +44 (0) 207 887 2793

## Abstract

The Paleocene clastic sediments encountered by recent exploration wells drilled in deep water in the Faroe-Shetland area have included a high proportion of sandstone. The dominance of sandstone causes seismic velocities to be higher in these distal wells than on the basin margins where the Paleocene deep-water sediments are, on average, finer-grained. A regional velocity model has been used together with averaged rock property trends from well logs to predict sand net-to-gross ratio, porosity and density within the Judd, Flett and Corona Basins. Integration of these three-dimensional parameter fields across the area, with allowance for the Faroes lavas, yields a solid volume estimate of Paleocene sediments of  $4.5 \pm 1 \times 10^4 \text{ km}^3$ , and a total mass estimate for these sediments of  $1.2 \pm 0.2 \times 10^{17} \text{ kg}$ . The Judd Basin has a higher volume of sand than either the Flett or the main Corona Basins, and a lower average sand density, reflecting its relatively shallow burial and resulting higher average porosity. Although significant thicknesses of Paleocene sediment are mapped within the main Corona Basin and the area to the west of the Corona Ridge, the overlying basalt lavas, averaging more than 2 km in thickness, act to reduce the prognosed sandstone porosity, and the westerly Judd Basin remains the most attractive area for the Paleocene sandstone play. The volumes of Paleocene sediment calculated in this study are greater than the volumes of material previously calculated to have been eroded from the catchment onshore in Britain and Ireland during the entire Cenozoic. This observation supports a westerly clastic sediment input to the Faroe-Shetland area prior to obstruction by flood basalt eruptions and continental rifting adjacent to the Faroe Islands.

## Introduction

During the initial phase of exploration of the Paleocene deep-water play in the Faroe-Shetland area, the principal challenge was the successful prediction of effective reservoir sandstones (Lamers and Carmichael, 1999), and several UK wells targeting Paleocene reservoirs failed to encounter good sands at key levels (e.g. well 205/14-3; Fig. 1; Smallwood *et al.*, 2004). However, the wells drilled in the Faroes Sector to date have encountered large quantities of sand within the Paleocene (Fig. 2). For example, well 6004/16-1Z (Fig. 1) penetrated sediments in the T36 to T28 sequences (of Ebdon *et al.*, 1995; Fig. 3) totalling c. 1500

m in thickness, with an overall average sand net-to-gross ratio (N:G) of 0.6-0.7. The high sand N:G has proved detrimental to the petroleum system, as sealing lithologies have been poorly developed (e.g. Sørensen, 2003; Woodfin *et al.*, this volume). Although oil shows were encountered at several levels within the T30s and T20s intervals in 6004/16-1Z, lack of a significant oil accumulation can be attributed to the lack of an integral top seal between T28 and T36 in this part of the basin. A similar high sand proportion and corresponding lack of shale seal development appears to have been a factor in the lack of an oil accumulation in the location tested by Svinoy well 6004/12-1 (Fig. 2; Hollingsworth, 2002).



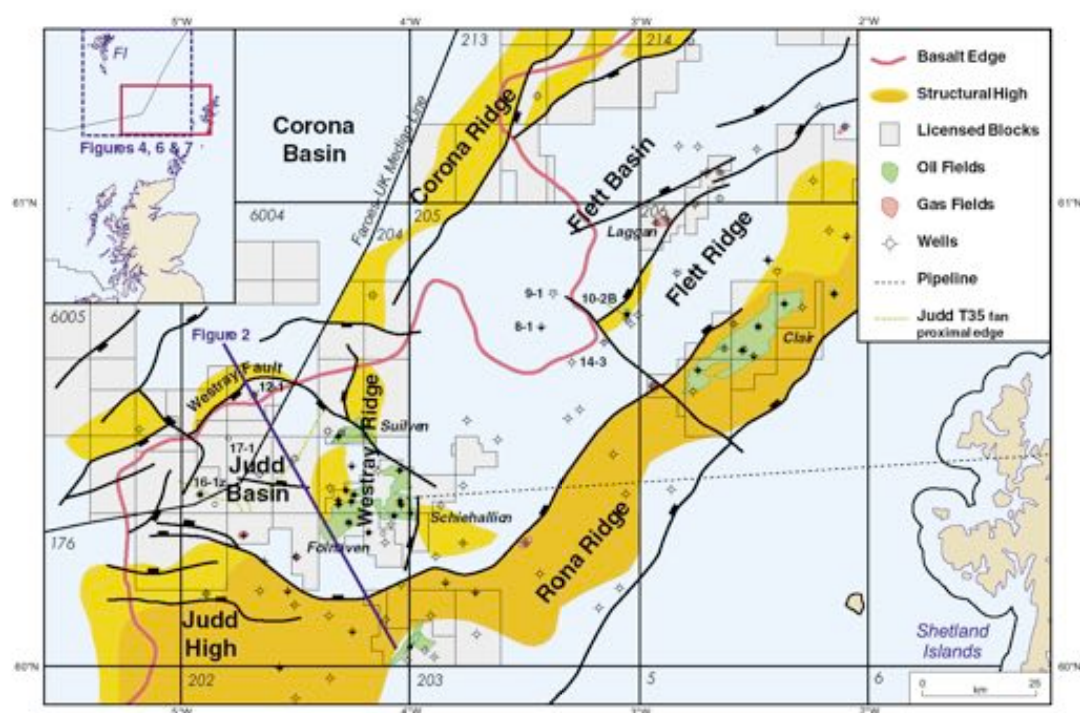


**Figure 1.** Location map with exploration licences (grey), Quadrants (numbered), oil fields, structural elements (faults shown as black lines) and wells discussed in text (numbered). Inset map shows the location of the main map between the Shetland Isles and the Faroe Islands (FI) and Figs 4, 6 & 7.

Predicting the areal distribution and vertical extent of both sand-prone and shale-prone intervals is therefore of great importance for hydrocarbon exploration, in order that the reservoir and seal aspects of the petroleum system can be correctly understood. In this paper, following a summary of the development of the Paleocene stratigraphy, a modelling technique in which sand N:G is inferred from compressional sonic velocity data is described briefly. Further details of the modelling procedure are discussed in Smallwood (this volume). The results of the regional modelling of lateral and vertical variations in sand N:G ratio throughout the Faroe-Shetland area and the distribution of clastic Paleocene sediments are then discussed. The regional lithology model includes representation of density and porosity variations, parameter fields which have been numerically integrated to yield estimates of the mass and solid volume of sediments in each sub-basin. These quantities are of interest for studies seeking to link the denudation from paleo-onshore areas with deposition in surrounding basins (e.g. Jones *et al.*, 2002; Clarke, 2002).

## Paleocene basin history and sediment provenance

Overall during the Cenozoic, the dominant process affecting the vertical movement of the basin was post-rift thermal subsidence (Turner and Scrutton, 1993). The accommodation space generated in the centre of the basin was filled with clastic sediments, which were deposited in environments ranging from shelfal on the basin periphery to deep-water in the basin centre. Ebdon *et al.* (1995) published a sequence stratigraphic system for the area on the basis of biostratigraphy and seismic mapping (Figs. 2 and 3). The first phase of uplift and denudation of the Shetland Platform occurred in the Early Palaeocene (the T10 sequence of Ebdon *et al.*, 1995) (Morton *et al.*, 2002), and caused sediments to be shed into the basin. Deposition was controlled by the underlying end-Cretaceous fault-induced topography. Submarine fans first filled the basin floor deeps, then progressed to onlap and eventually to cover the basin floor highs during the period of T20 deposition. The system continued to develop into a period of deep-water

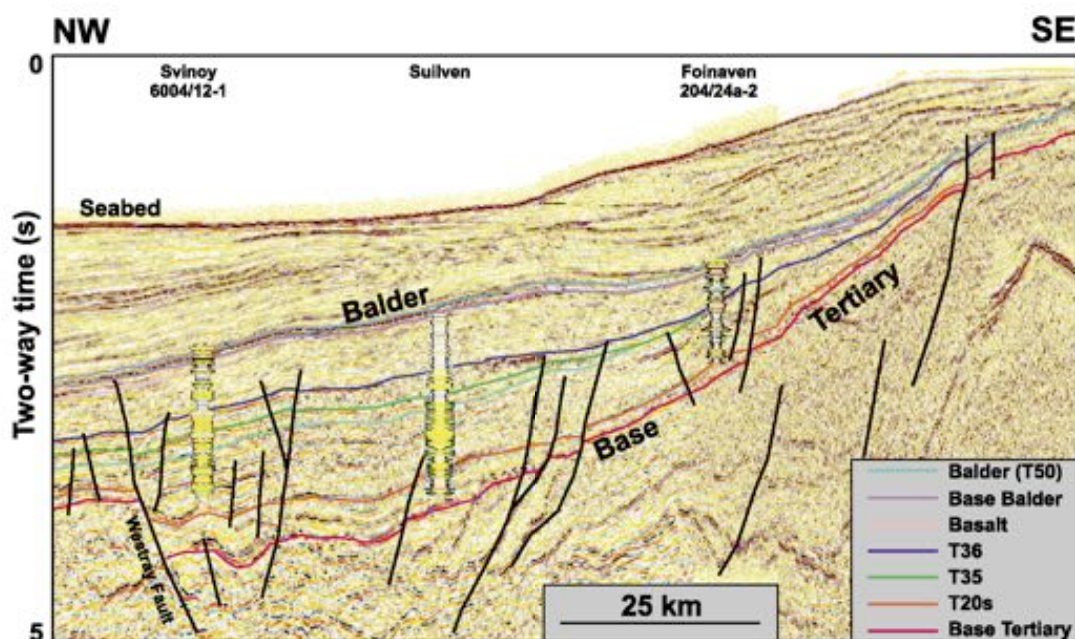


**Figure 2.** Semi-regional NW-SE seismic line (location indicated in Figs 1 & 4a). Interpreted seismic horizons are coloured and their stratigraphic position indicated in Figure 3. The interval between the 'Base Balder' seismic reflector and the 'Base Tertiary' seismic reflector, taken here to bracket rocks of Paleocene age, thickens into the deeper water areas. Representative well sticks from Hollingsworth (2002) show the increase in sand (yellow) proportion basinward in the Judd Basin.

fan sand progradation during the T30s, with sand input punctuating the background deep marine hemipelagic shale accumulation (Sullivan *et al.*, 1999).

During the T35 interval a major wedge of fine-grained clastic material accumulated to the east of the Judd Basin, later forming the top seal for the Foinaven and Schiehallion fields (Lamers and Carmichael, 1999). A shale bed at approximately the same level developed further north, in the Flett Basin, subsequently providing a regional seal separating overpressured (and in places hydrocarbon bearing) sands beneath from normally pressured

(and non-hydrocarbon bearing) sands above (Lamers and Carmichael, 1999).

The intersection of the Westray Ridge and Judd

**Figure 3.** Stratigraphic column for the Paleocene in the West of Shetlands area. The BGS nomenclature is from Knox *et al.* (1997). T sequence scheme is based on Ebdon *et al.* (1995) and Lamers & Carmichael (1999). The lithology column shows the approximate constituent lithologies encountered within the sequences from northwest to southeast: Green indicates fine-grained clastics, yellow indicates sand-grade clastics, purple indicates lava, red indicates volcanic tuff and black indicates coal (not to scale). U & L indicate Upper and Lower series lavas. LSW=Lowstand wedge. Coloured dotted lines indicate the stratigraphic positions of the seismic reflectors on Fig. 2.

Age	BGS Stratigraphic Nomenclature of the UK North West Margin		T Sequences	Lithology	
				NW	SE
Earliest Eocene Latest Paleocene	Moray Group	Balder Formation	B2		
			B1	T50	
			F3		
		Flett Formation	F2	T45	
Late Paleocene	Faroe Group	Flett Formation	F1b		
			F1a	T40	
		Lamba Formation	7L1-2	T38	
		Vaila Formation		T36	
				T35	
				low T35	
				T34	
				T32	
				T31	
			V2	T28	
				T25	
			V1	T22	
Early Paleocene	Shetland Group	Sullom Formation	S1-S2	T10	



High formed a major point of sediment input to the Judd Basin in the Paleocene (Fig. 1; Naylor *et al.*, 1999). The highest Paleocene sedimentation rates in the basin were reached in the Upper T35 to T36 interval (Jolley *et al.*, 2002), with input of a series of major fans (Ebdon *et al.*, 1995) into the basin from the south and west. The T36 Kettla Tuff (Fig. 3), overlying these fans, is a prominent seismic reflector, which is sparsely offset by faults, indicating the termination of the Paleocene phase of rift development.

Following the deposition of the Kettla Tuff, an abundant supply of clastic material, derived from the uplifted Scottish Highlands (e.g. Jones *et al.*, 2002), built two major progradational packages out across the basin. Palaeo-water depths of 500 m and 300 m have been reported from the Lamba and Flett Formations respectively, from delta-front clinoform sets on seismic data (Smallwood and Gill, 2002). The major extrusive igneous activity which generated the Faroes Lower Basalt Series commenced during deposition of the Flett Formation. Sediments within and equivalent to the oldest lavas (where penetrated by drilling in the Faroe-Shetland basin) allow them to be placed within the T40 sequence, as in East Greenland (Jolley *et al.*, 2002; Jolley and Whitham, 2004). Igneous activity continued during the T45 interval (Fig. 3) with the extrusion of the Middle and Upper Series of lavas in the Faroe Islands (Waagstein, 1988; Jolley *et al.*, 2002). While subaerial lava flows have been proved as far southeast as the UK sector (Figs 1 and 4), to the north the lavas encountered marine conditions, forming escarpments where major hyaloclastite wedges built out into the basin (Smythe, 1983; Gatliff *et al.*, 1984; Ritchie *et al.*, 1999; Kjørboe, 1999; Fig. 4d).

The elastic thickness of the region has been shown to be small, so that major vertical movements are unlikely to be caused by remote horizontal stress changes alone (Tiley *et al.*, 2003). Changes in the underlying asthenosphere have been invoked to explain observed departures from conventional post-rift subsidence patterns (e.g. Turner and Scrutton, 1993; Nadin *et al.*, 1997). The volcanism of the British Tertiary Igneous Province to the south and the Faroes to the west is thought to have been underpinned by anomalously hot asthenospheric mantle interacting with lithospheric thin spots early in the Paleocene (e.g.

White, 1988; Jones and White, 2003). Permanent uplift arising from igneous crustal underplating has also been postulated (Brodie and White, 1994), and Clift and Turner (1998) calculated that 1–2 km of underplating under the Shetland Isles and the sedimentary basins to the west could explain the observed subsidence anomalies. Although underplating has been detected under the Irish Sea with seismic techniques (Al-Kindi *et al.*, 2003), it has not been detected with similar methods around the Shetland Isles (R. England, pers. comm.), and debate continues about possible ‘pulsing’ of igneous activity and its relationship to sediment deposition offshore (White and Lovell, 1997; MacLennan and Lovell, 2002; Morton *et al.*, 2002). However, much of the Faroe-Shetland area was still submarine at the zenith of the regional uplift (Jones and White, 2003) at the end of the T40s interval, when a regional unconformity developed, forming the base of the Balder Formation (Figs 2 and 3). Rapid collapse of the regional uplift, attributed to the confinement of anomalously hot asthenospheric mantle to the nascent continental rift west of the Faroe Islands (Smallwood and Gill, 2002). The Balder Formation progressively overlapped basalt to the northwest, as the marine transgression proceeded and deep marine conditions were re-established across the basin in the Early Eocene. Apart from a few localised areas which have experienced subsequent uplift and erosion (Smallwood, 2004), Paleocene rocks are currently positioned at their maximum burial depth.

A suite of sills in the centre of the basin, intruding sediments as young as the Paleocene T31–T38 sequences, is thought to have been intruded mainly around the time of the Balder Formation (Hitchen and Ritchie, 1993; Smallwood and Maresch, 2002). Post-rift subsidence continued throughout the Cenozoic, punctuated by multiple minor compressional phases, possibly associated with relocations in the oceanic spreading centre to the west of the Faroe Islands and its interaction with the Iceland mantle plume (Boldreel and Andersen, 1993; Sørensen, 2003; Davies *et al.*, 2004; Smallwood, 2004).



## Summary of sediment distribution modelling

As outlined above, the thermal subsidence of the Faroe-Shetland basin provided accommodation space for the accumulation of clastic sediments throughout much of the Paleocene. The relatively predictable gross rock property trends of compacting clastic sediments in the basin offer the opportunity for simplified models to be developed

to describe the expected depth-varying behaviour of these sandstones and shales. Clean sandstones and shales with high natural radioactivity ("high gamma") were picked in twelve representative wells, and wireline data from the picked zones were compiled to establish depth trends in sonic velocity and density for sands and shales (fig 2 of Smallwood, this volume). Since the sonic velocity of sand and shales differs throughout the depth range, these well-log velocities were used together

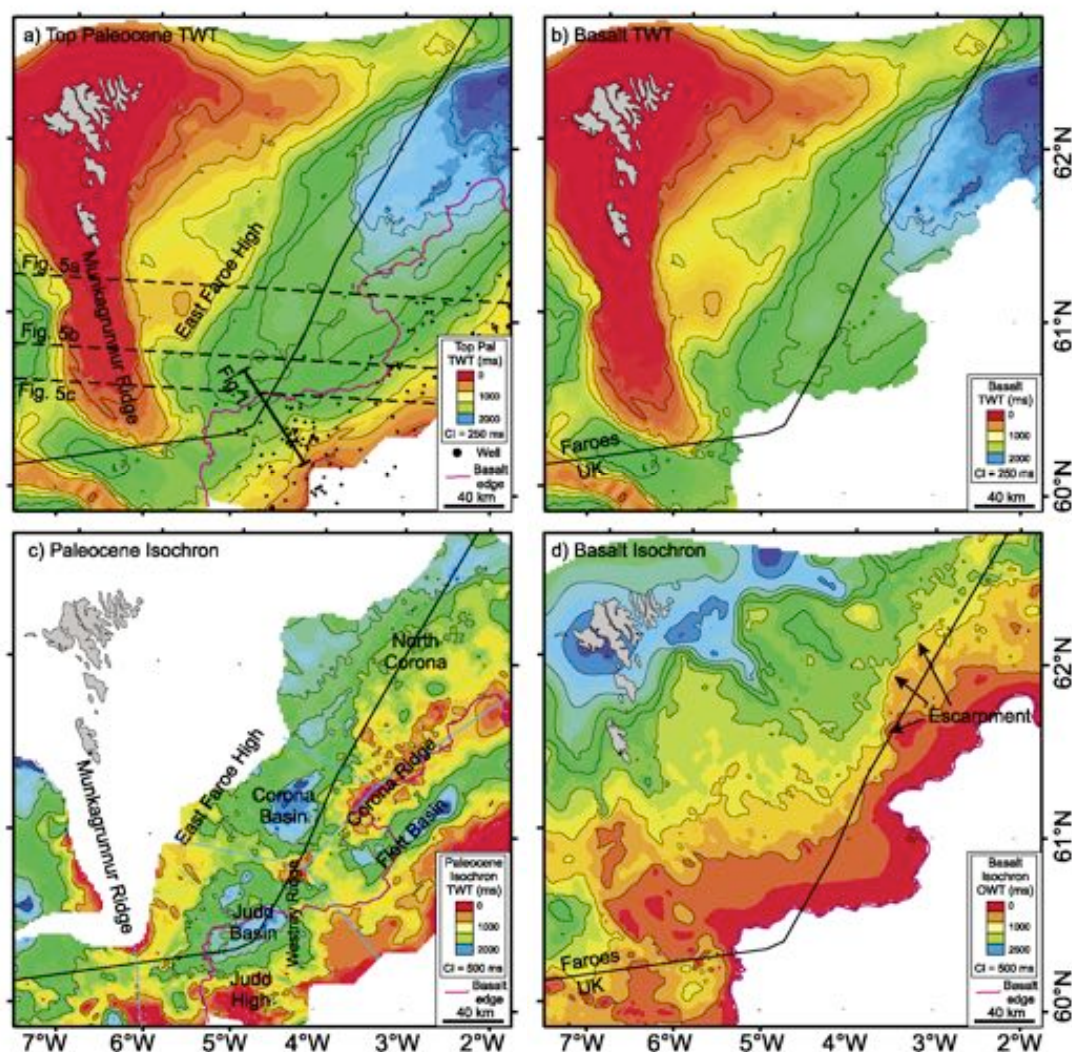


**Figure 4.** (a) Two-way time (TWT) map of 'Top Paleocene' seismic reflection (composite of 'Base Balder', 'Top Basalt' and 'Seabed' seismic reflections; see Fig. 5). The main trough running NE-SW reflects the Cenozoic post-rift thermal subsidence of the basin. Much of the UK sector is beyond the eastern extent of the basalt lava (pink line). Locations of Figs 1 & 5 shown. (b) TWT map of 'Top Basalt' seismic reflection, modified after White *et al.* (2003). (c) Isochronochore map, showing thickness of Paleocene (for Base Paleocene TWT map see fig 3c of Smallwood, this volume). Isochronochore thicks define the Judd, Flett and Corona Basins. Blue dotted lines indicate areas for which mass and volume of sediments are shown in Fig. 8. (d) Isochronochore map, showing one-way (OWT) time thickness of basalt, modified after White *et al.* (2003).

with independent seismic velocity measurements to estimate sand N:G in areas away from well control.

A regional velocity model was built using functions based on compilation of check-shot data from seventeen wells (Smallwood, 2002). This velocity model was used in conjunction with the well log-based trend models to estimate sand distribution across the area (see Smallwood, this volume, for a more detailed description of the modelling procedure). In Paleocene basin margin and slope settings (broadly located in areas with smaller present-day water depths), the regional velocity model shows a smaller rate of increase with depth than either the sand or shale well-based velocity trend curves (fig. 5a of Smallwood, this volume). This is interpreted to correspond to a decrease in the sand to shale ratio with depth, i.e. a decrease in sand net-to-gross (N:G) ratio, as observed in wells such as 205/8-1 (Fig. 1; fig. 4 of Smallwood *et al.*, 2004). In more distal positions in the Paleocene basin (mostly located in areas of larger present-day water depth), the regional velocity model shows overall higher velocities, and a higher rate of increase with depth than either sand or shale end member curves (fig. 5c of Smallwood, this volume). This is interpreted to correspond to overall sandier lithologies, and an increase in N:G ratio with depth, as observed in wells such as 205/9-1 (Fig. 1; fig. 4 of Smallwood *et al.*, 2004).

The velocity model was also used to depth convert regional two-way time maps of the 'Base Balder' (purple) and 'Base Tertiary' (maroon) seismic horizons (Figs 2, 3 and 4). The study area runs from 6°W to 1.75°W and from 50.9°N to 62.6°N, including the Paleocene Flett, Judd and Corona Basins (Fig. 4c). The basalt lava pile was taken into account during the depth conversion of the 'Base Tertiary' seismic horizon (Fig. 5), using a depth conversion velocity of 4.5 km s<sup>-1</sup>, as measured in well 164/7-1, in which over 1 km of basaltic lavas were penetrated. The Paleocene interval was then divided into eight layers of equal thickness. For each of the eight layers, the areally-varying proportion of sand to shale was estimated using the well-log based model, which also gives a prediction of the porosity and density of the sand and shale fractions.

## Results

### Sediment thickness

The mean thickness of Paleocene sediments varies between the sub-basins. The area northwest of the Corona Ridge has been subdivided into the deep area with a relatively thin basalt cover, the 'Corona Basin' and a northerly, less defined depocentre beneath thicker basalt, termed 'North Corona'. The laterally extensive North Corona area (Fig. 4c) is calculated to have a mean thickness of Paleocene sediments of 0.8 km, with Flett and Judd Basins averaging 0.9 and 1.1 km respectively. The Corona Basin is calculated to contain a mean thickness of 1.4 km of Paleocene sediments. Basalt cover varies across the basins (Fig. 4d). While the Flett Basin is largely basalt-free with a mean basalt cover of just 50 m, the Judd Basin averages 340 m basalt cover and the Corona Basin is calculated to have an average thickness of 2 km of basalts within the Paleocene. The North Corona area, which includes the area where an escarpment in the basalts indicated palaeo-shoreline (Fig. 4d; Kjørboe, 1999), averages 2.4 km of basalt cover over older Paleocene sediments. A volume of  $52 \times 10^4$  km<sup>3</sup> of basalt is calculated to overlie Paleocene sediments within the four sub-areas discussed here, although this is only a small fraction of the overall Faroes lava province, of which  $1.9 \times 10^6$  km<sup>3</sup> is calculated to lie within the area of Figure 4.

### Sand Net:Gross

Example maps of sand N:G from Layers 3 and 5 of the eight-layer Paleocene model (Fig. 5) are shown in Figure 6. A similar map for Layer 4 is shown in fig. 6d of Smallwood (this volume). The model suggests that within each of the layers, N:G increases into the centre of the Judd Basin, while a low N:G trend runs along the Corona Ridge. Where water depth is greater than about 750 m, as it is over the Corona Ridge, comparison of Figures 6a and 6b suggests that the N:G increases with depth (see also fig 5c of Smallwood, this volume).

### Porosity

Lateral porosity variation for the sand fraction of Layers 3 and 5 of the Paleocene model (Fig. 5) are shown in Figure 6. Sand porosity decreases into the basin centre and even in these layers, around half



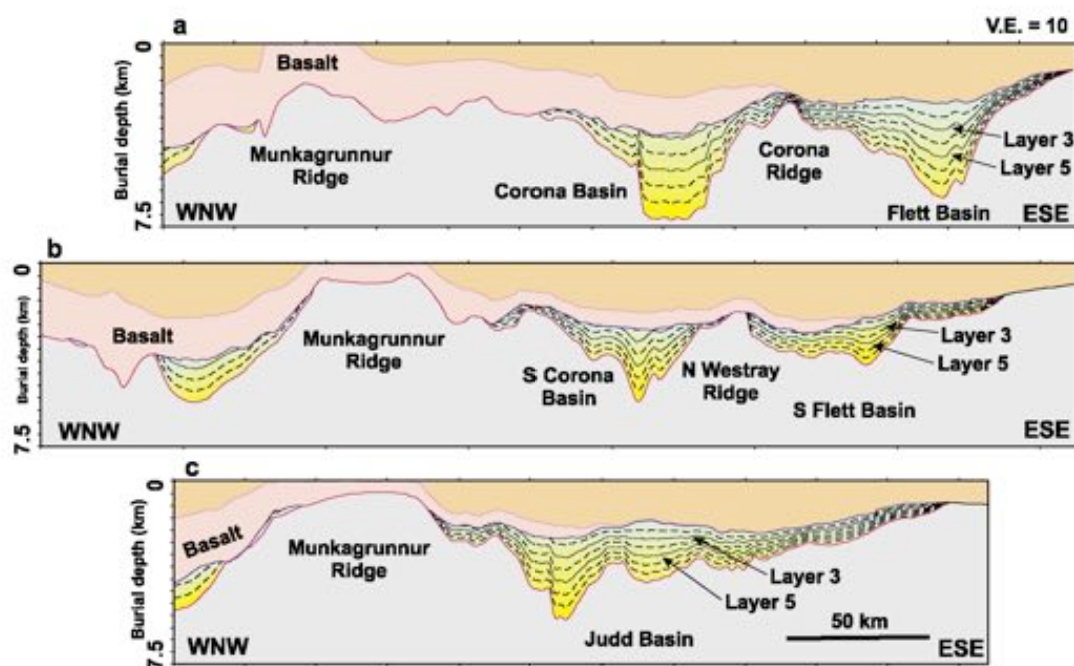


**Figure 5.** Cross-sections through the depth model (faults omitted). Depth conversion was made using functions described in Smallwood (2002) outside the basalt and  $4.5 \text{ km s}^{-1}$  within the basalt lava pile. Line locations shown in Fig. 4a. Main structural features named. The Top and Base Basalt surfaces and Top and Base Paleocene surfaces are shown as solid lines, colours match markers in Figs. 2 & 3. The Paleocene sedimentary interval is subdivided into eight layers of equal thickness (dashed lines). Properties of Layers 3 & 5 (dotted) are shown in Figs. 6 & 7. The basalt generally thickens to the north and west. (a) Line through Corona Basin and Flett Basin. (b) Line across northern part of Westray Ridge. (c) Line through northern section of Judd Basin.

the depth down through the Paleocene, is predicted to fall below 10% in the centre of the Flett Basin. Over much of the Corona Basin, and North Corona area, the porosity is predicted to be similarly low, largely due to compaction beneath the basalt lava pile. Good porosities are preserved (where sand is present) where burial depth is less severe (Fig. 6c), over much of the Judd Basin, Corona Ridge, and flanks of the Flett Basin.

#### Sediment density

Examples of the lateral variation in density through the Paleocene-age rocks are shown in Figure 7, plots which incorporate both the shale and sand fractions. The shale density has been limited to a maximum value of  $2.67 \text{ g cm}^{-3}$  to avoid extrapolation to unrealistic values outside the depth range constrained by well data. The mapped density increases towards the centre of each depocentre as the depth to the horizon increases, and higher densities are expected for Layer 5 than for the shallower Layer 3. The extra burial of the Paleocene sedi-

ments beneath the basalts contributes to the mean densities estimated by the model. Mean Paleocene sediment density in the Judd Basin is calculated to be  $2.36 \text{ g cm}^{-3}$ , compared to  $2.48 \text{ g cm}^{-3}$  in the Flett Basin, and nearly  $2.6 \text{ g cm}^{-3}$  in the Corona Basin and North Corona areas. The relatively thin Cenozoic section of the Judd Basin and lack of thick additional basalt contributes to its favourable position for oil exploration both for reservoir preservation and source rock maturity considerations (Lamers and Carmichael, 1999; Carr and Scotchman, 2003).

#### Solid grain thickness

The solid volume of the sediments is calculated by removing the volume accounted for by the porosity. For this treatment, the porosity parameter, (see Smallwood, this volume) has been limited to a maximum of 35% for sand and 45% for shale, although this only affects a small volume of Paleocene-age rocks, those which are shallower than approximately 1300 m below the sea floor at the



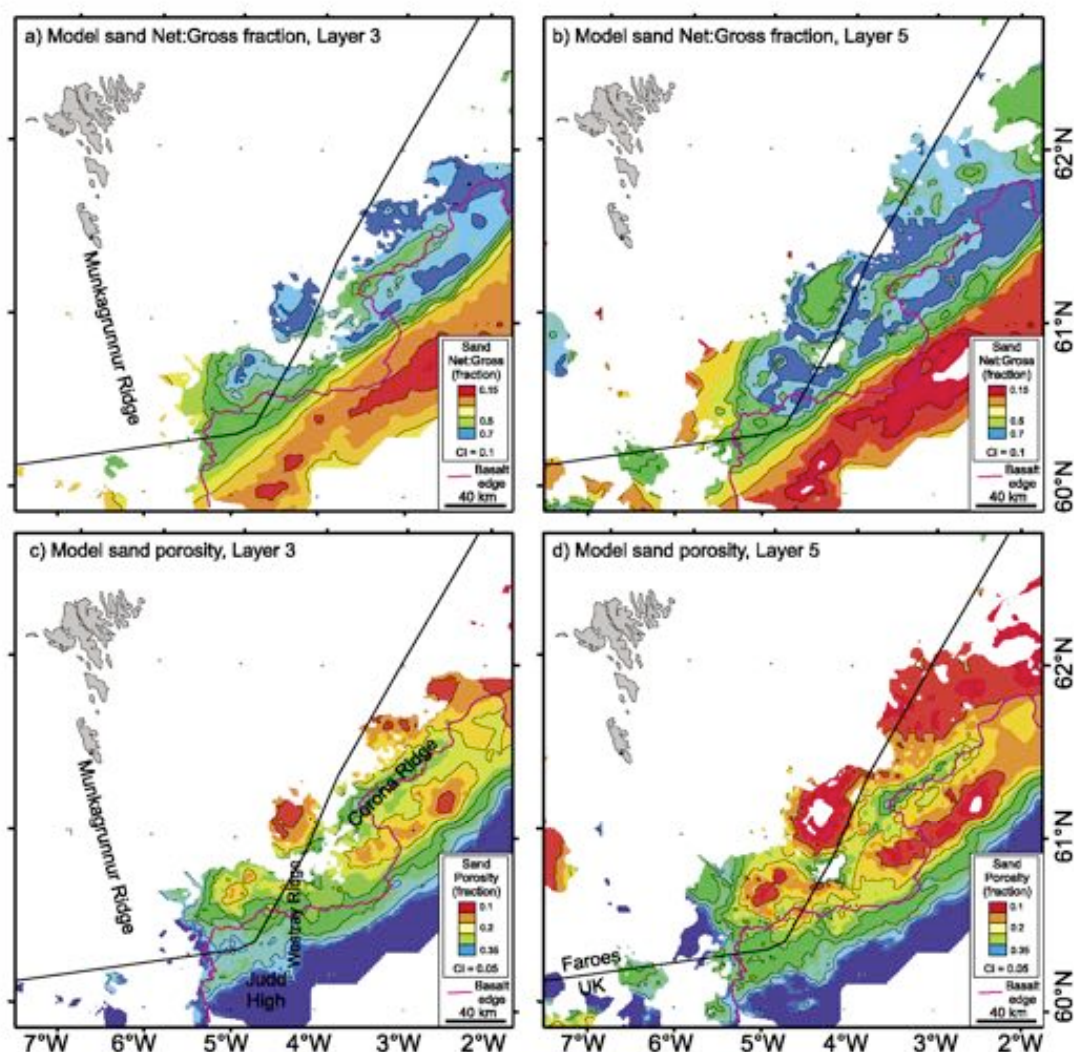


**Figure 6.** Illustrative maps from the eight-layer subdivided Paleocene model (Layer 4 shown in Smallwood, this volume). The data do not extend over the full area of the Paleocene basins (Fig. 4c) as the layers subcrop against the basalt (Fig. 5). (a) Model sand fraction (N:G), Layer 3. (b) Model sand fraction (N:G), Layer 5. Note at greater depths the sonic velocity cannot be used to distinguish sand and shale and the algorithm is designed to bring the N:G towards a value of 0.5. (c) Model sand porosity, Layer 3. (d) Model sand porosity, Layer 5.

present day (Fig. 5). Comparison of Figures 7c and 7d shows that overall, the majority of the sediment volume is occupied by sandstones, except in a few areas towards the flanks of the basins, which have formed by-pass zones for sands. The Flett Basin has a lower overall proportion of sand to shale than does the Judd Basin, and in general, as would be expected, the solid volume of shale is more constant across the area than the sand fraction of the basin fill.

### Sediment volumes

The solid grain thickness maps are integrated over depth and area to give sediment volumes in the sub-basins shown in Figure 4c (Fig. 8). The total volume of sand in the study area is calculated to be  $2.4 \times 10^4 \text{ km}^3$ , with approximately equal volumes in the Judd and Flett Basins and the North Corona area. The smaller Corona Basin is modelled to contain  $0.4 \times 10^4 \text{ km}^3$  of the total. The total volume of shale is calculated to be  $2.1 \times 10^4 \text{ km}^3$ , with a higher volume in the Flett Basin ( $6.5$

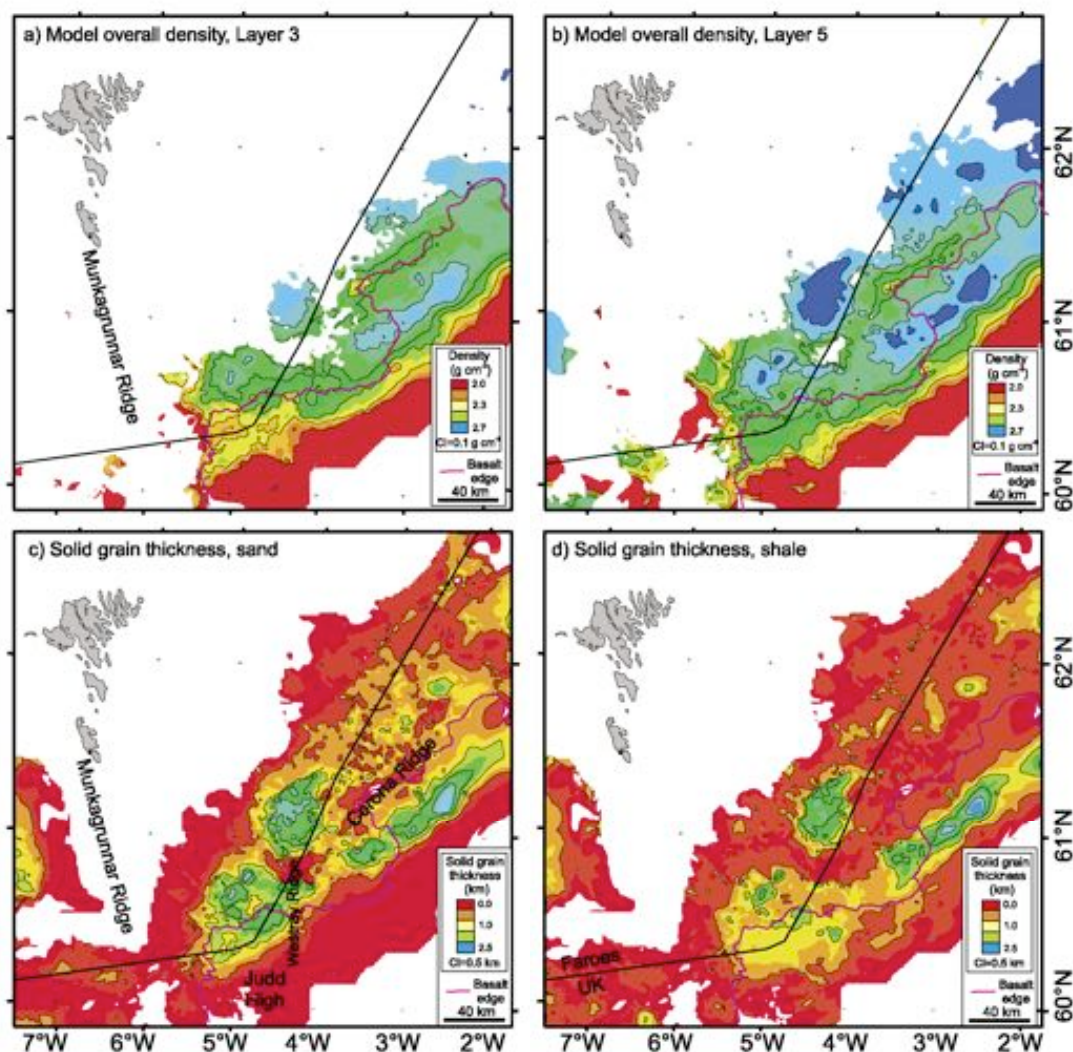


**Figure 7.** (a) Model bulk density, Layer 3 (Fig. 5). (b) Model bulk density, Layer 5. (c) Solid grain thickness of sand. (d) Solid grain thickness of shale.

$\times 10^3 \text{ km}^3$ ) than in the Judd Basin ( $6.0 \times 10^3 \text{ km}^3$ ), and a total of  $8.3 \times 10^3 \text{ km}^3$  present in the Corona Basin and North Corona area. The methodology outlined in this study is not expected to give very accurate measures of proportion of sand and shale although the overall solid sedimentary volume,  $4.5 \times 10^4 \text{ km}^3$  is a more robust figure.

### Mass

The bulk density maps were integrated across the area to calculate the mass of sediments within the study area, using an upper limit of  $2.67 \text{ g cm}^{-3}$  for the matrix density of shales. The total mass is calculated to be  $1.2 \times 10^{17} \text{ kg}$ , with mass being dis-

tributed between the four named sub-areas in the same proportions as the solid sediment volumes (Fig. 8).

### Uncertainties

In their estimation of solid sediment volumes around the British Isles, Jones *et al.* (2002) suggest that the largest error lies in the depth conversion, leading to an estimate ranging from  $5.3$  to  $7.1 \times 10^4 \text{ km}^3$  for Cenozoic sediment in the Faroe-Shetland area. Jones *et al.* (2002) state that uncertainty arising from choice of parameters to describe porosity decay with depth leads to an error range only 14% of that arising from a choice of depth



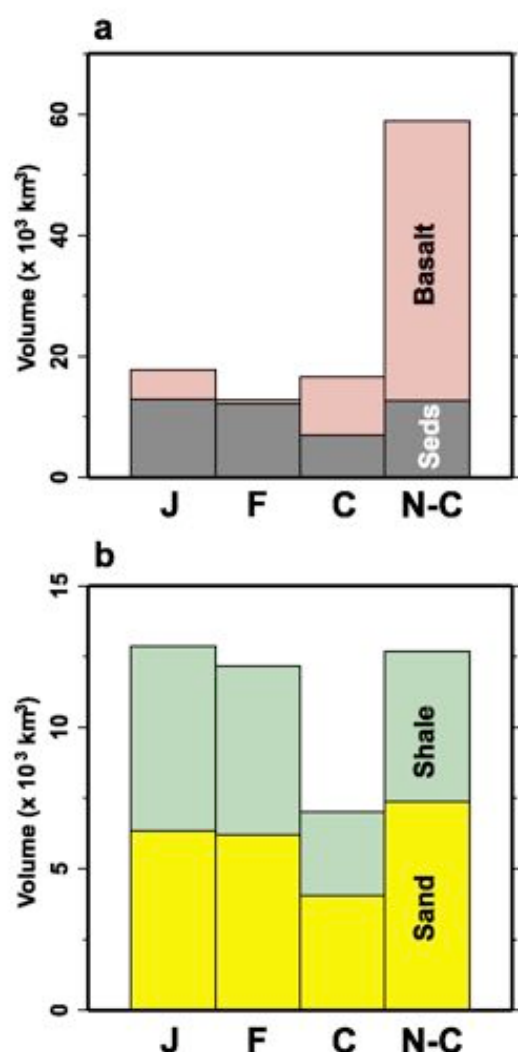


**Figure 8.** Volume and proportions of Paleocene rocks in the study area east of 6°W. Areas shown in Fig. 4c. J: Judd Basin, F: Flett Basin, C: Corona Basin, N-C: north part of Corona Basin. (a) Volume of sediment (grey) and basalt (pink). The volume of basalt was limited to that within the area overlying the maximum extent of Paleocene sediments. (b) Volume of sand (yellow) and shale (green).

conversion functions. Trials with a range of different compaction parameters in this study reach a similar conclusion, although the interpretation of the seismic data that has gone into the maps is a larger uncertainty than the depth conversion in this study, as the depth conversion has been carefully designed to tie the wells in the area. Picking uncertainty gives error bars estimated at 10% on the sediment volume figures for the Judd and Flett Basins, where many wells have penetrated

the entire Paleocene section, and up to 25% in the Corona Basin and North Corona area, which are undrilled to date. The overall error bar on sediment volume is therefore around  $\pm 20\%$  ( $1 \times 10^4 \text{ km}^3$ ), including consideration of the volume in the basin occupied by igneous sills (e.g. 205/10-2b; Smallwood and Maresh, 2002; Fig. 1). The equivalent mass error is around  $0.2 \times 10^{17} \text{ kg}$ . Error bars on the proportion of sand and shale are estimated to be about 20%.

## Discussion

The Faroes' wells drilled to date have all been drilled in deep water and published results suggest that all have high quantities of good quality sand within the Paleocene (Fig. 1; Oljumsáráðíð, 2001a; Oljumsáráðíð, 2001b; Hollingsworth, 2002; Oljumsáráðíð, 2003; Smallwood and Kirk, in press). This study suggests that towards the west flank of the Judd Basin the overall sand N:G will decrease and there may be areas more favourable to the development of sealing lithologies. The trade-off comes with the increasing thickness of basalt to the west which impedes seismic imaging, compacts the underlying sandstones and pushes the local source rock deeper. A second favourable area from a sand N:G perspective may lie immediately west of the Corona Ridge, although water depths in that area would make for high drilling costs.

While Clarke (2002) reports that overall, there is close volume balance between Cenozoic offshore sediments and British onshore denudation estimated from missing post-rift subsidence and thermal indicators, the volume of Cenozoic sediment in the Faroe-Shetland area reported by Jones *et al.* (2002) is greater, by a factor of approximately two, than the solid volume of material calculated to have been denuded from the onshore catchment associated with the area. Jones *et al.* (2002) calculated an overall solid sediment volume ranging from 5.3 to  $7.1 \times 10^4 \text{ km}^3$  for Cenozoic sediment in the Faroe-Shetland area, taken as extending from approximately 59.5 to 61.5°N and extending to 5.5°W. This study captures a slightly larger area than that mapped by Jones *et al.* (2002) and suggests a total solid sediment volume of  $4.5 \times 10^4 \text{ km}^3$  for the Paleocene alone. This figure is larger than the 1.8



to  $3.5 \times 10^4 \text{ km}^3$  of material estimated by Jones *et al.* (2002) to have been denuded from the relevant catchment area in the British Isles during the entire Cenozoic. Since post-Paleocene sediments occupy a larger volume than the Paleocene over much of the study area (Fig. 5; Clarke, 2002), this study exacerbates the discrepancy between the volume of sediment in the basin and that denuded from Britain and Ireland. Jones *et al.* (2002) offer three possible contributions to explain the volume discrepancy; incoming axially transported sediment, a sediment source to the west and temporal variation in drainage divides onshore UK. The introduction of material into the system by axial transport following the initiation of deep-water currents between the Faroe Islands and the Shetland Isles in the Oligocene (Davies *et al.*, 2001) cannot explain the observation made here that a larger volume of sediment accumulated in the basin in the Paleocene alone than was denuded from the catchment area throughout the whole Cenozoic. Temporal variation in the onshore drainage divide has been demonstrated, and recent work shows a much larger catchment draining to the Faroe-Shetland area at the end of the Paleocene than at the present day (Jones and White, 2003). However, the rapid uplift attributed to dynamic support from the Iceland swell appears to have occurred around T40 time, coincident with the onset of voluminous volcanism (Smallwood and Gill, 2002; Jolley and Whitham, 2004), later than the deposition of the majority of the Paleocene sediments. A combination of different drainage patterns and a westerly sediment input therefore appears to be the best explanation of the volume discrepancy.

Heavy mineral studies, which allow links to be made between sediment provenance areas and sand-grade sediments, suggest that vast majority of the Paleocene sandstone encountered in the UK sector has been sourced from the British Isles. Morton *et al.* (2002) identified the signature of the exhumed (Cretaceous) Shetland Platform in early Paleocene sands in the Foinaven area, and also recognised the signature of subsequent progressive erosional unroofing through to exposure of metamorphic basement terrains in the later Paleocene. Further, unpublished, heavy mineral reports also suggest a dominance of sediment sourcing to the Faroe-Shetland area from the southeast side of the basin (Clarke, 2002). Mapping from 3D seismic

data has identified sediment feeder systems which carried clastic material northwestwards from the area to the west of the Shetlands (e.g. Lamers and Carmichael, 1999; fig. 15 of Smallwood *et al.*, 2004).

However, some evidence is building for an additional, westerly, source area for Paleocene sediments in the Faroe-Shetland basin. A small component of westerly (volcanogenic) clastic input into the Flett Basin was recognised in the 1989 well 205/9-1 (Naylor *et al.*, 1999), but other geochemical, palynological, thermochronological and geological studies have started to yield indications of sediment input from the west into the Faroe-Shetland area. Similar characteristics in heavy mineral suites from Cretaceous–Paleocene sandstones from East Greenland and the Mid-Norwegian continental shelf has already indicated that sand was supplied from NE Greenland to western areas of the Vøring Basin (Morton and Grant, 1998) to the north of the Faroe-Shetland area.

The Faroes area was adjacent to southern East Greenland before the Northeast Atlantic Ocean basin rifted open (Smallwood and White, 2002). Palynological data from argillaceous Paleocene sediments West of Shetland suggest that sediment transport pathways periodically brought material from the west (Jolley *et al.*, in press). Additionally, results from radiometric dating of detrital white micas, zircon fission track and U/Pb dating are techniques which show promise in establishing the extent of cross-rift sediment transport from eastern Greenland to the Faroe-Shetland area (Carter *et al.*, 2002; Pickles, pers. comm. 2002; Whitham *et al.*, 2004). One possible sediment input point has been identified in the Kangerlussuaq area of southern East Greenland (Larsen *et al.*, 1999; Larsen and Whitham, in press). Further studies and drilling will be required to determine the extent to which westerly input to the Faroe-Shetland area contributed to the volumes of sediment that are inferred outside the areas constrained by existing wells (Fig. 4a).

## Conclusions

The method described uses the laterally and depth varying seismic velocity within a sedimentary basin with well-based depth trends to estimate the

proportion of sand and shale, porosity and sediment solid volumes. While the quantitative N/G predictions are subject to a number of assumptions, the overall sediment volume is relatively robust to variation in the model parameters and depends more heavily on the accuracy of the mapping of surfaces bounding the Paleocene basin and the lava pile within it. Application of the technique to the Faroe-Shetland area gives a solid sediment volume estimate for the Paleocene of  $4.5 \times 10^4 \text{ km}^3$ , which is significantly greater than previous estimates.

The Judd Basin has a higher volume of sand than either the Flett or the main Corona Basins, and a lower average sand density, reflecting its relatively shallow burial and resulting higher average porosity. Although significant thicknesses of Paleocene sediment are mapped within the main Corona Basin and the area to the west of the Corona Ridge, the overlying basalt lavas, averaging more than 2 km in thickness, act to reduce the prognosed sandstone porosity by compaction, and the westerly Judd Basin remains the most attractive area for the Paleocene sandstone play.

The volumes of Paleocene sediment calculated in this study are greater than the volumes of material calculated to have been eroded from the catchment onshore in Britain and Ireland during the whole Cenozoic (Jones *et al.*, 2002). This observation contributes to growing indications of a westerly clastic sediment input to the Faroe-Shetland area prior to obstruction by flood basalt eruptions and continental rifting adjacent to the Faroe Islands in T40 times (Jolley and Whitham, 2004).

## Acknowledgements

The regional mapping used in this study was carried out by Amerada Hess Ltd. (AHL) and the original Faroes Partnership: Brian Boslaugh, Wayne Kirk, Arnt Ove Bech, Jan Francois and others. This study benefited from discussion with Ben Clarke, and thorough, constructive reviews from Gregers Dam and Mark Woodfin. The seismic data are shown by kind permission of Veritas DGC (Fig. 1). Although the opinions and interpretations expressed herein are not necessarily theirs, thanks are also due to AHL and partner companies for permission to publish.

## References

- Al-Kindi, S., White, N., Sinha, M., England, R. and Tiley, R. 2003. Crustal trace of a hot convective sheet. *Geology* 31: 207-210.
- Boldreel, L.O. and Andersen, M.S. 1993. Late Paleocene to Miocene compression in the Faeroe-Rockall area. In: Parker, J.R. (ed.) *Petroleum Geology of Northwest Europe: Proceedings of the 4<sup>th</sup> Conference*. Geological Society, London: 1025-1034.
- Brodie, J. and White, N. 1994. Sedimentary basin inversion caused by igneous underplating: Northwest European continental shelf. *Geology* 22: 147-150.
- Carr, A.D. and Scotchman, I.C. 2003. Thermal history modelling in the southern Faroe-Shetland Basin. *Petroleum Geoscience* 9: 333-345.
- Carter, A., Sherlock, S., Kelley, S., Pickles, C., Whitham, A. and Morton, A. 2002. A geochronological approach to reconstructing sediment pathways and detecting sediment recycling in Palaeocene sediments from the Faroes-Shetland region. *Geophysical Research Abstracts* 4: EGS02-A02803.
- Clarke, B.J. 2002. Early Cenozoic denudation of the British Isles: a quantitative stratigraphic approach. Ph.D. dissertation, University of Cambridge, UK.
- Clift, P.D. and Turner, J. 1998. Paleogene igneous underplating and subsidence anomalies in the Rockall-Faeroe-Shetland area. *Marine and Petroleum Geology* 15: 223-243.
- Davies, R., Cartwright, J., Pike, J. and Line, C. 2001. Early Oligocene initiation of North Atlantic Deep Water formation. *Nature* 410: 917-920.
- Davies, R.J., Cloke, I.R., Cartwright, J.A., Robinson, A.M. and Ferrero, C. 2004. Post-breakup Compression of a Passive Margin and its Impact Upon Hydrocarbon Prospectivity: An Example from the Tertiary of the Faeroe-Shetland Basin, UK. *American Association of Petroleum Geologists Bulletin* 88: 1-20.
- Ebdon, C.C., Granger, P.J., Johnson, H.D. and Evans, A.M. 1995. Early Tertiary evolution and sequence stratigraphy of the Faeroe-Shetland Basin: Implications for hydrocarbon prospectivity. In: Scrutton, R.A., Stoker, M.S., Shimmield, G.B. and Tudhope, A.W. (eds.) *The Tectonics, Sedimentation and Palaeoceanography of the North Atlantic Region*. Geological Society, London, Special Publications 90: 51-69.
- Gatliff, R.W., Hitchen, K., Ritchie, J.D. and Smythe, D.K. 1984. Internal structure of the Erlend Tertiary volcanic complex, north of Scotland, revealed by seismic reflection. *Journal of the Geological Society, London* 141: 555-562.
- Hitchen, K. and Ritchie, J.D. 1993. New K-Ar ages, and a provisional chronology, for the offshore part of the British Tertiary Igneous Province. *Scottish Journal of Geology* 29: 73-85.
- Hollingsworth, R. 2002. BP Faroes Licence 004 Status Report. *Offshore Faroes Conference*, Torshavn.
- Jolley, D.W., Clarke, B. and Kelley, S. 2002. Paleogene time scale miscalibration: Evidence from the dating of the North Atlantic igneous province. *Geology* 30: 7-10.
- Jolley, D.W. and Whitham, A.G. 2004. A stratigraphical and paleoenvironmental analysis of the sub-basaltic Palaeogene sediments of East Greenland. *Petroleum Geoscience* 10: 53-60.



- Jolley, D.W., Morton, A. and Prince, I. in press. Volcanogenic impact on phytogeography and sediment dispersal patterns in the NE Atlantic. In: Doré, A. G. and Vining, B. (eds.) *Petroleum Geology: North-West Europe and Global Perspectives – Proceedings of the 6<sup>th</sup> Petroleum Geology Conference*. Geological Society, London.
- Jones, S.M. and White, N. 2003. Size and shape of the starting Iceland swell. *Earth and Planetary Science Letters* 216: 271-282.
- Jones, S.M., White, N., Clarke, B.J., Rowley, E. and Gallagher, K. 2002. Present and past influence of the Iceland Plume on sedimentation. In: Doré, A.G., Cartwright, J.A., Stoker, M.S., Turner, J.P. and White, N. (eds.) *Exhumation of the North Atlantic Margin: Timing, Mechanisms and Implications for Petroleum Exploration*. Geological Society, London, Special Publications 196: 13-25.
- Kjørboe, L. 1999. Stratigraphic relationships of the Lower Tertiary of the Faeroe Basalt Plateau and the Faeroe-Shetland Basin. In: Fleet A.J. and Boldy S.A.R. (eds.) *Petroleum Geology of Northwest Europe: Proceedings of the 5<sup>th</sup> Conference*. Geological Society, London: 559-572.
- Knox, R.W.O'B, Holloway, S. and Baily, H.E. 1997. Stratigraphic nomenclature of the UK North West Margin: 2. Early Paleogene lithostratigraphy and sequence stratigraphy. British Geological Survey, Nottingham.
- Lamers, E. and Carmichael, S.M.M. 1999. The Paleocene deepwater sandstone play west of Shetland. In: Fleet A.J. and Boldy S.A.R. (eds.) *Petroleum Geology of Northwest Europe: Proceedings of the 5<sup>th</sup> Conference*. Geological Society, London: 645-659.
- Larsen, M., Hamberg, L., Olaussen, S., Nørgaard-Pedersen, N. and Stemmerik, L. 1999. Basin evolution in Southern East Greenland: An outcrop analog for Cretaceous-Paleogene basins on the North Atlantic Volcanic Margin. *American Association of Petroleum Geologists Bulletin* 83: 1236-1261.
- Larsen, M. and Whitham, A.J. in press. Evidence for a major sediment input point into the Faroe-Shetland Basin from the Kangerlussuaq region of southern East Greenland. In: Doré, A. G. and Vining, B. (eds.) *Petroleum Geology: North-West Europe and Global Perspectives – Proceedings of the 6<sup>th</sup> Petroleum Geology Conference*. Geological Society, London.
- MacLennan, J. and Lovell, B. 2002. Control of regional sea level by surface uplift and subsidence caused by magmatic underplating of Earth's crust. *Geology* 30: 675-678.
- Morton, A.C. and Grant, S. 1998. Cretaceous depositional systems in the Norwegian Sea: Heavy mineral constraints. *American Association of Petroleum Geologists Bulletin* 82: 274-290.
- Morton, A.C., Boyd, J.D. and Ewen, D.F. 2002. Evolution of Paleocene sediment dispersal systems in the Foinaven Sub-basin, west of Shetland. In: Jolley, D.W. and Bell, B.R. (eds.) *The North Atlantic igneous province: stratigraphy, tectonic, volcanic and magmatic processes*. Geological Society, London, Special Publications 197: 69-93.
- Nadin, P.A., Kusznir, N.J. and Cheadle, M.J. 1997. Early Tertiary plume uplift of the North Sea and Faeroe-Shetland Basins. *Earth and Planetary Science Letters* 148: 109-127.
- Naylor, P.H., Bell, B.R., Jolley, D.W., Durnall, P. and Fredsted, R. 1999. Palaeogene magmatism in the Faeroe-Shetland Basin: influences on uplift history and sedimentation. In: Fleet, A.J. and Boldy, S.A.R. (eds.) *Petroleum Geology of Northwest Europe: Proceedings of the 5<sup>th</sup> Conference*. Geological Society, London: 545-558.
- Oljufáráððið. 2001a. BP Well 6004/12-1, *Faroe Islands Ministry of Petroleum Press Release* 26<sup>th</sup> September.
- Oljufáráððið. 2001b. Amerada Hess Well 6004/16-1z, *Faroe Islands Ministry of Petroleum Press Release* 19<sup>th</sup> November.
- Oljufáráððið. 2003. ENI Well 6004/17-1, *Faroe Islands Ministry of Petroleum Press Release* 4<sup>th</sup> August.
- Ritchie, J.D., Gatiloff, R.W. and Richards, P.C. 1999. Early Tertiary magmatism in the offshore NW UK margin and surrounds. In: Fleet A.J. and Boldy S.A.R. (eds.) *Petroleum Geology of Northwest Europe: Proceedings of the 5<sup>th</sup> Conference*. Geological Society, London: 573-584.
- Smallwood, J.R. 2002. Use of Vo-K depth conversion from shelf to deep-water: how deep is that brightspot? *First Break* 20: 99-107.
- Smallwood, J.R. 2004. Tertiary inversion in the Faroe-Shetland Channel and the development of major erosional scarps. In: Davies, R.J., Cartwright, J.A., Stewart, S.A., Lappin, M. and Underhill, J.R. (eds.) *3D Seismic Technology: Application to the Exploration of Sedimentary Basins*, Geological Society, London, Memoirs 29:187-198.
- Smallwood, J.R. this volume. Lithology prediction from velocity data: Paleocene sediments in the Faroe-Shetland area. In: Ziska, H., Varming, T. and Bloch, D. (eds.) *Faroe Islands Exploration Conference: Proceedings of the 1<sup>st</sup> Conference, Annales Societatis Scientiarum Faeroensis*, Supplementum 43, Tórshavn.
- Smallwood, J.R. and Gill, C.E. 2002. The rise and fall of the Faroe-Shetland Basin: evidence from seismic mapping of the Balder Formation. *Journal of the Geological Society, London* 159: 627-630.
- Smallwood J.R. and Kirk, W.J. in press. Exploration in the Faroe-Shetland Channel: Disappointments and Discoveries. In: Doré, A. G. and Vining, B. (eds.) *Petroleum Geology: North-West Europe and Global Perspectives – Proceedings of the 6<sup>th</sup> Petroleum Geology Conference*. Geological Society, London.
- Smallwood, J.R. and Maresch, J. 2002. The properties, morphology and distribution of igneous sills: Modelling, borehole data and 3D seismic from the Faroe-Shetland area. In: Jolley, D.W. and Bell, B.R. (eds.) *The North Atlantic Igneous Province: stratigraphy, tectonic, volcanic and magmatic processes*. Geological Society, London, Special Publications 197: 271-306.
- Smallwood, J.R., Prescott, D. and Kirk, W. J. 2004. Alternatives in Paleocene exploration West of Shetland: A



- case study. *Scottish Journal of Geology* 40 (2): 131-143.
- Smallwood, J.R. and White, R.S. 2002. Ridge-plume interaction in the North Atlantic and its influence on continental breakup and seafloor spreading. In: Jolley, D.W. and Bell, B.R. (eds.) *The North Atlantic Igneous Province: Stratigraphy, Tectonic, Volcanic and Magmatic Processes*. Geological Society, London, Special Publications 197: 15-37.
- Smythe, D. K. 1983. Faeroe-Shetland Escarpment and continental margin north of the Faeroes. In: Bott, M.H.P., Saxov, S., Talwani, M. and Thiede, J. (eds.) *Structure and Development of the Greenland-Scotland Ridge*. Plenum Press, New York: 77-90.
- Sullivan, M., Coombes, T., Imbert, P. and Ahmdach-De-mars, C. 1999. Reservoir quality and petrophysical evaluation of Paleocene sandstones in the West of Shetland area. In: Fleet A.J. and Boldy S.A.R. (eds.) *Petroleum Geology of Northwest Europe: Proceedings of the 5<sup>th</sup> Conference*. Geological Society, London: 627-633.
- Sørensen, A.B. 2003. Cenozoic basin development and stratigraphy of the Faroes area. *Petroleum Geoscience* 9: 189-207.
- Tiley, R., McKenzie, D.P. and White, N.J. 2003. The elastic thickness of the British Isles. *Journal of the Geological Society, London* 160: 499-502.
- Turner, J.D. and Scrutton, R.A. 1993. Subsidence patterns in western margin basins: evidence from the Faeroe-Shetland Basin. In: Parker, J. R. (ed.) *Petroleum geology of Northwest Europe: Proceedings of the 4<sup>th</sup> Conference*. Geological Society, London: 975-983.
- Waagstein, R. 1988. Structure, composition and age of the Faeroe basalt plateau. In: Morton, A.C. and Parson, L.M. (eds.) *Early Tertiary Volcanism and the Opening of the NE Atlantic*. Geological Society, London, Special Publications 39: 225-238.
- White, N. and Lovell, B. 1997. Measuring the pulse of a plume with the sedimentary record. *Nature* 387: 888-891.
- White, R.S. 1988. A hot-spot model for early tertiary volcanism in the N Atlantic. In: Morton, A.C. and Parson, L.M. (eds.) *Early Tertiary Volcanism and the Opening of the NE Atlantic*. Geological Society, London, Special Publications 39: 3-13.
- White, R.S., Smallwood, J.R., Flidner, M.M., Boslaugh, B., Maresch, J. and Fruehn, J. 2003. Imaging and regional distribution of basalt flows in the Faeroe-Shetland Basin. *Geophysical Prospecting* 51: 215-231.
- Whitham, A.G., Morton, A.C. and Fanning, C.M. 2004. Insights into Cretaceous-Palaeogene sediment transport paths and basin evolution in the North Atlantic from a heavy mineral study of sandstones from southern East Greenland. *Petroleum Geoscience* 10: 61-72.
- Woodfin, M., Seedhouse, J., Spadini, G. and Cardamone, M. this volume. Elastic Impedance Inversion to aid lithology prediction in the Palaeocene of the Judd sub-basin. In: Ziska, H. Varming, T. and Bloch, D. (eds.) *Faroe Islands Exploration Conference: Proceedings of the 1<sup>st</sup> Conference, Annales Societatis Scientiarum Faeroensis*, Supplementum 43, Tórshavn.

# New Methods and Techniques for Innovative, Integrated Provenance Studies

DIRK FREI<sup>1\*</sup>, THOMAS RASMUSSEN<sup>1</sup>, CHRISTIAN KNUDSEN<sup>1</sup>, MICHAEL LARSEN<sup>1</sup>, ANDREW WHITHAM<sup>2</sup> AND ANDREW MORTON<sup>3</sup>

1: GEUS, Øster Voldgade 10, DK-1350 København K, Danmark.

\*E-mail: df@geus.dk; Tel: +45 3814 2000, Fax: +45 3814 2050

2: CASP Department of Earth Sciences, University of Cambridge, West Building, 181a Huntingdon Rd, Cambridge, CB3 0DH, UK.

3: HM Research Associates, 100 Main Street, Woodhouse Eaves, Leicestershire, LE12 8RZ, UK.

Department of Geology and Petroleum Geology, University of Aberdeen, Kings College, Aberdeen, AB24 3UE, UK.

## Abstract

When evaluating the petroleum potential of the Faroe-Shetland basin, an understanding of the sand transport processes into the basin during the Maastrichtian to Paleocene is of primary importance. Therefore, detailed provenance analysis that integrate bulk rock chemostratigraphic data with compositional data and age information of a large number of detrital heavy mineral grains are needed. Because conventional methods employed in provenance studies, such as SHRIMP and EMPA, require tedious and time-consuming sample preparation, and hence are relatively expensive, the development of analytical techniques which are more cost-efficient is therefore highly desirable. This paper describes CCSEM and LA-ICP-MS, alternative analytical techniques that are capable of providing the same, or even more detailed information with sufficient precision more rapidly and economically compared to SHRIMP and EMPA. CCSEM and LA-ICP-MS are characterised by straightforward sample preparation, are relatively rapid, and yield the same (and additional) information at a fraction of the costs compared with the conventional methods used in provenance studies. Therefore, CCSEM and LA-ICP-MS are powerful tools that will allow much more detailed insight into the provenance of sedimentary rocks in the future. Additionally, we briefly describe methods suitable for the rapid and cost-effective acquisition of the bulk rock chemostratigraphic data needed in advanced provenance studies.

## Introduction

A key issue for hydrocarbon exploration in the Faroes region is the development of an understanding of sediment dispersal patterns prior to continental break up in the Late Paleocene to Eocene. Sediment provenance studies on Cretaceous and Paleogene strata in the Greenland-Faroes-Shetland region are just beginning to provide an understanding of sediment transport paths (Whitham *et al.*, 2004). The latter authors have shown the benefits of linking the age distributions recorded in specific heavy mineral suites, such as zircon, to conventional heavy mineral data and heavy mineral geochemistry of sandstones.

The appearance of Laser Ablation – Inductively

Coupled Plasma – Mass Spectrometry (LA-ICP-MS) has made it possible to determine, for example, age distributions recorded in populations of detrital zircons rapidly and relatively inexpensively compared with other age dating techniques, such as Sensitive High Resolution Ion MicroProbe (SHRIMP) or Isotope Dilution - Thermal Ionization Mass Spectrometry (ID-TIMS). In addition, LA-ICP-MS can provide information about trace element distributions in detrital garnet and ilmenite that might be used for fingerprinting these minerals.

The Computer Controlled Scanning Electron Microscopy (CCSEM) method, developed and applied for provenance analysis at the Geological Survey of Denmark and Greenland (GEUS), offers

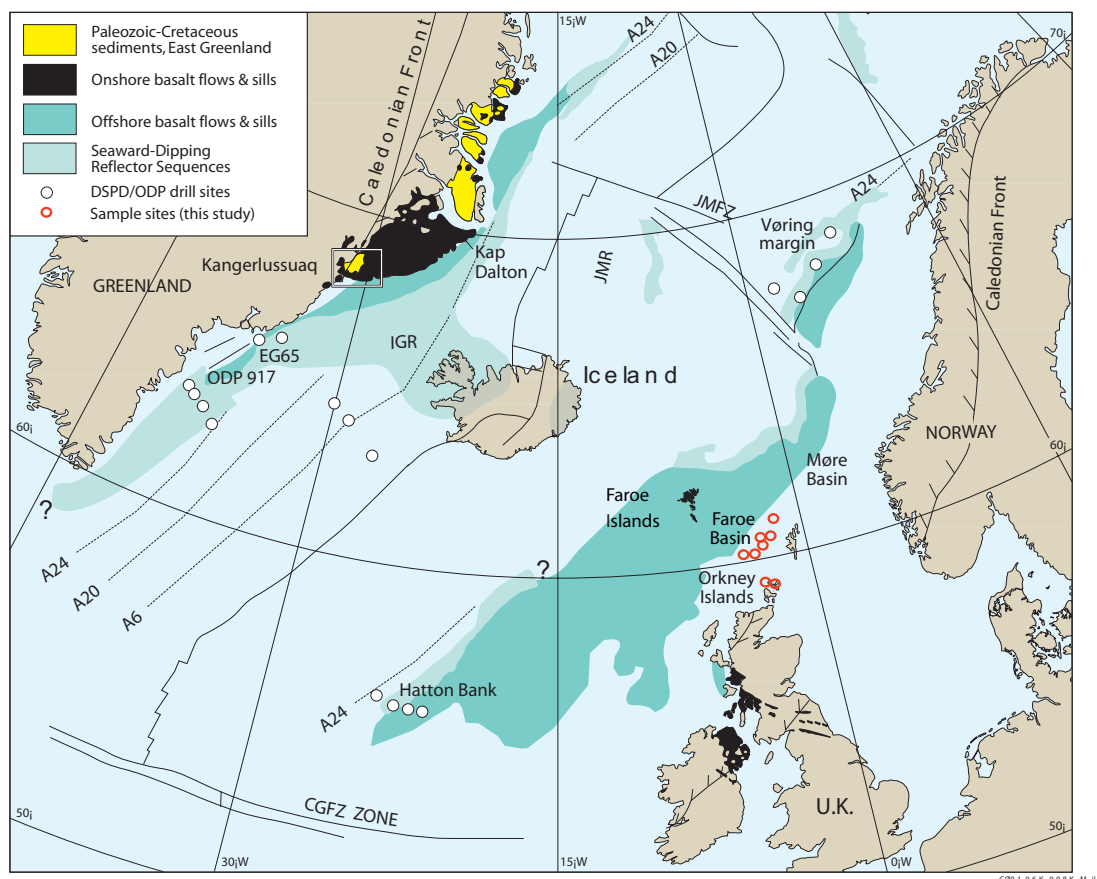


**Figure 1.** Map depicting the location of the samples that are used in this study and the main geological features of the investigated area.

several exciting new possibilities such as the rapid generation of combined mineral chemical, grain size and grain shape data for a large number of grains. However, there is a need to test these methods against those that are conventionally used in provenance studies in order to assess the validity of the results and to delineate the areas for further development. A detailed investigation of sediment dispersal patterns in the Cretaceous and Paleogene strata in the Greenland-Faroes-Shetland region, where a large dataset derived by conventional methods already exists (e.g. Whitham *et al.*, 2004; and references therein), therefore offers the perfect background to test these new methods against a range of hydrocarbon exploration problems.

### Objectives

The primary goal of this part of the SINDRI programme is to conduct a provenance study that helps to establish a depositional model for Creta-

ceous and Paleocene sediments in the East Greenland – Faroese – West of Shetland region. An overview of the study area is provided in Figure 1. Our approach is to integrate data derived by a number of different analytical techniques, i.e. bulk rock major- and trace element geochemistry, CCSEM, and LA-ICP-MS, of which the last two are novel in provenance analysis. Here, we give an overview of the different techniques applied in order to accomplish this goal. In addition to a brief description of the bulk rock geochemical techniques used, we provide a more detailed description of the potential that CCSEM and LA-ICP-MS offer for modern, integrated provenance studies. To this end, we present an introduction to the basic principles of CCSEM and LA-ICP-MS, describe the information that can be derived by these techniques, and compare the results obtained by CCSEM and LA-ICP-MS with those derived by conventional methods. By doing so, we demonstrate the validity of



the data derived by CCSEM and LA-ICP-MS, two methods that are much less work- and cost-intensive compared than those conventionally used in provenance studies.

### Samples

The samples investigated in this study are sandstones from wells and outcrops in three main areas. The geographical distribution of samples is illustrated in Figure 1: (1) Cretaceous and Paleocene sediments from outcrops in the Kangerlussuaq region, East Greenland; (2) cuttings from wells in the West of Shetland region; and (3) samples from outcrops in the Orkney Islands.

### Bulk rock major- and trace element geochemistry

The degree of sediment maturity is very variable in the sediments in the studied area. Apart from classical optical microscopy, major- and trace element analysis provides a rapid insight into the bulk rock composition and the changes it may have suffered during diagenesis and/or transport. Accordingly, a large number of samples have been analysed for their major and trace element compositions. This data offers the possibility of delineating chemostratigraphical correlations within the basin. Additionally, trace element data provides information about the content of heavy minerals such as zircon, monazite, xenotime and Ti-minerals (i.e. rutile, ilmenite, and leucoxene). This allows comparison between the bulk rock data and data obtained through point-counting of individual heavy mineral grains by e.g. conventional methods and by CCSEM.

All samples are analyzed for major-, minor-, and trace elements by XRF and solution ICP-MS to establish a large database for chemostratigraphy. Two grams of each sample are ground to fineness (i.e. particle sizes of 63  $\mu\text{m}$  and below) using a tungsten carbide ball mill and subsequently dried at 110°C for 2 hours. Aliquots of about 1 to 1.5 grams of the resulting powder are subsequently used for bulk chemical analysis.

### Fusion XRF

Homogeneous glass discs are produced by fusing 1 gram of sample powder together with a borate flux. The glass discs are analysed with a Phillips

PW1606 multichannel X-ray fluorescence (XRF) spectrometer at GEUS for all major elements excluding Na, which is determined by atomic absorption spectrometry (AAS). Ba and Sr are determined by XRF because of the better precision compared with ICP-MS due to the very high contents of these elements in most of the samples. Trace element contents are routinely determined by ICP-MS. The combined content of organic material and volatiles are analysed by combustion of the samples. Analytical details, including precision, accuracy, and detection limits are reported by Kystol and Larsen (1999).

### AAS

For the determination of Na by AAS, about 0.25 to 0.5 g of the dried sample is treated with hydrofluoric acid in a PTFE beaker on a hot plate. After evaporation to dryness the residue is dissolved in a hydrochloric acid - potassium chloride solution and Na is determined using a Perkin Elmer PE2280 instrument at GEUS (Kystol and Larsen, 1999).

### ICP-MS

For solution ICP-MS a piece of the glass disc previously used for XRF (see above) is dissolved in a HF-HNO<sub>3</sub> mixture, evaporated to dryness and subsequently redissolved with HNO<sub>3</sub> and evaporated to dryness twice. The dry residue is then dissolved in HNO<sub>3</sub>, and diluted; the resulting solution is analysed for trace elements using a Perkin Elmer 6100 DRC quadrupole ICP-MS at GEUS. The fusion method ensures that refractory minerals such as zircon and chromite are brought completely into solution. Routine analysis of international and in-house geo-standards demonstrated that the precision and accuracy are usually better than 5 % relative for the majority of the elements analysed.

### Computer controlled scanning electron microscopy (CCSEM)

CCSEM is used for the rapid determination of modal abundances, average chemical compositions, grain size distributions, and grain shape parameters of heavy minerals and, where possible, silicates. Furthermore, the maturity of the Ti-minerals (i.e. the average Ti-content of ilmenite, leucoxene and rutile) is determined. Ideally, for CCSEM analysis all mineral grains should not be in grain-to-grain

contact. The CCSEM is consequently vulnerable to poor liberation of mineral grains when dealing with highly indurated rocks such as sandstones from the Kangerlussuaq region. A major task therefore involves ensuring good liberation of individual mineral grains, without seriously affecting the grain-size parameters.

### Basic principles of CCSEM

The CCSEM method was originally developed for the determination of the size, shape, and semi-quantitative composition of particles in environmentally relevant materials, e.g. minerals in coal and fly ashes (Lee *et al.*, 1978; Huggins *et al.*, 1980; Zygarić and Steadman, 1990). However, the method can be used to characterise any particulate matter that can be distinguished, by image analysis techniques, from the surrounding material (usually an embedding resin) by its back-scattered electron reflection. In the scanning electron microscope laboratory at GEUS, a dedicated CCSEM technique was initially set up for the rapid, and hence labour- and cost efficient, screening of the mineralogy, titanium grade and grain size distribution of heavy mineral sands (Laursen, 1997; Sørensen, 1998) during exploration for heavy mineral deposits in Denmark (Knudsen, 1998).

Based on this, the CCSEM method was subsequently developed and refined for the fully automated, rapid and simultaneous determination of the average semi-quantitative chemical composition, grain size distribution, grain size parameters (such as aspect ratio and circularity) and modal abundance of a variety of environmentally stable heavy minerals, such as apatite, chrome spinel, garnet, monazite, rutile, and zircon, which show similar hydraulic and diagenetic behaviour and hence are provenance-sensitive (e.g. Morton and Hallsworth, 1994; 1999).

The basic principle of CCSEM is demonstrated in Figure 2: First, a back-scattered electron (BSE) image with  $512 \times 512$  pixels and with magnifications typically ranging from 30 to 100 times is generated (Figure 2a). Subsequently, grains are segmented from the background by applying grey-level thresholds and the binary image is processed by a “hole-fill” function which fills out minor voids and cracks to simplify the image for subsequent analysis (Figure 2b). This processed binary image is utilized to control the beam during CCSEM

analysis. Clusters of interconnecting pixels are recognized as individual grains and the electron beam is scanned across each grain for 10 seconds in order to acquire data for grain size and shape parameters and energy-dispersive X-ray intensities for specified regions of interest. A guard region filter ensures omission of grains that are cross-cut by the margin of the generated image (Figure 2c).

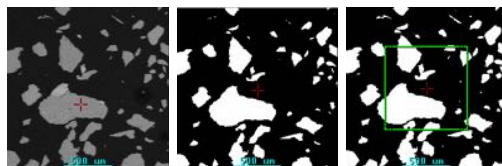


**Figure 2.** Steps involved in fully-automated CCSEM analysis of particulate samples: (a) BSE image ( $512 \times 512$  pixels). (b) “hole-fill” processing of the BSE image generates a processed binary image for microscope control. (c) guard region filter applied. For further explanations see text.

### CCSEM sample preparation and operating conditions

For CCSEM analysis, the bulk sample and a heavy mineral fraction obtained by heavy liquid separation from the bulk sample are embedded in epoxy in 5 mm diameter plastic vials in such a way that no sedimentation occurs during curing of the epoxy and that the majority of the grains do not touch each other. The vials are cut in half longitudinally to obtain a representative section and the section is mounted in epoxy for subsequent grinding and polishing. Prior to analysis, all samples are carbon-coated to facilitate conductivity.

The data presented in this study were acquired using a Philips XL 40 SEM equipped with a ThermoNoran Voyager 2.7 energy dispersive X-ray analysis (EDX) system with integrated control of sample stage and electron beam. The electron beam was generated using a tungsten filament operated at an accelerating voltage of 17 kV and a sample current of typically 50 to 60  $\mu\text{A}$ . A CCSEM analysis typically contains data from between 500 to 1500 measured mineral grains. The collected X-ray data are corrected for e.g. atomic number, absorption or fluorescence effects by the Proza correction scheme. Data reduction is performed on in-house developed software-based spreadsheet calculation programs (Laursen, 1997; Sørensen, 1998).

**Table 1:** Semi-quantitative, average chemical compositions of minerals present in a beach sand from Kulusuk, East Greenland, as determined by CCSEM. A total of 1359 grains have been analysed.

Category	TiO <sub>2</sub>	Fe <sub>2</sub> O <sub>3</sub>	MnO	Cr <sub>2</sub> O <sub>3</sub>	SiO <sub>2</sub>	Al <sub>2</sub> O <sub>3</sub>	MgO	CaO	ZrO <sub>2</sub>	Total
Ilmenite	50.1	39.1	0.7	0.2	4.2	0.9	0.6	2.7	0.2	98.6
Leucoxene	84.0	3.3	0.1	0.5	4.6	4.4	0.3	0.1	0.3	97.6
Rutile	97.2	0.4	0.1	0.0	0.2	0.1	0.1	0.0	0.3	98.4
Ti magnetite	30.9	62.1	0.6	0.3	2.0	0.9	0.8	0.3	0.3	98.2
Magnetite	2.1	84.9	0.4	0.2	1.1	0.6	0.2	0.3	0.4	90.2
Phosphate	0.1	0.3	0.1	0.1	0.5	0.0	0.1	56.2	1.0	58.5 <sup>1</sup>
Garnet	0.1	29.6	0.6	0.1	38.2	20.1	7.9	1.3	0.3	98.2
Kya/Sill	0.1	0.8	0.1	0.5	43.0	54.0	0.1	0.0	0.0	98.5
Zircon	0.1	0.2	0.0	0.0	29.6	0.0	0.0	0.1	64.5	94.4
Pyriboles	0.7	17.0	0.4	0.2	49.6	6.5	14.0	8.1	0.3	96.7

<sup>1</sup>total does not include P<sub>2</sub>O<sub>5</sub>

**CCSEM results**

An example of the information provided by CCSEM analysis is presented in Tables 1 and 2, where the analytical results for beach sand from Kulusuk, East Greenland, are displayed. The data reported comprise the average chemical composition of the mineral species detected (Table 1) and parameters such as aspect ratio, circularity, perimeter length and number of grains counted (Table 2). This information is used to calculate the modal abun-

dances and grain size distributions of the detected minerals.

The grain size distributions obtained for the heavy minerals ilmenite, rutile, magnetite, titanomagnetite, garnet, monazite and mafic silicates (i.e. amphibole, pyroxene and epidote) in beach sands from two contrasting depositional environments in East Greenland are graphically displayed in Figure 3. The different depositional environments of the samples are clearly reflected by the

**Table 2:** Average grain size parameters of minerals present in a beach sand from Kulusuk, East Greenland, as determined by CCSEM. Additional minerals studied but not detected are chromite, monazite, xenotime, sphene, and staurolite. “Silicate” minerals comprise quartz, feldspars, mafic silicates (i.e. pyroxenes, amphiboles and epidote group minerals), and micas.

Category	Aspect ratio	Circularity	Perimeter (µm)	Length (µm)	Area (µm <sup>2</sup> )	Grains counted
Ilmenite	1.6	1.9	638	250	18261	23
Leucoxene	1.4	2.0	896	362	31153	2
Rutile	1.3	1.9	1099	441	68624	8
Ti magnetite	1.5	1.8	655	255	24915	80
Magnetite	1.5	1.8	428	163	10274	16
Pyrite	1.3	2.2	683	282	16769	1
Phosphate	1.5	1.8	790	297	31707	13
Garnet	1.6	2.0	729	292	27366	557
Kya/Sill	1.3	1.7	341	128	5412	1
Zircon	1.6	1.6	520	189	13819	2
Silicate	1.6	1.9	656	260	21766	621
Unclassified	1.3	1.3	274	107	10417	26



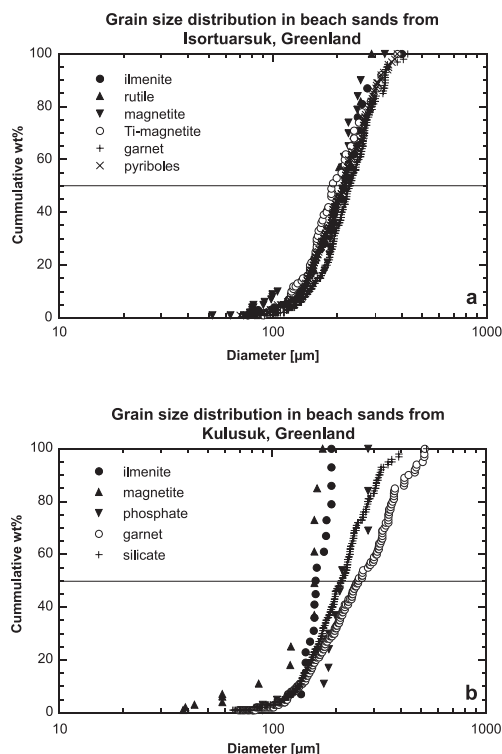


**Figure 3.** Grain size distributions of selected heavy minerals in beach sand samples from Eastern Greenland determined by CCSEM. (a) sand from an active beach foreshore; and (b) sand from uplifted beach terraces. For further explanations see text.

marked difference in observed grain size curves. The sample from an active present-day foreshore (Isortuasuk, Figure 3a) displays the steep, well-sorted and very uniform grain size distribution curves characteristic for this high-energy depositional environment. In contrast, in the sample from an uplifted beach terrace (Kulusuk, Figure 3b) the grain size distribution curves are inhomogeneous and less well-sorted. In this lower-energy depositional environment, the differing hydraulic properties and grain densities of the analysed minerals result in much better sorted grain size distributions and finer grain sizes of very heavy minerals.

The  $\text{TiO}_2$ -distribution in the Ti-mineral fraction (i.e. ilmenite, rutile, and leucosene) of a sediment is a very sensitive indicator for the maturity of the sediment. The continuous alteration of primary ilmenite (with an average stoichiometric  $\text{TiO}_2$  content around 50 wt%; Deer et al., 1992) via pseudorutile to leucosene by leaching of iron, leads to a significant increase in the  $\text{TiO}_2$ -grade of the Ti-min-

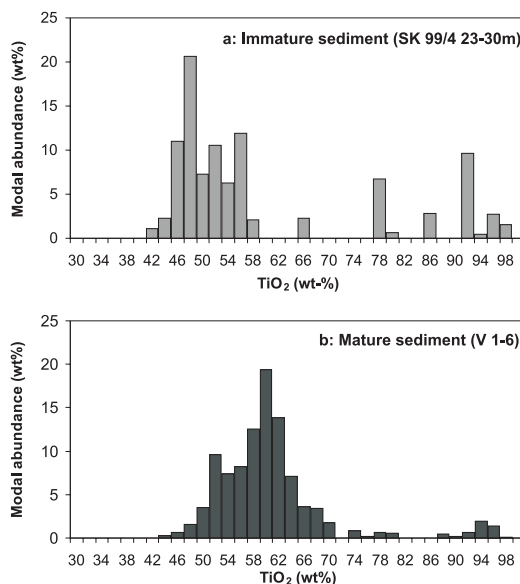


**Figure 4.** Average  $\text{TiO}_2$ -content of the Ti-mineral fraction in immature (a) and mature sediments (b) from wells in Jutland, Denmark, determined by CCSEM (Sk = Skjern; V = Voerslund).

eral fraction in a mature sediment (e.g. Mücke and Bhadra Chaudhuri, 1991). Since CCSEM yields the average chemical compositions of all minerals present in a given sample, the  $\text{TiO}_2$ -distribution of the Ti-mineral fraction can be easily calculated without the need for tedious and time-consuming mineral separation. This is demonstrated in Figure 4a and b, where the average  $\text{TiO}_2$ -contents of the Ti-mineral fraction of sediments from wells in Jutland, Denmark, are graphically displayed. In the sample from Skjern (Figure 4a), the majority of the data scatters around the average  $\text{TiO}_2$  content of about 50 wt%, characteristic of primary, unleached ilmenite, and is pointing to an immature sediment. In contrast, the shift in average  $\text{TiO}_2$ -contents to values around 62 wt% observed in the Voerslund sample (Figure 4 b) is indicative of a more mature sediment.

The compositional variability of the detrital garnet fraction in sediments is a very useful provenance indicator (e.g. Morton, 1985; Morton and Hallsworth, 1994). Garnet compositions are conventionally determined by point-counting a representative number of grains by electron microprobe analyses (EMPA). Grains are hand-picked from dry residues during optical examination under a polarising microscope (Morton, 1985), which is a

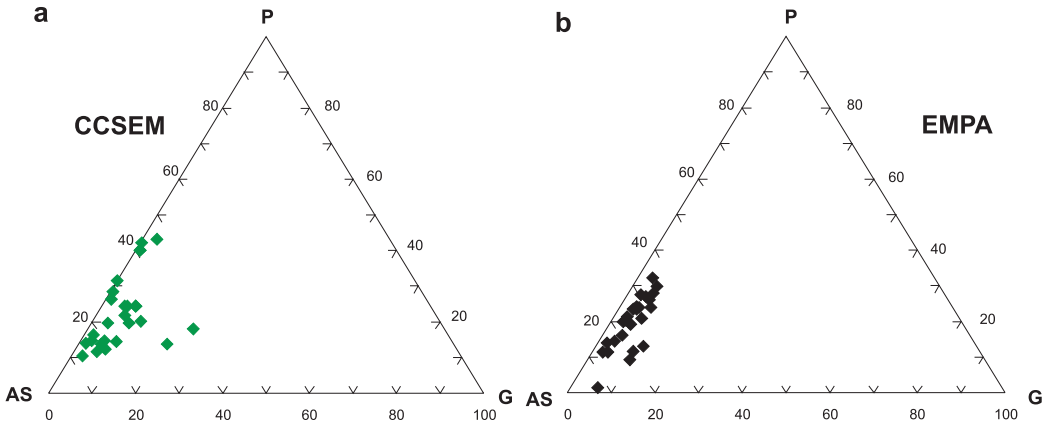


**Figure 5.** Detrital garnet compositions in an Albian sandstone (sample W4629) from Kangerlussuaq, East Greenland: (a) determined by CCSEM (this study); and (b) determined by EMPA (Whitham *et al.*, 2004). AS = almandine + spessartine; P = pyrope; G = grossular.

tedious and time-consuming process. In CCSEM, information on the chemical variability of the garnet fraction in a sample is acquired during routine operation, i.e. no further sample preparation or analytical steps are required.

In order to compare the results obtained by CCSEM with those obtained by conventional methods, we have determined the chemical variability of detrital garnets in an Albian sandstone from Kangerlussuaq, Eastern Greenland. The compositions of detrital garnets have previously been analysed by electron microprobe (Whitham *et al.*, 2004). The results obtained by the two techniques are plotted on ternary diagrams in Fig. 5 using the end-member molecules almandine plus spessartine (AS), pyrope (P), and grossular (G) as poles. Within error, the results obtained by CCSEM are

in excellent agreement with those obtained by conventional EMPA. The apparent minor differences can be readily explained by the fact that the CCSEM analyses are performed as a scan across the whole grain, whereas EMPA analyses are usually conducted by analyzing a point in the core of a grain, with a much higher spatial resolution. Hence, in the case of zoned grains, it is likely that EMPA analyses overrepresent core compositions. In contrast, CCSEM analyses yield chemical data that is more representative of the composition of the entire grain. The only marked difference observed is the presence of two grains with elevated grossular contents detected by CCSEM. Since CCSEM is capable of detecting every grain in a given garnet population, it is likely that these grains have been omitted during EMPA analyses where

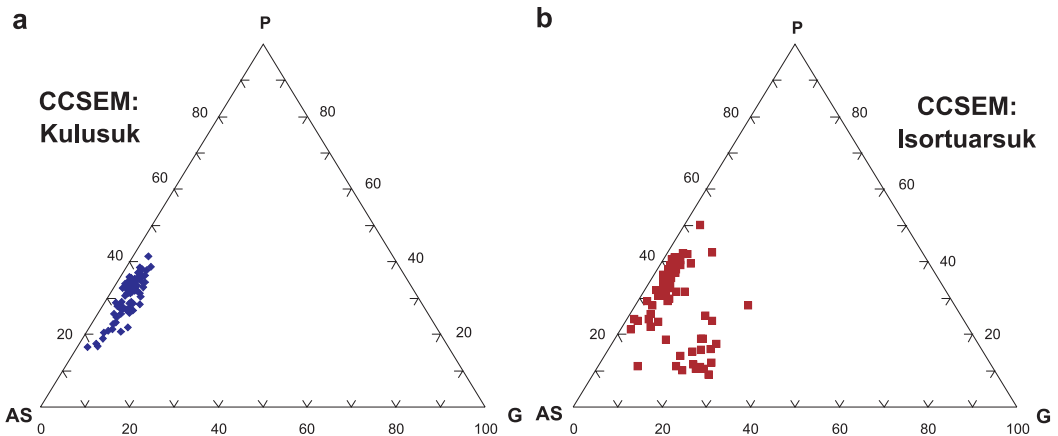


**Figure 6** Detrital garnet compositions in beach sands from East Greenland: (a) Kulusuk and (b) Isortuarsuk. AS = almandine + spessartine; P = pyrope; G = grossular.

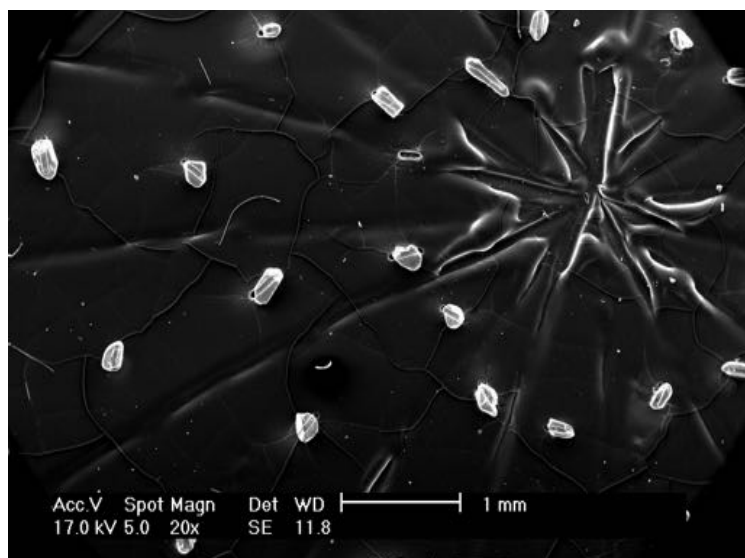


**Figure 7.** Secondary electron photomicrograph of detrital zircon grains mounted on adhesive tape for  $^{207}\text{Pb}$ - $^{206}\text{Pb}$  age dating by LA-ICP-MS. Note the analysis tracks on each grain resulting from laser sampling.

grains are hand-picked and only a selected number of grains from the entire population are therefore analysed.

The potential of CCSEM for the rapid and cost-effective determination of garnet populations from different source regions is further illustrated in Figure 6, where the compositions of detrital garnets determined by CCSEM in beach sands from Kulusuk (Figure 5a) and Isortuasuk (Figure 5b), East Greenland, are plotted on ternary diagrams in the same fashion as in Figure 4. The garnets from Kulusuk display a unimodal distribution along the almandine/spessartine-pyrope join, pointing to a single source. In marked contrast, garnets from Isortuasuk plot into two distinctive groups: (1) a group with compositions along the almandine/spessartine-pyrope join; and (2) a second group with higher grossular and lower pyrope contents, pointing to a sediment input from at least two different sources.

### Laser Ablation–Inductively Coupled Plasma–Mass Spectrometry (LA-ICP-MS)

Two different types of analysis using LA-ICP-MS are of significance for integrated provenance studies: (1) Dating of detrital zircons using  $^{207}\text{Pb}/^{206}\text{Pb}$ -ratios; and (2) determination of trace element distributions in garnets and ilmenites for fingerprinting these phases. Here, we present the

age-dating results for detrital zircons in three different sandstones from the Kangerlussuaq area using  $^{207}\text{Pb}/^{206}\text{Pb}$ -ratios. The results are compared with conventional SHRIMP data obtained on the same set of samples in order to evaluate the extent to which the much faster and cheaper LA-ICP-MS technique can produce data of sufficient precision.

### Basic principles of LA-ICP-MS

Laser ablation – inductively coupled plasma – mass spectrometry (LA-ICP-MS) was developed as a trace element microprobe for geomaterials in the early nineties (e.g. Arrowsmith, 1987; Denoyer *et al.*, 1991; Pearce *et al.*, 1992). In LA-ICP-MS, a

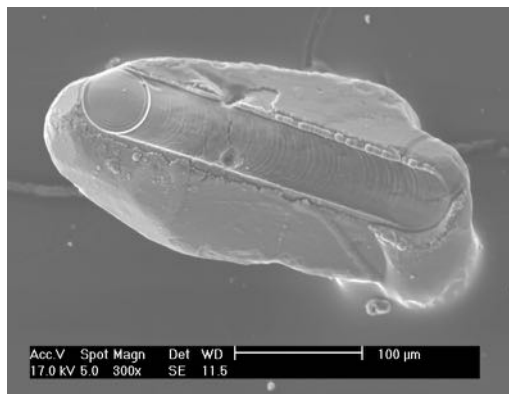


**Figure 8.** Secondary electron photomicrograph of a detrital zircon grain after  $^{207}\text{Pb}$ - $^{206}\text{Pb}$  age analysis by LA-ICP-MS. Note that the laser has sampled only the outer rim of the grain.



laser ablation sampling device is coupled to a mass spectrometer analyser; this combination utilizes a relatively simple and inexpensive instrument capable of analysing elemental concentrations in-situ in solid samples with a high spatial resolution and low detection limits. In addition, isotopic ratios can be determined simultaneously with moderate precision (0.1 to 2% relative standard deviation, depending on the operating conditions, the isotopic system investigated and the equipment used). Solid samples are held in a cell at atmospheric pressure and sub-micron particles are ablated from the surface using a laser. The ablated particles are dispersed into an Ar carrier-gas and flushed into the mass spectrometer for analysis. This setup requires only minimum sample preparation and allows quick sample exchange. For an in-depth description and discussion of the capabilities of modern, state-of-the-art LA-ICP-MS systems, the reader is referred to Sylvester (2001).

#### **LA-ICP-MS sample preparation and operating conditions**

For LA-ICP-MS age determinations, zircons were separated from the bulk samples using conventional heavy liquid and magnetic separation methods. The final separation step was made by hand-picking individual zircon grains from the heavy and non-magnetic fraction using an optical microscope. For analysis, the individual zircon grains are mounted on adhesive tape in a fashion where each grain can be unequivocally related to its LA-ICP-MS age determination for subsequent optical inspection (Figure 7).

All analyses were performed using a Cetac LSX 200 laser ablation system equipped with a frequency quadrupled ND-YAG laser emitting at a wavelength of 266 nm, coupled to a Perkin Elmer 6100 DRC quadrupole ICP-MS at GEUS. The nominal pulse width of the laser is < 4 ns with a pulse-to-pulse stability of 1%. The laser was operated at a repetition rate and pulse energy of 20 Hz and 6 mJ, respectively, for the analyses presented in this study. All data presented here were acquired with a single line scan on each individual zircon grain and with beam diameters of approximately 40 to 50  $\mu\text{m}$ . An example of a single line scan used for analysis is displayed in Figure 8. All measurements were performed in time-resolved analysis (TRA) mode

using peak jumping with 1 point per peak. The total acquisition time for each analysis varied between 60 to ~70 s depending on grain size with the first ~20 s used to measure the gas blank. The instrument was tuned to give large, stable signals for the  $^{207}\text{Pb}$  and  $^{238}\text{U}$  peaks, low background count rates (typically below 10 counts per second for  $^{207}\text{Pb}$ ) and low oxide production rates ( $^{232}\text{Th}^{16}\text{O}/^{232}\text{Th} < 0.2\%$ ). The following isotopes were measured:  $^{204}\text{Pb}$ ,  $^{206}\text{Pb}$ ,  $^{207}\text{Pb}$ ,  $^{208}\text{Pb}$ , and  $^{202}\text{Hg}$  to monitor the  $^{204}\text{Hg}$  interference on  $^{204}\text{Pb}$  (using a  $^{202}\text{Hg}/^{204}\text{Hg}$ -ratio of 4.36). It was found that the net intensities for mass 204, corrected for  $^{204}\text{Hg}$ , are below the limit of detection (defined as three times the standard deviation of the background intensity) and hence no common Pb-correction was performed. Given the fact that limpid zircons have only a very small amount of common Pb and the average precision of  $^{207}\text{Pb}$ - $^{206}\text{Pb}$  age measurements (usually 5 - 10 % relative), the inability to correct for the presence of common Pb in the sample and standard is insignificant for the accuracy of the  $^{207}\text{Pb}$ - $^{206}\text{Pb}$  ages presented here. The instrumental mass bias during ablation on  $^{207}\text{Pb}/^{206}\text{Pb}$ -ratios was corrected using the NIST SRM 612 glass reference material. The use of an external standard implies that the mass bias factor remains constant during a reasonable time interval. In order to minimise time-dependent variations in the mass bias factor, the standard was analysed every 20 to 25 minutes. Data reduction and concentration calculations were performed off-line using in-house developed spreadsheets. The computer program IsoplotEx v. 2.60 (Ludwig, 1999) was used to carry out the final computation of Pb-Pb ages.

#### **LA-ICP-MS results**

##### *Lead-lead geochronology of zircon – comparison of LA-ICP-MS and SHRIMP*

Analysis of the crystallisation ages of detrital zircon grains in clastic sediments has proved to be a powerful tool in sedimentary provenance studies. Zircon is very resistant to physical and chemical alteration and U-Pb dating of detrital zircons can therefore yield the age of their sources, even after metamorphism and deformation. Previous studies have demonstrated that accurate and precise U-Pb ages of about 80 to 100 zircon grains in a sample are sufficient to detect the major sedimentary source components (Dodson *et al.*, 1988; Morton

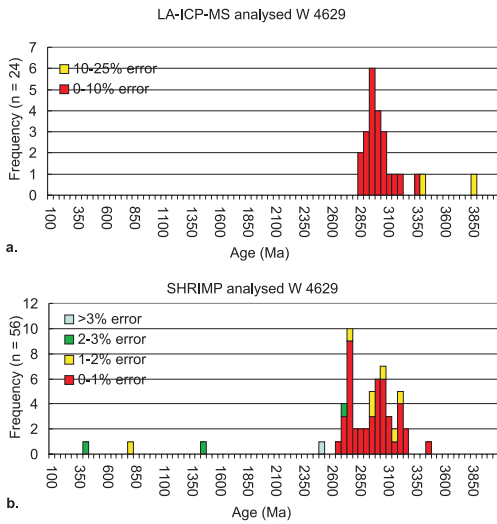


**Figure 9.** (a) Histogram of  $^{207}\text{Pb}/^{206}\text{Pb}$  zircon ages from Albian sandstones (sample W4629, cf. Whitham *et al.*, 2004) from Kangerlussuaq, southern East Greenland, determined by LA-ICP-MS. (b) Histogram of U-Pb zircon ages from the same sample obtained by SHRIMP (Whitham *et al.*, 2004).

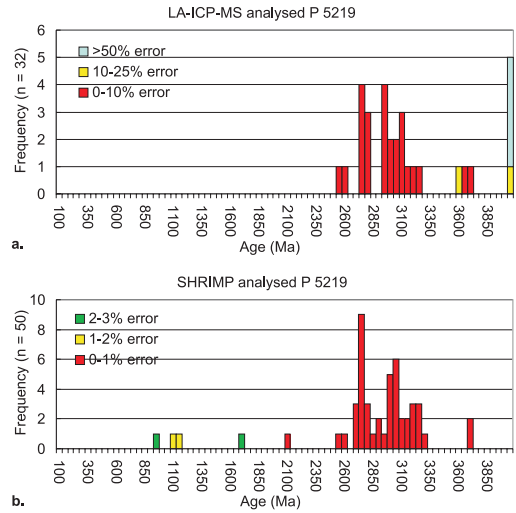


**Figure 11.** (a) Histogram of  $^{207}\text{Pb}/^{206}\text{Pb}$  zircon ages from Paleocene sandstones (sample P5219, cf. Whitham *et al.*, 2004) from Kangerlussuaq, southern East Greenland, determined by LA-ICP-MS. (b) Histogram of U-Pb zircon ages from the same sample obtained by SHRIMP (Whitham *et al.*, 2004).

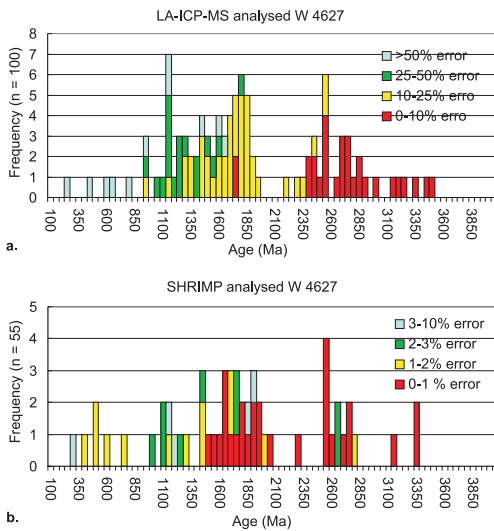


**Figure 10.** (a) Histogram of  $^{207}\text{Pb}/^{206}\text{Pb}$  zircon ages from Maastrichtian sandstones (sample W4627, cf. Whitham *et al.*, 2004) from Kangerlussuaq, southern East Greenland, determined by LA-ICP-MS. (b) Histogram of U-Pb zircon ages from the same sample obtained by SHRIMP (Whitham *et al.*, 2004).

*et al.*, 1996; Whitehouse *et al.*, 1997; Fernandez-Suarez *et al.*, 2000).

The currently most widely accepted and used techniques for the determination of U-Pb ages are SHRIMP and ID-TIMS. When combined with air

abrasion and low analytical blanks, these techniques yield the most precise and accurate ages for single zircon grains or domains of single grains (Krogh, 1973; 1982). Besides the high purchasing and operating costs for instrumentation, the major drawback of these techniques is that they need highly specialized personnel and time-consuming sample preparation.

The potential of LA-ICP-MS as a low cost alternative for U-Pb zircon dating was recognized relatively early (e.g. Feng *et al.*, 1993; Fryer *et al.*, 1993), but its application was hampered by the inability to yield reliable U/Pb values. Although this drawback has been overcome by the recent technical developments (e.g. Kösler *et al.*, 2002), the most attractive feature of LA-ICP-MS with respect to provenance studies remains its ability to produce  $^{207}\text{Pb}$ - $^{206}\text{Pb}$  ages of detrital zircon grains with sufficient precision (usually in the 1 to 10% range), minimal sample preparation, high sample throughput and low costs (Machado and Gauthier, 1996). It is therefore surprising that its application in sedimentary provenance studies is still in its infancy. This might be partly due to the absence of studies that compare age information derived by  $^{207}\text{Pb}$ - $^{206}\text{Pb}$  dating using LA-ICP-MS with those derived by conventional U-Pb dating using

SHRIMP or ID-TIMS that document the reliability of the age information derived by LA-ICP-MS. We have therefore carried out a comparison study based on Cretaceous to Paleogene sandstones from the Kangerlussuaq area, East Greenland, where the age distributions of detrital zircon populations have previously been analysed by U-Pb-dating using SHRIMP (Whitham *et al.*, 2004).

The results obtained are displayed in histograms in Figures 9 to 11. The most important result is that, within analytical error, the age distributions of the zircon populations determined by the two methods are in excellent agreement. For all three investigated samples, the overall patterns are identical and all significant age groups identified by SHRIMP are also recognized by LA-ICP-MS. Moreover, the relative frequency of occurrence in each age group is, apart from minor deviations, strikingly similar. The zircon ages in the Albian sandstone (sample W 4629; Figure 9) all fall in one large age group between 2600 to 3300 Ma. Within this group, three minor clusters at 2720 Ma, 2960 to 3120 Ma, and 3180 Ma can be distinguished in the SHRIMP determinations. Additionally, the SHRIMP method reveals individual occurrences of relatively young zircons and a single zircon with a Paleoproterozoic age undetected by LA-ICP-MS. This is probably due to the small number of zircon grains (total number = 24) that could be separated and analysed by LA-ICP-MS. In contrast, the observed zircon age distribution in the Maastrichtian sandstone (sample W 4627; Figure 10) is relatively complex. However, the same five groups of zircon ages (900 to 1300, 1450 to 1500, 1600 to 2000, 2500 to 2600, and 2700 to 2800 Ma) are distinguished by both techniques. Furthermore, both techniques indicate the minor presence of young Caledonian (~450 Ma) and old Archean (~3100 to 3500 Ma) zircons, and several relatively young zircons (< 800 Ma). The zircon age distribution in the Early Eocene sandstone (sample P 5219; Figure 11) is similar to the age distribution observed in the Albian sandstone (sample W 4629; cf. Figure 9) with one large age group ranging from ~2600 to ~3300 Ma that can be subdivided into three distinctive clusters around 2700 to 2750, 2950 to 3100, and 3200 Ma. Both methods reveal the presence of older, Paleoproterozoic grains (~3700 Ma).

## Conclusions

The most important result of this contribution is that, within analytical error, the age distributions of the zircon populations determined by SHRIMP U-Pb-dating and LA-ICP-MS  $^{207}\text{Pb}$ - $^{206}\text{Pb}$ -dating are in excellent agreement. Although the patterns for all three investigated samples are not identical, they are reassuringly similar and all significant age groups identified by SHRIMP are also recognized by LA-ICP-MS. It has been shown that it is possible to analyse up to 200 grains per day using the LA-ICP-MS, with a minimum of sample preparation, and using simpler, more robust equipment than with the SHRIMP.

Another finding is that it is possible to determine the compositional variations of detrital garnet populations using CCSEM. Within error, the results obtained by CCSEM are in excellent agreement with those obtained by conventional EMPA. The apparent minor differences can be readily explained by the fact that the CCSEM analyses are performed as a scan across the whole grain, whereas EMPA analyses are usually conducted by analyzing a point in the core of a grain, with a much higher spatial resolution. Hence, in the case of zoned grains, it is likely that EMPA analyses overrepresent core compositions. In contrast, CCSEM analyses yield chemical data that is more representative of the composition of the whole grain.

Finally the CCSEM analyses yield data concerning other properties, such as the titanium content of ilmenite/leucosene, which reflects the chemical maturity of the host sediment. The CCSEM analyses further have the potential of yielding information on grain sizes and grain shapes. However, because of the highly indurated character of the sediments analysed there are apparent problems with the liberation of the heavy mineral fraction without affecting the size- and shape-characteristics of the minerals. Further research is needed to reconcile the observed differences between classical grain size and grain shape analytical techniques and CCSEM in order to establish CCSEM as a reliable method for the determination of grain sizes and grain shape parameters of the heavy mineral suite present in highly indurated sediments.



## Acknowledgements

The results presented here are a part of a study conducted by GEUS and CASP in the period October 2001 to March 2005 generously supported by the SINDRI programme, which the authors gratefully acknowledge. Many thanks are due to Ingerlise Nørgaard and Hanne Lamberts for sample preparation and to Jørgen Kystøl for support during CCSEM and LA-ICP-MS analysis. We would also like to thank Julie Alison Hollis for an unofficial review of this contribution. The comments and suggestions of J. Richard Wilson helped to improve the final shape of the manuscript and are greatly appreciated. This paper is published with the permission of the Geological Survey of Denmark and Greenland.

## References

- Arrowsmith, P. 1987. Laser ablation of solids for elemental analysis by inductively coupled plasma mass spectrometry. *Analytical Chemistry* 59: 1437-1444.
- Deer, W.A., Howie, R.A. and Zussman, J. 1992. An introduction to the rock forming minerals. Longman Scientific & Technical, Harlow, Essex, England.
- Denoyer, E.R., Kenneth, J.F. and Hager, J.W. 1991. Laser solid sampling for inductively coupled plasma mass spectrometry. *Analytical Chemistry* 63: 445A-457A.
- Dodson, M.H., Compston, W., Williams, I.S. and Wilson, J.F. 1988. A search for ancient detrital zircons from Zimbabwean sediments. *Journal of the Geological Society, London* 145: 977-983.
- Feng, R., Machado, N. and Ludden, J. 1993. Lead geochronology of zircon by LaserProbe - Inductively Coupled Plasma Mass Spectrometry (LP-ICPMS). *Geochimica et Cosmochimica Acta* 57: 3479-3486.
- Fernandez-Suarez, J., Gutierrez-Alfonso, G., Jenner, G.A. and Turbrett, M.N. 2000. New ideas on the Proterozoic-Early Paleozoic evolution of NW Iberia: insights from U-Pb detrital zircon ages. *Precambrian Research* 102: 185-206.
- Fryer, B.J., Jackson, S.E. and Longerich, H.P. 1993. The application of laser microprobe-inductively coupled plasma-mass spectrometry (LAM-ICP-MS) to in situ (U)-Pb geochronology. *Chemical Geology* 109: 1-8.
- Huggins, F.E., Kosmack, D.A., Huffman, G.P. and Lee, R.J. 1980. Coal mineralogies by SEM automatic image analysis. *Scanning Electron Microscopy* 1: 531-540.
- Köslér, J., Fonneland, H., Sylvester, P., Tubrett, M. and Pedersen, R.-B. 2002. U-Pb dating of zircons for sediment provenance studies - a comparison of laser ablation ICPMS and SIMS techniques. *Chemical Geology* 182: 605-618.
- Knudsen, C. 1998. Heavy mineral exploration in Miocene sediments, Jylland. *Danmarks og Grønlands Geologiske Undersøgelse Rapport* 1998/45.
- Krogh, T.E. 1973. A low-contamination method for hydrothermal decomposition of zircon and extraction of U and Pd for isotopic age determinations. *Geochimica et Cosmochimica Acta* 37: 485-494.
- Krogh, T.E. 1982. Improved accuracy of U-Pb ages by the creation of more concordant systems using an air abrasion technique. *Geochimica et Cosmochimica Acta* 46: 637-649.
- Kystøl, J. and Larsen, L.M. 1999. Analytical procedures in the Rock Geochemical Laboratory of the Geological Survey of Denmark and Greenland. *Geology of Greenland Survey Bulletin* 184: 59-62.
- Laursen, K. 1997. Advanced scanning electron microscope analysis at GEUS. *Danmarks og Grønlands Geologiske Undersøgelse Rapport* 1997/1.
- Lee, R.J., Huggins, F.E. and Huffman, G.P. 1978. Correlated Mössbauer-SEM studies of coal mineralogy. *Scanning Electron Microscopy* 1: 561-568.
- Ludwig, K.R. 1999. IsoplotEx 2.6. *Berkeley Geochronological Center Publication* 1a
- Machado, N. and Gauthier, G. 1996. Determination of <sup>207</sup>Pb/<sup>206</sup>Pb ages on zircon and monazite by laser-ablation ICPMS and application to a study of sedimentary provenance and metamorphism in southeastern Brazil. *Geochimica et Cosmochimica Acta* 60: 5063-5073.
- Morton, A.C. 1985. A new approach to provenance studies: electron microprobe analysis of detrital garnets from Middle Jurassic sandstones of the northern North Sea. *Sedimentology* 32: 553-566.
- Morton, A.C. and Hallsworth, C.R. 1994. Identifying provenance-specific features of detrital heavy mineral assemblages in sandstones. *Sedimentary Geology* 90: 241-256.
- Morton, A.C., Claué-Long, J.C. and Berge, C. 1996. SHRIMP constraints on sediment provenance and transport history in the Mesozoic Statfjord formation, North Sea. *Journal of the Geological Society, London* 153: 915-929.
- Morton, A.C. and Hallsworth, C.R. 1999. Processes controlling the composition of heavy mineral assemblages in sandstones. *Sedimentary Geology* 124: 3-29.
- Mücke, A. and Bhadra Chaudhuri, J.N. 1991. The continuous alteration of ilmenite through pseudorutile to leucocene. *Ore Geology Reviews* 6: 25-44.
- Pearce, N.J., Perkins W.P., Abell, L., Duller, G.A. and Fuge, R. 1992 Mineral microanalysis by laser ablation inductively coupled mass spectrometry. *Journal of Analytical Atomic Spectroscopy* 7: 53-57.
- Sørensen, H.S. 1998. Computer controlled scanning electron microscopy (CCSEM) of heavy minerals. *Danmarks og Grønlands Geologiske Undersøgelse Rapport* 1998/74.
- Sylvester P. 2001 (ed). Laser-Ablation-ICPMS in the Earth Sciences - principles and applications. *Mineralogical Association of Canada Short Course Series* 29.
- Whitham, A.G., Morton, A.C. and Fanning, C.M. 2004. Insights into Cretaceous-Palaeogene sediment transport paths and basin evolution in the North Atlantic from a heavy mineral study of sandstones from southern East Greenland. *Petroleum Geoscience* 10: 61-72
- Whitehouse, M.J., Bridgewater, D. and Park, R.G. 1997. Detrital zircon ages from the Loch Maree Group, Lewisian Complex, NW Scotland: confirmation of

Paleoproterozoic Laurentia-Fennoscandia connection.  
*Terra Nova* 9: 260-263.

Zygarlicke, C.J. and Steadman, E.N. 1990. Advanced SEM techniques to characterise coal minerals. *Scanning Electron Microscopy* 4: 579-590.

# An Updated View of the Faroes-Shetland Petroleum System

STEVE CAWLEY<sup>1\*</sup>, HAMISH MATHESON<sup>2</sup> AND GORDON STALKER<sup>3</sup>

1: BP Exploration Ltd., Farburn Industrial Estate, Dyce, Aberdeen, AB21 7PB, UK.

\*E-mail: cawleysj@bp.com; Tel: +44 1224 833937; Fax: +44 1224 833882.

2: BP Exploration Ltd., Chertsey Road, Sunbury-on-Thames, Middlesex, TW16 7LN, UK.

3: RML Consulting Ltd, 7 Bon Accord Square, Aberdeen, AB11 6DJ, UK.

## Abstract

After disappointing drilling results, BP (for BP:Shell in Faroes License 004) reviewed their risking of the Petroleum System components of the Faroes-Shetland Basin:

- Reservoir Presence
- Reservoir Effectiveness
- Top Seal Effectiveness
- Charge Access

A risk model was built from the Base Tertiary to the top of the Palaeocene T36 Sequence. This had three aims:

1. Identify areas of regional prospectivity.
2. Quantify and visualize charge risk via migration fetch-area mapping.
3. Communicate predicted modes of failure in high-risk areas.

### Conclusions:

Basin general:

- Reservoir presence is generally low risk but effectiveness is highly variable.
- Seal effectiveness is variable and a key control on charge access.
- Charge is generally medium risk but access is a complex plumbing issue governed by 3D seal distribution.

License 004 specific (Figure 1.1):

- T36 is the most prospective sequence; low geological model risk and medium charge risk.
- T34 Kunoy Prospect has medium risk on reservoir effectiveness, seal presence and access to charge.
- T31 Kunoy Prospect has medium/high risk on reservoir presence and high risk on seal effectiveness.

## 1. Introduction

There are four risk components that define the Petroleum System of a sedimentary basin:

- Reservoir Presence
- Reservoir Effectiveness
- Seal (Presence and) Effectiveness
- Charge Access

This paper describes an updated view of these risk components, built into an integrated composite risk model for the Faroes-Shetland Basin. The

structure of the paper follows a workflow of risk component evaluation and addresses recent drilling results. Note that Trap formation was not part of this basin-scale risk analysis.

The area of interest (AOI) of the evaluation was defined by the limits of a set of merged 3D seismic surveys (Figure 1.1). Figure 1.2 presents a summary chronostratigraphy of the general area whilst Figure 1.3 is a schematic of the general play system.



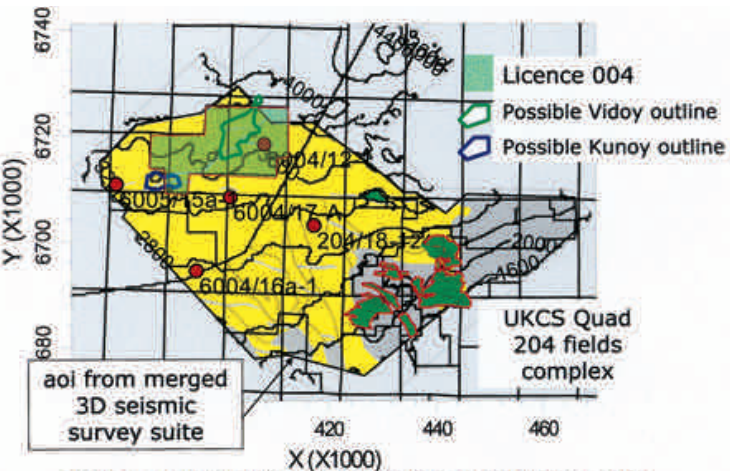
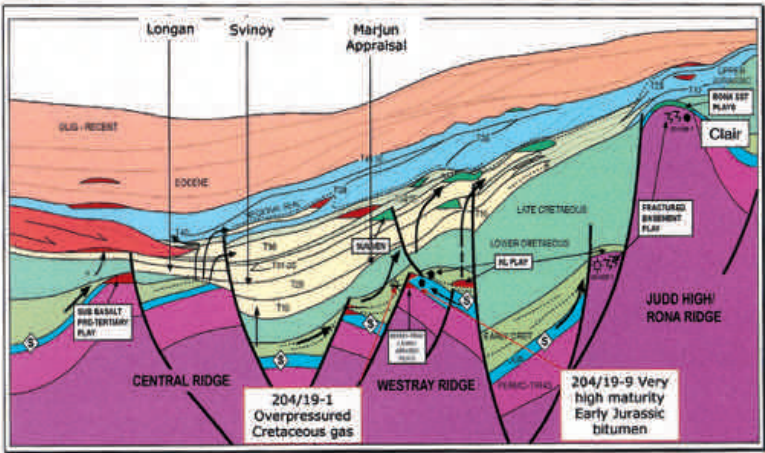


**Figure 1.3.** Faroes-Shetland Play Summary. This schematically illustrates the critical elements of the petroleum system (Jurassic source rocks and Tertiary reservoirs). The main Tertiary and pre-Tertiary pools are shown as are the approximate locations of some recent Faroes licence wells.



3. Reservoir Presence and Effectiveness Risk

Reservoir Presence risk in each Tertiary sequence was assessed using a G(ross)D(epositional)E(nvironment) approach:

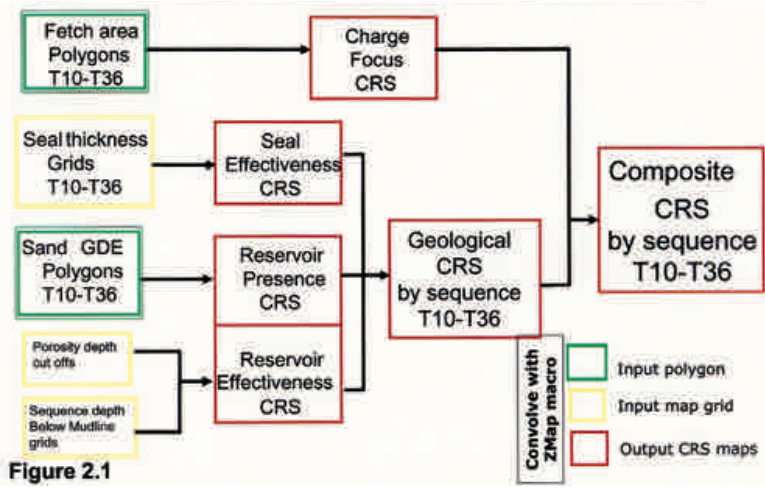
1. Net Sand thickness and sequence Net:Gross were estimated using gamma ray log cut-offs in wells.
2. Sequence seismic isochores, tied to wells using updated biostratigraphic control, were used as trend forms to interpret areal sand distribution – isochore thicks were interpreted to be areas of higher general sequence Net:Gross.
3. Intra-sequence seismic architecture and character were used to identify sand-prone deposition
4. RMS amplitude extraction windowed between defined levels and strongly tied to the

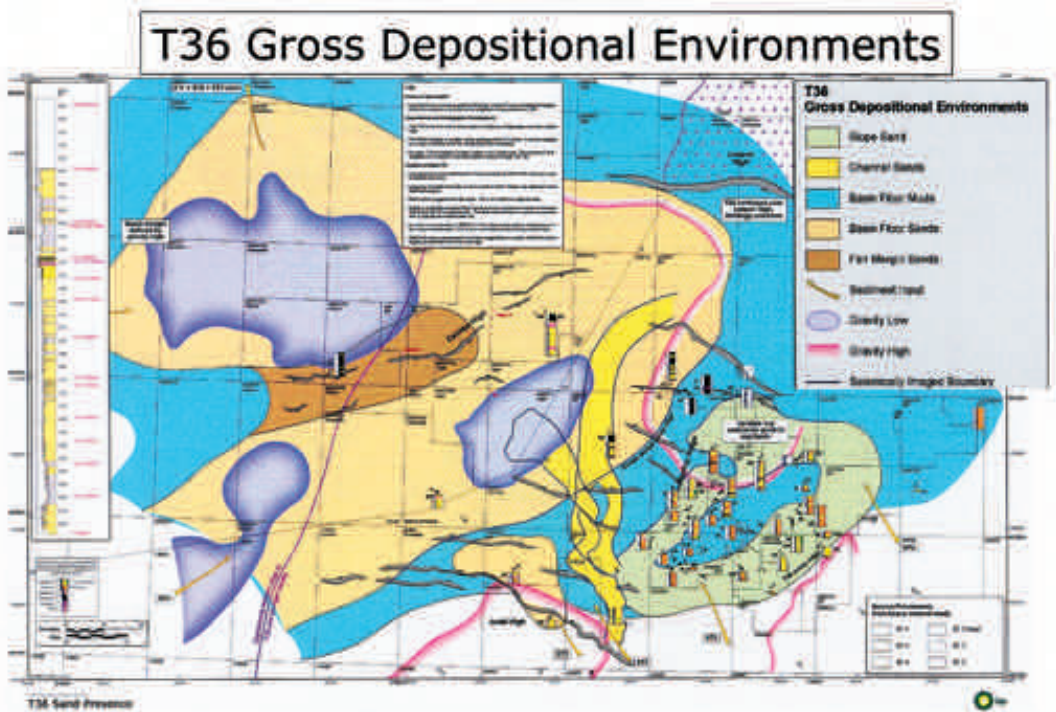
recent Faroes wells completed the interpretation.

Figure 3.1 shows an example GDE map, for the T36 Sequence. The interpreted facies distribution was translated into Reservoir Presence risk as shown in Figure 3.2. Note that all sand presence interpretation from outside the study AOI (e.g. from pre-existing GDE interpretations) has been risked at a “Medium risk” level. Basin floor muds are High Risk for Reservoir Presence.

Reservoir Effectiveness risk was defined from compaction trends and porosity:permeability relationships for the Palaeocene sequences. These trends were derived from quantitative log, core and sidewall core data. The object was to define

**Figure 2.1.** Petroleum Systems Evaluation through Common Risk Segment (CRS) mapping. This shows the workflow and inputs into the overall risking process and the deliverables – Composite Common Risk Segment maps for each Tertiary sequence

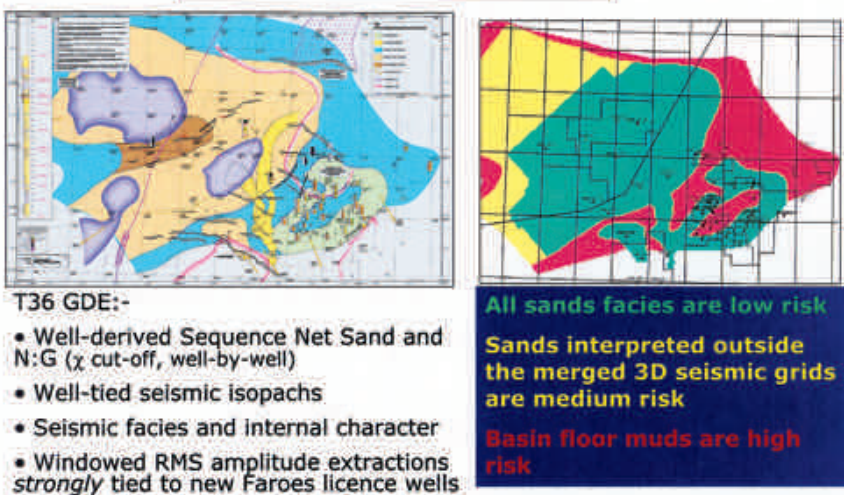




**Figure 3.1.** T36 Gross Depositional Environments. This figure shows the G(ross)D(epositional)E(nvironment) for an example Tertiary sequence – the T36. Well logs and well-tied seismic mapping of bounding surfaces, internal depositional structure and windowed amplitude expression all contribute to the lithological interpretation for the presence/absence of sand, reservoir Net:Gross and overall depositional environment.

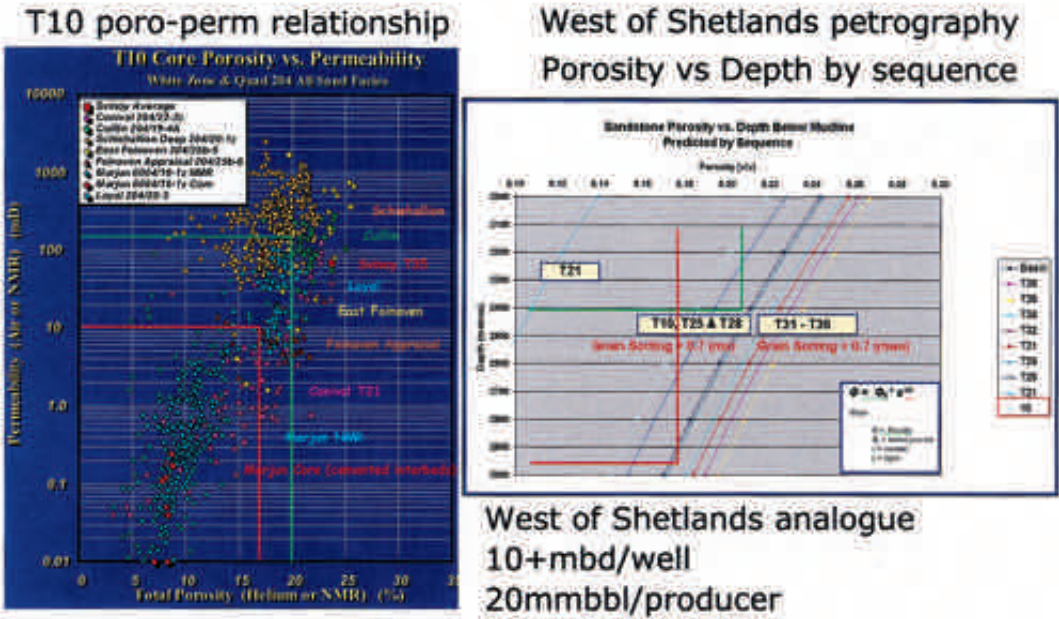
simple but robust depth cut-offs for Effectiveness risk bins which could be mapped across the whole AOI. The West Shetlands fields provided the analogue data to describe an economic limit for risk bins. Reservoirs should be able to flow at approximately 10,000+ bbl/day and producers should access 20mmbbl of reserves.

Figures 3.3 and 3.4 show the poro-perm ranges estimated to deliver the economic rates and their depth below mudline windows. Figure 3.5 translates the depth:risk windows into a CRS distribution for an example sequence, the T10 (the deepest Palaeocene unit). The Reservoir Effectiveness map is very much a function of burial depth.

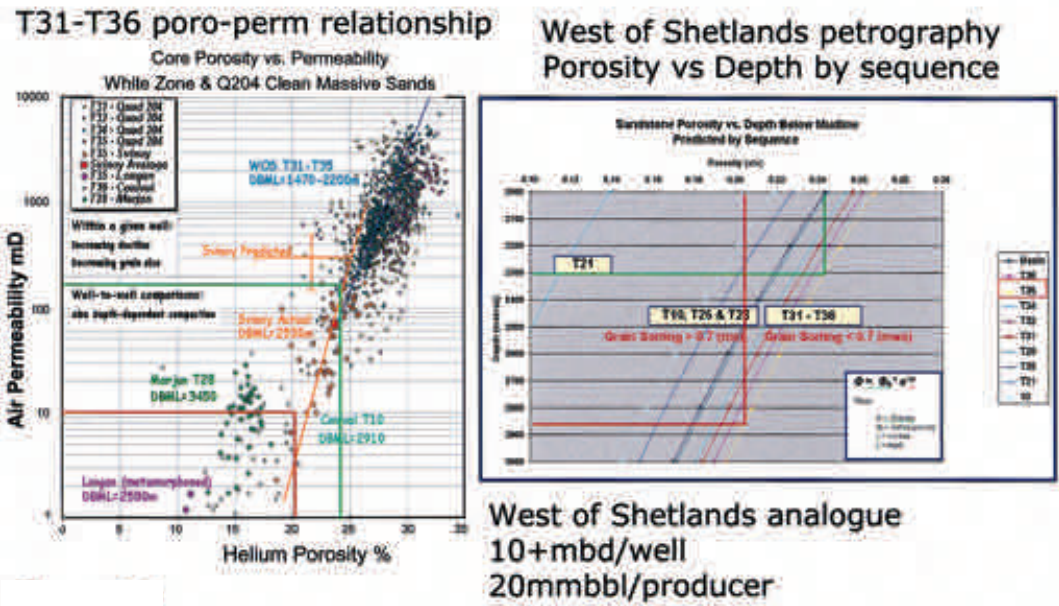


**Figure 3.2.** Reservoir Presence CRS. This shows how a sequence GDE (here the T36) interpretation for presence/absence of sand, Net:Gross etc., is converted into areas of Common Risk at Low, Medium or High levels for Reservoir Presence.

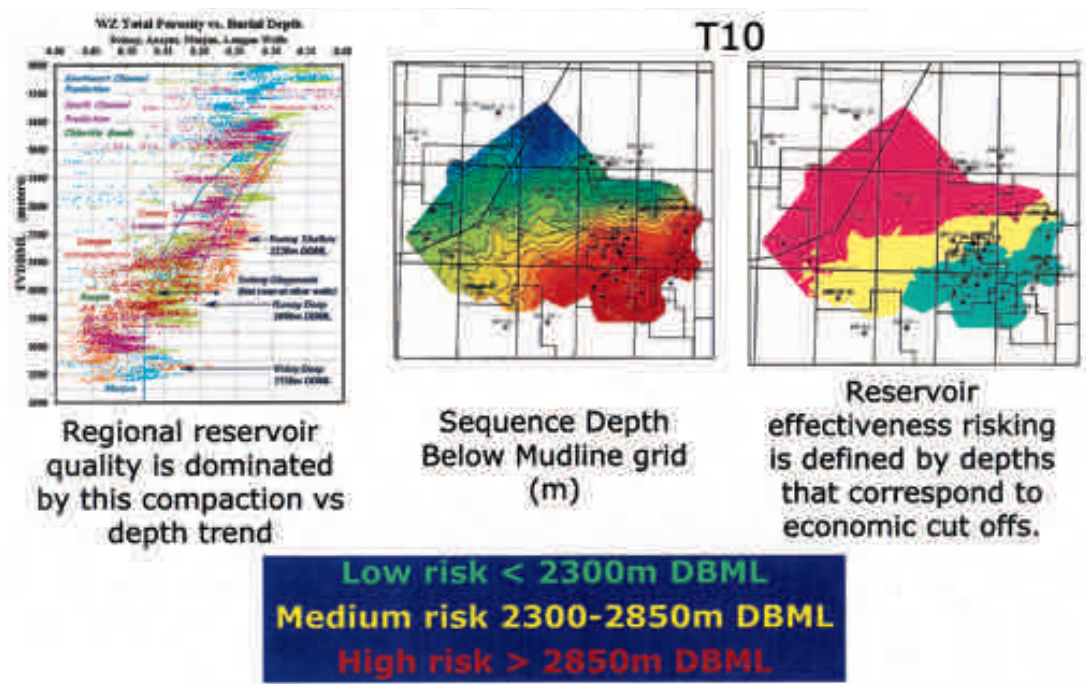




**Figure 3.3.** T10-T28 Reservoir Effectiveness. The figure shows predicted compaction curves for each Tertiary sequence based on BP-in house lithology and provenance studies. Core and SWC porosity:permeability correlations are also shown. These two parameter sets combine to create a prediction of reservoir deliverability properties as a function of depth below mudline (seabed). Low and High Risks are governed by porosity (volume) and permeability (flow) limits for the rates and reserves required to meet Q204 fields analogue economics.



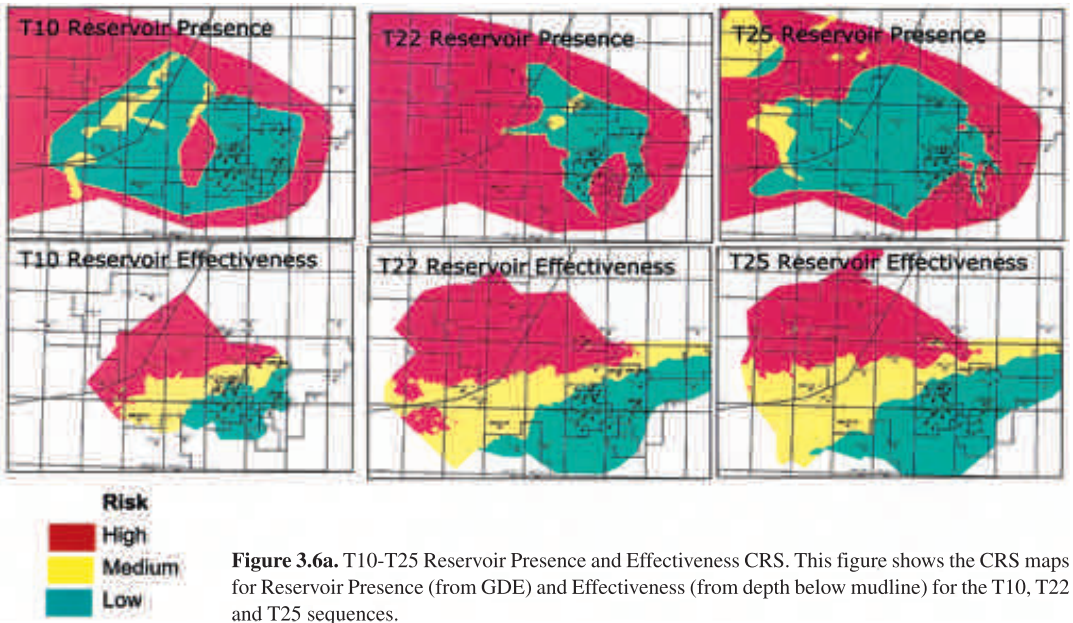
**Figure 3.4.** T31-T36 Reservoir Effectiveness. The figure shows predicted compaction curves for each Tertiary sequence based on BP-in house lithology and provenance studies. Core porosity:permeability correlations are also shown. These two parameter sets combine to create a prediction of reservoir deliverability properties as a function of depth below mudline (seabed). Low and High Risks are governed by porosity (volume) and permeability (flow) limits for the rates and reserves required to meet Q204 fields analogues economics



**Figure 3.5.** Reservoir Effectiveness CRS. This shows how compaction trends, poro-perm limits and depth below mudline for a sequence (example T10) convert into Common Risk Segments for Reservoir Effectiveness risk.

Figures 3.6a to 3.6c show Reservoir Presence and Effectiveness CRS maps for the T10 to T36 sequences which contain the vast majority of the discovered and produced fluids of the Faroes-Shetland Petroleum System (excluding the Clair Field). The increasingly large areas of Medium and High

Reservoir Effectiveness risk in progressively older Palaeocene sequences reflects the distribution of the Palaeocene and Eocene depocentres. This primarily reflects increasing burial with compaction-destruction of porosity and permeability.





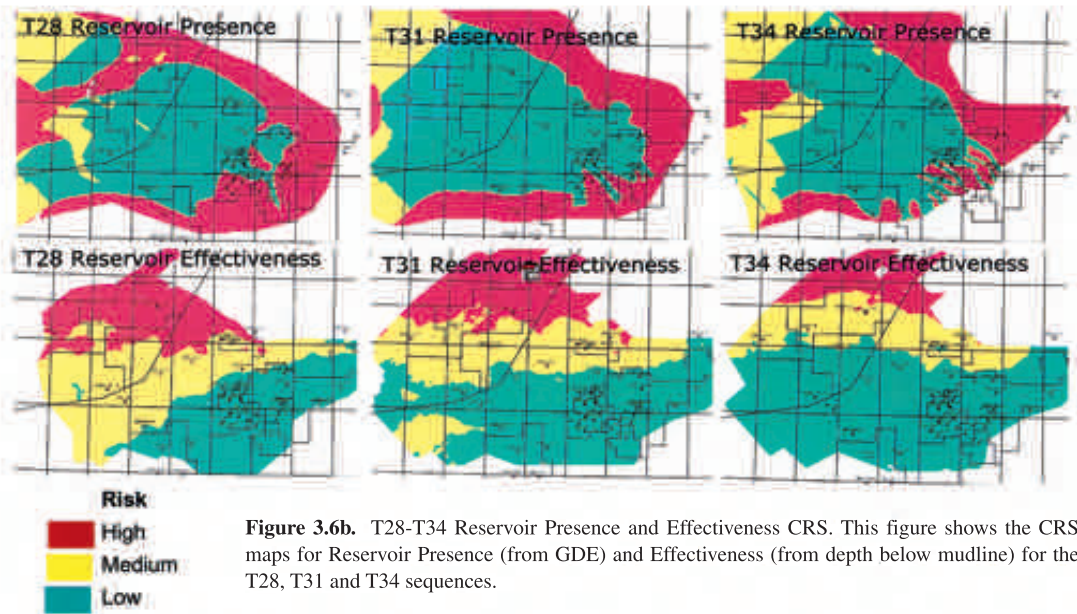


**Figure 3.6b.** T28-T34 Reservoir Presence and Effectiveness CRS. This figure shows the CRS maps for Reservoir Presence (from GDE) and Effectiveness (from depth below mudline) for the T28, T31 and T34 sequences.

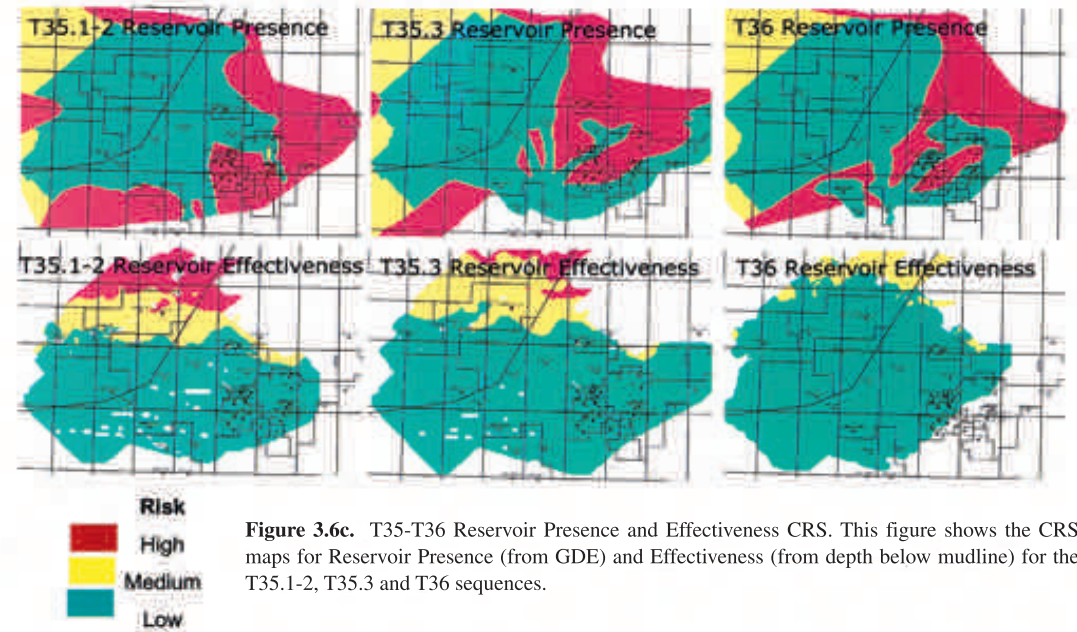


**Figure 3.6c.** T35-T36 Reservoir Presence and Effectiveness CRS. This figure shows the CRS maps for Reservoir Presence (from GDE) and Effectiveness (from depth below mudline) for the T35.1-2, T35.3 and T36 sequences.

4. Seal Presence and Effectiveness Risk

Seal Presence has been mapped via well-tied mudstones at or near sequence tops and sometimes extending into the lower parts of overlying sequences. This is shown in the BP-Shell Assynt well 204/18-1 where a 130m thick mudstone straddles the (top) T34 sequence boundary (Figure 4.1).

Seal thickness distribution was evaluated by initial gridding of well-tied, “top sequence” mudstone isochores. To extend the isochores away from well control, the initial grids were constrained by the overall sequence seismic isochores as trend-forms. The end results were Seal thickness grids that were used as controls in the Seal Effectiveness CRS mapping process.



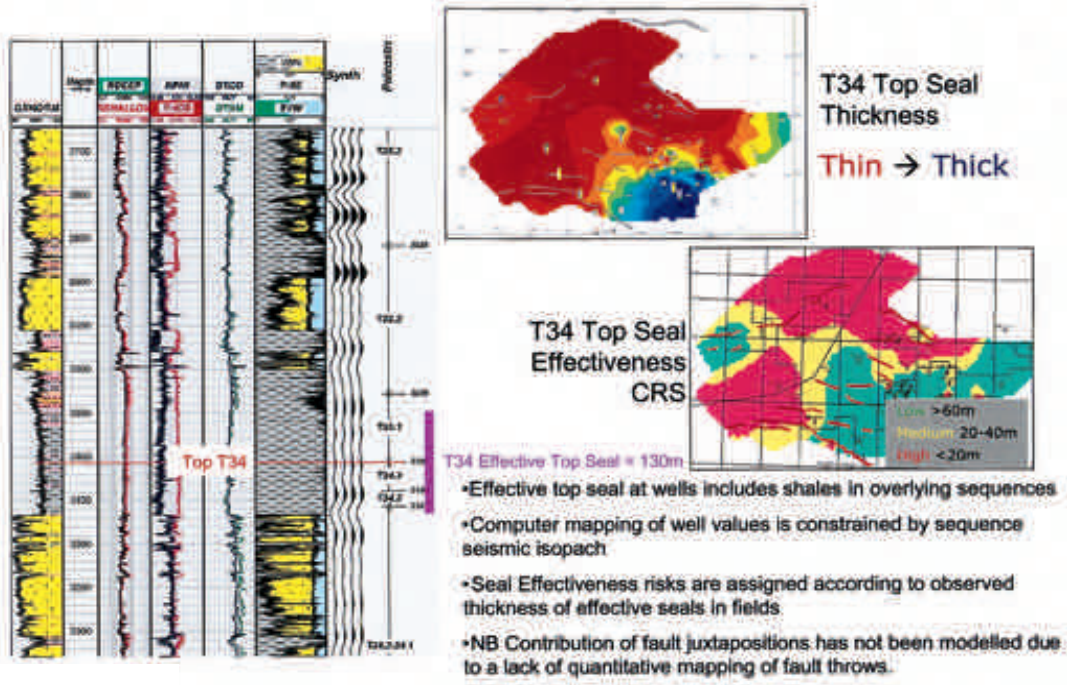


**Figure 4.1.** Top Seal Effectiveness CRS. Top Seal thickness was interpreted from well-tied, top or near-top sequence mudstones, mapped away from well control by overall sequence seismic isopach trend forms. Top Seal Effectiveness was risk-binned by sealing mudstone thickness in relation to the distribution of column heights in the UKCS Q204 fields and shows in carriers.

Rather than treat Seal presence and effectiveness separately, this study considered only a single risk component – Seal Effectiveness.

Seal Effectiveness was risked on the probability of a given thickness being able to prevent petroleum migration. The key calibrant for this value range was petroleum column occurrence in the West Shetlands fields (the UKCS Quad 204-205 area). A less reliable calibrant was the presence or absence of shows in Tertiary sands in wells. The absence of shows does not necessarily mean seal failure and leakage; it could mean that the sands that were drilled never received a petroleum charge.

However, there was a reasonable overall trend of agreement between column occurrence and shows distribution in given sequences to suggest the following risks:

**Table 1**

Seal thickness (m)	Seal Effectiveness Risk
<20	High
20-60	Medium
>60	Low

Establishing these guideline thickness: risk ranges meant that regional Seal Effectiveness CRS maps could be drawn at roughly top sequence level, as shown in Figure 4.2 .

5. Geological CRS Maps

The next step in the CRS process was to convolve the Reservoir Presence, Reservoir Effectiveness and Seal Effectiveness maps into “Geological” CRS maps. This was done using ZMap macros as each CRS map was in ZMap grid format. Figure 5.1 shows an example for the T34 sequence. Risk component convolvement followed the BP internal rules of assigning the highest risk component to the convolved map.

Figures 5.2 summarises Geological CRS maps for the Palaeocene T10 to T36 sequences. They show risk distribution and highlight reasons for risk assignment in certain areas.

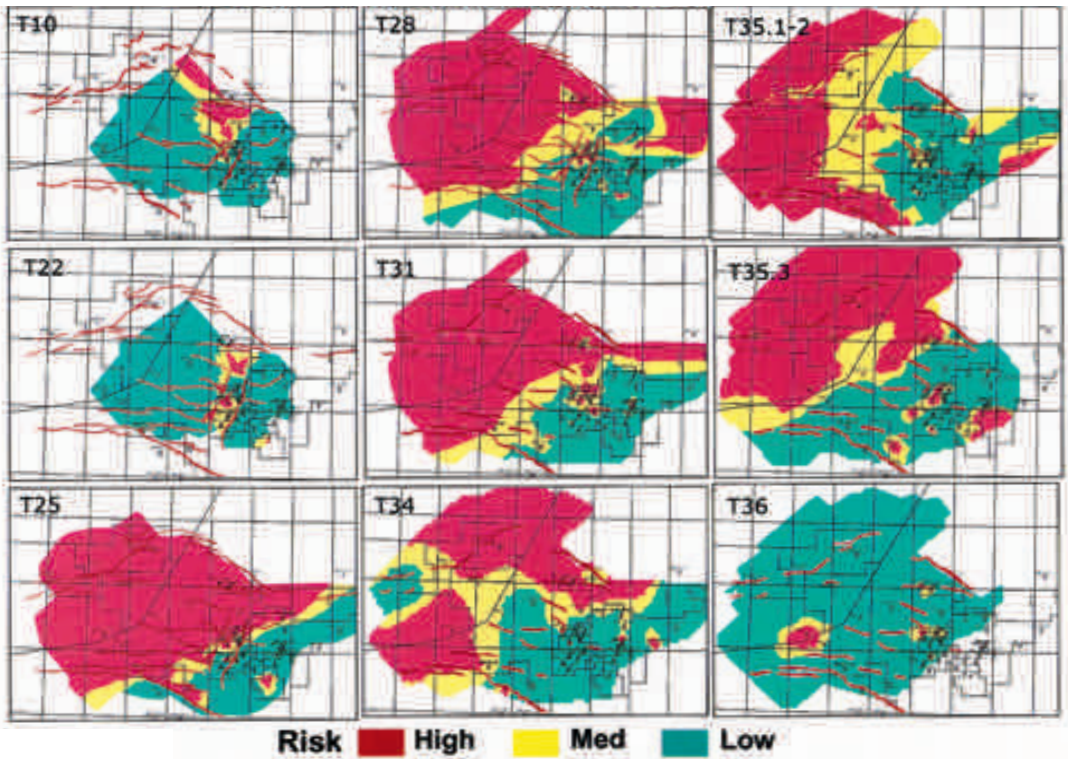


**Figure 4.2.** Seal Effectiveness CRS. This figure shows the distribution of risked Top Seal Effectiveness for all of the Palaeocene sequences.

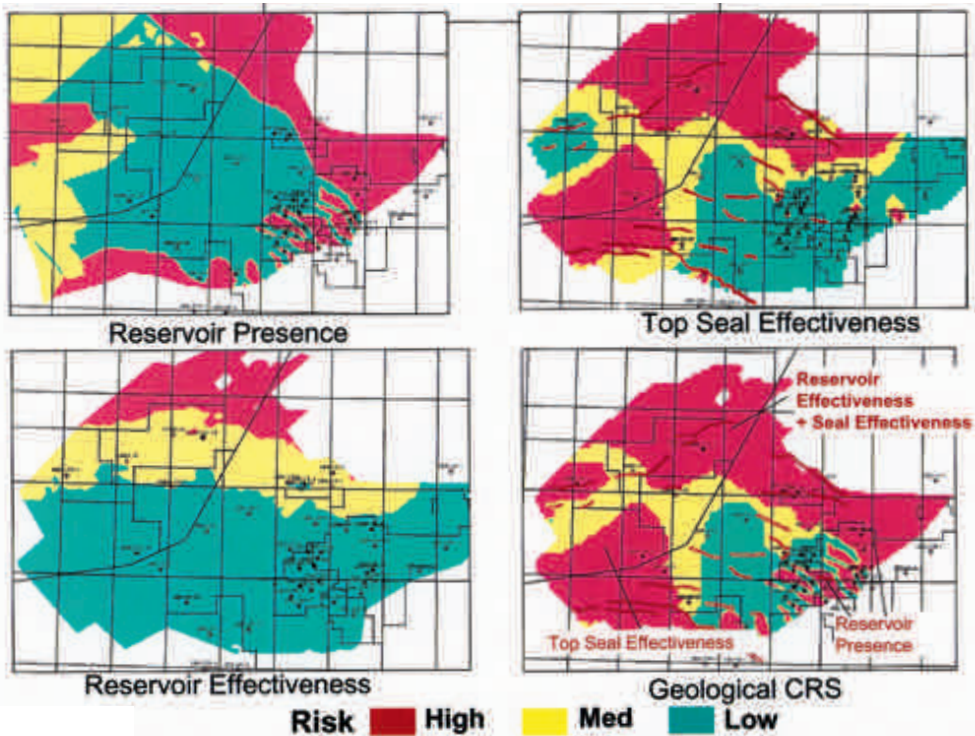


**Figure 5.1.** Geological CRS. Reservoir Presence, Reservoir Effectiveness and Seal Effectiveness were convolved into one “Geological CRS” map per Palaeocene sequence. This CRS map type illustrates all the non-Charge related risk evaluations.



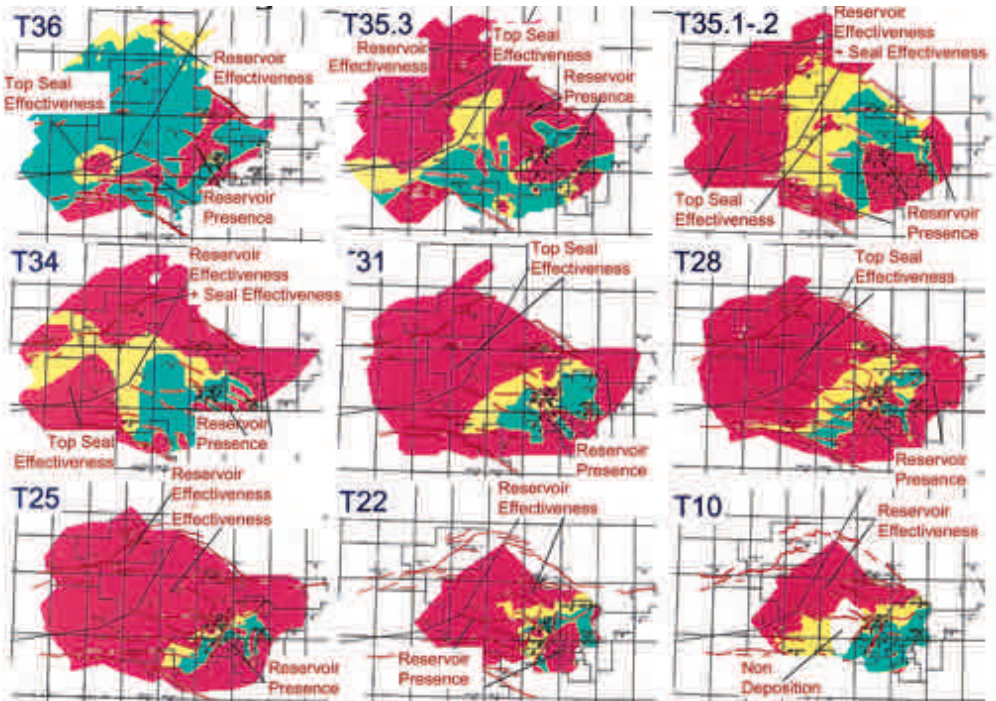


**Figure 5.2.** Geological CRS maps – Summary. Each Palaeocene sequence has a Geological CRS map to illustrate the distribution of non-Charge related risks. Critical risks in certain areas are highlighted.

## 6. Charge Access Risk

Charge Access Risk is governed by 3 sub-components:

1. Source rock presence
2. Source rock maturity
3. Fluid migration

Source rock presence risk has direct and indirect indicators. Direct indicators are sample geochemical data from drilled source rocks. Indirect indicators are from thermogenic fluids that can be geochemically correlated to the drilled source rocks. These form the forensic evidence of a working Petroleum System.

### 6.1 Source rock presence

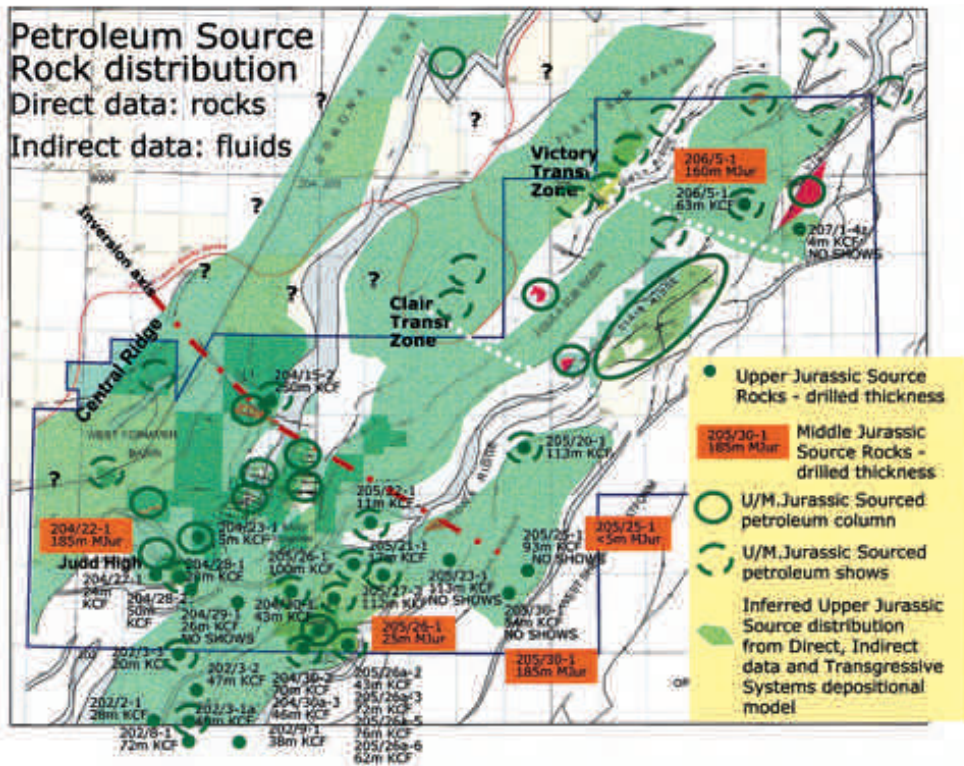
Figure 6.1.1 summarises direct and indirect evidence of source rock deposition in the general area of the Faroes-Shetland Basin.

There are 30 wells in the area that penetrate organic-rich, highly oil-prone source rocks of Late Jurassic age. The Kimmeridge Clay Formation (J64-76, Middle Kimmeridgian to Late Ryazanian)

is widespread on this margin (Stoker *et al.*, 1993) and a world-class source rock in NW Europe. It is the main source for much of the produced petroleum in the UKCS. The organic-rich, gamma-active mudstones were deposited in fully marine, outer shelf to bathyal conditions. They were deposited in a series of marine transgressions that succeed the transgressive marine Rona Sandstone unit and progressively overstep previously exposed basement highs. The transgressive marine environment suggests basin-scale source rock deposition.

The Kimmeridge Clay Formation is typically many 10's to <250 m thick with TOC >5% and petroleum potential yields of up to 50Kg/t where immature. There is usually a good correlation between gamma ray intensity and organic richness due to the concentration of uranium in the preserved organic matter. Since the organic matter is dominantly of marine algal origin oils generated and expelled from this source rock are usually low-wax. They may have slightly elevated sulphur concentrations where the host source lithology was more carbonate-rich (probably reflecting shallower water but more oxygen-depleted, reducing conditions).





The Middle Jurassic (J26-34, Late Bajocian to Late Bathonian; Stoker *et al.*, 1993) is sometimes organic-rich (Figure 6.1.1). There are few penetrations of this age in the basin and fewer in source rock facies. Where they have been drilled, the Middle Jurassic source rocks are usually thin but have very good oil-potential (TOC >4%, petroleum potential >15-20 Kg/t). Since their depositional environment was restricted marine but relatively nearshore/lagoonal, one would expect a large amount of preserved terrigenous organic matter in the source rocks. However, the very waxy nature of the oils (typically >20% Wax) correlated to these source rocks is mainly due to abundant amorphous algal material (supported by palynological evidence) probably similar to Botryococcus, which could have survived in restricted, brackish water conditions.

that can be geochemically correlated to the known source rocks in the area. A key correlation parameter in the Faroes-Shetland area is the presence or absence of a certain biological marker in the oils called 28,30 Bisnorhopane. This biomarker may be related to sulphur-oxidising bacterial mats living in highly oxygen-depleted conditions (Peters and Moldowan, 1993). It occurs in the Kimmeridge Clay Formation source rocks but *not* in the Middle Jurassic. Therefore its relative concentration in an oils population compared to end-members may give an estimate of the areal occurrence of both Middle and Late Jurassic source rocks. This index is strengthened by the good (negative) correlation between 28,30 Bisnorhopane concentration and wax levels in the oils of this area.

Figure 6.1.2 shows the occurrence and concentration of 28,30 Bisnorhopane (relative to the ubiquitous C30 Hopane of bacterial origin Peters and Moldowan 1993; H13 = Integrated 28,30 Bisnorhopane peak as relative % to integrated C30 Hopane peak) in oils and reservoir rock extracts



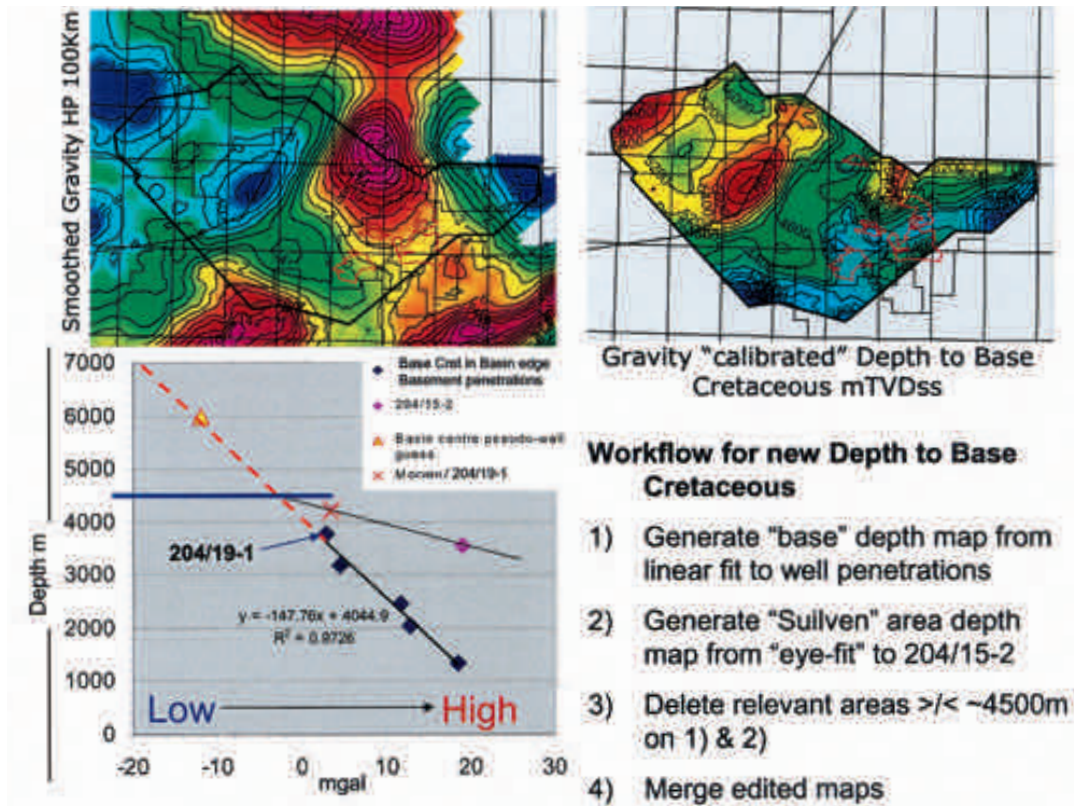


**Figure 6.2.1.** Workflow for Depth to Base Cretaceous. There are a few wells within the AOI where the Base Cretaceous is penetrated and many more in basin-margin areas outside the AOI but still within an area of coverage by satellite gravity data. Seismic identification of the Base Cretaceous/top Jurassic source rock system is possible in shallow basin-margin areas outside the study AOI. Seismic mapping away from well control into the basin is not possible. Therefore a correlation was built between the satellite gravity and depth to Base Cretaceous as penetrated to create an AOI-wide depth to Base Cretaceous for use in source rock maturity evaluation.

satellite gravity data at well locations. Although the well tie-to-gravity data population was small, the correlation was very good ( $r^2=0.97$ ) except in the Suilven area (204/19-8, 204/14-1, 204/15-1). A depth to base Cretaceous/top source rock map was generated from the correlation and hand-edited using a "Suilven" gravity correction for that area (Figure 6.2.1).

Application of the current geothermal gradient (derived from corrected BHT data and RFT, MDT, DST etc. temperature data from the very large wells suite in the UKCS West Shetlands area) enables a present day thermal stress model to be built (Figure 6.2.1).

Source rock maturity, i.e. kitchen thermal stress, can also be evaluated using oils biomarker data that indicate petroleum expulsion temperatures.

Figure 6.2.2 shows the probable expulsion temperature windows of UKCS Quad 204 Tertiary-reservoired oils and shows from the recent Faroes licence wells within a general North Sea data set. The Methylidibenzothiophene Ratio (MDR) is the most reliable fluid maturity parameter as it is very resistant to the post-charge alteration (biodegradation and water-washing) common in Faroes-Shetlands oils.

The thermal reaction kinetics of the MDR biomarker ratio are well understood and have been incorporated into the map-based Petroleum Systems modelling software used by BP (Trinity by ZetaWare Inc.). Fluids biomarker data suggest that an MDR window of approximately 2-8 will capture the kitchen maturity range of the charge migrating into the UKCS fields and the shows in the Faroes



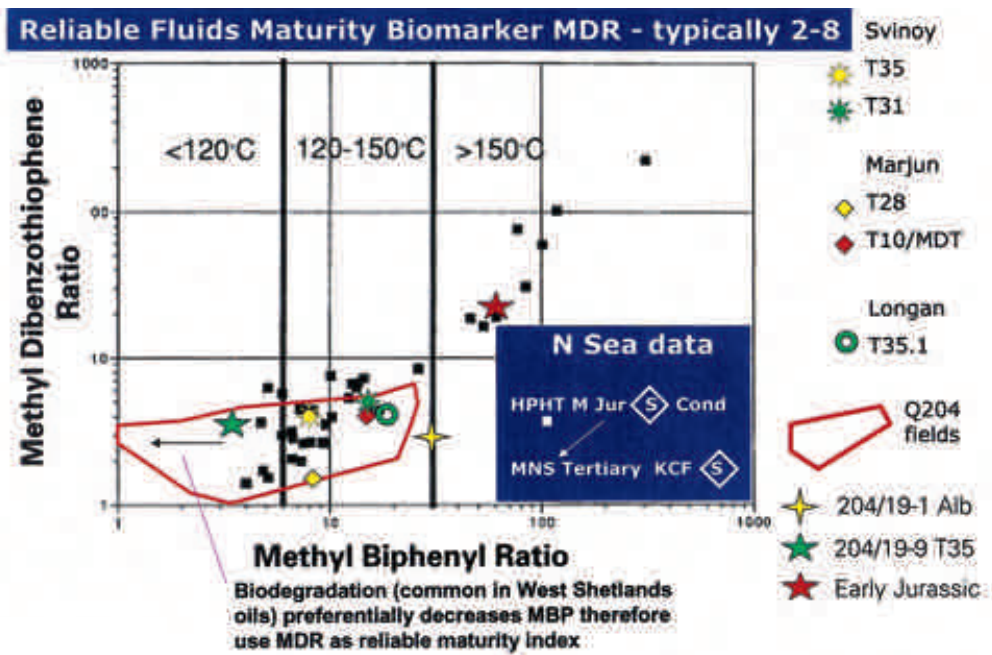


**Figure 6.2.2.** Faroes-Shetland Fluids maturity. Source rock kitchen maturity can also be estimated from the maturity and expulsion temperature of petroleum fluids via biomarker analysis. BP in-house research has concluded that the biomarker ratios of 4-Methyldibenzothiophene/1-Methyldibenzothiophene (MDR) and 3-Methyl Biphenyl/2- Methyl Biphenyl (MBP) are the best for estimating petroleum fluid expulsion temperatures. The expulsion temperature estimations have been corroborated particularly in the North Sea using BPs large fluids database and regional kitchen maturity mapping. Most of the Faroes-Shetland Basin fluids sit within an MDR window of 2-8 (MDR selected as MBP may be affected by the post-emplacement alteration processes commonly seen in oils from this margin).

wells. Figure 6.2.3 illustrates the present day modelled thermal stress and extent of the MDR=2-8 window in the basin. Note that the deep basin centre is far too mature to represent the trapped/analysed (shows) fluids population but that basin shoulders appear more likely as effective kitchen-

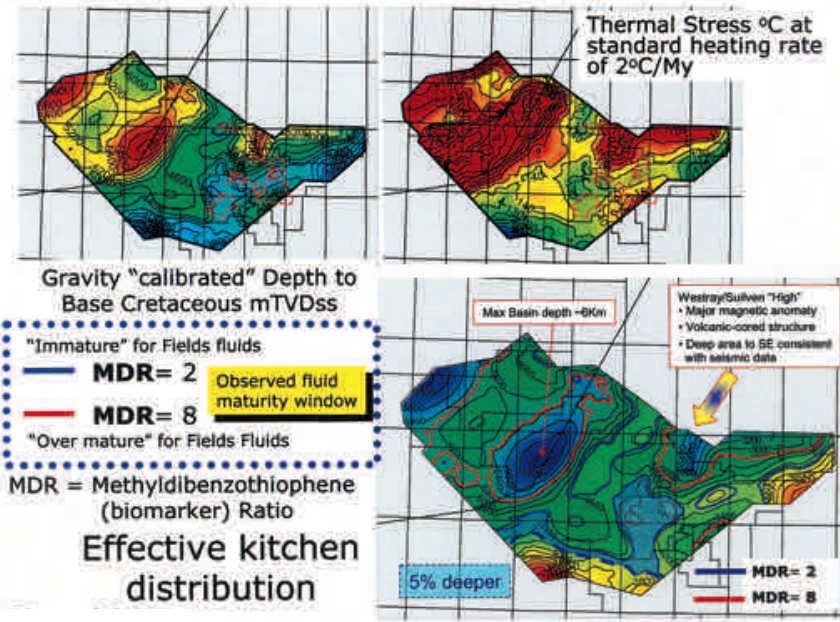


**Figure 6.2.3.** Effective kitchen distribution. The gravity-derived depth to Base Cretaceous (top source rock), present day thermal stress (estimated at a typical heating rate of 2°C/My) and biomarker window (MDR=2-8) for oil maturity combine to allow the mapping of the effective kitchen for the petroleum fluids discovered in the basin to date.

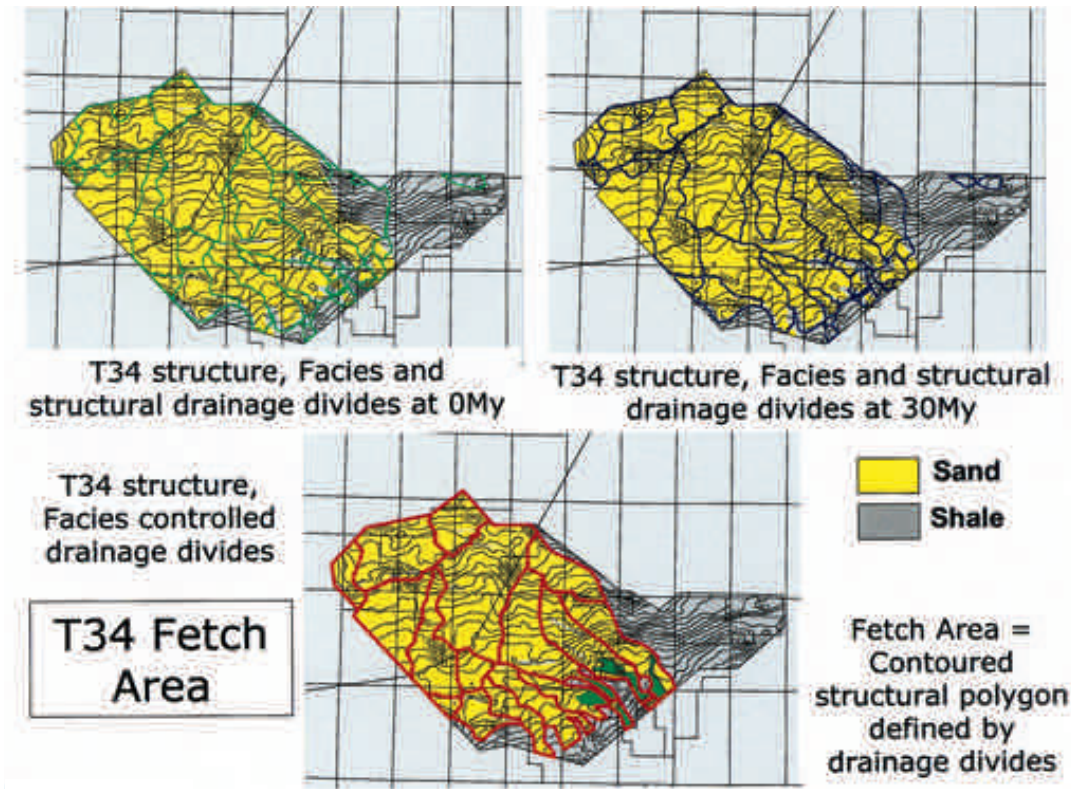


**Figure 6.3.1.** T34 Fetch Area. Carrier structural surfaces provide the basis for simple petroleum migration streamline mapping. Structurally-defined drainage divides create fetch cells, the distribution of which on the T34 for example have changed little in the past 30 My. Lateral migration only occurs in carriers therefore the facies distribution governed by a sequence GDE provides the major control on distribution of effective fetch cells.

ens, particularly to the southwest of the Foinaven-Schiehallion giant field complex.

This analysis suggests that, like source rock presence, maturity is low risk almost everywhere in the study AOL.

### 6.3 Fluid migration

The key risk component in the Faroes-Shetland petroleum system is Charge Access, i.e. petroleum fluid migration. The approach used in this study was to assume vertical migration out of the dominantly muddy Cretaceous section into the first Palaeocene carrier (T10). This assumption was made in the absence of extensive mapping of any significant Cretaceous carriers, although for example overpressured, gas-bearing Apto-Albian sands have been drilled in 204/19-1. But the widespread occurrence of Tertiary-reservoired petroleum suggests that access to the first Palaeocene carrier is low risk. Access risks dramatically increase once into the complex, turbidite-dominated Palaeocene

carrier/reservoir system.

The Petroleum Systems software used in BP is map-based and works by modelling ortho-contoured migration streamlines on structural surfaces to constrain lateral migration. Structural foci in each carrier create fluid flow fetch cells delineated by drainage divides. Solely structure-contoured fetch cell distributions for the T34 are shown in Figure 6.3.1. Fetch cell distributions show little change over the past 30 My. Previous basin modelling work in BP has suggested that the most likely timing of the low-moderate maturity charge described by fluids biomarkers, was post-Eocene suggesting that the present day fetch cell distributions are reasonable proxies for the past (Figure 6.3.1).

Lateral fluid migration is further constrained in the modelling software by lithology. This is achieved by using pseudo-capillary entry pressure distributions as stratigraphic surface-associated facies



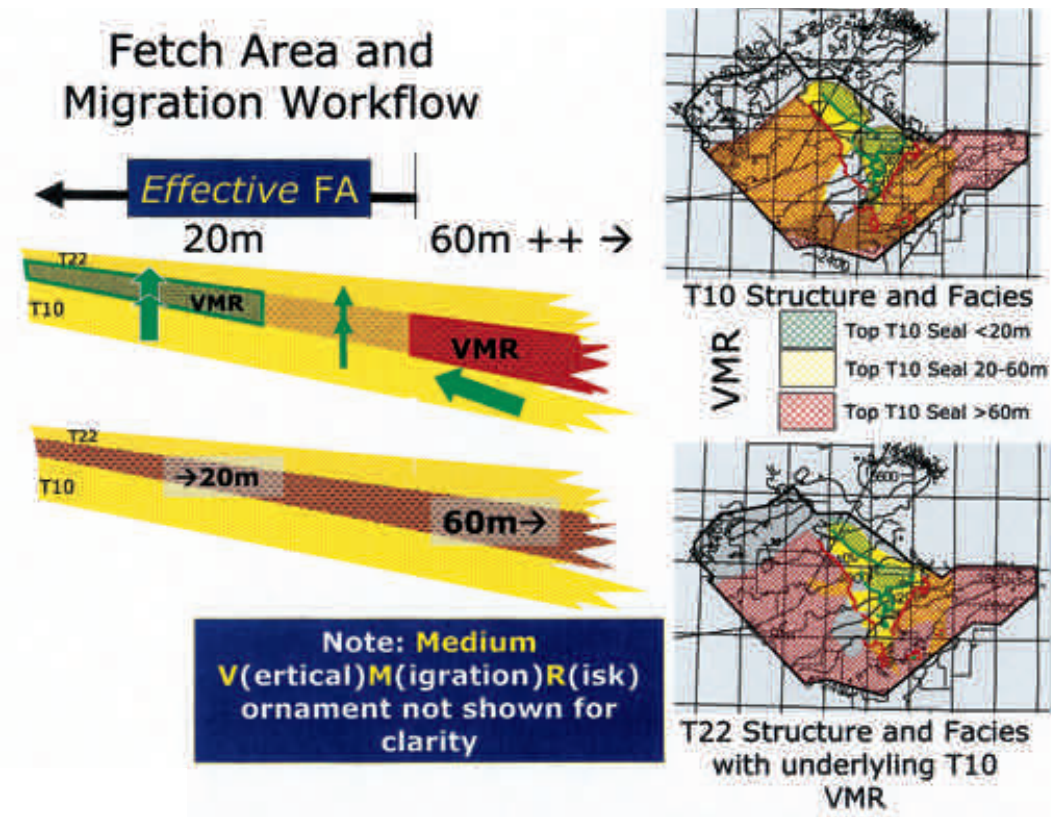


**Figure 6.3.2.** Fetch Area and Migration Workflow. Lateral petroleum migration in a (post-T10) carrier also depends on vertical delivery of petroleum from the carrier below. This is controlled by the inverse of Seal Effectiveness Risk; i.e. a Vertical Migration Risk (VMR). This risks the vertical connectivity between one carrier and another. Field column heights and the general distribution of shows in the system suggest a range of top seal thickness to allow (VMR green/Low at top seal thickness <20m) or prevent (VMR red/High at top seal thickness >60m) vertical migration. Lateral migration only occurs in carriers and hence is dependent on sequence Reservoir Presence Risk. (Note the Medium risk VMR ornament is not shown for diagram clarity.)

maps (Figure 6.3.2). A low pseudo-capillary entry pressure value allows migration (e.g. sands=0) whilst a high value (e.g. mudstones=1000) prevents migration. The distributions of sands and muds for each carrier/reservoir sequence were taken from the GDE maps described previously. By definition, a fetch cell can only occur in a GDE-defined sand. Fetch cell distribution is therefore conditional on Reservoir Presence Risk. A fetch cell cannot occur where Reservoir Presence Risk is High as this risk category has been defined from sequence GDEs as a basin floor mud.

Vertical fluid connectivity in the Palaeocene carrier/reservoir system is between one “T” sequence and the overlying one. In this study, vertical connectivity is a risk sub-component known as Verti-

cal Migration Risk (VMR). Vertical connectivity (i.e. VMR) depends on top-sequence Seal Effectiveness Risk (see Section 4). VMR is therefore the inverse of Seal Effectiveness Risk (Figure 6.3.2):

**Table 2**

Seal thick-ness m	Seal Effec-tiveness Risk	Vertical migration Risk
<20	High	Low
20-60	Medium	Medium
>60	Low	High

Consequently, the distribution of fetch cells in (post-T10) carriers which can be charged from sands in the sequence below depends on the distribution of Seal Effectiveness Risk of the underlying sequence. This is illustrated in Figure 6.3.3. The



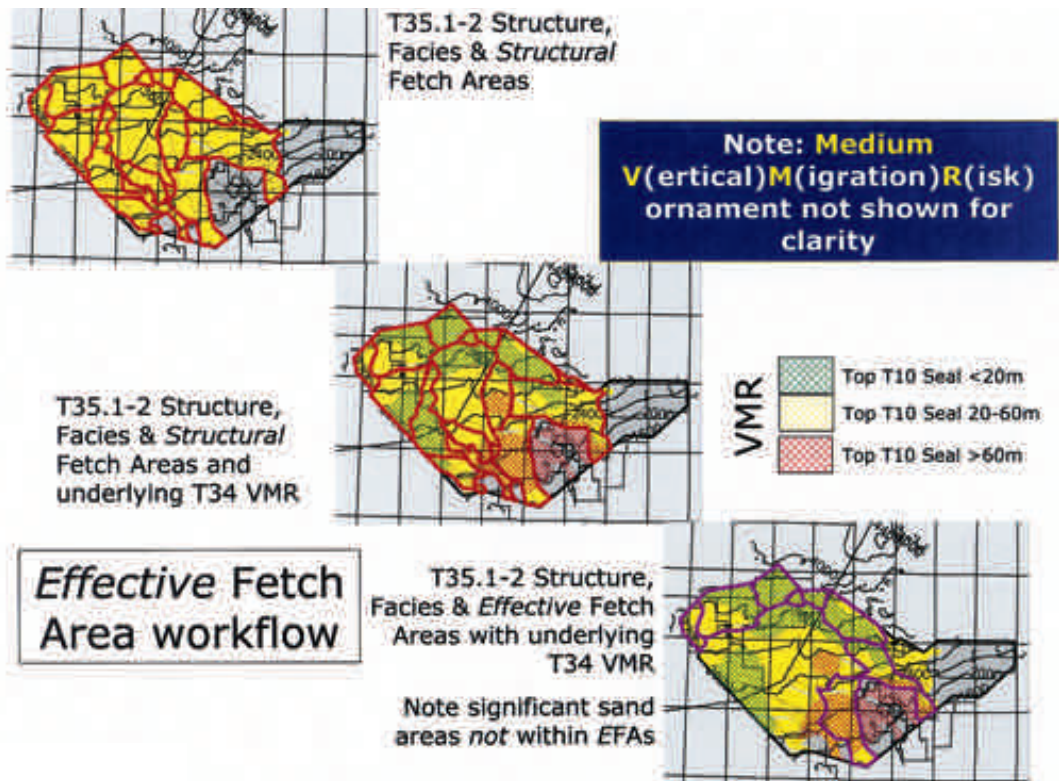


**Figure 6.3.3.** Effective Fetch Area workflow. The combination of (facies-controlled) structural fetch cell distribution with VMR from an underlying carrier creates Effective Fetch Areas which may have a very different geometry from purely structural and facies alone.

net result is that some structurally defined fetch cells in a given Palaeocene sequence have a significant probability of not being charged from below as they overlie areas of Low Seal Effectiveness Risk, i.e. High VMR (Figure 6.3.3).

This creates a distribution of Effective fetch cells per sequence defined as:

1. overlying areas of (GDE-constrained) Low to Medium Reservoir Presence Risk

AND

2. which have High Seal Effectiveness Risk.

Fetch cells above an area of High VMR (Low Seal Effectiveness Risk) are not Effective and not used as polygons in the final CCRS process. This means that there are no High Risk Effective fetch cell polygons in this evaluation.

From a vertical migration point of view, Low Seal Effectiveness Risk is bad. However, from a lateral migration and trapping point of view, Low Seal Effectiveness Risk is naturally very good.

Figure 6.3.4 shows the distribution of Effective Fetch cells for the Palaeocene sequences with the VMR for the underlying carrier. Note that Medium Risk VMR ornament is not shown for diagram clarity but occurs between Low and High risk VMR areas from the underlying sequence. These fetch cell/risk polygons are Charge Focus CRS maps. The dominant or down-dip VMR value in the effective fetch cell defines the Charge Focus CRS assignment.

The Charge Focus CRS maps were convolved with the Geological CRS maps to deliver a series of Composite CRS maps for the T10 to T36 sequences in the Faroes-Shetland area.

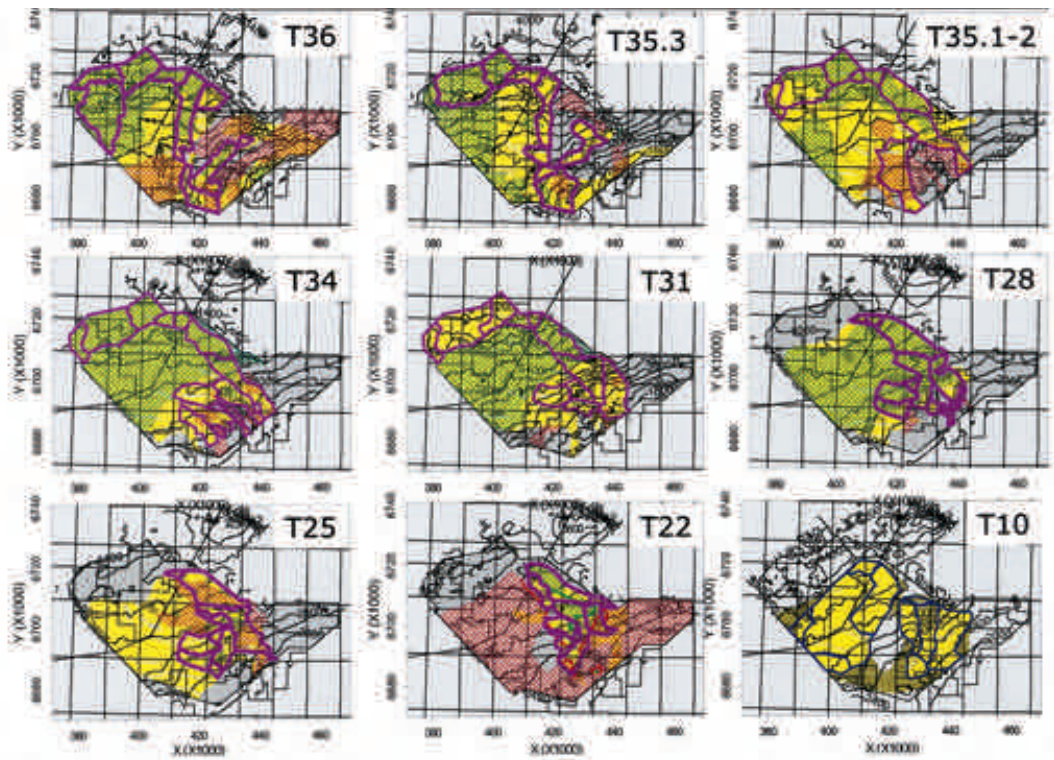


**Figure 6.3.4.** Effective Fetch Area distribution by Sequence. Each map shows:

- Structural surface (contours) Facies overlay (yellow=sand, grey=mudstone block ornament)
- VMR from the underlying carrier (except T10; Red=High, Green=Low hachured ornament; Note the Medium risk VMR ornament is not shown for diagram clarity)
- Effective fetch area distribution (heavy purple polygons)

7. Composite Common Risk  
Segment mapping

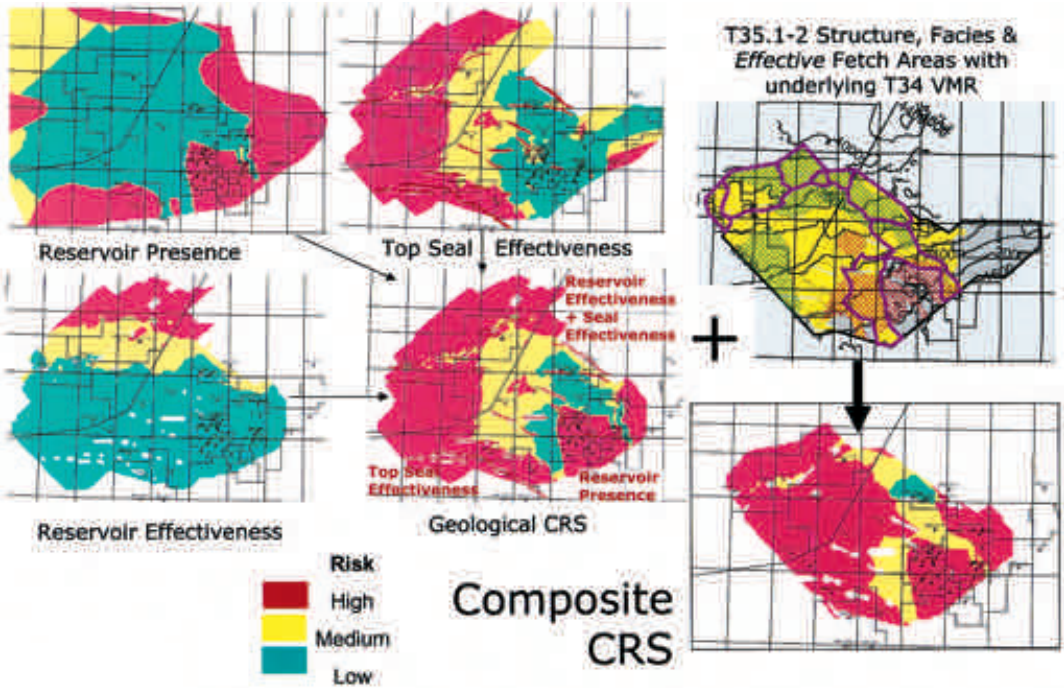
A Composite CRS (CCRS) map convolves the component risks for any given level. In the Faroes-Shetland area this refers to the Palaeocene T10 to T36 sequences. The risk rules dictate that the CCRS is assigned the riskiest component CRS. For example (table 3):

Figure 7.1 shows the workflow of convolving the Geological CRS maps with the sequence Effective Fetch Area polygons, the example shown being the T35.1-2. Figure 7.2 summarises the convolved CCRS maps for the Palaeocene T10-T36 sequences. Risk boundary rules require that Medium Risk always separates Low from High Risk. Therefore some maps show Medium Risk “rims” separating Low from High Risk areas.

Table 3

	Reservoir Presence	Reservoir Effectiveness	Seal Effective-ness	Charge Access	CCRS
RISK	●	●	●	●	●
RISK	●	●	●	●	●
RISK	●	●	●	●	●





**Figure 7.1.** Composite CRS workflow – example T35.1-2. Each of the sequence CRS maps are convolved into a “Geological” CRS map. This is then convolved with a Charge Focus CRS which is the distribution of Effective Fetch Areas per sequence as a set of polygons with attached risks. The Geological and Charge Focus CRS maps are then convolved to create an overall Composite CRS map for each sequence.

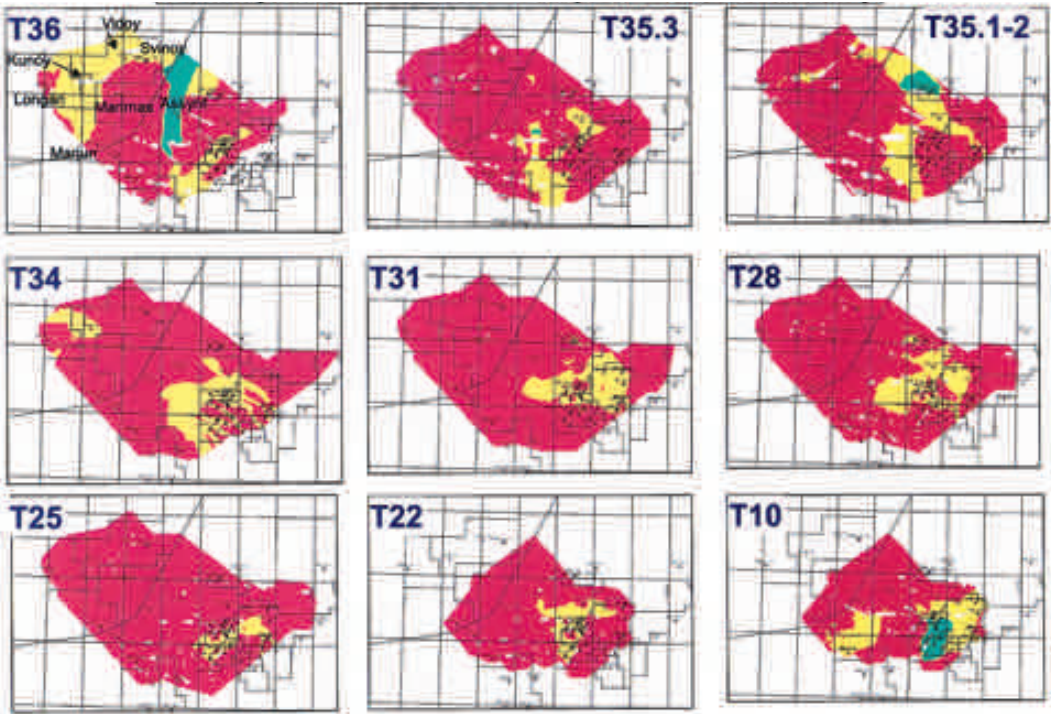


**Figure 7.2.** Composite CRS Maps – Summary. Each Palaeocene sequence has a CCRS map. The VMR, Charge Focus risk etc., mean that the CCRS maps are linked into an integrated holistic risk model. Note Trap risk was not addressed in this study.



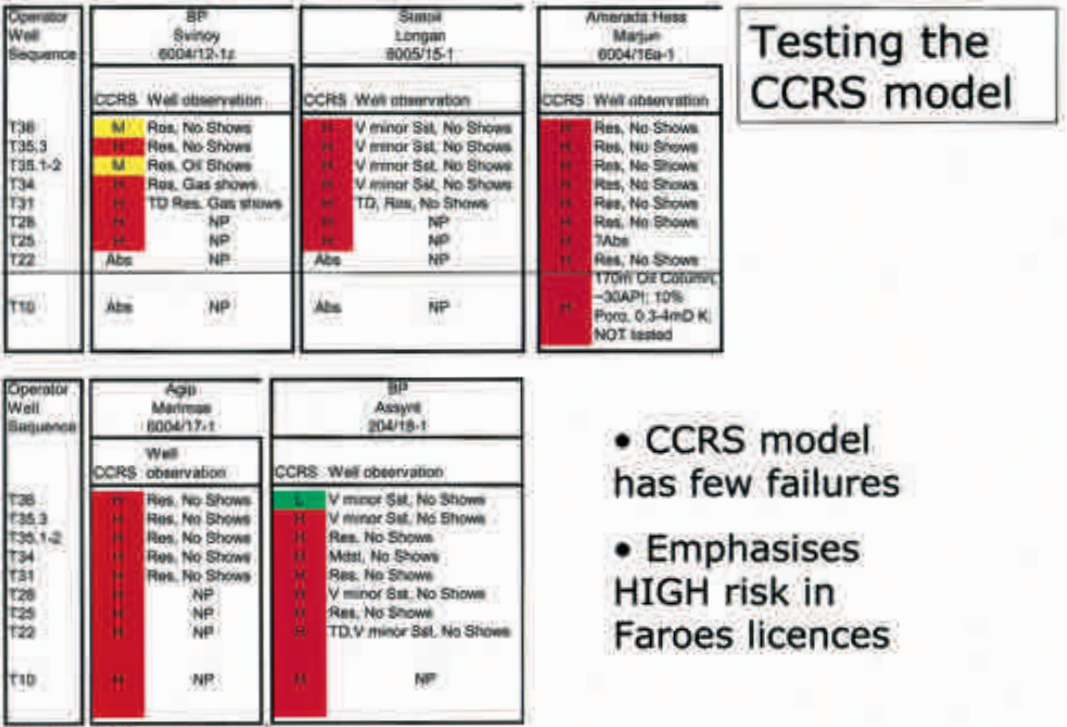


**Figure 8.1.** Testing the CCRS Model. Recent UKCS and Faroes well results allow the integrated CCRS model to be tested.

Model failures:  
Svinoy 6004/12-1  
Marjun 6004/16a-1  
Assynt (UKCS) 204/18-1

T36: thick intra-T35 seal not mapped  
T10 has ~170m petroleum column BUT was not able to be flow tested down-hole hence critical High Reservoir Effectiveness risk may still be correct  
T36 Low CCRS dependent on Low Charge Focus risk with lateral migration from the north dependent on a small vertical migration access window.

Considering each sequence penetrated as a potential target in these wells then the CCRS Model has a correct prediction rate of 90%.

8. Testing the Risk Model

Figure 8.1 shows the CCRS predictions for recent Faroes and UKCS wells, testing the model against well results. The well results/failures are correctly predicted for most in terms of overall risk outcome. Risk model prediction failures are the T36 in Assynt and Svinoy.

The Svinoy (6004/12-1) well at T36 confirmed all the individual CRS risk assignments except for Seal Effectiveness and Charge Access. The occurrence of significant shows in the underlying good quality T35.3 sands and their interpretation as being a migration pathway, suggests that the risk

of Top Seal Effectiveness at Svinoy was Low to Medium rather than High as mapped which would have had a significant effect on the Charge Access risk (Effective fetch cell distribution). The T35.3 “A” Sand was topped by ~40 m of Tuff.

The Petroleum Systems project post-dates drilling the BP-operated UKCS Assynt well (204/18-1). The CCRS evaluation places all Tertiary sequences at High risk except the T36 which has an overall Low CCRS. This well was dry with no shows of any description despite abundant good quality reservoir sands. Interpretation of the mud-log gas data suggests this well never received any thermogenic petroleum charge. The well is also thought to have failed due to absence of trap. The

model prediction failure at Assynt T36 was due to predicted Low risk for Reservoir Presence/Effectiveness and Charge Access. There were minor, poor quality T36 sands at the Assynt location. The Effective Fetch cell for Assynt required significant southwards lateral migration from a relatively small “vertical migration access” window in the northern half of UKCS Quad 204/13. However, Low Top Seal Effectiveness Risk was confirmed by ~100 m mudstone at Top T36 to Base T38.

Another possible CCRS Model failure is the approximately 170 m petroleum column reported in the Amerada Hess-operated Marjun well (6004/16a-1). Reservoir Effectiveness is the critical High risk component for this well. As the well could not be flow-tested down-hole, this risk assignment could still prove correct. The Marjun discovery is currently being appraised.













































## 9. Implications for Faroes Licence 004

BP has mapped the Kunoy and Vidoy prospects at Palaeocene T31 to T35 levels in Faroes Licence 004 (Figure 1.1). The Petroleum Systems CRS mapping has identified the T36 as the most prospective sequence from Reservoir and Seal risk perspectives.

The upper and lower T35 sequences which were shows-bearing in the BP:Shell Svinoy well (6004/12-1) have major risks associated with Seal Effectiveness. Geochemical analysis of the shows in the Svinoy well suggests the T35 was in fact a migration pathway.

The T34 sequence is moderately prospective in CRS terms but the T31 has significant Reservoir and Seal Effectiveness risks. The deep T10 to T28 sequences have varied cause but generally Reser-

**Table 4**

RISK	Reservoir Presence	Reservoir Effectiveness	Top Seal Effectiveness	Charge Focus	CCRS
T36					
T35.3		 Kunoy  Vidoy	 		
T35.1-2		 Kunoy  Vidoy	 		 
T34		 Kunoy  Vidoy	 		
T31		 Kunoy  Vidoy			
T28			 North  South		 
T25					
T22					
T10					

voir-related individual High CRS components.

Of 9 potential Tertiary sequence targets, 5 have High CCRS, 2 Medium CCRS and 2 Medium-High CCRS.

## 10. Conclusions

1. A BP study, focused on risking the Petroleum System of the Faroes-Shetland Basin and specifically incorporating new well data from recent wells in the Faroes and UKCS, has highlighted most areas in the Faroes Six Year Licences to have a high risk of failure.
2. The primary failure modes are:
  - T35: Reservoir and Seal Effectiveness
  - T34: Seal Effectiveness
  - T31: Seal Effectiveness
  - T28: Seal Effectiveness
  - T25: Reservoir Effectiveness
  - T22: Reservoir Presence
  - T10: Reservoir Presence
3. Recent well results have confirmed the Composite Common Risk Segment model and most of the individual risk component assignments; the overall model prediction success rate is 90%.
4. Model prediction failures are usually because of failure at a finer scale or resolution than the model scale can handle, typically Seal Effectiveness risk.

## References

- Ebdon, C.C., Granger, P.J., Johnson, H.D. and Evans, A.M. 1995 Early Tertiary evolution and sequence stratigraphy of the Faeroe-Shetland Basin: implications for hydrocarbon prospectivity. *In: Scrutton R.A., Stoker, M.S., Shimmield, G.B. and Tudhope, A.W. (eds.) The Tectonics, Sedimentation and Palaeoceanography of the North Atlantic Region.* Geological Society, London, Special Publications 90: 51-69
- Green, P.F., Duddy, I.R., Hegarty, K.A. and Bray, R.J. 1999. Early Tertiary Heatflow along the UK Atlantic margin and adjacent areas. *In: Fleet, A.J. and Boldy, S.A.R. (eds.) Petroleum Geology of Northwest Europe: Proceedings of the 5<sup>th</sup> Conference.* Geological Society, London: 349-357.
- Peters, K.E. and Moldowan, J.M. 1993. The Biomarker Guide. Prentice Hall
- Stoker, M.S., Hitchen, K. and Graham, C.C. 1993 The Geology of the Hebrides and the West Shetland Shelves and Adjacent Deep-water areas. British Geological Survey, London, HMSO.



# Faroese Area: Structural Interpretation of Seismic Data in a Basalt Environment

JUDITH KESER NEISH

Geophysical Consultant, Faroese Geological Survey (JFS), Tórshavn, Faroe Islands

Email: judy@jfs.fo

## Abstract

The Faroe Islands and associated offshore shelf area are located on the North Atlantic Margin of Europe, and form one of the principal components of the North Atlantic Large Igneous Province. A significant amount of volcanic material was laid down over this area in the Paleocene and Eocene, consequently blanketing the geological structure. This presents a substantial challenge for geophysical exploration in the region, where precise geological information is sparse, as well control is confined to a small, restricted corner of the area.

However, over the last ten years, advances in seismic data acquisition and processing technology have resulted in specific data sets which allow imaging of intra and sub-basalt units in the more basinal areas, where basalt is not present at outcrop. These data were analyzed to determine the geophysical characteristics of the geological units present, and a system was developed for the differentiation, categorization, and correlation of geological units and structures based upon these geophysical characteristics. The corresponding areal mapping of these units can assist in documenting the definition and evolution of structural relationships of the basalt and sub-basalt units throughout the region.

In areas adjacent to the Faroese Platform, Paleocene flow basalts are overlain by a post-basalt sedimentary section which is thick and well-developed towards basin centres. The flow basalt units are underlain by older interpreted sedimentary units which may be considered to be of interest to hydrocarbon exploration. These units are in turn underlain by a block-faulted basement whose fault and structural trends define the pre-existing features of the area.

Although structure throughout the area has been strongly influenced by Paleocene volcanism and subsidence, the main controls upon formation and orientation of structural features have been exerted by the basement faults. The predominant trend direction in the area is SW-NE (Caledonian). Later Eocene-Miocene compressional events are also evident within the area. Another key to the structural evolution is given by the presence of NW-SE trending transfer zones, which serve to offset and terminate structures as well as providing sediment entry points into the basinal features which they may influence or control.

These factors indicate that the evolution of margin features as a result of changing stress regimes has played a major role in defining the Faroese area in its current form.

## Geological setting

The Faroe Islands and their associated offshore area are located on the Northeast Atlantic Margin of Europe. This passive continental margin consists of many basins which have developed from the Devonian to the Paleogene (Fig. 1) and has a complex developmental history (Doré *et al.*, 1997). This is shown by the predominant NE-SW early Caledonian trend, which has been influenced by rifting events commencing in the Permo-Triassic and continuing episodically until the early

Tertiary, when extensive volcanism commenced within the area (Dean *et al.*, 1999). Uplift, erosion, subsidence and fault activity related to these rift phases has allowed deposition of Devonian to Cretaceous material in the evolving basin and associated ridge systems which were defined prior to the Tertiary and enhanced by subsequent tectonic events (Keser Neish and Ziska, 2004). NW-SE trending transfer zones have had a major influence on the structural and depositional pattern of the area (Mitchell *et al.*, 1993).

During the Eocene, a series of compressional

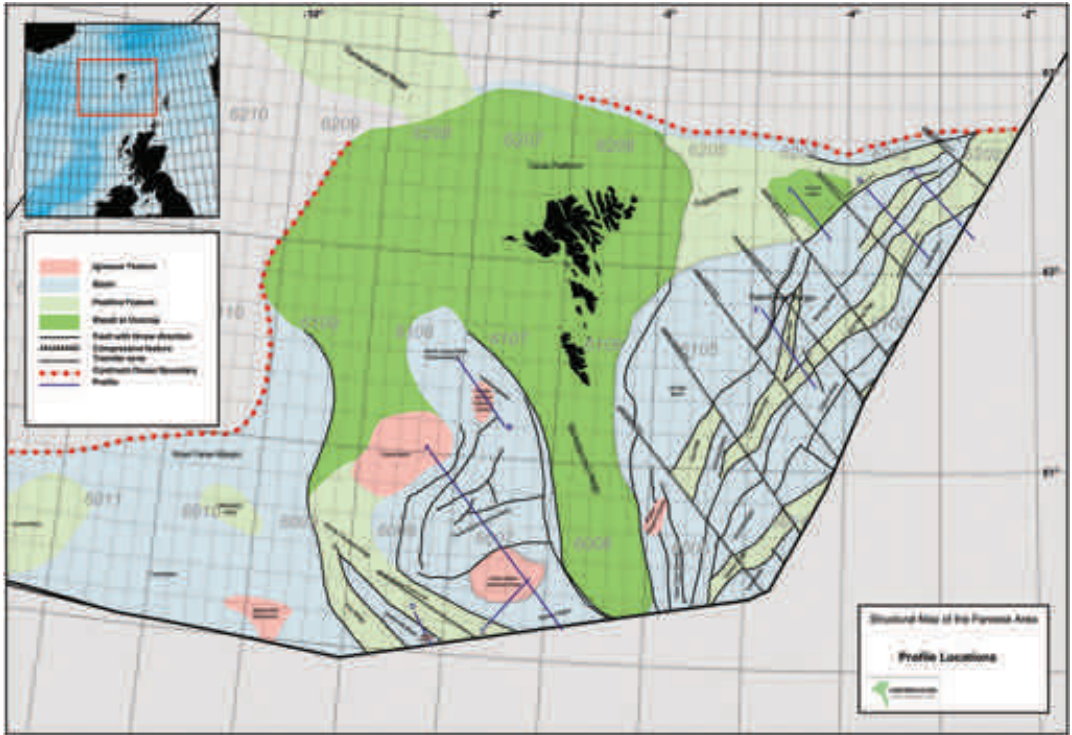


**Figure 1.** Principal structural and igneous elements of the Faroese offshore area, with seismic profile locations denoted. Faults have been derived from the regional Basement time structure map. Major correlated faults only are shown. Inset map shows the study area location on the North Atlantic Margin of Europe. DI denotes the location of the Drekaeya Intrusion.

tectonic phases related to the opening of the North Atlantic Ocean commenced, re-activating pre-existing fault trends and creating the present-day form of such positive features as the Wyville-Thomson Ridge, Munkagrinnur Ridge, and East Faroe High (Keser Neish and Ziska, 2004). Subsidence with related sedimentation and compressional events, leading to inversion during the late-Eocene-Miocene have dominated the recent history of the area (Boldreel and Andersen, 1993).

## Volcanic sequences in the Faroese area

Major eruptive episodes began in the early Tertiary, associated with the rifting and formation of the Faroese margin prior to the separation of the Faroese Plateau from Greenland (Ritchie *et al.*, 1999). The entire region was affected by thermal activity, associated with the suggested Icelandic mantle plume (Naylor *et al.*, 1999). The interaction of regional uplift and volcanic activity has resulted in the emplacement of large volumes of plateau basalt la-

vas, intrusive igneous centres, sill complexes, and volcanoclastic sequences. The thickness of the sequence at any given location is governed by the pre-existing topography, eruptive volume, rate, and stage of volcanism; intraepisodic weathering, deposition, erosion, and subsidence history. The interactions and relationships of all these factors, over millions of years, are reflected in the seismic record today. This thick succession of lower Tertiary volcanic rocks is present over most of the area and is the dominant feature observed, acting as an effective cover to the prior structural and stratigraphic fabric (Keser Neish and Ziska, 1996).

Onshore, a known thickness of approximately 3000 m above sea level is seen. At the Lopra-1 location a further 3565 m were drilled (Ellis *et al.*, 2002). The thickness of the volcanic column offshore is not known absolutely, but, as shall be discussed, various conclusions can be drawn from the interpretation of seismic data.

## Data Base

The seismic data base evaluated in this study con-





Or geologically related:

- High variability in acoustic impedance and Q, in three dimensions
- Thin beds
- Complex earth-induced multiple generation and ringing
- Generation of mode conversions, both simple and complex, with associated energy loss
- Presence of disrupted/rough weathered surfaces
- Generation of high-amplitude events from high acoustic impedance boundaries may mask weaker events

## Characterization and interpretation of seismic units

Interpretation of seismic data does not commence when the final data is available; interpretation is accomplished as a synergistic process from the time it is first decided to explore an area, throughout all the many stages of the acquisition and processing process: survey layout and parameter selection, signal and noise analysis, velocity determinations, and all the myriad adjustments for ray path geometry and image focussing analysis. However, it must be remembered at all times that the ultimate goal of all this effort is to *translate the seismic information into geological terms*: that is, to create a geologically valid structural picture.

Throughout all phases of the seismic 'interpretation' process, the analysis is ongoing. Questions being continually asked include: what do we see? Why is it there? Is it real? Noise? Artefact? What method of formation can be derived for what we observe? This procedure involves the use of geological judgement. If it is not possible to develop a sound geological model for the interpretation, the process must be repeated until a sensible solution can be derived; the more information which can be incorporated into this process, the better the process becomes.

This seismic interpretation process was undertaken without the benefit of well ties. UK wells were tied to seismic data, and it was attempted to carry this horizon information across into the Faroese basins, but this proved highly impractical for anything below the Eocene Balder level, because of the basalt/structural barriers which inhibit

the continuity of reflections.

Traditionally, seismic velocities and seismic stratigraphic concepts are used to define lithology and depositional environment. Because of the complexities of the volcanic environment and the lack of absolute geologic control, application of the principles of seismic stratigraphy has not been possible within the majority of the Faroese area. It was therefore necessary to use the seismic data to define both the structure and geology; e.g. the time/stratigraphic units by necessity had to be defined in seismic terms.

In order to enable interpretation and correlation of seismic units within this environment, a system was developed whereby geological units could be differentiated, categorized, and correlated based on their geophysical characteristics. Analysis of these characteristics leads to an interpretation model for each geological/geophysical unit. Subsequent mapping of these units is then used to document the structure and evolution of the region.

## Development of unit geophysical characteristics

Table 1 summarizes the seismic characteristics which have been derived for units within the Faroese area. A comprehensive description of the seismic unit geophysical characteristics used in this work may be found in Keser Neish and Ziska (2004).

Figure 3 displays the individual characteristic unit response, or unit signatures, described in Table 1. In general, the post-basalt units were interpreted as a whole, but two individual units immediately overlying the Top Basalt reflection will be described, as they give important information concerning volcanic processes in the area. The first unit surface is represented by the beige reflector, or Eocene tuffaceous Balder Formation, which is generally seismically opaque. It is often taken as the latest volcanic product. The red reflection interpreted below it is thought to be volcanoclastic in nature and to consist of material which has been eroded from volcanic highs and deposited downslope. It can display bedding and generally onlaps or downlaps upon the Top Basalt reflector.

The Top Basalt reflection itself, denoted by the green marker (Fig.3) is the strongest and most distinctive event observed in the region, exhibit-

Seismic Unit	Marker	Reflec- tion	Seismic Characteristics	Velo- city, km/sec	Age
<b>Post-Basalt</b>					
Sediment 1				1.6-1.8	Recent
Sediment 2				1.9-2.0	Miocene
Sediment 3				2.1-2.3	Oligocene
Volcaniclas- tics	Beige	Top	High amplitude, narrow, continuous peak	2.4-2.6	Eocene
		Internal	If present, layered, conformable; if absent, opaque		
		Base	Top Basalt reflection		
<b>Pyroclastics</b>	Magenta	Top	Moderate amplitude, continuous	3.3-3.7	Eocene
		Internal	Opaque		
		Base	Volcaniclastic or Top Basalt reflection		
<b>Basalt</b>	Light	Top	Moderate amplitude, rough	3.9-4.8	Eocene
	Green	Internal	Discrete, weak	(4.5 ave)	(Upper Series)
		Base	Not determined		
<b>Basalt</b>	Dark	Top	High amplitude peak-trough-peak doublet	3.9-4.8	Paleocene
	Green	Internal	Generally parallel-layered flows	(4.5 ave)	(Lower Series)
		Base	When observed, deepest parallel reflection		
<b>Subbasalt 1</b>	Orange	Top	Deepest parallel basalt reflection	N/a	Paleocene
		Internal	Variable amplitude and continuity		
		Base	Local onlap/downlap		
<b>Subbasalt 2</b>	Lavender	Top	High amplitude peak-trough-weak peak	4.8-5.21	Early Paleocene
		Internal	Locally strong amplitude, internal bedding		
		Base	Local onlap		
<b>Subbasalt 3</b>	Yellow	Top	High amplitude peak-wide trough-variable peak		Base Tertiary/
		Internal	Marginal coherent reflectivity		Top Cretaceous
		Base	Reflection character change		
<b>Subbasalt 4</b>	Red	Top	Narrow peak-broad trough-weak peak		?Mesozoic
		Internal	Weakly reflective		
		Base	High amplitude trough, variable following peak		
<b>Subbasalt 5</b>	Blue	Top	High-amplitude trough-variable amplitude peak pair		?Mesozoic/ Paleozoic

**Table 1.** Correlation of Seismic Units

ing a sharp, strong acoustic impedance response. Most commonly, internal reflections are parallel to subparallel, with an apparent bedded character believed to represent differing flows or eruptive

episodes. These can be of variable amplitude and continuity.

The primary factor to remember concerning the subbasalt units is that, although it is not possible to

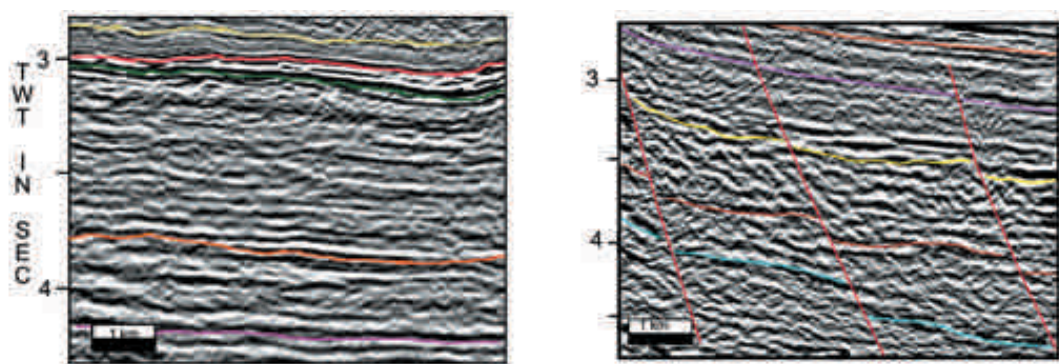


**Figure 3.** Detail showing seismic response of units interpreted as: Pyroclastic – beige marker; Volcaniclastic – red marker; Top Basalt – green marker; Base Basalt – orange marker; Subbasalt 2 – magenta marker; Base Tertiary (Subbasalt 3) – yellow marker; Subbasalt 4 – brown marker; Basement – blue marker. Seismic data shown courtesy of WesternGeco.

say absolutely what the units are, it is possible to make some conclusions based upon the behaviour and characteristics of these units.

The Base Basalt reflection, or top of the Subbasalt 1 unit, is shown by the orange marker, and can be difficult to identify, dependent upon the seismic data quality and geological environment. It often suffers from the effects of multiple superposition and composite interferences. On high platform or bank areas, where the basalt surface is present at or near outcrop, this reflector cannot be determined at all. When observed, this surface reflection is taken as the deepest parallel reflector seen, and the underlying unit usually exhibits weak, discontinuous reflection segments and may possibly represent a mixture of sedimentary and volcaniclastic products of Paleocene age.

The Subbasalt 2 unit, whose upper surface is given by the magenta marker, is usually quite highly reflective and shows strong internal reflectivity. It can infill depressions and form mound-like features. Localized sills may also occur. Because of its generally reflective character, internal features, and position in the geologic column, it is thought to be sedimentary in nature and Paleocene in age.

The yellow marker denotes the upper surface of the Subbasalt 3 unit and appears to represent a surface of non-deposition: on a regional scale, its form is quite smooth and relatively featureless; as a unit it is fairly massive, shows little in the way of coherent reflectivity, its structure is controlled by deeper features, and overlying units drape over its surface. Because of these indications, and the fact that the behaviour of the units above differs

markedly from the behaviour of units below, this surface is interpreted as the Base Tertiary Unconformity.

The interpretation of the Subbasalt 4, or brown, reflection response is tentative, but correlatable. The reflection event itself is generally composed of shorter, discrete segments whose overall character response is consistent. Little coherent internal reflectivity is seen within this unit, and given its position on the seismic data it is interpreted as Mesozoic in age.

The Subbasalt 5 unit, demonstrated by the blue reflection event, lies at the base of the section. It is the deepest discernible reflection event which can be correlated and mapped on the seismic data and it is therefore interpreted as acoustic basement. This event can be difficult to interpret above the surrounding background noise, but throughout the basinal environments of the Faroese area this reflection can be identified and carried. This level, thought to be Mesozoic/Paleozoic in age, not only helps to define the structural form and shape of the region, but appears to control it as well.

## Major structural features derived from seismic interpretation

Many diverse types of geological features formed from the units described above can be seismically defined within the Faroese area. Profile locations for all the seismic lines described in this section are given in Fig. 1.

Profile A (Fig. 4) trends from Faroe Bank (FB) in the northwest and crosses Faroe Bank Chan-



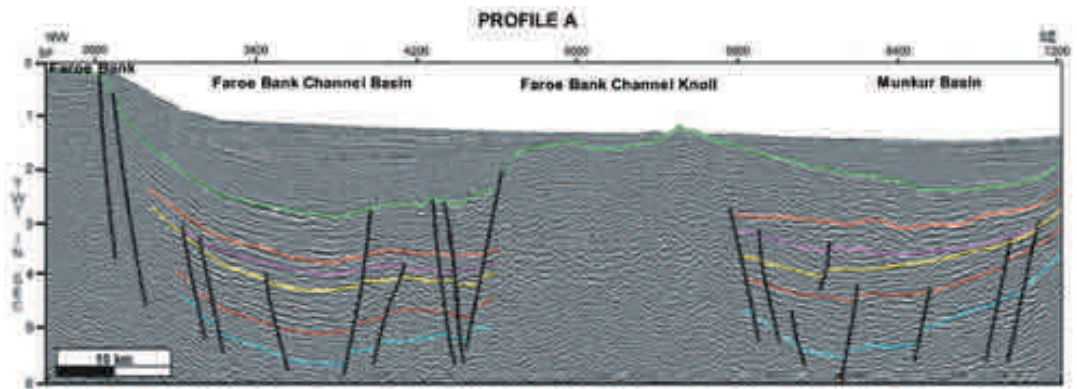


**Figure 4.** Descriptive seismic line showing primary structural elements of the Faroe Bank Channel Basin and its surrounds. Principal horizons interpreted as described in Fig.3; of particular note are the block faulted deeper layers and the disturbed area within the volcanics immediately to the northwest of Faroe Bank Channel Knoll. Seismic data shown courtesy of WesternGeco.

nel Basin (FBCB), Faroe Bank Channel Knoll (FBCK), and Munkur Basin. Within the two basins, all the major units are seen. Basalts are thicker in FBCB, but thin markedly to the southeastern part of Munkur Basin. Also notable is the disturbed zone which affects the basalt layer only, immediately northwestwards of FBCK. This is thought to be the result of transcurrent fault activity during the time of basalt emplacement (Keser Neish and Ziska, 2004).

Substantial features of volcanic origin are found within the Faroese area; many of these seem to lie to the west of the Faroe Platform (Fig.1). The characteristics of these features in relation to the surrounding structure can provide useful information concerning the structural orientation, age, and timing of volcanic episodes and tectonic activity in the area. Faroe Bank, which is thought to represent

an igneous centre based largely on its characteristic gravity response (Roberts *et al.*, 1983; Keser Neish and Ziska, 2004), is basalt covered and has steep sides. However, it is not possible on currently available data to determine an intrusive body, feeder dykes and vents, or basement fault block structures. Faroe Bank Channel Knoll separates FBCB from Munkur Basin and appears to have been erupted above sea level, as escarpments can be mapped (Keser Neish and Ziska, 2004). Later subsidence lowered the knoll below the wave base, but at a rate which allowed neither erosion or deposition at its crest. Fig. 5 shows the onlap of knoll volcanics onto the adjacent Wyville-Thomson Ridge (WTR), clearly demonstrating that the WTR existed as a positive flow-volcanic covered feature prior to the eruption of the knoll volcanics. This relationship suggests an age coincident with that

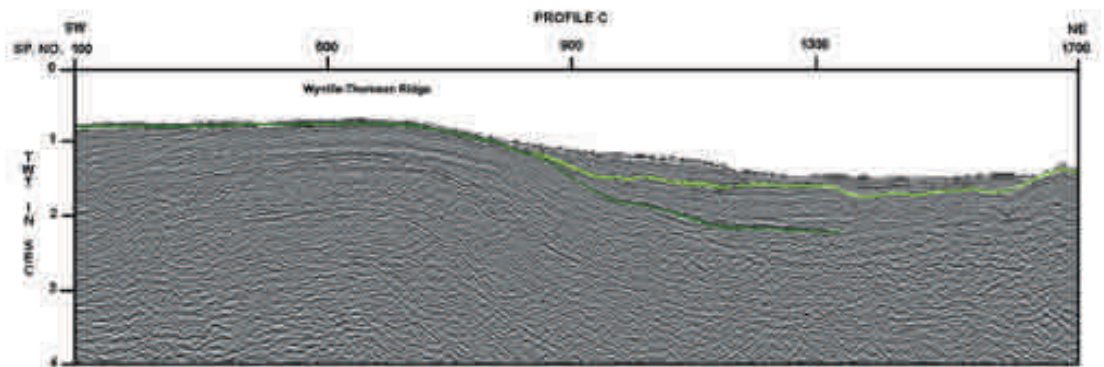


**Figure 5.** Seismic profile across Faroe Bank Channel Knoll and the Wyville-Thomson Ridge showing the clear onlap of younger (light green) knoll volcanics onto the older (dark green) WTR flows. Seismic data shown courtesy of Veritas.

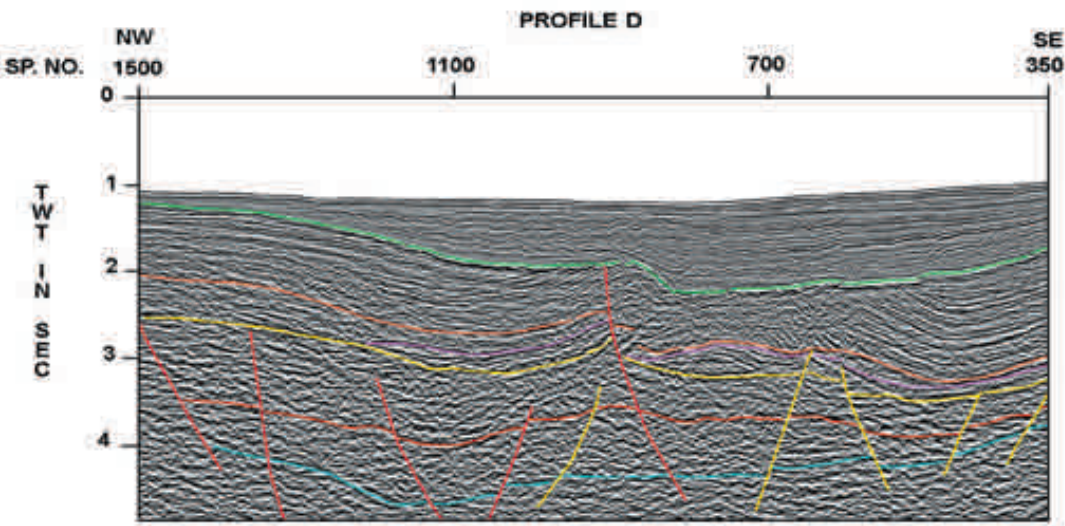


**Figure 6.** Seismic profile in Audhumla Basin demonstrating Drekaeyia Intrusion at SP 800, TWT 3 sec. and the folded, truncated volcanic structure above and block-faulted deeper layers. Units are interpreted as described in Fig. 3. Seismic data shown courtesy of WesternGeco.

of the Faroese Lower Series Basalts for the flow units, and Middle-Upper Series for the knoll volcanics (Keser Neish and Ziska, 2004). The ridge was probably even further uplifted by reactivation of older faults during a later compressive phase.

A different type of volcanic feature is shown in Fig. 6. Drekaeyia intrusion, in Audhumla Basin, displays this igneous element, which is overlain by flow basalts which appear to have been arched or folded upwards and eroded. The deeper structure is also highly faulted. These faults may have acted as conduits for the transport of volcanic material.

To the eastern side of the Faroe Platform, the structural dynamic is more similar to a ridge and basin style. Profile E (Fig. 7) traverses the two ‘paired’ highs of the East Faroe High and Trondur High. Neither of these features has bathymetric expression, and both are controlled by basement fault blocks over which parallel-layered basalts have flowed. It is highly possible that these, and similar highs, acted as sediment sources for the adjacent basins during more emergent periods (Keser Neish and Ziska, 2004). The majority of the fault activity stops at the yellow, or interpreted Base

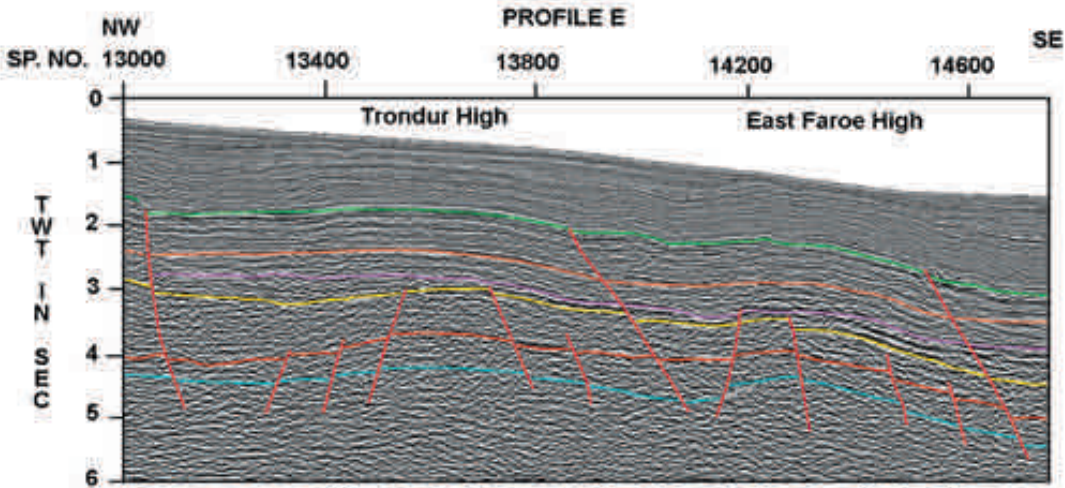


**Figure 7.** Seismic profile crossing Trondur and East Faroe Highs. Units interpreted as described in Fig. 3. Seismic data shown courtesy of WesternGeco.



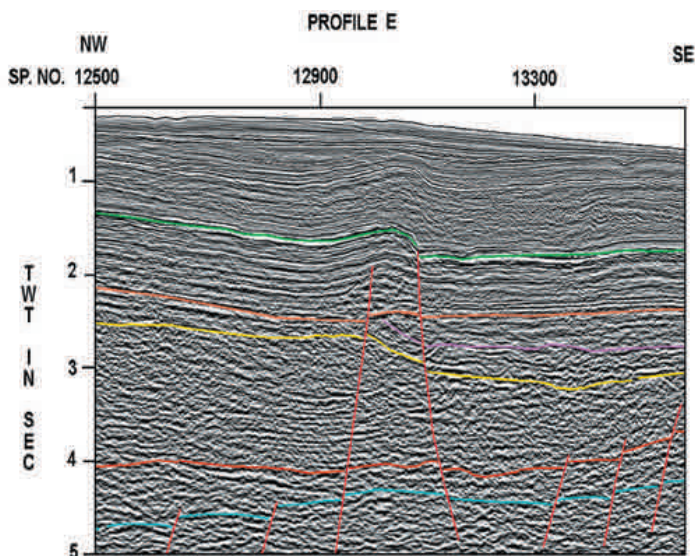


**Figure 8.** Extension of profile shown in Fig. 7 showing an interpreted compressional feature formed by probable Miocene-Oligocene reactivation of pre-existing deeper faulting. Seismic data shown courtesy of WesternGeco.

Tertiary, level and through-faulting is attributed to late-stage reactivation of earlier, pre-existing fault trends. This layer also displays a marked change in reflection character.

Further northwestwards on the same profile (Fig. 8) a prominent feature is seen which is ultimately fault controlled, but seems to have been formed primarily from this type of reactivation, probably during a Miocene-Oligocene compressional phase. This feature can be mapped for at least 60 km along the East Farøe Margin and it further displays a corresponding distinctive mag-

netic response (Keser Neish and Ziska, 1996; T. Varming, personal communication).

Profile F (Fig. 9) crosses Fugloy Bank, whose southeastern edge exhibits a fault-controlled escarpment. The top of Fugloy Bank is flat, featureless, and may be eroded; identification of units below this surface is quite tentative. It is not possible to say if Fugloy Bank is an igneous feature. However, basalts are present at the sea floor.

Further to the northeast, another high is seen (Fig. 10, Profile G) whose location again is clearly determined by a basement fault-controlled block.

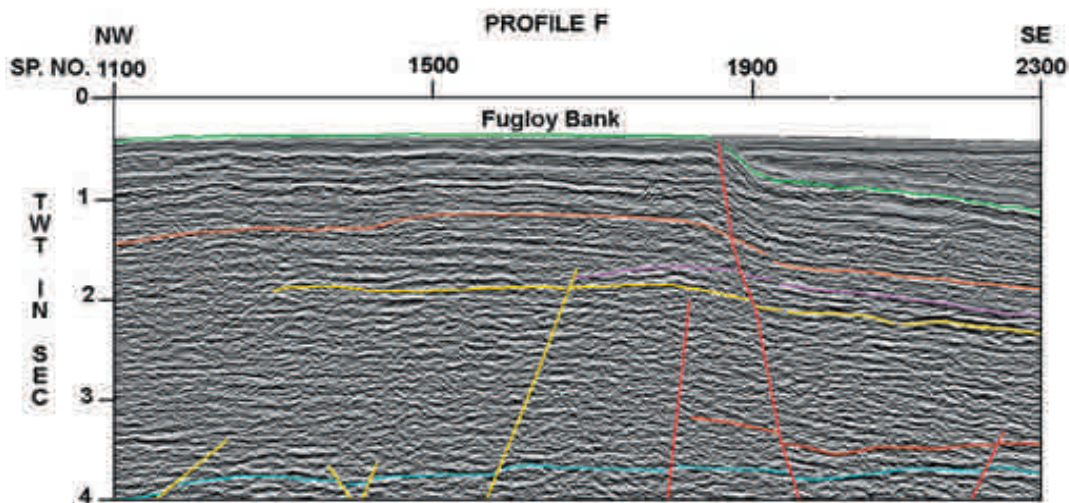


**Figure 9.** Profile showing the seismic character of Fugloy Bank. Units interpreted as described in Fig. 3. Seismic data shown courtesy of WesternGeco.



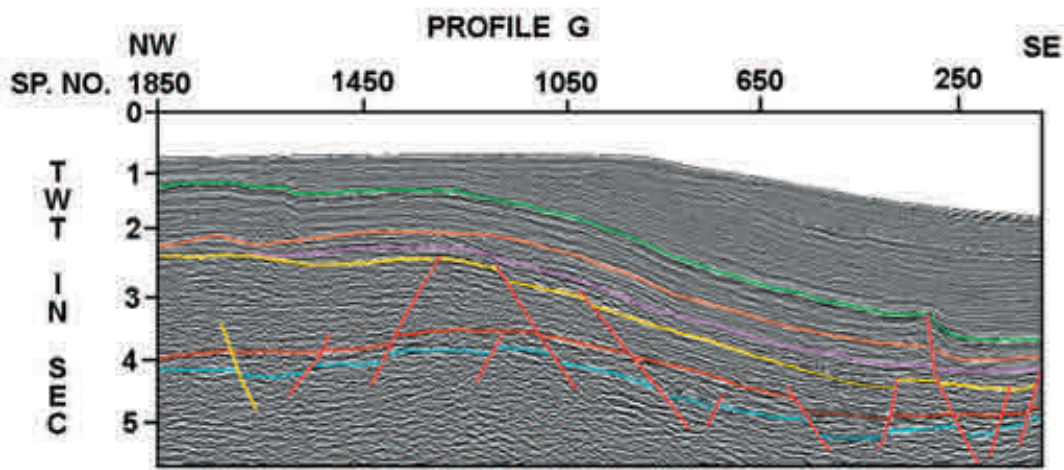


**Figure 10.** Seismic profile crossing the Faroe-Shetland Escarpment (SP 250) and a subparallel, SW-NE trending basement ridge lying between SPs 1450-900. Interpreted units as described in Fig. 3; seismic data shown courtesy of WesternGeco.

Faulting terminates at the Base Tertiary level and the overlying units have the appearance of a drape. This high is subparallel to the deep-seated fault which apparently controls the Faroe-Shetland Escarpment. The Faroe-Shetland Escarpment is thought to have been formed as a foreset breccia when subaerial lavas flowed over a paleocoastline (Smythe, 1983; Kjørboe, 1999). However, the position of this paleocoastline appears to be fault-controlled (Keser Neish, 2004).

Profile H (Fig. 11), documents the detail of this controlling fault, and further displays an adjacent,

downdip fault-controlled structure. This line demonstrates clearly the seismic character of the units: the parallel-bedded nature of the flow basalts, the relatively opaque underlying unit, local strong reflectivity and mounding in the Lower Paleocene (magenta) as well as the marked change in reflection character above and below the Base Tertiary (yellow) level. Although the brown unit is largely absent here, the basement reflection character is quite clear. Also visible, southeastwards from SP 3300, are younger, localized volcanics which rest upon and overlap the older flow basalts. This can

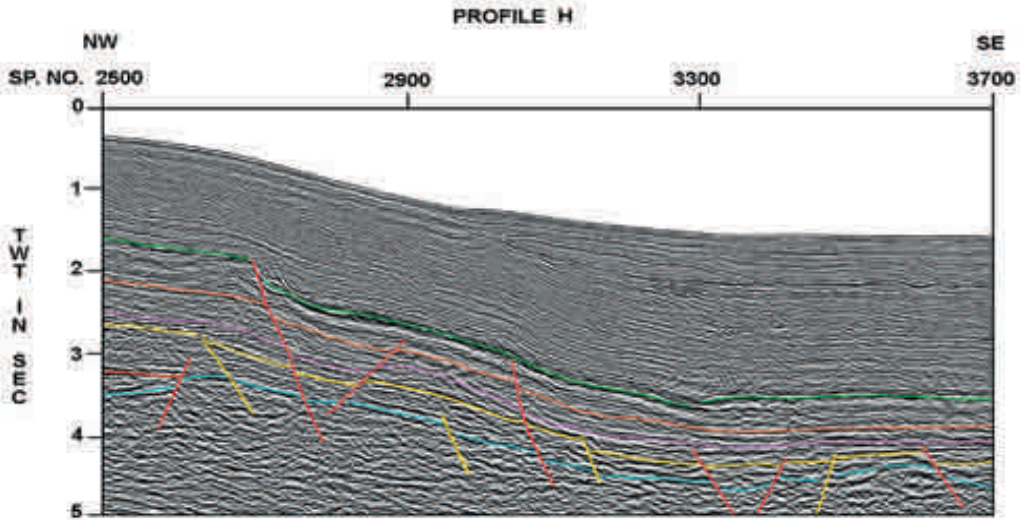


**Figure 11.** Seismic profile showing the basement fault control (SP 2750) for the Faroe-Shetland Escarpment, a further basement fault block lying southeastwards (SP 2850-SP 3100) and tongue of younger volcanics trending southeastwards from SP 3300. Units as described in Fig. 3 and seismic data shown courtesy of WesternGeco.

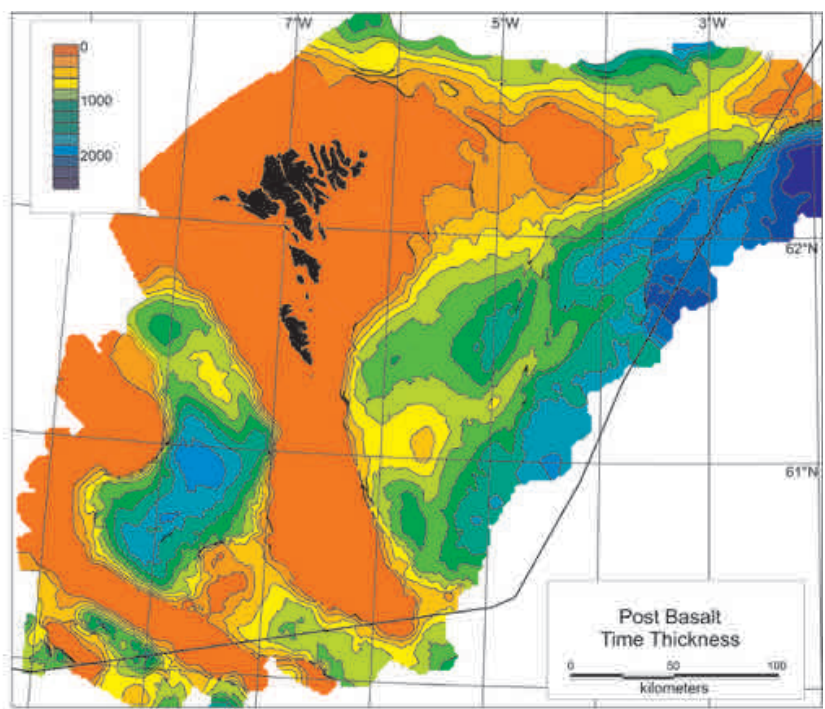


**Figure 12.** Post Basalt Time Thickness Map displaying the sediment interval between the water bottom and the Top Basalt. Contour interval is 200 ms.

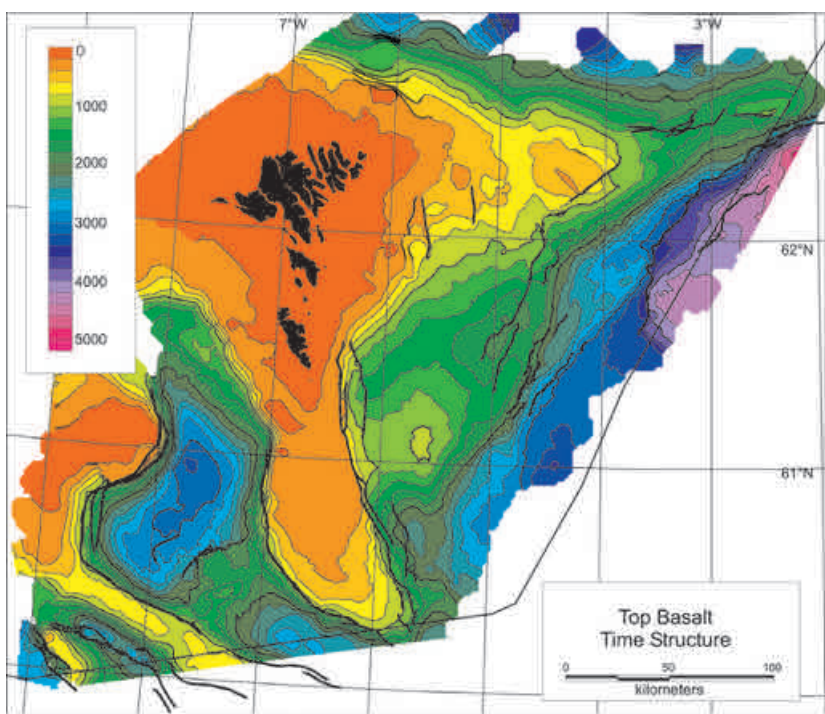


**Figure 13.** Top Basalt Time Structure Map. Contour interval is 200 ms.

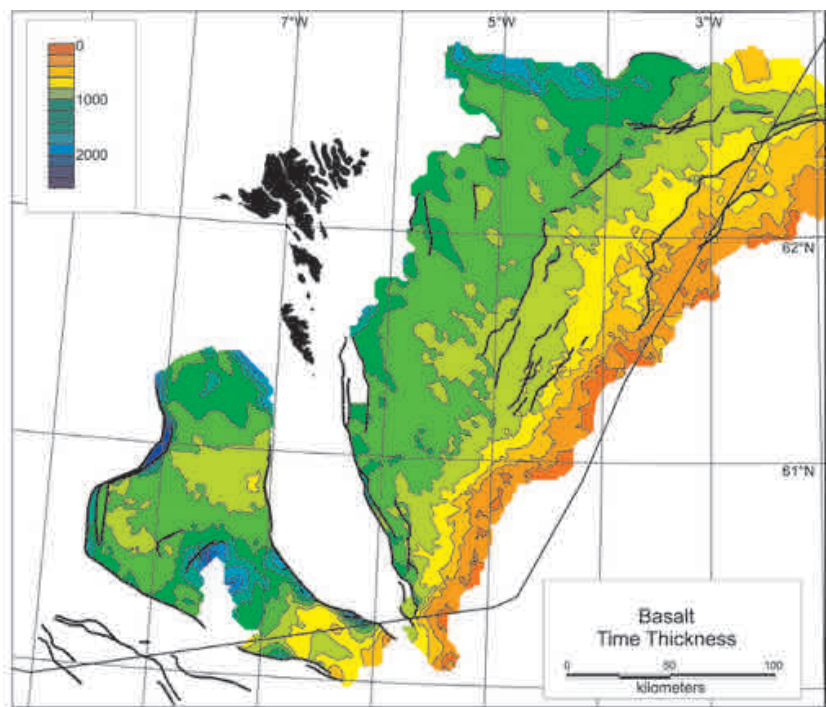


**Figure 14.** Basalt Time Thickness Map. The extent of this map is constrained by the ability to interpret and map the Base Basalt reflection. Contour interval is 200 ms.

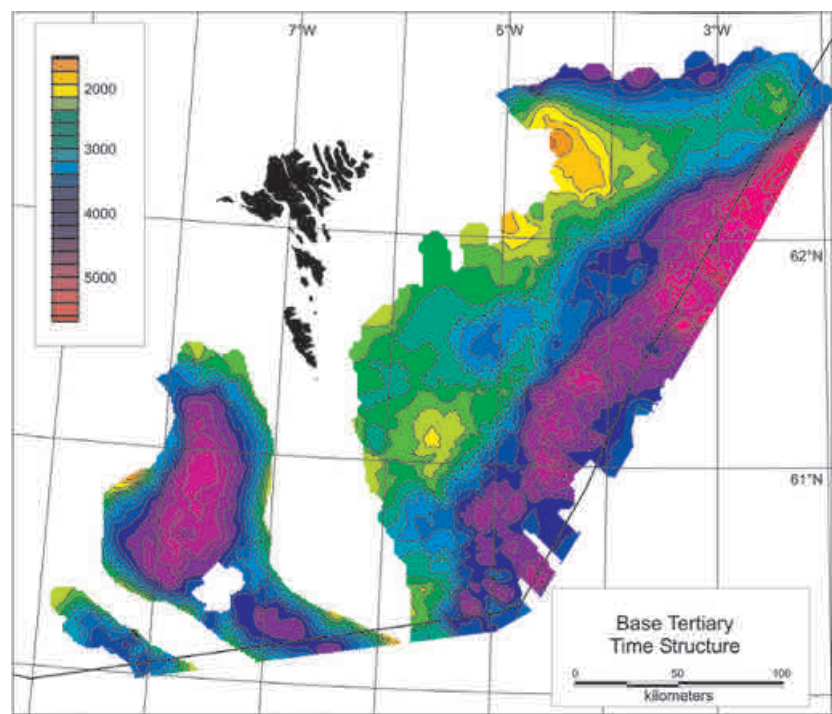


**Figure 15.** Base Tertiary Time Structure Map with major correlated faults. Contour interval is 200 ms.



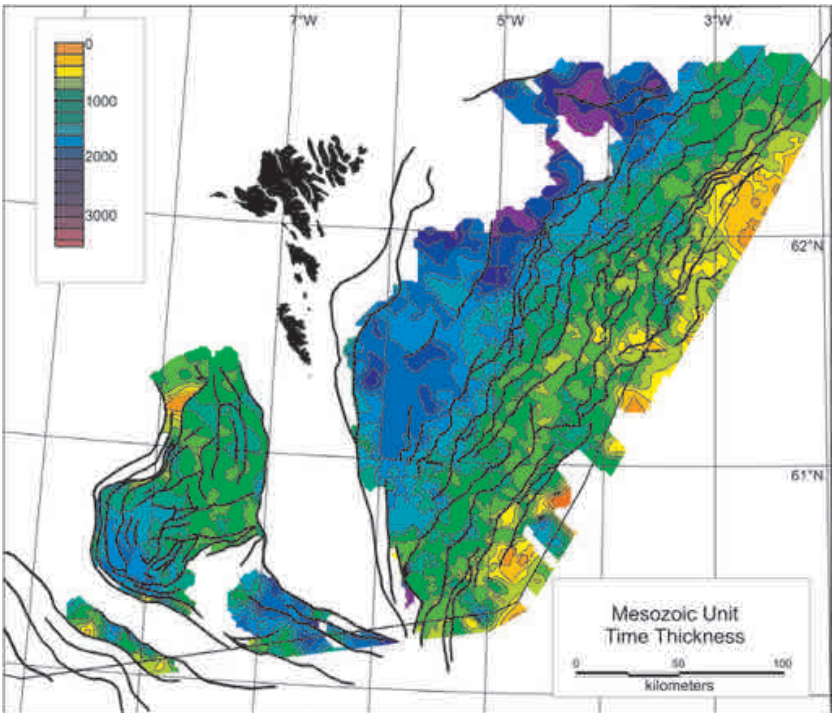


**Figure 16.** Mesozoic Unit Time Thickness Map displaying the interval thickness between the interpreted Base Tertiary and Basement reflections. The extent of this map is constrained by the ability to interpret and map the Basement reflection. Basement level faults are superimposed (see Fig. 17). Contour interval is 200 ms.

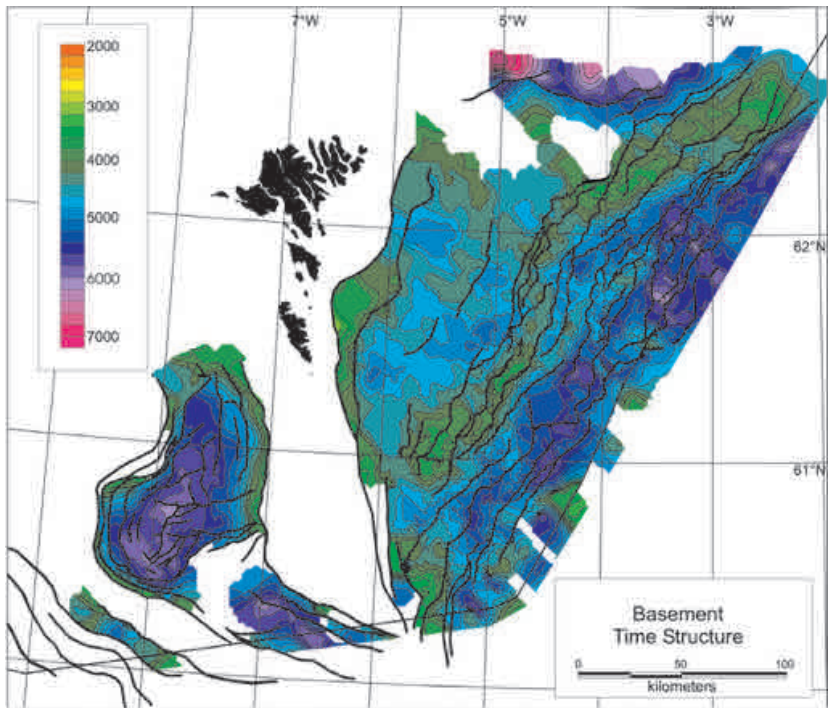


**Figure 17.** Basement Time Structure map with major correlated faults. Contour interval is 200 ms.

be mapped as a tongue of younger volcanic material beneath the Faroe-Shetland Channel, most probably originating from a local source.

## Structural characteristics derived from mapping and interpretation

The geophysical interpretation procedure previously described can be used to generate unit maps (Figs. 12-17) which illustrate the depositional and geological characteristics of the area at individual unit levels. The relationships between the successive maps can be readily observed, and possible structures suitable for further investigation can be located.

The Post-Basalt time-thickness map (Fig. 12) shows the basinal areas which have acted as post-basalt depocentres. The Top Basalt time structure map (Fig. 13) defines the interpreted extent of the basalt, the depth in time to its surface, and areas where the basalt is either present at the surface or has been uplifted. The Basalt time-thickness map (Fig. 14) demonstrates the thinning of the basalt away from the platform area southeastwards, and also in Munkur Basin; a further thinned area is noted within FBCB. The Base Tertiary Time structure map (Fig. 15) defines the interpretational limit of this reflection event towards the Faroe Platform and the depth in time to this surface. The entire geologic interval present beneath the Base Tertiary (yellow) horizon is interpreted as being Mesozoic or older, and the Mesozoic Unit time-thickness map (Fig. 16) describes the relationship between the Base Tertiary and Basement (Fig. 17) structural levels. It is not possible here to derive any information regarding the age of any individual units, or even determine between Paleozoic or Mesozoic intervals, based on the available geophysical data.

## Fault Behaviour

It is notable that the predominant fault trend is Caldonian (SW-NE), although a strong N-S trend, interpreted as Jurassic (Keser Neish and Ziska, 2004) is noted both in the Judd Basin and the North Faroe Bank Channel Basin.

In general, two types of fault behaviour are observed within the area: normal faulting and transfer zone, or deep transcurrent, faults. Most apparent from this series of maps is the evidence for the controlling influence which the basement faults

have had upon the architecture of the area. The basement level, as shown by the Basement time-structure map (Fig. 17) displays the oldest and greatest degree of faulting seen; these define the platform, basinal, and high or ridge structures.

Generally magnitude of throw decreases upwards within the section. Within the deeper Mesozoic levels, unit thickness is generally quite uniform but some growth activity may be observed, indicative of deposition during fault activity (Figs. 10 and 11). This growth is not observed in the overlying Base Tertiary interval, and fault movement at this level is minimal. The basic form of this unit has resulted from the deeper structural features and fault activity, but the unit itself is not greatly affected. Other than at the basin margins, very little faulting occurs above the Base Tertiary, and in general only minor, unrelated fault activity has been interpreted above the basalt; essentially, units above the Base Tertiary are largely 'decoupled' from fault activity other than for unit termination at marginal bounding faults.

An example of an exception to this would appear to be apparent transverse-basin faulting within the FBCB, as described by Keser Neish and Ziska (2004). Only the basalt unit is disturbed by this activity. Underlying units display normal faulting only, and any disturbance in the overlying units is attributed to sedimentary drape over the affected basalts. This behaviour is attributed to re-activation of pre-existing fault trends during the time of basalt extrusion. Although this movement is interpreted as normal in throw, a strong element of transverse fault activity could be present.

The pronounced affect of transfer zones upon the structural and depositional grain of the area is most evident from the mapping. It can be readily observed that the location of the NW-SE trending transfer zones in Fig. 1 correspond with offset and termination of structural and depositional features displayed on the unit maps (Fig. 12-17).

## Conclusions

Key points arising from the analysis and interpretation of seismic data within the Faroese area are:

- Seismic data of usable quality can be acquired in the Faroese area.

- Geological units, which can be defined and correlated in terms of their inherent seismic reflection characteristics can be derived from this data
- Broad geological identification of these units, based upon this technique, is possible
- Seismic data interpreted systematically in this manner can provide useful information concerning the structure, history, and evolution of this area
- The area to the west of the Faroe Platform exhibits a predominance of volcanic features; the area to the eastwards displays a more 'ridge and basin' structural style
- Both Caledonian (SW-NE) trending normal faults and NW-SE trending transfer zones have strongly influenced the structural form of the area.

## Acknowledgements

The seismic interpretation and mapping shown in this study was accomplished using data with the permission of WesternGeco, Veritas DGC, and Fugro Geoteam and their cooperation is gratefully acknowledged.

## References

- Boldreel, L.O. and Andersen, M.S. 1993. Late Paleocene to Miocene compression in the Faroe-Rockall area. *In: Parker, J.R. (ed.) Petroleum Geology of Northwest Europe: Proceedings of the 4<sup>th</sup> Conference*. Geological Society, London: 1025-1034.
- Dean, K., McLachlan, K., and Chambers, A. 1999. Rifting and the development of the Faroe-Shetland Basin. *In: Fleet, A.J., and Boldy, S.A.R. (eds.) Petroleum Geology of Northwest Europe: Proceedings of the 5<sup>th</sup> Conference*. Geological Society, London: 533-544.
- Doré, A.G., Lundin, E.R., Fichler, C. and Olesen, O. 1997. Patterns of basement structure and reactivation along the NE Atlantic Margin. *Journal of the Geological Society, London*, 154: 85-92.
- Ellis, D., Bell, B.R., Jolley, D.W. and O'Callaghan, M. 2002. The stratigraphy, environment of eruption and age of the Faroes Lava Group, NE Atlantic Ocean. *In: Jolley, D.W. and Bell, B.R. (eds.) The North Atlantic Igneous Province: Stratigraphy, Tectonic, Volcanic, and Magmatic Processes*. Geological Society, London, Special Publication 197: 253-269.
- Keser Neish, J.C. and Ziska, H. in press. Structural Interpretation of the Faroe Bank Channel Basin. *In: Dore, A.G. and Vining, B. (eds.) Petroleum Geology: North West Europe and Global Perspectives -Proceedings of the 6<sup>th</sup> Petroleum Geology Conference*. Geological Society, London.
- Keser Neish, J.C. 2004. *Faroeese Region: A Standard Structural Nomenclature System*. Jarðfrøðisavnið, Tórshavn, Faroe Islands, 66 pp.
- Keser Neish, J.C. and Ziska, H. 1996. Imaging of Basalts and Underlying Structures in the Faroeese Offshore Area. *Frøðskaparrit*, 44: 119-129.
- Kjørboe, L. 1999. Stratigraphic relationships of the Lower Tertiary of the Faroe Basalt Plateau and the Faroe-Shetland Basin. *In: Fleet, A.J., and Boldy, S.A.R. (eds.) Petroleum Geology of Northwest Europe: Proceedings of the 5<sup>th</sup> Conference*. Geological Society, London: 5559-572.
- Mitchell, S.M., Beamish, G.W.J., Wood, M.V., Malacek, S.J., Armentrout, J.A., Damuth, J.E. and Olson, H.C. 1993. Paleogene sequence stratigraphic framework of the Faeroe Basin. *In: Parker, J.R. (ed.) Petroleum Geology of Northwest Europe: Proceedings of the 4<sup>th</sup> Conference*. Geological Society, London: 1011-1023.
- Naylor, P.H., Bell, B.R., Jolley, D.W., Durnall, P. and Fredsted, P. 1999. Palaeogene magmatism in the Faeroe-Shetland Basin: influences on uplift history and sedimentation. *In: Fleet, A.J. and Boldy, S.A.R. (eds.) Petroleum Geology of Northwest Europe: Proceedings of the 5<sup>th</sup> Conference*. Geological Society, London: 545-588.
- Ritchie, J.D., Gatliff, R.W. and Richards, P.C. 1999. Early Tertiary magmatism in the offshore NW UK margin and surrounds. *In: Fleet, A.J. and S.A.R. Boldy (eds.) Petroleum Geology of Northwest Europe: Proceedings of the 5<sup>th</sup> Conference*. Geological Society, London: 573-584.
- Roberts, D.G., Bott, M.H.P and Uruski, C. 1983. Structure and Origin of the Wyville-Thomson Ridge, *In: Bott, M.H.P., Saxov, S., Talwani, M. & Thiede, J. (eds.) Structure and Development of the Greenland – Scotland Ridge*. Nato Conference Series, Serie IV: Marine Science, Plenum Press, London: 133-158.
- Smythe, D.K. 1983. Faroe-Shetland Escarpment and Continental Margin north of the Faroes. *In: Bott, M.H.P., Saxov, S., Talwani, M. and Thiede, J. (eds.) Structure and Development of the Greenland – Scotland Ridge*. Nato Conference Series, Serie IV: Marine Science, Plenum Press, London: 109-119.



# Exploration Opportunities in the Faroe Islands

HERI ZISKA<sup>1</sup> AND CLAUS ANDERSEN<sup>1,2</sup>

1: Faroese Geological Survey (JFS), Tórshavn, Faroe Islands, hziska@jfs.fo

2: present address: Geological Survey of Denmark and Greenland (GEUS), Copenhagen, ca@geus.dk

## Abstract

The exploration of the Faroese Continental Shelf (FoCS) saw a surge of activity in 2000, when the first offshore licensing round resulted in award of 7 licenses with a total of 8 commitment wells, a number of geophysical data acquisition commitments and a number of committed geological studies. The first drilling campaign, which only targeted one play in one basin, did not live up to the immense expectations. Much of the area and stratigraphic column has not been tested. Sub-basalt imaging problems were initially quoted as the reason to focus on the Judd Basin without basalt cover. It is demonstrated that sub-basalt imaging has improved to such an extent that large structures, which bear striking resemblances to structures on the UK side of the Faroe-Shetland Channel, can be mapped. An active hydrocarbon system exists in UK waters and geochemistry of seabed cores support extension into FoCS. Numerous reservoir sections have been proven in the West of Shetlands offshore and by analogy may also be present on the neighbouring FoCS. A westerly sediment provenance, Greenland and/or the Faroese Platform is anticipated to dominate in large parts. The existence of basinwide seals has been proven by many wells and is considered a minor risk when exploring large sub-basalt structural traps on the FoCS.

## Introduction

The Faroese continental shelf is at an early stage of hydrocarbon exploration and remains one of the least explored parts of the NW European Atlantic Margin. The exploration activities have been focussed on a confined area to the SE of the Faroe Islands, adjacent to the international border with UK. The remaining part of the Faroese shelf is characterised by Palaeogene flood basalts of varying thickness, which reduce seismic imaging quality of pre-basalt exploration targets, adding an extra challenge to this frontier area.

Important events leading to hydrocarbon exploration on the Faroese Continental Shelf (FoCS) include the agreement made between the Faroese Home Rule authorities and the Danish government in 1992 on the transfer of legislative and administrative competence concerning 'mineral resources

in the subsoil' to the Faroese Home Rule authorities. Interest for petroleum exploration was boosted by the discovery in the same year of the Paleocene Foinaven field in UK Quadrant 204 close to the so-called 'White Zone', which was at that time a disputed area in the Faroe-Shetland Channel. The international continental shelf boundary between the Faroe Islands and the United Kingdom was finally defined in an agreement signed by the parties in summer 1999. As the legal framework and legislation already was in place the first Faroese Licence Round could be launched in 2000 within a contiguous area covering approx. 14,000 km<sup>2</sup> located to the east and south-east of the islands.

The period between 1992 and 2000 was not just a period of 'wait and see' with respect to geophysical data acquisition. Western Geophysical Co. (now WesternGeco) received exclusive rights to acquire seismic data in 1994 and 1995 in return for a com-

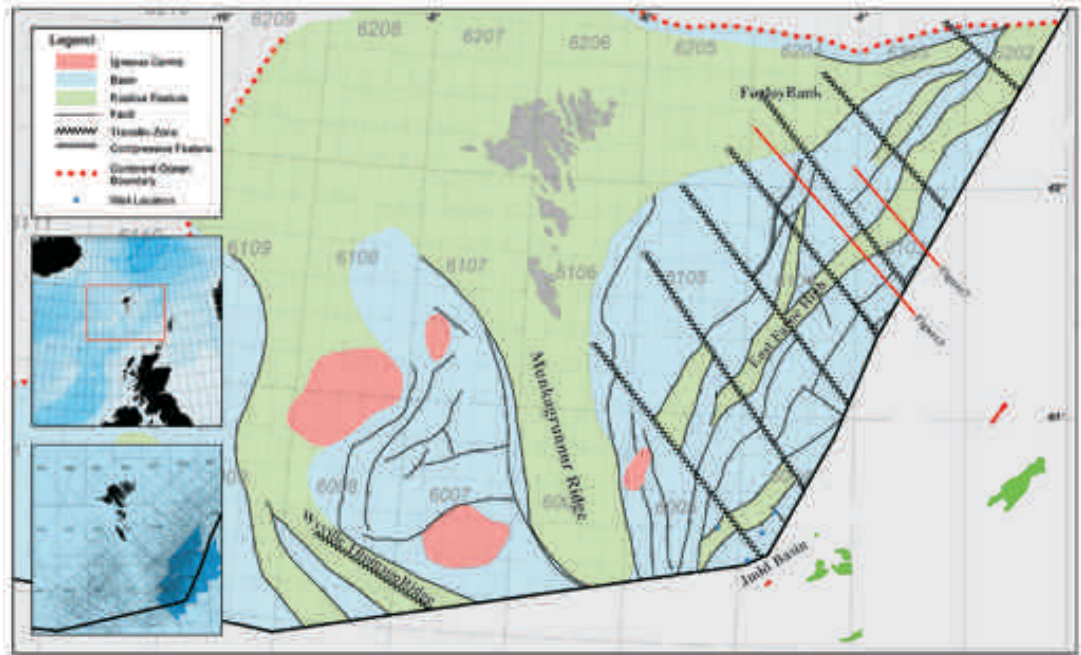


**Figure 1.** Structural Elements of the Faroese Continental Shelf. Inset Location map and seismic data coverage map.

mitment to acquire a pre-defined amount of data. A similar exclusive licence was awarded to World Geoscience Corporation (now part of Fugro) to acquire aeromagnetic and seep data in 1995 and 1996. In the following years a lot of seismic activity took place, mostly concentrated to the area to the east and southeast of the islands. This resulted in acquisition of almost 50,000 km of 2D data and about 8,000 km<sup>2</sup> of 3D data, almost exclusively as non-proprietary surveys prior to opening the 1<sup>st</sup> round (Fig. 1, inset).

The level of interest was high in spite of turmoil in the oil industry with big fluctuations in the price of crude oil and several large company mergers. The round resulted in award of seven licences on 17<sup>th</sup> August, 2000 (Fig. 1). Four of the licences are located in the Judd Basin, an area with no or insignificant Palaeogene basalt and covered with pre-existing 3D seismic. The firm work programme here included drilling of a total of eight exploration wells. The remaining three licences are located in basalt covered areas and are without initial drilling commitments.

The exploration objectives in the Judd Basin licences with water depth of about 1000 m were focussed on Paleocene sandstones deposited in slope and basin floor environments. The producing West

of Shetland fields located on the eastern flank of the basin were used as analogues. Identification of prospects with a high stratigraphic component was seismic amplitude driven with various degrees of AVO support.

So far four wells have been drilled with somewhat mixed and surprising results. Three wells encountered oil shows of varying magnitude in the Upper Palaeocene section. Reservoir sandstones of high quality were drilled, but the section in the basin centre was overall much more sandy than expected and thus flawing trap integrity (Hollingsworth, 2002). Due to the differing lithologies the WOS fields proved poor analogies and AVO techniques failed as fluid prediction tools in this setting. Although disappointing, the well results showed that an active petroleum system exists on the Faroese Continental Shelf.

The 6004/16-1z well, drilled by Amerada Hess and partners, on a structural high of a Tertiary inversion anticline was deepened below the sand dominated Upper Paleocene section through underlying siltstones/shales. The resulting 'Marjun' discovery consisted of a 170 m gross hydrocarbon column in the T10 Lower Palaeocene interval (Smallwood and Kirk, 2003). Although the interval was not flow tested, and therefore reservoir





volumes of locally derived coarse clastic sediments and allowed dominance of shale deposition during this time interval. Many deeper faults terminate in the ductile upper Cretaceous shales. Larsen *et al.* (1999) suggest that Greenland might have acted as a provenance area to the Faroes region during Cretaceous and continuing into the Early Paleocene.

Initiation of extensive volcanism prior to separation of the Faroe Plateau from Greenland was preceded by regional uplift, which resulted in widespread sub-areal environments in the Paleocene at basin margins (e.g. Dean *et al.*, 1999). Reworking of Cretaceous and Jurassic sediments during the early-mid Paleocene has been documented on the Shetland Platform. There was a shift in the orientation of the depocentres in the Paleocene compared to the Cretaceous. The Judd Basin has experienced a massive influx of sediments in the Paleocene (Smallwood, this volume). New well data from the Faroes area has revealed that copious amounts of sand were shed into this basin (Poulsen *et al.*, 2004). Provenance studies indicate that sediments were sourced from both the Shetland Platform and from the East Greenland margin to the west. Dean *et al.* (1999) suggested major rifting allowed massive Paleocene subsidence and resultant sediment deposition, in contrast to Mudge and Rashid (1987) who suggested post-rift thermal subsidence was associated with earlier Cretaceous rifting.

The onset of volcanism in the North Atlantic Igneous Province took place 60.5 Ma (Ellis *et al.*, 2002). Most parts of the Faroese Continental Shelf were covered by flood basalts as result of the volcanism. The total stratigraphic thickness established onshore Faroe Islands is in excess of 6 km. The flood basalts have been subdivided into a Lower, Middle and Upper Formation with the Lower and Middle Formation separated by a thin sedimentary section. The extent of the different formations is disputed with e.g. Ritchie *et al.* (1999) suggesting that the Upper Formation is most widespread towards the Faroe-Shetland Channel. In contrast Neish and Ziska (in press) suggest that the Lower Formation is the most widespread, at least in the Faroe Bank Channel area to the south.

Post-rift subsidence continued throughout the Cenozoic in the Faroe-Shetland Channel and Faroe Bank Channel area, punctuated by multiple compressional phases. Oligo-Miocene compression has been suggested as the cause of some of

the large scale features such as Munkagrunnur and Wyville-Thomson Ridges (Boldreel and Andersen, 1993). Neish and Ziska (in press) suggest however that pre-existing ridges were present prior to the Oligo-Miocene compressional events.

## Challenges

It is postulated above that several untested exploration opportunities are left in the Faroese offshore area. The question is why have these opportunities not been explored as actively as the Foinaven/Schiehallion analogues in the Judd basin?

There are at least three answers:

- Firstly; a layer of flood basalts of varying thickness covering most parts of the Faroese Continental Shelf and inhibiting exploration due to serious imaging problems with geophysical techniques available today.
- Secondly; it is a frontier area. By the late 1990's a large number of wells had been drilled on the flank of the Judd Basin in the UKCS, and the industry expected, based on wells and advanced geophysical techniques, to find certain types of geology in the deeper parts of the basin. This concept did not deliver the expected results. The remaining part of the area does not have any nearby correlation wells, and advanced geophysical techniques are not possible or applicable.
- Thirdly; the perception of sub-basalt exploration has met a lot of apprehension within some oil companies, where any basalt is considered to be a barrier too great to overcome partly due to the mentioned issues and partly due to expected technical issues regarding drilling through basalt.

## Imaging problems

The flood basalts form a barrier to seismic imaging because of the very high impedance contrast between the overlying sediments and the basalts themselves (White *et al.*, 2003). Another issue is a very uneven surface, and internal in-homogeneity resulting in scattering of energy.

It has been attempted to overcome the problems by use of large low frequency energy sources and the use of long acquisition cables which enable recording of a higher fold and also to utilise converted wave arrivals (Van der Baan *et al.*, 2003). Other seismic experiments have also been attempt-

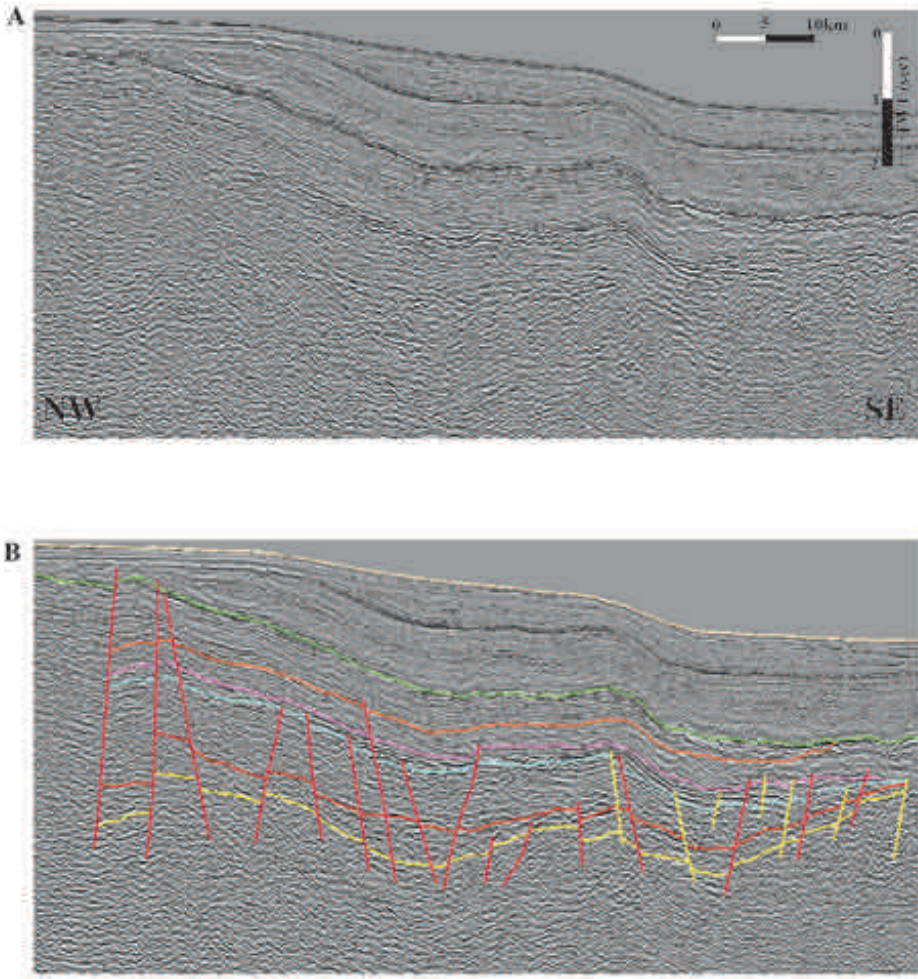


**Figure 3.** A: Seismic section across East Faroe High. B: Interpreted version of same seismic line. Seismic data shown courtesy of WesternGeco.

ed, such as: Ocean bottom Seismometers (OBS), Ocean Bottom Cable (OBC), Dragged Array, Vertical Cable and multi-pass shooting, the latter with a total offset up to 38 km.

The method which has given the most promising results with regard to detailed mapping of possible prospects, is conventional seismic data acquired with 6–8 km cables and large low frequency airgun arrays. These data can be used in conjunction with other geophysical methods in order to mitigate the weaknesses of one method with the corresponding strength of other methods.

Several geo-scientists have independently attempted to map the sub-basalt section in the Faroese area applying techniques, which are variations on the one mentioned above. The resulting maps have

over the years converged towards a point where today most maps are very similar, both with respect to the large scale structures, and the TWT to mapped horizons. Figure 3 shows an interpreted seismic section across the East Faroe High. Top basalt is the green horizon. A number of horizons have been mapped below the top basalt. It is not possible to state conclusively which one represents the base basalt/volcanics. The authors favour the second interpreted horizon below the top basalt (Violet) as the base of the volcanic rocks with the one above (Orange) defining the base of the sub-aerial flood basalts. What remains, however, is that sub-basalt imaging appears possible with methods in use at present.

## Frontier area issues

It is not possible to suggest with any confidence what the geological sections mapped below the basalt cover represent. There have been many attempts to tie wells to seismic and in that way to get an idea on the pre-basalt stratigraphy. The long distance to the nearest wells, which are either located in the Judd Basin or on the Corona Ridge, limits the value of attempted well ties significantly.

Advanced geophysical techniques are frequently used to derive lithological information from seismic data and access to nearby wells for calibration. However, data quality is an issue, which is very likely going to limit the value of advanced geophysical techniques in a sub-basalt environment, until a significant breakthrough in sub-basalt imaging has been achieved.

## Opportunities

The basalt covered Faroese Continental Shelf is a frontier area with lack of 'hard' data, where standard exploration techniques are difficult to use due to seismic imaging problems. This reduces the possibility to carry out a risk reduction process of mapped structures. It is therefore necessary to establish exploration models based on robust geological models in a basinwide context. A review and discussion of individual play elements extracted from neighbouring areas is attempted in the following section.

### Source rocks and maturity

The presence and effectiveness of source rocks in the UK part of the Mesozoic-Tertiary basins in the Faroe-Shetland Channel area has been described by among others Scotchman *et al.* (1998) and Holmes *et al.* (1999). Amounts, type and timing of hydrocarbon generation remain only partly understood.

The main source rock in the WOS area is the Late Jurassic Kimmeridge Clay equivalent with lacustrine Middle Jurassic shales forming a secondary co-source. The Kimmeridge Clay equivalents have been penetrated in a large number of wells and believed to be widespread on the margin (Fig. 4). It is a world-class source rock with TOC > 5% and S<sub>2</sub> yields up to 50 kg/t when immature. Since the organic matter dominantly is of marine algae origin, it generates oils low in wax.

Middle Jurassic oil-prone source rocks were deposited along basin edges in restricted marine/lagoonal-lacustrine environments. However, their present-day extent may be further restricted by later erosion (Lamers and Carmichael, 1999). When present, they are rich in organic matter and are dominated by kerogen type I and type I/II. Upon maturation they will generate waxy oils.

There is at present no evidence for Cretaceous source rocks in the UK part of the Faroe-Shetland Channel area. However, well data from the deep-water Vøring and Møre Basins offshore Mid-Norway suggest possible Cretaceous source rock intervals although their quality still has to be confirmed (Kristensen *et al.*, 2004). Their possible southward extent into Faroese waters can be speculated.

The filling history of the WOS fields is complex. There have been three periods of hydrocarbon charging into the Palaeocene reservoirs in the Foinaven Field, with the first the two charges having been subsequently biodegraded before the final live oil charge (Scotchman *et al.*, 1998). Both Late Jurassic and Middle Jurassic sourced oils have contributed to the accumulation. Extracts from reservoirs in the Faroese wells has also shown source rock mixing, based on biomarker distributions (Cawley *et al.*, this volume).

The multiple charging history has proved enigmatic. The source in the central part of the Faroe-Shetland Basin is deep-seated and most published maturity modelling studies suggest that the oil prone Jurassic source rocks are either mature for gas generation or overmature and that large volumes of oil was generated prior to deposition of the Upper Palaeocene reservoir. The 'motel' (Lamers and Carmichael, 1999) and the 'whoopie-cushion' model (Iliffe *et al.*, 1999) have been introduced to explain predicted Cretaceous generation and post-Palaeocene charging. Alternative maturation models have been presented by Carr and Scotchman (2003). They apply different heat flow history and pressure dependent vitrinite reflectance models. The predicted vitrinite values for the Kimmeridge Clay Formation at 8 km depth in the centre of the Judd Basin indicate that the source is still mature for oil generation due to extensive retardation by highly overpressured Mesozoic sediments.

The extent of the upper Jurassic Kimmeridge Clay Formation deposited during a series of marine transgressions (Stoker *et al.*, 1993) can only



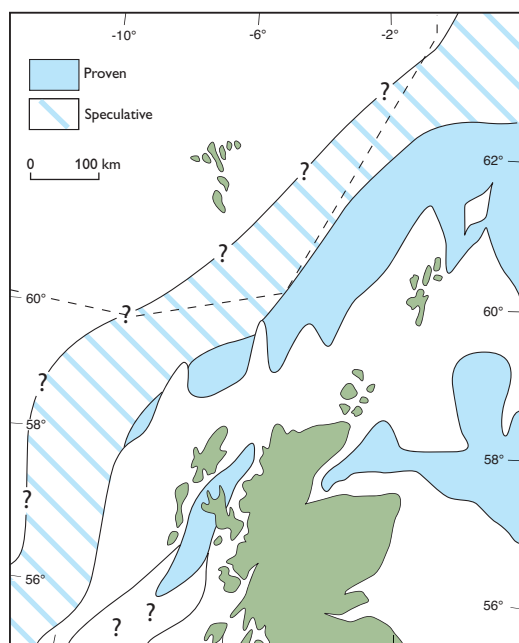


**Figure 4.** Distribution of Upper Jurassic shales. Modified from Holmes *et al.*, 1999.

be inferred as proper seismic well ties only exist on the shallower basin-margin areas on the UK shelf. Figure 4 shows the estimated extent proposed by Holmes *et al.* (1999). They suggest possible widespread occurrence covering a large part of the eastern Faroese Shelf. Due to lack of proper seismic identification, uncertainties with respect to appropriate velocities for depth conversion, thermal history, kerogen kinetics and pressure regime any prediction on timing of HC generation and phase is conjectural in the basalt-covered areas. Satellite and airborne slick detection and geochemical investigations on seabed cores support however the proven hydrocarbon system in neighbouring UKCS can be extended westwards to include basalt-covered areas on the Faroese Shelf. Timing of charge into sub-basalt structural highs may be an important issue due to reactivation during Oligo-Miocene compressional events. The hydrocarbon phase may have spilled during these structural reorganisations (Davies *et al.*, 2004).

## Reservoirs

One of the biggest issues regarding exploration potential below the flood basalts in the Faroese area

is reservoir presence and quality. Reservoirs have been found throughout the stratigraphic column on the UK side of the Faroe-Shetland Channel (Fig. 2). The quality has been variable due to different factors. But where does this leave the Faroese Continental Shelf with regard to reservoir presence and quality?

## Provenance areas

The proven primary provenance area for the eastern part of the Faroe-Shetland Channel is the Shetland Platform. Another much speculated provenance area relevant for the Faroes is Greenland, prior to continental break-up in the early Eocene. There is, however, a third option, namely the Faroese Platform. This last option has generally been left out of most discussions on provenance areas. This section will briefly review all three options as potential sources for reservoirs in the Faroes.

### Shetland Platform

All discoveries made so far on the UK side of the boundary have one thing in common. The reservoir section is sourced from the Shetland Platform. The level of sediment sourcing has varied through time, and the quality of the different sandstones varies based on depth of burial, cleanliness and diagenetic history. End members are Triassic sandstones acting as top seal in the Strathmore field (Herries *et al.*, 1999) to very high porosities recorded in the Eocene section.

Main concerns with the Shetland Platform acting as the dominant provenance area to parts of FoCS are on the one hand the large distance to the Shetland Platform, and on the other parallel intra-basinal elevated ridges, which would have acted as barriers. Material transported from the east will be dumped in the accommodation space on the landward sub-basins after rifting pulses until they have been filled. The ridges themselves may still have acted as sediment sources, but these are, due to their limited size, not expected to have been able to source sediments over large distances.

Jolley *et al.* (in press) demonstrate a westerly source in the Paleocene in several wells on the UK side of the Faroe-Shetland Channel. This puts a question mark over the Shetland Platform acting as dominant provenance area of sediments below the flood basalts in the area towards the Faroese Platform.

### Greenland

The East Greenland margin, prior to continental break-up, was situated close to the present day Faroese Platform. Pre-drift reconstructions place the East Greenland Kangerlussuaq Basin with Cretaceous and Palaeogene sediments less than 100 km from the Faroes Islands. Several authors (e.g. Larsen *et al.*, 1999) have suggested Greenland as a major provenance area for sediments to the western part of the Faroe-Shetland Channel area. A western source area for the majority of Upper Cretaceous sandstones has been demonstrated in the Møre Basin offshore Mid-Norway (Kristensen *et al.*, 2004).

Supporting evidence for Greenland provenance areas are heavy mineral analyses, which based on reference samples from Greenland, indicate that at least part of the Paleocene sands from the central part of the Faroe-Shetland Channel have a westerly source (Jolley *et al.*, in press). Palynological investigations have also identified North American floral assemblages suggesting Greenland as a source of sediments. Poulsen *et al.* (2004) report, that new well results in the Judd Basin demonstrate mixed west and east sourcing in the early Paleocene sections.

Several authors (e.g. Jolley *et al.*, in press) have suggested that NW-SE trending lineaments related to transfer elements may have acted both as entry points and conduits for sediment transport from the Greenland margin towards the Faroe-Shetland Channel in the Cretaceous and Paleocene. The distribution of North American floral assemblages in the Paleocene here appears to be constrained by transfer zones. Whitham *et al.* (2004) favour a model, where rifting in the Albian known from Kangerlussuaq was followed by a long period of thermal subsidence and infilling leading to creation of a shelf break and a rather smooth topography along the margin. This basin configuration was conducive to long distance transport of sandstones and may have been responsible for the sand deposition offshore Mid-Norway. Similar sand plays might exist on the Faroese Continental Shelf.

### Faroese Platform

The least discussed potential provenance area for coarse clastics is local, namely the Faroese Platform and intra-basinal ridges in the Faroe-Shetland Channel area. The first may be speculated to

be the mirror image of the Shetland Platform (see later) and thus provide for similar sediment source mechanisms forming the reservoirs in WOS.

It is argued that there is evidence for continental crust below the Palaeogene flood basalts on the Faroese Platform. These include gravity modelling (e.g. Schröder, 1971), refraction velocities (e.g. Pálmason, 1965), magnetic data (Ziska and Morgan, 2004) and geochemical evidence for contamination of the Faroese basalts by Precambrian continental crust (e.g. Gariépy *et al.*, 1983). The Sub Faroe continental crust has never been sampled and therefore it is not possible to delineate it as a provenance area using heavy mineral analysis as an analytical tool (lack of source control data).

Therefore it can only be speculated when and if and the Faroese Platform or parts of it was emergent. However, a substantial uplift took place in connection with initiation of Paleocene volcanism. This uplift probably resulted in the Faroese Platform and intra-basinal highs becoming emergent, and thus acting as provenance areas for adjacent basins as suggested by Neish and Ziska (2005). The Shetland Platform and intra-basinal ridges on the UK part of the Faroe-Shetland Channel have been emergent at different times (e.g. Goodchild *et al.*, 1999). A similar story may have occurred on FoCS due to the close proximity and similar evolutionary story, apart from the much thicker volcanic section in the late Paleocene to Early Eocene. Larsen and Olaussen (2004) have argued along the same lines, based on the succession of the Lower Cretaceous estuarine and shallow marine sandstones described in Kangerlussuaq and suggesting a Lower Cretaceous play on the FoCS, where reservoirs are predicted along structurally controlled basin margins.

### Proven reservoirs (WOS)

Since the start of exploration in the 1970's more than 200 wells have been drilled on the UK side of the Faroe-Shetland Channel. Discoveries have been made throughout the geological column (Fig. 2). Proven high quality reservoirs are present at several different stratigraphic levels. Structural mapping of the Faroe-Shetland Channel (e.g. Neish, this volume) has demonstrated that the series of NE/SW trending ridges in the UK also exist on the Faroes side of the international boundary

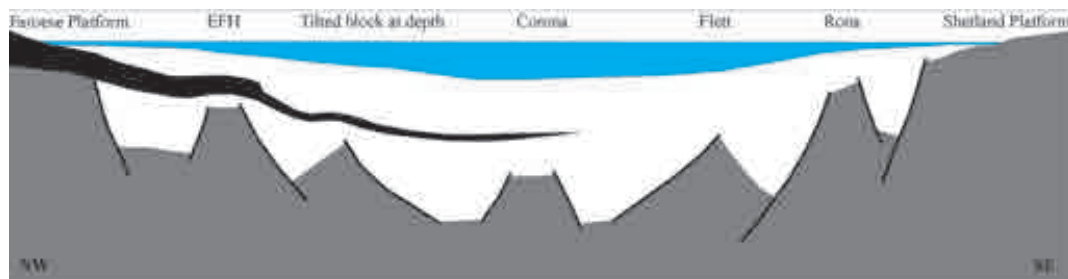


**Figure 5.** Conceptual cross section across the Faroe-Shetland Channel. EFH: East Farøe High. Black: volcanics.

below the flood basalts with the East Farøe High being the most prominent to the NW. A conceptual cross section (Fig. 5) through the mapped ridges illustrates basin symmetry. The Farøe-Shetland Channel has been subject to several episodes of extension through time with the Cretaceous and Paleocene rifting events having dominating influence on present day basin geometry. A more or less symmetric basin geometry is anticipated, unless differences in pre-rift architecture were prevailing.

The suggested symmetry influences the way the age of mapped sub-basalt horizons are interpreted. It is possible, based on the basin symmetry model, to suggest the age of the mapped sub-basalt horizons. This can be further supported by the knowledge of the general regional evolution of the area. Here pre-rift sections are expected to be pre Mid-Cretaceous in age. Dean *et al.* (1999) describe fault detachments between the pre-Paleocene and the Paleocene with the deeper faults seemingly terminating within the Upper Cretaceous shales. This information can further be used to infer approximate ages of mapped sections.

We can examine the reservoir sections at various stratigraphic levels found on the UK side of the Farøe-Shetland Channel and by analogy suggest that these possibly occur in neighbouring Farøese waters.

### Devonian - Carboniferous

The oldest reservoir found in the Farøe-Shetland Channel, with the exception of fractured basement in the Clair Field, is the Devonian-Carboniferous Old Red Sandstone of the Clair group. It constitutes the primary reservoir in the Clair field.

The Clair group is found on the Rona Ridge, in well 204/19-1 on the Westray Ridge and in well

213/23-1 on the Corona Ridge. The thickness on the Rona Ridge varies from absent to more than 1000 m proving a complicated evolutionary history.

The lower reservoir section is sourced from Lewisian gneiss on the West Shetland Platform while the upper section is possibly sourced from Archaean rocks in East Greenland (Allen and Mange-Rajetzky, 1992). The depositional environment was fluvial to aeolian in intra-montane rift basins.

### Triassic

The Early Triassic Otter Bank Sandstone is the reservoir in the Strathmore field (Herries *et al.*, 1999), discovered in the area between the East and South Solan Basins in 1990. This discovery demonstrated that the Triassic has provided reservoir sand in the back basins of the Farøe-Shetland Channel. Well 213/23-1 encountered hydrocarbon bearing Triassic sandstones on the Corona Ridge in the central part of the Farøe-Shetland Channel.

Herries *et al.* (1999) suggested that the Otter Bank sandstone in Strathmore was deposited in a broad, low relief setting. The lower part of the sandstone was deposited in a fluvial setting, while the upper part was a mixture of fluvial, aeolian and sabkha deposits.

Another Triassic sandstone is the Middle-Upper Triassic Foula Sandstone, which acts as top seal for the Strathmore discovery. The reason for the difference in reservoir quality is assumed to be the immature nature of the Foula Sandstone compared to the Otter Bank Sandstone (Herries *et al.*, 1999). The authors also stated that porosity preservation was caused by chlorite coating in the Otter Bank Sandstone, while no such chlorite coating is found in the Foula Sandstone.



## Jurassic

Middle Jurassic has only been found in a few released wells in the Faroe-Shetland Channel. Most of these wells are located on the Rona Ridge and in the southern part of the Faroe-Shetland Channel.

The Upper Jurassic Rona Member is a Kimmeridge Clay Formation time-equivalent, which includes coarse-grained subaerial fan delta deposits to shoreface/shallow marine grading into deep marine deposits (Verstralen *et al.*, 1995). The only hydrocarbon discovery so far in the Jurassic is the Solan discovery (Herries *et al.*, 1999), with the reservoir section belonging to the Rona Member.

Reservoir quality in the Solan discovery was very good in the discovery well which is also farthest up-dip on the structure. Down-dip wells have shown a decrease in reservoir quality with depth. This is thought to be a result of early hydrocarbon charge preserving updip of 25.7% porosity (mean) and 185 mD effective permeability. The effective permeability decreases to 63 mD and further to 13 mD in the two down-dip wells (Herries *et al.*, 1999).

The Solan sands in well 205/26a are believed to have been fed axially by reworking of Devonian sandstones, or having a shared provenance area with sands found on the Rona Ridge. The depositional mechanisms were structurally constrained mass flows (Herries *et al.*, 1999).

## Cretaceous

The only Cretaceous discovery in the in the Faroe-Shetland Channel is the Victory field on the Rona Ridge. It is a gas discovery in the Lower Cretaceous Victory Formation with generally high reservoir quality (Goodchild *et al.*, 1999).

The reservoir parameters are dependent on the depositional setting, with calcite cemented sandstones and poorly sorted conglomerates providing inferior reservoir parameters and clean sandstones of different sorts providing high quality reservoirs.

The provenance area for the reservoir sections in the Victory discovery is partly the Rona Ridge itself and partly the West Shetland Platform. The sediments were deposited in a fan delta to shallow to marginal marine setting (Goodchild *et al.*, 1999). Lower Cretaceous potential reservoir rocks have also been found in well 204/19-1 on the Westray Ridge.

There is an additional Cretaceous play in the

Faroe-Shetland Channel. This is the Turonian Sandstone play which is a pinch-out play, where the reservoir is sands deposited in basin slope to basin floor fans (Grant *et al.*, 1999).

Reservoir quality is dependent on the depositional style and the average porosity is 5-10% in thinly bedded sandstone while it is 20-30% in thick massive sandstones. Present day depth to the reservoir is a problem and Grant *et al.* (1999) speculate that overpressure is needed for preserving good reservoir quality at depth. Provenance areas for this succession are local ridges such as the Rona ridge.

These sandstones have been found close to the Faroese area on the Corona Ridge, where well 213/23-1 encountered both Turonian and Cenomanian sands with oil shows.

## Palaecene

Presently the only producing fields in the Faroe-Shetland Channel are the Paleocene Foinaven and Schiehallion fields with satellites. These fields are all located on the eastern flank of the Judd basin. The Flett Basin further north has also provided some good reservoirs as demonstrated by the Laggan and Torridon discoveries, the former having recently been re-visited in order to assess the possibility of initiation of production. The reservoir quality of the Paleocene slope and basin floor fan sandstones is generally good, but decreasing with depth. Lamers and Carmichael (1999) have shown the relationship between depth below mudline (BML) and porosity.

The provenance area for the UK Paleocene sands in the Judd Basin are sub basins to the South and East, where reworking of Jurassic and Triassic strata has resulted in the sands found in Foinaven and Schiehallion (Ebdon *et al.*, 1995).

The first four wells in the Faroese area, all located in the central Judd Basin, showed the presence of thick sands in the Paleocene section. The section was more sandy than what is known from the Foinaven/Schiehallion and adjacent discoveries.

The upper part of the Paleocene is dominated by volcanic rocks on the Faroese Continental Shelf. These are normally not a primary exploration target, but Schutter (2003) lists a large number of discoveries and fields in volcanic rocks throughout the world. This could indicate that further investi-

gations into the prospectivity of the volcanic section are warranted.

### Eocene

Three large Eocene deep-water fans have been mapped in the Faroe-Shetland Channel (e.g. Davies *et al.*, 2004). These are sandy in nature and have been proven to contain high quality reservoirs. Well 214/14-1 penetrated a 4-way dip closure on one of these fans (Strachan) and found hydrocarbon bearing sandstone with very good reservoir quality.

The presence of Eocene reservoir rocks on the Faroese Continental shelf is not fully investigated. The three large mapped fans are mostly found within UK waters, but the edges of these are extending into Faroese waters. The central parts of the fans are very sandy and this has prevented the creation of stratigraphic traps. The sands thin towards the Faroese area, and it is worth considering if some up-dip pinch-outs of these or equivalent sands exist on the Faroese Continental Shelf.

### Seals

Sealing is, despite the setback in the Judd Basin, not expected to be a significant risk in the greater Faroe-Shetland Channel area. There are several seals, which have been demonstrated on the UK side of the Faroe-Shetland Channel. The most promising candidates for regional seals are the Kimmeridge Clay Formation (KCF), Upper Cretaceous shales, Paleocene T36 shales and the basaltic succession itself.

The KCF is a deep marine shale, which has been penetrated in a number of wells in the Faroe-Shetland Basin, and it is expected to be present in most parts of the Faroe-Shetland Channel and adjacent areas as discussed previously. The sealing capacity of the KCF is demonstrated in the Solan discovery (Herries *et al.*, 1999).

The entire area was drowned during the late Late Cretaceous. This resulted in the deposition of deep marine shales, which in places reach a thickness in excess of one kilometre. These shales are expected to be the primary seal for any pre-Tertiary structural play, and also for the Turonian stratigraphic play. Upper Cretaceous shales seal the Victory discovery (Goodchild *et al.*, 1999).

The Upper Paleocene stratigraphic play was the most contested play in the first Faroese licensing

round, and wells based on this play demonstrated that the primary risk factor was lack of seal (Woodfin *et al.*, this volume). The wells did, however, show that the T36 shales acted as a basin wide seal, as it has previously been demonstrated in the Flett Basin (Lamers and Carmichael, 1999). The T36 sequence may, according to some authors, be contemporaneous with the Faroese Lower Basalt Formation (e.g. Kiørboe, 1999). The basalt formations have at times been suggested as a seal, but sills in Japan act as reservoirs (Magara, 2003) and live oil has been found in basalt in West Greenland (Christiansen *et al.*, 1997). These observations cast some doubt on the validity of the basalts themselves as possible seals. The Lower Basalt Formation has an increasing abundance of tuffs separating the flows towards the upper part of the formation onshore Faroes. The sealing capacity of these tuffs is unknown, but tuffaceous sediments are known to be sealing in other places, such as the Kettle Member in the Judd Basin.

### Structures

The primary focus in the 1<sup>st</sup> licensing round on the FoCS was the Upper Paleocene stratigraphic play in the Judd Basin. This is very unusual compared to what has been experienced in most other frontier areas, where large structures are the focus of the first phase of exploration.

The presence of large structures at top and post basalt levels has been known for a long time. These include large structures such as the Fugloy Bank and the Wyville-Thomson Ridge (Fig 1 and 6). It has, however, been more of a challenge to confidently map structures below the flood basalts.

Progress in sub-basalt imaging has led to better data being available and enabled geo-scientists more confidently to map sub-basalt features (e.g. Neish and Ziska, in press). There seems to be very good correlation between post basalt highs and basement highs. This suggests that the topography of the top basalt surface is controlled by underlying basement topography. This relationship might be related to post depositional differential compaction or continued activity of the bounding faults. The latter is only partly supported by fault interpretations. Late Tertiary compression may have further enhanced these structures.

The most prominent sub basalt structure, which

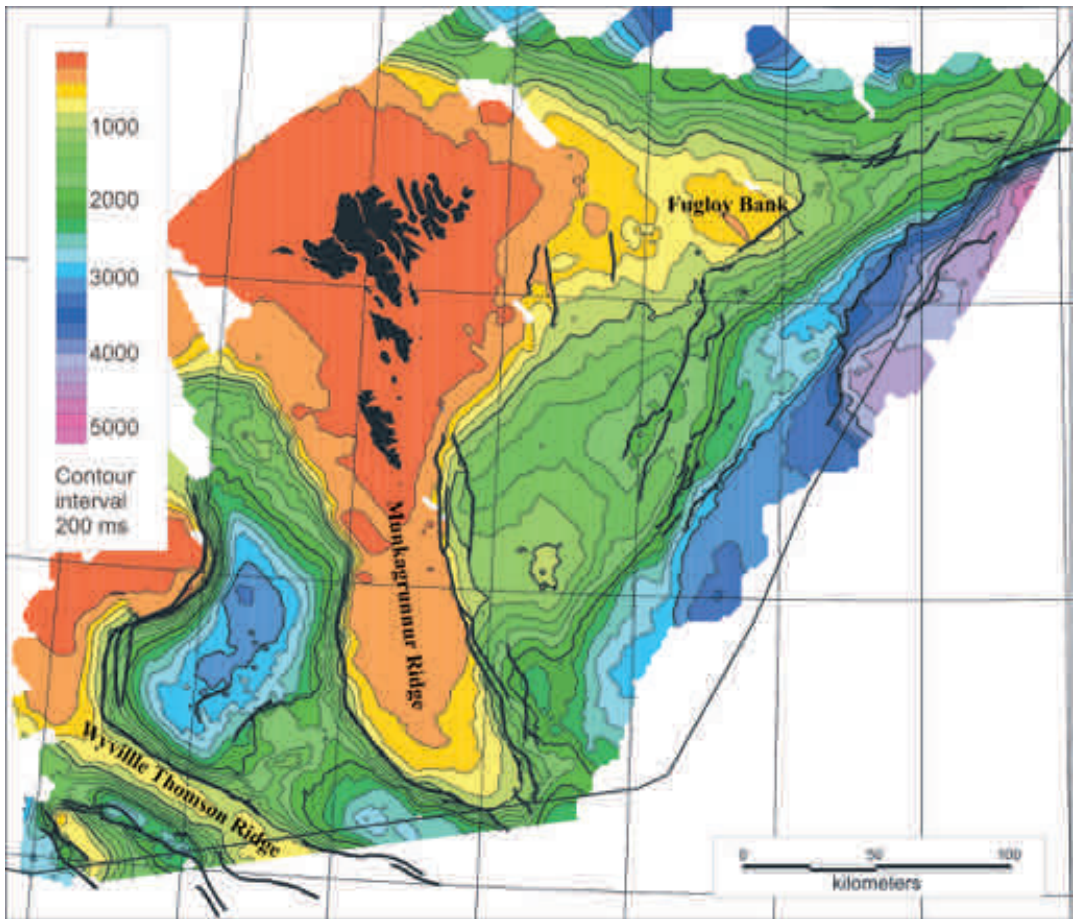


**Figure 6.** Top Basalt TWT map.

incidentally was identified on potential field data prior to being mapped by seismic data, is the East Faroe High Complex (Fig. 3). This is a structure with the same orientation and style as other major ridges in the Faroe-Shetland Basin. It is mapped as the closest ridge to an inferred palaeo-Faroese Platform at sub-basalt level. This would make it the mirror image of the Rona Ridge. The Devonian-Carboniferous Clair discovery and the Cretaceous Victory discoveries are located on the Rona Ridge.

Other structures of varying size have been identified within the Faroese area, some very similar to recently drilled structures on the UK side, while others are very different. The structural range includes tilted fault blocks at depth, which in turn generate closures at more shallow levels, sometimes into the Eocene. Other structures are depositional mounds which have become positive

features due to post depositional differential compaction and inversion structures created by late Tertiary compressional events.

There are still areas where imaging under the basalt has remained a hindrance to the development of leads and prospects. Some of these features are, however, still interesting due to their sheer size. The Fugloy Bank and the Wyville-Thomson Ridge (Fig. 1 and 6) each cover several blocks, and potential field modelling give ambiguous results. Potential Field modelling of the Wyville-Thomson Ridge has given varying results and include shallow basement with little sedimentary cover (Tate *et al.*, 1999) or the presence of a deep sedimentary basin under the Ridge (Waddams and Cordingley, 1999). These ambiguities, coupled with the size of these structures make further studies warranted.



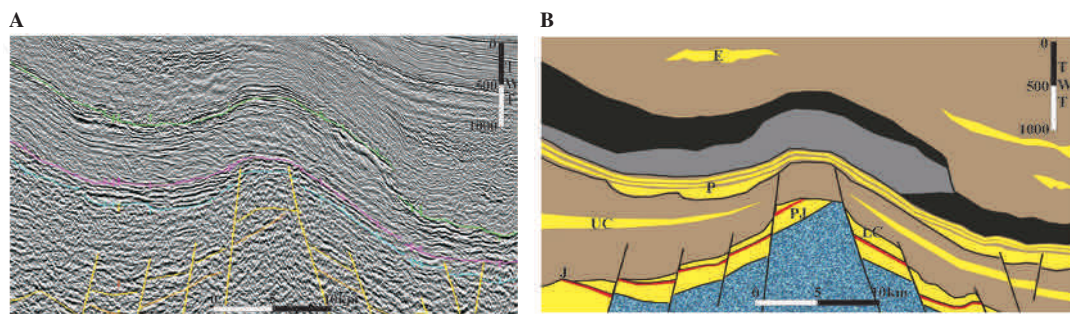


**Figure 7.** **A:** Seismic section across the East Faroe High. **B:** Interpreted reservoir configurations based on analogies from UK side of the Faroe Shetland Channel. E: Eocene, P: Paleocene, UC: Upper Cretaceous, LC: Lower Cretaceous, J: Jurassic source rock and PJ: Pre Kimmeridge Clay. Seismic data shown courtesy of WesternGeco.

### Traps

In order to illustrate exploration opportunities an example of a large sub-basalt structural lead identified on the slope of the Faroe-Shetland Channel in the NW part of Quadrant 6103 at a water depth of 850 m is commented upon. It is situated above a deep-seated Mesozoic horst block along the East Faroe High trend with a sediment section preserved below the interpreted base of volcanic rocks (Fig. 7). The volcanic section comprises an upper part dominated by high amplitude parallel to sub-parallel reflections, interpreted to represent sub-aerial flood basalts, and a lower part characterised by progrades typical for a lava delta with hyaloclastites. The basaltic rocks decrease in thickness on the eastern flank across the Faroe-Shetland Escarpment. This feature has been described by Kjørboe (1999). The relief of the progrades indicates that the water depth during deposition was high (500 m or more).

Any clastic reservoir of Palaeocene or Cretaceous age, located below the basalts and above deeper fault block features, is in a favourable position to be charged by hydrocarbons as the rotated fault blocks may have focussed migrating fluids. There is evidence that suggests that the East Faroe High Complex has been a positive feature relative to surrounding areas during much of geological record. The significance of this is that timing with respect hydrocarbon generation and trap formation is less of an issue. Late Tertiary compression has enhanced the structure, but may have led to remigration of early trapped hydrocarbons.

A simple exercise to estimate the trapping potential of a lead based on a regional depth structure map at the presumed base of the volcanics (Fig. 8)

has been carried out. The crest of the structure is at about 4300 ms. The vertical 4-way dip closure is 250 m and covers an area of 240 km<sup>2</sup>. Only an oil case has been considered although great uncertainty exists with respect to the hydrocarbon phase due to lack of control on the depth of the Base Cretaceous and the Upper Jurassic organic rich Kimmeridge Clay. The following parameters have been used to estimate the trapping capacity of the rock volume under closure:  $B_o$ : 1.8, net/gross: 0.4,  $S_o$ : 0.7 and porosity: 12%. The modest porosity value is used to allow for reservoir degradation due to depth of burial. The crest is situated about 3450 mBML below a thick basalt cover. Early chlorite over-growth of quartz, early hydrocarbon invasion and development of overpressure may have preserved or enhanced reservoir characteristics. A STOIP of 1 billion barrels require a hydrocarbon column of 120 m. Filled to spill the trapping capacity is 3.9 billion barrels in-place.

Realising the frontier nature of the area with a thick basalt cover and considerable uncertainties (e.g. depositional nature and subsequent diagenesis of any sands) this large structural lead with high up-side potential deserves further attention.

### Discussion

The Faroese Continental Shelf is a vastly underexplored area, with only a small part being drilled, and only the Paleocene tested so far. Knowledge on the geology of the area is based primarily on analogues with adjacent areas and on the general geological evolution of the region. Several different hydrocarbon source scenarios are possible based on the present knowledge of the North At-

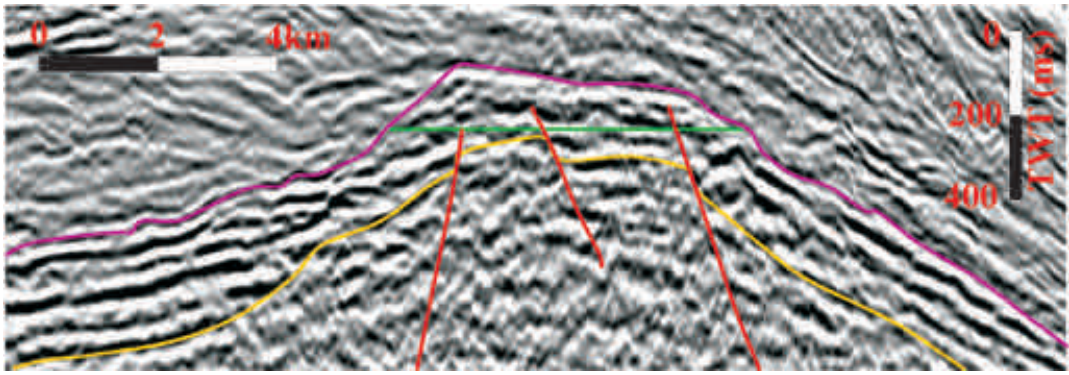


**Figure 8.** Part of Figure 7 Seismic line. (Violet: interpreted base volcanics, yellow: interpreted base Tertiary, green: spill point of mapped structural closure). Seismic data shown courtesy of WesternGeco.

lantic Margin in general and the Faroe-Shetland Channel in particular. There are two proven source rocks within the Jurassic, and in addition the possibility of a Cretaceous source rock. It has not been possible to map the depths to specific source rock intervals in basalt-covered areas due to lack of well ties and poor seismic imaging. The depths are varying from relatively shallow near and over the ridges, to very deep in the central parts of the basin. This provides for many different source scenarios where the fetch area for any structures might include both immature, oil mature, gas mature and over mature source rocks.

The mapped structure points to the basin being symmetrically developed provides for the possibility of finding similar reservoir sections on the Faroese side of the basin, as have been found on the UK side of the Faroe-Shetland Channel. Reservoirs have been found here in all stratigraphic levels ranging from the Devonian-Carboniferous Old Red Sandstone to the Eocene deepwater fans.

There are three possible sediment provenance areas, which may have sourced sediments to the FoCS. These are the Shetland Platform, Greenland and the Faroese Platform itself. The Shetland platform has been shown to have sourced the UK side of the Faroe-Shetland Channel. A westerly Greenlandic source has been documented based on heavy mineral analyses and palynology. We suggest that the Faroese Platform and intra-basinal ridges may have acted as sediment sources through time in a similar manner as on the UK side of the Faroe-Shetland Channel. This suggestion is based partly on mapped basin symmetry partly, on a similar evolutionary history; with the exception of the

extensive volcanism in the Early Tertiary. Seismic mapping has indicated analogous fault behaviour and fault trends below the flood basalts as found to the East on the UK side of the international boundary.

Reservoir quality is a major issue due to the presence of thick basalts and their possible baking effects on the sediments. Depth to possible reservoirs under an unknown thickness of basalts and sediments is also a concern. Structural closures have been mapped which are at depth levels where reservoir quality is not expected to be a problem. Deeper structures also exist, where porosity preserving mechanisms may have to be invoked in order to maintain potential reservoir quality. Porosity preserving mechanisms include early charge, overpressure and chlorite coating on quartz, all of which have been proved to work in the area.

Seals are not considered a major risk with the KCF and Upper Cretaceous shales acting as regional seals. The latter has been proven to be sealing several of the discoveries on the UK side of the Faroe-Shetland Channel. The Paleocene T36 shale interval has proven to be a basin wide seal in the Judd and Flett Basins. It is further possible that the basalts and especially the intra-basaltic tuffs can act as seal for underlying Paleocene reservoirs.

## Conclusions

Exploratory drilling to date only focussed on the Paleocene in the Judd basin and the result is that the stratigraphic play here is a lot more risky than expected prior to the 1st Licence Round. This

leaves a huge part of the area and the major part of the stratigraphic column virtually unexplored.

There is still some apprehension within companies with regard to hydrocarbon exploration in a basalt province like the Faroese Continental Shelf. It is demonstrated that sub-basalt exploration has moved to a level where the risk attached to structural mapping and the presence of a hydrocarbon system is reduced. The primary geological risk is presently reservoir presence and effectiveness. This risk can be lowered somewhat by using knowledge of the general geological evolution of the area coupled with analogies from the adjacent margin of the Faroe-Shetland Channel.

## References

- Allen, P.A. and Mange-Rajetzky, M.A. 1992. Devonian-Carboniferous sedimentary evolution of the Clair area, offshore north-western UK: impact of changing provenance. *Marine and Petroleum Geology* 9, February: 29-52.
- Boldreel, L.O. and Andersen, M.S. 1993. Late Paleocene to Miocene compression in the Faroe-Rockall area. In: Parker, J. R. (ed.) *Petroleum Geology of Northwest Europe: Proceedings of the 4<sup>th</sup> Conference*. Geological Society, London: 1025-1034.
- Carr, A.D. and Scotchman, I.C. 2003. Thermal history modelling in the southern Faroe-Shetland Basin. *Petroleum Geoscience* 9: 333-345.
- Cawley, S., Matheson, H. and Stalker, G. This volume. An Updated View of the Faroe-Shetland Petroleum System. In: Ziska, H. Varming, T. and Bloch, D. (eds.) *Faroe Islands Exploration Conference: Proceedings of the 1<sup>st</sup> Conference, Annales Societatis Scientiarum Feroensis*, Supplementum 43, Tórshavn.
- Christiansen, F.G., Bosenen, A., Dalhoff, F., Pedersen, A.K., Pedersen, G.K., Riisager, P. and Zinck-Jørgensen, K. 1997. Petroleum geological activities onshore West Greenland in 1996, and drilling of a deep exploration well. *Geology of Greenland Survey Bulletin* 176: 17-23.
- Davies, R.J., Cloke, I.R., Cartwright, J.A., Robinson A. and Ferrero, C. 2004. Post-breakup compression of a passive margin and its impact on hydrocarbon prospectivity: An example from the Tertiary of the Faroe-Shetland Basin, United Kingdom. *American Association of Petroleum Geologists Bulletin* 88(1): 1-20.
- Dean, K., McLachlan, K. and Chambers, A. 1999. Rifting and the development of the Faeroe-Shetland Basin. In: Fleet, A.J. and Boldy, S.A.R. (eds.) *Petroleum Geology of Northwest Europe: Proceedings of the 5<sup>th</sup> Conference*. Geological Society, London: 533-544.
- Doré, A. G., Lundin, E. R., Fichler, C. and Olesen, O. 1997. Patterns of basement structures and reactivation along the NE Atlantic Margin. *Journal of the Geological Society, London* 154: 85-92.
- Earle, M.M., Jankowski, E.J., and Vann, I.R. 1989. Structural and stratigraphic evolution of the Faeroes-Shetland trough and northern Rockall Trough. *American Association of Petroleum Geologists Memoir* 46: 461-469.
- Ebdon, C.C., Granger, P.J., Johnson, H.D. and Evans, A.M. 1995. Early Tertiary evolution and stratigraphy of the Faeroe-Shetland Basin: implications for hydrocarbon prospectivity. In: Scrutton, R.A., Stoker, M.S., Shimmiel, G.B. and Tudhope, A.W. (eds.) *Sedimentation and Palaeoceanography of the North Atlantic Region*. Geological Society, London, Special Publications 90: 51-69.
- Ellis, D., Bell, B.R., Jolley, D.W. and O'Callaghan, M. 2002. The stratigraphy, environment of eruption and age of the Faroes Lava Group, NE Atlantic Ocean. In: Jolley, D.W. and Bell, B. R. (eds.) *The North Atlantic Igneous Province: Stratigraphy, Tectonic, Volcanic and Magmatic Processes*. Geological Society, London, Special Publications 197: 253-269.
- Gariépy, C., Ludden, J. and Brooks, C. 1983. Isotopic and trace element constraints on the genesis of the Faeroe lava pile. *Earth and Planetary Science Letters* 63: 257-272.
- Goodchild, M.W., Henry, K.L., Hinkley, R.J. and Imbus, S.W. 1999. The Victory gas field, West of Shetland. In: Fleet, A.J. and Boldy, S.A.R. (eds.) *Petroleum Geology of Northwest Europe: Proceedings of the 5<sup>th</sup> Conference*. Geological Society, London: 713-724.
- Grant, N., Bouma, A. and McIntyre, A. 1999. The Turonian play in the Faeroe-Shetland Basin. In: Fleet, A.J. and Boldy, S.A.R. (eds.) *Petroleum Geology of Northwest Europe: Proceedings of the 5<sup>th</sup> Conference*. Geological Society, London: 661-673.
- Herries, R., Poddubiuk R. and Wilcockson, P. 1999. Solan, Strathmore and the back basin play, West of Shetland. In: Fleet, A.J. and Boldy S.A.R. (eds.) *Petroleum Geology of Northwest Europe: Proceedings of the 5<sup>th</sup> Conference*. Geological Society, London: 693-712.
- Hollingsworth, R. 2002. BP Faroes Licence 004 Status Report, *Offshore Faroes Conference*, Tórshavn.
- Holmes, A.J., Griffith, C.E. and Scotchman, I.C. 1999. The Jurassic Petroleum System of the West of Britain Atlantic Margin – an integration of tectonics, geochemistry and basin modelling. In: Fleet, A.J. and Boldy, S.A.R. (eds.) *Petroleum Geology of Northwest Europe: Proceedings of the 5<sup>th</sup> Conference*. Geological Society, London: 1351-1365.
- Iliffe, J.E., Robertson, A.G., Ward, G.H.F., Wynn, C., Pead, S.D.M. and Cameron, N. 1999. The importance of fluid pressures and migration to the hydrocarbon prospectivity of the Faeroe-Shetland White Zone. In: Fleet, A.J. and Boldy, S.A.R. (eds.) *Petroleum Geology of Northwest Europe: Proceedings of the 5<sup>th</sup> Conference*. Geological Society, London: 601-611.
- Jolley, D.W., Morton, A. and Prince, I. in Press. Volcanogenic impact on phytogeography and sediment dispersal patterns in the NE Atlantic. In: Doré, A.G.



- and Vining, B. (eds.) *Petroleum Geology: North-West Europe and Global Perspectives-Proceedings of the 6<sup>th</sup> Petroleum Geology Conference*. Geological Society, London.
- Kiørboe, L. 1999. Stratigraphic relationships of the Lower Tertiary of the Faeroe Basalt Plateau and the Faeroe Shetland Basin. In: Fleet, A.J. and Boldy, S.A.R. (eds.) *Petroleum Geology of Northwest Europe: Proceedings of the 5<sup>th</sup> Conference*. Geological Society, London: 559-572.
- Kristensen, E.B., Brekke, H., Magnus, C., Høy, T. and Williams, R. 2004. The Deepwater Cretaceous Frontier Geology and Exploration of the Vøring and Møre Basins. *Faroe Islands Exploration Conference 2004*, abstract.
- Lamers, E and Carmichael, S.M.M. 1999. The Paleocene deepwater sandstone play West of Shetland. In: Fleet, A.J. and Boldy, S.A.R. (eds.) *Petroleum Geology of Northwest Europe: Proceedings of the 5<sup>th</sup> Conference*. Geological Society, London: 645-659.
- Larsen, M., Hamberg, L., Olausen, S., Preuss, T. and Stemmerik, L. 1999. Sandstone wedges of Cretaceous-Lower Tertiary Kangerlussuaq Basin, East Greenland – outcrop analogues to the offshore North Atlantic. In: Fleet, A.J. and Boldy, S.A.R. (eds.) *Petroleum Geology of Northwest Europe: Proceedings of the 5<sup>th</sup> Conference*. Geological Society, London: 337-348.
- Larsen, M. and Olausen, S. 2004. The Lower Cretaceous play in the Faroes – A comparative study from the North Atlantic western margin (Kangerlussuaq, southern East Greenland). *Faroe Islands Exploration Conference 2004*, abstract.
- Magara, K. 2003. Volcanic reservoir rocks of northwestern Honshu Island, Japan. In: Petford, N. and McCaffrey, K.J.W. (eds.) *Hydrocarbons in Crystalline Rocks*. Geological Society, London, Special Publications 214: 69-81.
- Mudge, D.C. and Rashid, B. 1987. The Geology of the Faroe Basin. In: Brooks, J. and Glennie, K. (eds.) *Petroleum Geology of NW Europe*. Graham and Trotman, London: 751-763.
- Neish, J.K. This volume. Faroese Area: Structural interpretation of seismic data in a basalt environment. In Ziska, H., Varming, T. and Bloch, D. (eds.) *Faroe Islands Exploration Conference: Proceedings of the 1<sup>st</sup> Conference*. *Annales Societatis Scientiarum Faeroensis*, Supplementum 43, Tórshavn.
- Neish, J. K., and Ziska, H. in Press. Structure of the Faroe Bank Channel Basin, offshore Faroe Islands. In: Doré, A.G. and Vining, B. (eds.) *Petroleum Geology: North-West Europe and Global Perspectives-Proceedings of the 6<sup>th</sup> Petroleum Geology Conference*. Geological Society, London.
- Pálmason, G. 1965. Seismic refraction Measurement of the Basalt lavas of the Faeroe Islands. *Tectonophysics* 2: 475-482.
- Poulsen, R., Ellis, D., Callaghan, J.W., Lundstrøm, R. and Dromgoole, P. 2004. Paleocene development of the Faroes area. *Faroe Islands Exploration Conference 2004*, abstract.
- Ritchie, J.D., Gatliff, R.W. and Richards, P.C. 1999. Early Tertiary magmatism on the offshore NW UK margin and surrounds. In: Fleet, A.J. and Boldy, S.A.R. (eds.) *Petroleum Geology of Northwest Europe: Proceedings of the 5<sup>th</sup> Conference*. Geological Society, London: 573-584.
- Rumph, B., Reaves, C.M., Orange, V.G. and Robinson, D.L. 1993. Structuring and transfer zones in the Faeroe Basin in a regional tectonic context. In: Parker, J.R. (ed.) *Petroleum Geology of Northwest Europe: Proceedings of the 4<sup>th</sup> Conference*. Geological Society, London: 999-1009.
- Schrøder, N.F. 1971. Magnetic Anomalies Around the Faeroe Islands. *Fróðskaparrit (annal. Societ. Scient. Faeroensis)* 19. bók, Tórshavn: 20-29.
- Schutter, S.R. 2003. Occurrences of hydrocarbons in and around igneous rocks. In: Petford, N. and McCaffrey, K.J.W. (eds.) *Hydrocarbons in Crystalline Rocks*. Geological Society, London, Special Publications 214: 35-68.
- Scotchman, I.C., Griffith, C.E., Holmes, A.J. and Jones, D.M. 1998. The Jurassic petroleum system north and west of Britain: a geochemical oil – source correlation study. *Organic Geochemistry* 29: 671-700.
- Smallwood, J.R and Kirk, W.J. 2003. Exploration in Faroe-Shetland Channel: Disappointments and Discoveries. *6<sup>th</sup> Petroleum Geology Conference: North West Europe and Global Perspectives*, abstract
- Smallwood, J.R. This volume. Lithology prediction from velocity data: Quantity and distribution of Paleocene sediments in the Faroe-Shetland area. In Ziska, H., Varming, T. and Bloch D. (eds.) *Faroe Islands Exploration Conference: Proceedings of the 1<sup>st</sup> Conference*. *Annales Societatis Scientiarum Faeroensis*, Supplementum 43, Tórshavn.
- Stoker, M.S., Hitchen, K. and Graham, C.C. 1993. The Geology of the Hebrides and West Shetland Shelves, and adjacent deep-water areas. British Geological Survey, London, HMSO.
- Tate, M.P.O., Dodd, C.D. and Grant, N.T. 1999. The North-east Rockall Basin and its significance in the evolution of the Rockall-Faeroes/East Greenland rift system. In: Fleet, A.J. and Boldy S.A.R. (eds.) *Petroleum Geology of Northwest Europe: Proceedings of the 5<sup>th</sup> Conference*. Geological Society, London: 391-406.
- Van der Baan, M., Kerrane, T., Kendall, J-M. and Taylor, N. 2003. Imaging sub-basalt structures using locally converted waves. *First Break* 21: 29-36.
- Verstralen, I., Hartley, A. and Hurst, A. 1995. The sedimentological record of a late Jurassic transgression: Rona Member (Kimmeridge Clay Formation equivalent), West Shetland Basin, UKCS. In: Hartley, A.J. and Prosser, D.J. (eds.) *Characterization of Deep Marine Clastic Systems*, Geological Society; London, Special Publication 94: 155-176.
- Waddams, P. and Cordingley, T. 1999. The regional geology and exploration potential of NE Rockall Basin. In: Fleet, A.J. and Boldy S.A.R. (eds.) *Petroleum Geology of Northwest Europe: Proceedings of the 5<sup>th</sup> Conference*. Geological Society, London: 379-390.

- White, R.S., Smallwood, J.R., Fliedner, M.M., Boslaugh, B., Maresh, J and Fruehn, J. 2003. Imaging and regional distribution of basalt flows in the Faeroe-Shetland Basin. *Geophysical Prospecting* 51: 215-231.
- Whitham, A.G., Morton, A.C. and Fanning, C.M. 2004. Insights into Cretaceous- Palaeogene sediment transport paths and basin evolution in the North Atlantic from a heavy mineral study of sandstones from southern East Greenland. *Petroleum Geoscience* 10(1): 61-72.
- Woodfin, M., Seedhouse, J., Spadini, G. and Cardamone, M. This volume. Elastic Impedance Inversion to aid lithology prediction in the Palaeocene of the Judd sub-basin. In Ziska, H., Varming, T. and Bloch, D. (eds.) *Faroe Islands Exploration Conference: Proceedings of the 1<sup>st</sup> Conference*. *Annales Societatis Scientiarum Faeroensis*, Supplementum 43, Tórshavn.
- Ziska, H. and Morgan, R. 2004. Interpreting Aeromagnetic Data in a Basalt Province: Case study from the Faroe Islands. *Faroe Islands Exploration Conference 2004*, abstract.

# Outline of a Joint Inversion of Gravity, MT and Seismic Data

MARION JEGEN-KULCSAR<sup>1</sup> AND RICHARD HOBBS<sup>2</sup>

1: Bullard Labs, Dept of Earth Science, University of Cambridge, Madingly Road, Cambridge CB3 0EZ, UK.

E-mail: jegen@esc.cam.ac.uk

2: Dept of Earth Science, University of Durham, South Road, Durham DH1 3LE, UK.

E-mail: r.w.hobbs@durham.ac.uk

The aim of our study is to combine the information about sub basalt sediments contained in the gravity, seismic and electromagnetic data. This can be achieved by interpreting the data sets independently and comparing the results after the interpretation looking for consistent feature.

An alternative way would be to interpret the different data sets simultaneously. This can be done by using information obtained in one method to constrain inversion results in the other, or alternatively to jointly invert the data. We have tried this latter novel approach in the interpretation of sub basalt imaging data in the framework of the EC SIMBA project (ENK6-CT-2000-00075).

In figure 1 I try to demonstrate the benefits of a joint inversion based on a trivial, one layer in air model with a gravity and electromagnetic response. The gravity response of such a layer is also trivial and given by  $g = 2 \pi \gamma h d$ , where  $\gamma$  is the gravity response and  $h$  and  $d$  the thickness and density of the layer. Any model with the appropriate thickness density product shown by a black line in figure 1, will produce an equally well fitting response, thus the amount of solutions to the gravity inversion problem are infinite.

At low frequencies, inversion of EM data will also yield infinite amount of solutions, since the EM response is then governed by the conductance  $S = h/\rho$  and the thickness  $h$  and resistivity  $\rho$  of the layer may not be resolved separately. The red line shows the solutions of the EM response, assuming a mapping of the resistivity and density

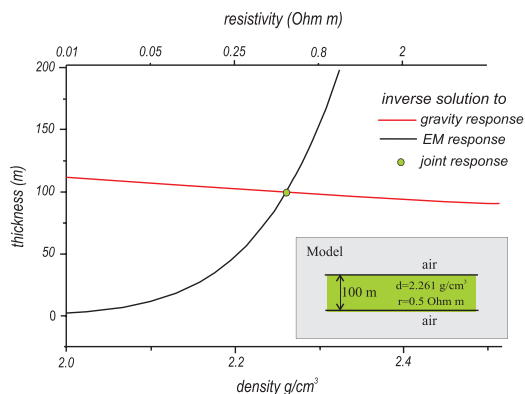


**Figure 1.** Possible, *infinite* amount of solutions of a gravity response inversion (red line) and an EM response inversion (black line) based on synthetic gravity and EM data calculated for the model depicted in the bottom right corner (see text for further explanation). The solutions, layer rock property and thickness, are plotted as a function of density or resistivity on the x axis and thickness on the y-axis. In order to overlay the plots, we have assumed a relationship of density into resistivity values. The green circle depicts the *unique* solution of a joint gravity and EM inversion process.

derived from borehole data such that the plots may be overlaid. While there is an indiscriminate, infinite amount of solutions to the inversion process for each one method, there is only *one* solution, where the two lines intersect, which fits both data sets. This model, marked by a green circle in figure 1, would be the solution to a joint inversion problem.



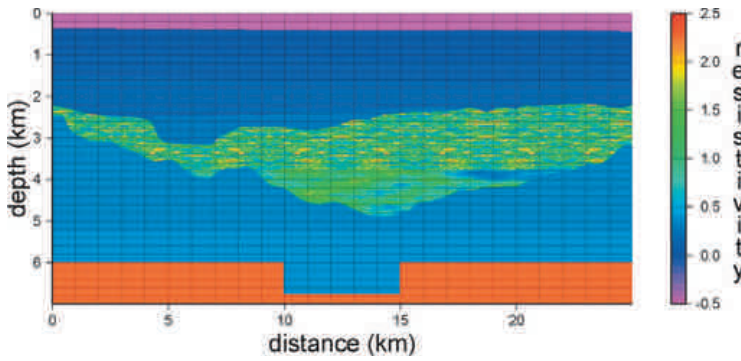


**Figure 2.** Synthetic fine structured model based on geological and geophysical data representing a typical sediment-basalt sequence in the North Sea. The model is represented in resistivity values, but, based on a relationship derived from nearby borehole data, may be represented in terms of velocity and density as well.

The model chosen is extreme in its non-uniqueness, however it illustrates nicely how a joint inversion process may find the true model out of the large amount of possible technical solutions of the inverse problem.

We have developed a joint inversion algorithm based on a synthetic 2 D model representing a feasible geological sub basalt sediment earth model (Figure 2) for which we calculated synthetic reflection seismic, gravity and EM, that is magneto telluric (MT), responses.

The conversion from seismic velocities, in which the model was designed, into densities and resistivities was based on borehole data in the region where the actual experimental part of the project took place. Figure 3 shows the seismic response of this model. While sediment layers above the basalt can be clearly identified and characterized, the base of the basalt is not visible in the seismic section.

Figure 4 shows the coarser representation of the original model used in our 2D MT and gravity forward response calculation for the synthetic data.

The inversion code we developed incorporates a full 2D gravity response, and an approximated 2D MT forward response consisting of a succession of 1D layered strips underneath each station. We tested that this approximation is justified in a smoothly varying model as the one shown and it was used to speed up the inversion code in order to investigate the principals of the joint inversion scheme. Using the entire gravity and EM data set we inverted for thickness and physical parameters (density and electrical resistivity) of all 1D layer strips simultaneously.

We started out with an inversion of MT and gravity data of 11 stations equally spaced across the model without seismic constrains of the upper sequence. The results produced (not shown here) were somewhat random models, which showed

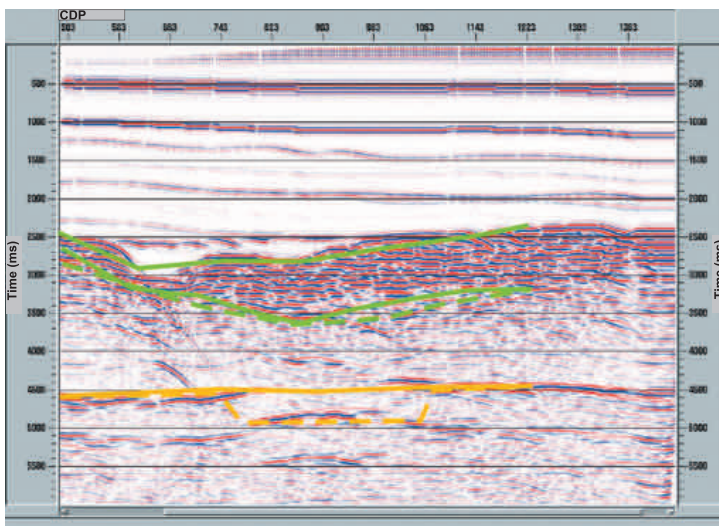


**Figure 3.** Seismic section of the above model. Dashed lines show true reflectors, solid line is the position of reflectors predicted by joint MT and gravity inversion. Green lines upper and lower boundaries of basalt layer (note that the upper green dashed and solid line are coincident), yellow lines basement.

**Figure 4.** Coarser representation of the model in figure 2 for calculation of 2D MT and gravity response.

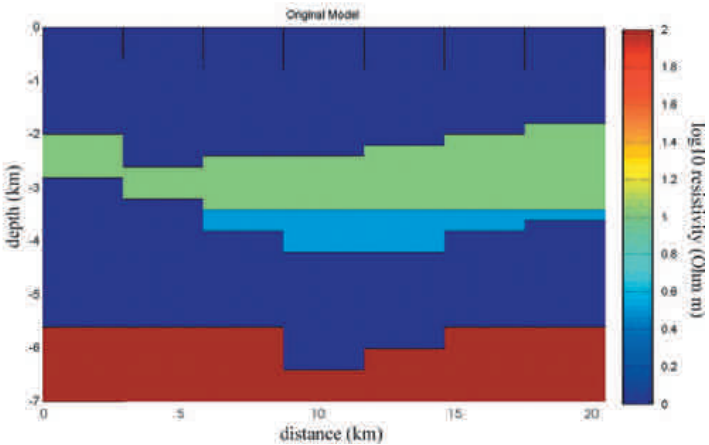


**Figure 5.** Inversion results of MT with seismic a priori input. Inversion was run on synthetic MT data produced by the model shown in figure 3. In the inversion process, a priori information from seismic reflection data shown in figure 2 have been used to fix model parameters down to top of basalt layer.

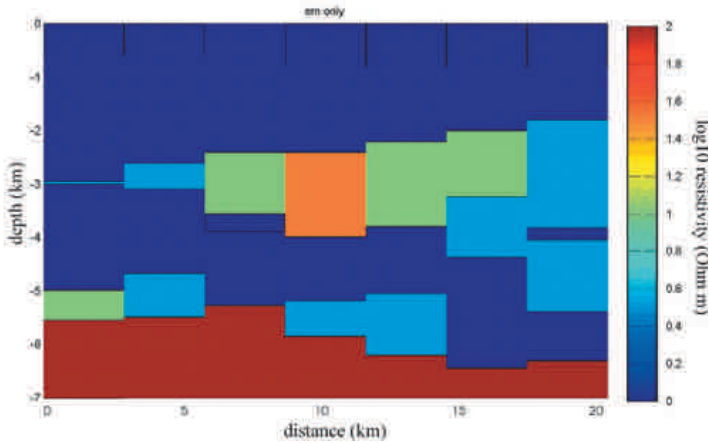
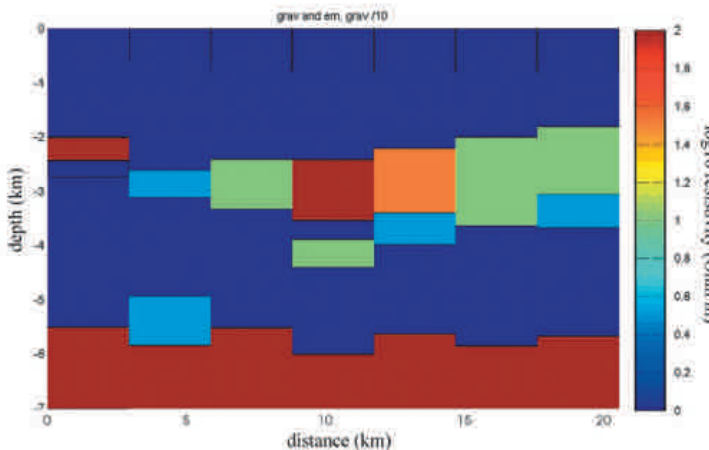


**Figure 6.** Joint inversion results of MT and gravity response with seismic a priori input.



the presence of a basalt material whose position and thickness differed significantly from the true model and in which the basalt layer did not appear as a coherent layer across the 2D section. As a next step we incorporated the seismic information to constrain structure and physical parameters of

the upper sediment sequence. Physical parameters underneath the upper sediment sequence were set to a constant half-space value.

Figure 5 shows the result if only the MT data was incorporated in the inversion. A coherent basalt layer becomes visible, however, the thick-

ness of the basalt layer and furthermore the depth to the basement does not consistently correspond to the true model. Figure 6 shows the results of a joint inversion, incorporating gravity and EM data with seismic a priori information. Now the basalt layer comes clearly into focus and the thickness and characteristic features are consistent with the original model. However, while the overall depth of the basement has been fixed at the right level, variations in the depth of the basement have not been resolved. Most likely for such a relatively fine structure at this depth, the approximated 2D MT response calculated is not suitable and a full 2D response has to be calculated. For comparison, we have converted our resulting model expressed in resistivities into a two-way travel time section and overlain the obtained structure on the seismic section shown in figure 3.

We have tried our inversion code on a data set collected during the project. Amerada Hess made reflection seismic data along the 150 km long Flare 10 profile line accessible to our project. Together with Prof. Tarits at the University of Brittany I recorded 17 MT stations along the FLARE10 line with the instruments that we built in the framework of the SIMBA project.

Figure 7 shows a summary of the experiment and inversion results so far. In the seismic migrated depth section the upper sediment sequence is visible. At three MT stations, where processed MT data is yet available, we inverted the MT data together with satellite free air gravity and a priori seismic information about the upper sedimentary layers. The measured and by the models predicted MT data are shown on the top right panel. The resulting earth models are overlain on the seismic section. The inversion results clearly shows the base of the basalt layer in the western section and thus pinpoints the unidentified reflector in the seismic section as such. The basalt layer is underlain by a less resistive layer, whose resistivity, density or velocity values could be interpreted as hydroclastites or sedimentary structures. Unfortunately, due to lack of low frequency MT data, the basement could not be identified.



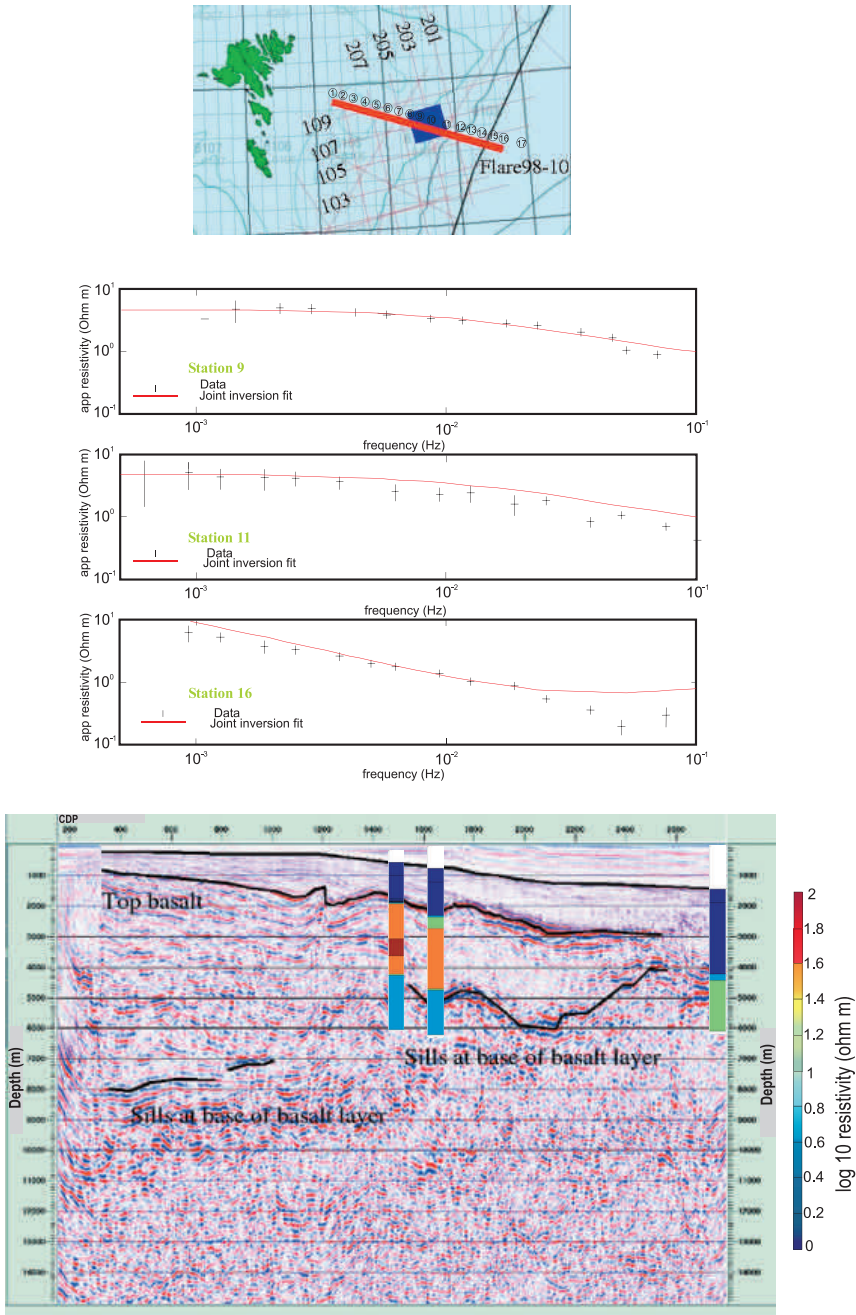


**Figure 7.** Summary of SIMBA experiment. Top left panel shows the Flare 10 seismic reflection line (red solid line) and MT stations (circles) measured in a profile off the Faeroe Ridge towards the Shetland Islands. The MT profile extends over a length of 180 km. Top right panel shows the apparent resistivity measured (crosses) at station 9, 11 and 16. The MT data and satellite free air gravity data has been inverted for basalt and sub basalt parameters. Seismic information about upper sediment sequence parameters have been used as a priori information. The solid line in the upper top right panel shows the fit of the model obtained by joint inversion to the MT data. The models are overlaid on the reflection seismic depth section (1 cdp interval equals 50 m). Orange and red colours are high resistivity/seismic velocity structures indicating basalt. Blue colours are lower resistivity values indicating the presence of sediments. The joint inversion results identify the intermittent reflector seen in the seismic section as the base of basalt and indicate the presence of potentially oil-bearing sediments underneath.

# Imaging Sub-Basalt with Deep Towed Streamer: A Case Study from the Faroe Islands

RUPERT HOARE<sup>1\*</sup>, PHIL SCHEARER<sup>1</sup>, ANDREW LANGRIDGE<sup>1</sup> AND EMMANUEL SARAGOUSSI<sup>1</sup>,  
PHILIP CHRISTIE<sup>2</sup> AND THE ISIMM TEAM<sup>3</sup>

1: WesternGeco, Schlumberger, Kirkton Avenue, Dyce, Aberdeen AB21 0YA, UK.

\*E-mail: rupert.hoare@westerngeco.com

2: Schlumberger Cambridge Research, High Cross, Madingley Road, Cambridge CB3 0EL, UK. E-mail: pafc1@slb.com

3: R. White, R. Spitzer, Z. Lunnnon, C. Parkin, A.W. Roberts, L. Smith, N. Kuszniir, D. Healey, V. Tymms, N. Hurst and A. Roberts

## Abstract

The integrated Seismic Imaging and Modelling of Margins (iSIMM) project is a joint industry-university research project seeking to characterize magmatic ocean margins and develop new models for their evolution. The iSIMM project aims to tackle two of the biggest problems facing hydrocarbon explorationists on the NW European Atlantic margin, and on all other volcanically dominated margins. These are the inability of conventional seismic reflection methods to image through basalt layers overlying sediments, and the failure of current methods and software to model properly the stretching, subsidence, and thermal history of rifted continental margins.

The seismic components of iSIMM seek to address the seismic imaging problem by developing techniques using very long-offset, low-frequency, streamer acquisition, together with wide-angle imaging using ocean-bottom seismometers (OBS) to penetrate through the basalts. It will then be possible to develop a structural model from seabed to Moho to image the stretched crust and the extruded, intruded, and under-plated igneous material, and to use these constraints in magmatic margin basin modeling.

In summer 2002, seismic data were acquired successfully over two such margins: the Hatton-Rockall margin and the margin to the northeast of the Faroe Islands, using a combination of towed streamers and ocean-bottom seismometers (OBS). This paper describes the towed-streamer survey over the Faroes margin, where a 385 km profile was acquired by WesternGeco using three single-sensor streamers.

The acquisition used a source array tuned for low frequencies, building upon reported experiences of imaging below shallow basalts west of Ireland, and seismic characterisation of Lower Series basalts in the Lopra borehole. The time and depth processing of the towed-streamer data has been completed and, in this paper, we describe key features of the acquisition and the processing, and we present examples of the data.

## Introduction

The early Tertiary onset of seafloor spreading in the North Atlantic was accompanied by extensive volcanism, probably caused by lithospheric rifting interacting with the Iceland mantle plume (Barton and White, 1997). Massive lava flows extend away from the rift zone across the potential hydrocarbon-prospective basins of the Atlantic margin (e.g., Richardson *et al.*, 1999). The extruded material ap-

pears to be accompanied, in places, by intrusion of sills into the sedimentary sequence, lower-crustal sill intrusion and/or igneous underplating. This resulted in permanent uplift in the affected areas.

The iSIMM project integrates strategies for imaging and then modeling the effects of extrusive lavas, sills, and lower-crustal intrusions at magmatic ocean margins. Intracratonic basin models can successfully predict heat flow and subsidence, and hence, broad-brush hydrocarbon maturation,

from basin stretching. However, these models cannot easily be extended to magmatic margins due to melt underplating and extrusion (i.e., crustal non-conservation), and depth-dependent stretching.

The Tertiary volcanic material which comprises the Faroese component of the North Atlantic igneous province provides a substantial barrier to seismic imaging of basin structure and, hence, to modeling the subsidence and development of continental margins. The seismic component of the iSIMM project seeks to develop seismic acquisition and processing technology, focusing on low frequencies, to image the crust from surface to Moho using a combination of towed-streamer and OBS acquisition.

Combinations of new streamer, OBS, gravity and magnetometer data were acquired in two long transects across contrasting continental margins at Hatton Bank and the margin east of the Faroes (White *et al.*, 2002). This paper focuses on Line ISIMM02A, the towed-streamer component of the transect in the Faroes area. This line passes over the complete range of basalt environments from no basalt at all on the southeast flank of the Faroe-Shetland Trough, through increasing basalt cover and the basalt escarpment, over the Fugløy Ridge, across the continent-ocean transition east of the Faroe Islands and out over basaltic oceanic crust (Figure 1).

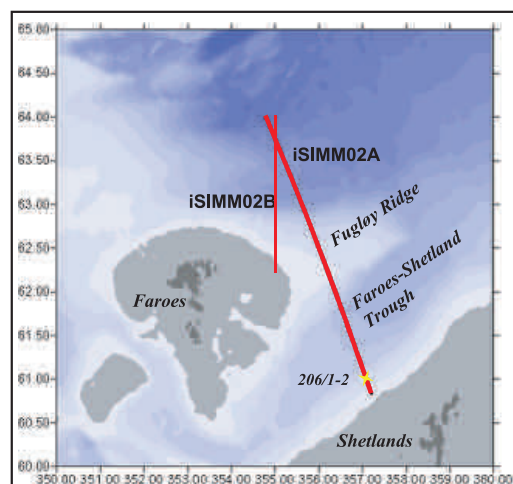


**Figure 1.** Long-offset, multi-streamer swaths acquired by *M/V Geco Topaz*. This paper presents the results from line ISIMM02A.

## Motivation for low frequencies and long offsets

Stacked basalt flows are highly heterogeneous. Flow boundaries are characterised by lower velocities and densities than flow centres, caused by vesicles at the top and base of the flow (Planke and Cambray, 1998), and by weathering and alteration. The heterogeneity causes spectral colouration and scattering loss in seismic transmission. Rough flow boundaries also cause further scattering loss. However, Dancer and Pillar (2002) used low-frequency seismic energy to image the gas-bearing sands of the Corrib field, west of Ireland, which are overlain by shallow basalts. Mack (1997) modelled the effects of layered basalt flows and proposed low frequencies to minimise scattering loss. Christie *et al.* (2002 and in press) estimated an effective  $Q$  of 35 in layered basalts from a VSP in the Lopra 1/1A borehole, which penetrated some 3.6 km of Lower Series basalts. This is consistent with more recent estimates of basalt scattering loss by Maresh *et al.* (2003). Ziolkowski *et al.* (2001) also proposed low frequencies for sub-basalt imaging and advocated large airguns towed deep to generate the low-frequency bandwidth. In the iSIMM towed-streamer profile, low frequencies were produced by adapting the bubble-tuned airgun method of Avedik (1993).

The requirement for long-offset data has been understood for a number of years following the two-boat acquisition of long-offset data by Geco-Prakla in 1998 (Brown *et al.*, 1998; Kostov *et al.*, 2000) and by Western Geophysical in the FLARE experiment in 1999 (White *et al.*, 1999).

## Data acquisition

The towed-streamer line ISIMM02A was acquired by *M/V Geco Topaz* in August 2002. The *Topaz* towed three, single-sensor streamers, two of 4 km and one of 12 km, to provide both long offsets and crossline protection at shorter offsets (Figure 2). To date, only data from the 12 km streamer has been processed. The streamers were towed at 18 m depth. The combination of deep tow, good weather and on-board digital group forming (Martin *et al.*, 2000) gave data sampled at 12.5 m, with exceptionally high signal-to-noise ratio (Figure 3). The



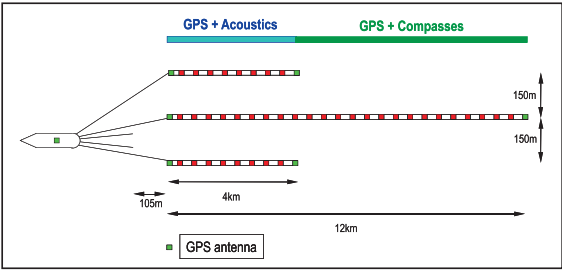


**Figure 2.** The three-streamer towing configuration for Line ISIMM02A acquired by *M/V Geco Topaz*.

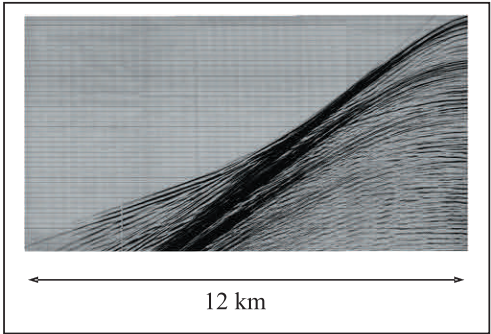


**Figure 3.** An example 12 km shot gather. The trace interval is 12.5 m.

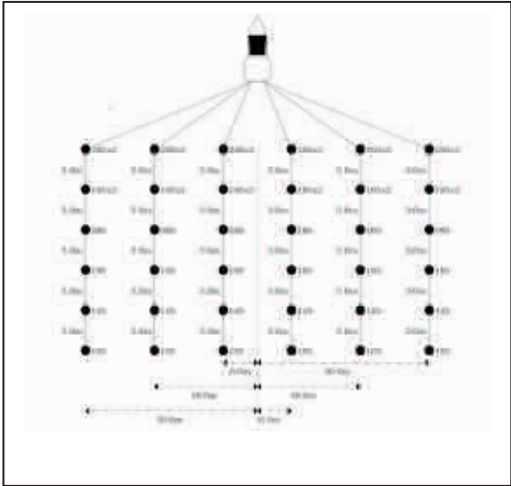


**Figure 4.** A diagram showing the 10,170 in<sup>3</sup> source array used for Line ISIMM02A.

long-offset seismic data show events with linear moveout at larger offsets, which will permit correlation with the OBS.

A large volume, wide source was carefully designed by combining two standard source arrays (Figure 4). The source was also towed deep and tuned on the first bubble. The source volume was

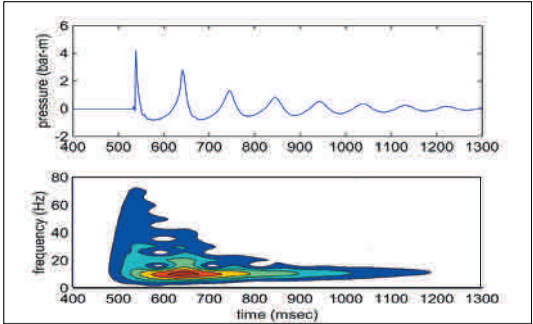


**Figure 5.** Amplitude and frequency spectrum from a single 400 in<sup>3</sup> gun at ten-m depth with no ghost, showing the greater low-frequency content in the bubble

fired at 140 bar with a 50 m pop interval to acquire 18 s records. This would allow the acquisition of doubly mode-converted shear events at long offsets which elsewhere have been used successfully to image beneath basalt (Emsley *et al.*, 1998). Presurvey modeling showed a benefit at low frequencies for the bubble-tuned source (Figure 5) (Lunnon *et al.*, 2003). The TRISOR source controller enabled

**Table 1. Acquisition parameters for line ISIMM02A**

Vessel	M/V Geco Topaz	No. streamers x separation	3 x 150 m
Energy source	Airgun array	Group interval	3.125 m single sensor
Type: Volume	Bolt: 10,170 in <sup>3</sup>	Streamer depth	18 m
Gun depth	18 m	Active length	4-12-4 km
String separation	12 m	Near trace offset	105 m
TRISOR/CMS	Yes	Record length	18 s
Gun tuning	First bubble	Sample interval	2 ms
Shotpoint interval	50 m (~20 s)	Acquisition filters	3 Hz/18 – 200 Hz/477
		Streamer positioning	Acoustic + Q-Fins

bubble tuning and acquired near-gun hydrophone traces to compute a calibrated marine signature (CMS) using the Notional Source algorithm (Ziolkowski *et al.*, 1982). On-board QC showed that the CMS far-field signature was stable and a good match to the presurvey-modelled signature.

## Data Processing

The WesternGeco Gatwick processing group has completed time and depth processing of the 12 km streamer data. A key enabler for the bubble-tuned source was the shot-by-shot estimate of the mixed-phase, far-field signature. After convolution with the streamer ghost, an average source signature was estimated and a shot-by-shot shaping filter was applied to remove any residual source variation. Detailed testing determined the optimal working signature and bandwidth. Because conventional seismic technology is effective in imaging the post-basalt sequence, it was decided to focus on the low-frequency bandwidth for sub-basalt penetration. Consequently, the source wavelet was whitened and shaped to a zero-phase wavelet in the band below the first ghost notch. Figure 6 shows the field signature, with a streamer ghost, in comparison to the final shaped signature. This signature processing strategy has been effective for the sub-critically reflected data.

In sub-basalt imaging, long-period multiples generated between the major impedance boundaries of free surface, seabed, top basalt, and base basalt require careful processing. Our strategy combined

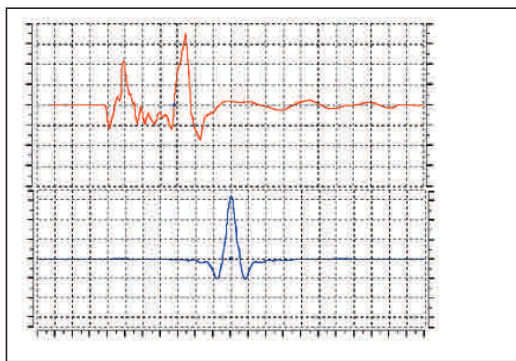


**Figure 6.** Comparison of field estimated signature convolved with the streamer ghost (upper, red) and the processing wavelet after designature (lower, blue). Timing lines are at 30 ms.

a Kirchhoff wavefield inversion method with a moveout-dependent, Radon transform method. For the former, the WesternGeco implementation of surface-related multiple elimination was the preferred approach (e.g. Dragoset, 1999). Because the algorithm is not velocity-dependent, it was effective on water-column multiples even when the sub-basalt velocities were uncertain. Two passes of Radon demultiple, with multiple-trend velocity picking, removed faster multiples and remaining energy at longer offsets. Prediction of the multiples generated by the top basalt horizon allowed picking of the second multiple trend. A primary-retaining Radon transform was applied only at the pre-stacking stage, after a significant amount of multiple had already been removed. This used a velocity mute at 85% of the (now more confident) picked primary velocities. True-offset CMP gathering accommodated the fairly significant feather angles on the 12 km cable. Fourth-order moveout flattened the farther offsets. Partial pre-stack migration, comprising constant-velocity NMO, DMO, and Stolt migration, removed stacking conflicts and improved primary velocity picking. The migration was backed-off post-stack, before applying a full Kirchhoff migration using the smoothed primary velocity field. Careful angle muting at top basalt and outer and inner muting deeper in the section, maintained stacked event resolution.

A 40 km part of line ISIMM02A was also pre-stack depth migrated. Pre-stack depth migration is the most accurate form of seismic imaging, where, through an iterative sequence, information embedded in seismic data is extracted to derive an accurate interval velocity model, which is subsequently used in the migration to produce the final image in depth. The high-fidelity algorithm accounts for any vertical or lateral velocity variations and maps seismic energy in its correct subsurface position.

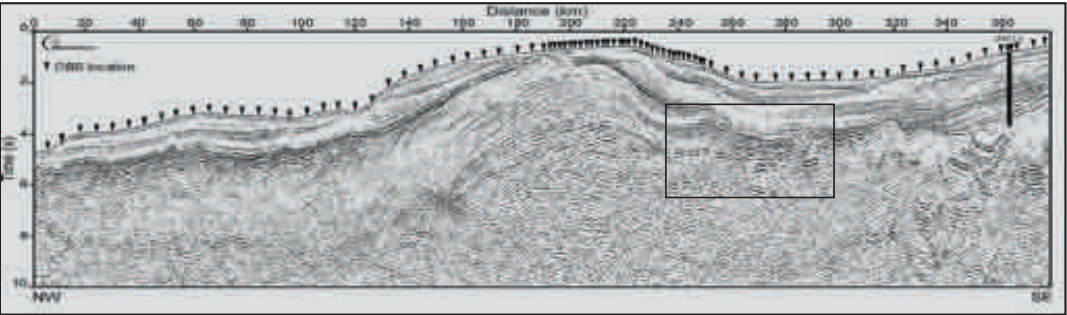
The method propagates seismic energy through the high-velocity basaltic layers, which act as a powerful lens, and correctly focuses it to image the sub-basalt regions. Its success, however, depends on the accuracy of the velocity model; the more accurate the velocity model, the more likely it is to optimally image the deeper geology. It is, therefore, imperative that the derived velocity model satisfies the conditions of seismic data, and at the same time, is geologically meaningful.

Table 2: Data processing flow for Line ISIMM02A	
REFORMAT from SEG.D. Record length 18 s	SORT TO COMMON OFFSET
NAVIGATION/SEISMIC MERGE	DIFFERENTIAL NMO. Picked 10 km velocities
CMS DESIGNATURE to zero phase debubbled wavelet	NMO constant velocity 2000 m/s
RESTRICT RECORD LENGTH TO 10.5 s	DMO Kirchhoff
RESAMPLE TO 6 ms	F/K STOLT MIGRATION constant velocity 2000 m/s
F/K FILTER	INVERSE NMO constant velocity 2000 m/s
RETAIN ODD NUMBERED TRACES	SORT TO CMP 120 offsets
F/K SHOT INTERPOLATION	RETAIN ODD NUMBERED CMPs
OFFSET RECONSTRUCTION FOR SMA	HIGHER-ORDER NMO picked 1 km DZO velocities
SURFACE MULTIPLE PREDICTION	NMO Picked 500 m DZO velocities
MULTIPLE SUBTRACTION	RADON TRANSFORM DEMULTIPLE
GEOMETRIC SPREADING CORRECTION	F/K NOTCH FILTER
SORT TO CMP	OUTSIDE AND INSIDE MUTES
NMO Constant velocity 1470 m/s	STACK
RADON TRANSFORM DEMULTIPLE (Pass 1).	F/K STOLT DEMIGRATION const. velocity 2000 m/s
INVERSE NMO Constant velocity 1470 m/s	F-X DECONVOLUTION constant velocity 2000 m/s
NMO. Picked 1 km Multiple velocities	AMPLITUDE SCALING
RADON TRANSFORM DEMULTIPLE (Pass 2)	T-X KIRCHHOFF MIGRATION
INVERSE NMO. Picked 1 km Multiple velocities	TIME VARIANT FILTER
MERGE 2 PARTS OF LINE	AGC SCALING
ASSIGN CMPS ON WIDE GRID Using true offsets	GUN/CABLE correction

The initial velocity model was provided by the Faroese Geological Survey. Built top-down, layer-by-layer, it was based on an interpretation of the time-migrated data, with initial velocities based on well data and regional knowledge. It was subsequently further constrained by automatic tomographic inversion routines applied to each layer.

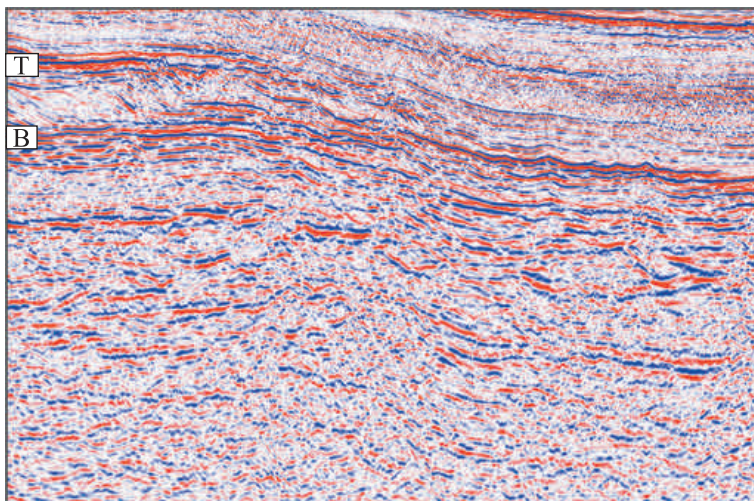
Results

Figure 7 shows a squash plot of the final time migration of the whole 385 km line ISIMM02A. The southeast end of the line lies in UK waters and ties well 206/1-2. The southwest limit of the basalt lavas is at approximately 310 km and the wedge of basaltic lavas thickens to the northwest. The major structure in the centre of the section is



**Figure 7.** A squash plot of the whole 385-km line ISIMM02A. The rectangle shows the area enlarged in Figure 8





**Figure 8.** A detailed TWT section of approx 60 km of line ISIMM02A.

the Fugløy Ridge (160 – 240 km). The top basalt event is the strong event only a short way below the seabed at the crest of the ridge (210 km). The continent /ocean boundary lies in the approximate distance range 140-160 km. Note the characteristic seaward-dipping reflectors in this area.

Figure 8 is an enlargement of the area marked by the rectangle in Figure 7. It shows a sample section from the final migration that crosses the basalt escarpment on the northwestern flank of the Faroe-

Shetland Trough. The image comprises 60 km of data and displays a two-way time interval from approximately 3.0 sec to 6.5 sec. Northwest is to the left of the image. The basalt top is at about 2700 ms at the left edge of the image (marked by "T") and is probably just below the strong, smooth reflector which may be the Balder ash marker. Below top basalt is a sequence of sigmoidal structures that are probably palaeo-shorelines of the basalt flows. Down-dip from this sequence is the basalt escarpment identified by other authors (e.g. Kiør-

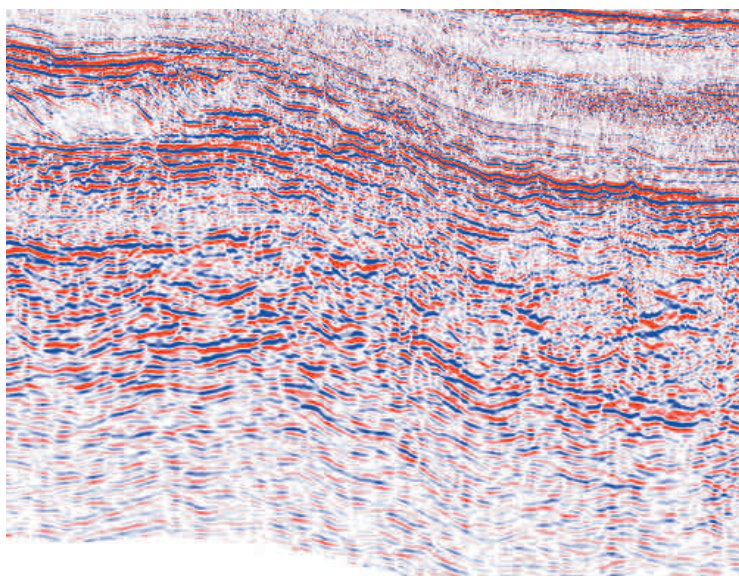


**Figure 9.** A detailed depth section of the same part of line ISIMM02A shown in Figure 8 (displayed in time to ease comparison).

boe, 1999). The base basalt is unsure, but the base of the flows is interpreted by the letter "B". Further support will come from integrated velocity analysis of the 2 km-spaced OBS over this area, with the long-offset arrivals from the streamer data. Both approaches will be supported by analysis of the gravity data acquired over this line. The imaging of sub-basalt reflections is a considerably improved, compared to any previous seismic data acquired in this region.

Figure 9 shows the depth migration of the same part of the line as Figure 8 (displayed in time to ease comparison). Note how the depth migration has improved the quality of sub-basalt imaging with better reflector continuity and fault definition.

## Conclusions

In 2002, the iSIMM project acquired both towed-streamer and OBS data over two margins in the Hatton-Rockall area and northeast of the Faroe Islands. One goal is to characterise magmatic margins and drive the development of models capable of simulating the spatio-temporal evolution of subsidence and heatflow. In the Faroes region, a 385 km profile was shot with long-offset, single-sensor streamers, using a bubble-tuned source designed for low frequencies. Key aspects of the processing included shot-by-shot signature monitoring allowing waveshaping, and careful demultiple.

The resulting TWT-migrated data revealed good imaging of structures beneath the top basalt. This imaging was further improved by depth migration. Further analysis, integrating the OBS data, and focusing on the long-offset arrivals will help to identify the base of the basalts and illuminate deeper structure using wide-angle imaging techniques, as used by White *et al.* (2003) in estimating the regional distribution of basalt flows in the Faroe-Shetland Trough.

## Acknowledgements

We thank the crew the *M/V Geco Topaz* for their expertise in acquiring high-quality data. We acknowledge Peter Sabel, Jon-Fredrik Hopperstad, and Andy Harber of

WesternGeco for valuable support during the pre-survey modeling. John Bacon and colleagues in the WesternGeco data processing group brought insight to the data analysis. Velocity data provided by the Faroese Geological Survey was invaluable in the depth migration. iSIMM is supported by Liverpool and Cambridge Universities, Schlumberger Cambridge Research, Badley Geoscience Limited, WesternGeco, Amerada Hess, Anadarko, BP, ConocoPhillips, ENI UK, Statoil, Shell, the Natural Environment Research Council and the Department of Trade and Industry. However, the views expressed here are those of the authors who are solely responsible for any errors.

## References

- Avedik, F., Renard, V., Allenou, J.P., and Morvan, B. 1993. Single bubble air-gun array for deep exploration. *Geophysics* 58: 366–382.
- Barton, A.J., and White, R.S. 1997. Crustal structure of the Edoras Bank continental margin and mantle thermal anomalies beneath the North Atlantic. *Journal of Geophysical Research* 102: 3109–3129.
- Brown, G., Hoare, R.J.S., Morice, S., Roberts, G., and Ronen, S. 1998. The design and implementation of long offset seismic profiling for sub-basalt imaging. PETEX.
- Christie, P.A.F., Gollifer, I., and Cowper, D. 2002. Borehole seismic results from the Lopra Deepening Project. *Journal of Conference Abstracts* 7(2): 138–139.
- Christie, P.A.F., Gollifer, I., and Cowper, D. in press. Borehole seismic studies of a volcanic succession from the Lopra1/1A borehole in the Faroe Islands, NE Atlantic. *Geology of Denmark Survey Bulletin*.
- Dancer, P.N., and Pillar, N.W. 2002. Successful sub-basalt imaging with enhanced low frequency 3D seismic data: Corrib Field, West of Ireland. *Presented at: Frontier Exploration of Volcanic Continental Margins. Geological Society of London*, 17–18 September 2002.
- Dragoset, B. 1999. A practical approach to surface multiple attenuation. *The Leading Edge* 18(1): 104–108.
- Emsley, D., Boswell, P. and Davis, P. 1998. Sub-basalt imaging using long offset reflection seismic data. *60<sup>th</sup> Ann. Mtg., Eur. Assn. Geosci. Eng., Expanded Abstracts*: 1–48.
- Kjørboe, L. 1999. Stratigraphic relationships of the Lower Tertiary of the Faeroe Basalt Plateau and the Faeroe-Shetland Basin. In: Fleet, A.J., and Boldy, S.A.R. (eds.) *Petroleum Geology of Northwest Europe: Proceedings of the 5<sup>th</sup> Conference*. Geological Society, London: 559–572.
- Kostov, C., Hoare, R.J.S., Jaasund, S., and Larssen, B. 2000. Advances in sub-basalt p-wave imaging with long offset streamer data. *62<sup>nd</sup> Mtg., Eur. Assn. Geosci. Eng., Expanded Abstracts*.
- Lunnon, Z., Christie, P., and White, R. 2003. An evaluation of peak and bubble tuning in sub-basalt seismology: modelling and results from OBS data. *First Break* 21(12): 51–56.

- Mack, H. 1997. Seismic response of Tertiary basalt flows in the northeast Atlantic - a modelling study. *59<sup>th</sup> Mtg., Eur. Assn. Geosci. Eng., Expanded Abstracts*: B017.
- Maresh, J., Hobbs, R.W., White, R.S. and Smallwood, J.R. 2003. Attenuation of Atlantic margin basalts using downhole VSP. *73<sup>rd</sup> Ann. Internat. Mtg., Soc. Expl. Geophys.*, Dallas: 1310–1313.
- Martin, J., Ozbek, A., Combee, L., Lunde, N., Bittleston, S. and Kragh, E. 2000. Acquisition of marine point receiver seismic data with a towed streamer. *70<sup>th</sup> Ann. Internat. Mtg., Soc. Expl. Geophys., Expanded Abstracts*: 37–40.
- Planke, S., and Cambray, H. 1998. Seismic properties of flood basalts from Hole 917A downhole data, southeast Greenland volcanic margin. *In: Sanders, A.D., Larsen, H.C. and Wise, S.W. Jr., (eds.) Proceedings of the Ocean Drilling Program, Scientific Results* 152: 453–462.
- Richardson, K., White, R., England, R.W., and Fruehn, J. 1999. Crustal structure east of the Faroe Islands. *Petroleum Geoscience* 5: 161–172.
- White, R.S., Christie, P.A.F., Kusznir, N.J., Roberts, A., Hurst, N., Lunnon, Z., Parkin, C.J., Roberts, A.W., Smith, L.K., Spitzer, R., Surendra, A., and Tymms, V., 2002. iSIMM pushes frontiers of marine seismic acquisition. *First Break* 20: 782–786.
- White, R.S., Fruehn, J., Richardson, K.R., Cullen, E., Kirk, W., Smallwood, J.R., and Latkiewicz, C. 1999. Faroes Large Aperture Research Experiment (FLARE): Imaging through basalts. *In: Fleet, A.J., and Boldy, S.A.R. (eds.) Petroleum Geology of Northwest Europe: Proceedings of the 5<sup>th</sup> Conference*. Geological Society, London: 1243–1252.
- White, R.S., Smallwood, J.R., Flidner, M.M., Boslaugh, B., Maresh, J. and Fruehn, J. 2003. Imaging and regional distribution of basalt flows in the Faroe-Shetland Basin. *Geophysical Prospecting* 51: 215–231.
- Ziolkowski, A., Hanssen, P., Gatliff, R., Li, X., and Jakubowicz, H. 2001. The use of low frequencies for sub-basalt imaging. *71<sup>st</sup> Ann. Internat. Mtg., Soc. Expl. Geophys., Expanded Abstracts*: 74–77.
- Ziolkowski, A., Parkes, G., Hatton, L. and Haugland, T. 1982. The signature of an air-gun array - Computation from near-field measurements including interactions. *Geophysics* 47: 1413–1421.



# PGS Faroe Shetland Basin MegaSurvey – the Key to New Discoveries in a Maturing Frontier Area?

NICHOLAS TERRELL<sup>1</sup>, HUW EDWARDS<sup>1</sup>, PERRY SCOFFIELD<sup>2</sup> AND MARK MARTIN<sup>3</sup>

1: PGS Reservoir

PGS Thames House, 17 Marlow Road, Maidenhead Berkshire, SL6 7AA, UK.

E-mail: [nicholas.terrell@pgs.com](mailto:nicholas.terrell@pgs.com); [huw.edwards@pgs.com](mailto:huw.edwards@pgs.com);

Tel: +44 1628 641000; Fax: +44 1628 641200

2: PGS Geophysical (New Ventures)

PGS Court, Halfway Green, Walton-on-Thames, Surrey, KT12 1RS, UK.

E-mail: [perry.scofield@pgs.com](mailto:perry.scofield@pgs.com); Tel: +44 1932 260001; Fax: +44 1932 266465

3: PGS Geophysical (Data Sales)

PGS Court, Halfway Green, Walton-on-Thames, Surrey, KT12 1RS, UK.

E-mail: [mark.martin@pgs.com](mailto:mark.martin@pgs.com); Tel: +44 1932 260001; Fax: +44 1932 266465

This paper focuses on the initial results from the interpretation of the Faroe-Shetland Basin (FSB) MegaSurvey - Phase I (figure 1) which focused on key regional horizons in order to create a consistent structural and stratigraphic framework. The MegaSurvey dataset allows visualisation and analysis of the subsurface on a scale and resolution that has not previously been fully recognised in this frontier province, providing detailed depositional and structural information over much of the basin. This new regional scale interpretation has been integrated with potential field modelling and attribute analysis to provide answers to localised as well as regional questions. Combined with dramatic visualisations of the subsurface, it has allowed a step change in our understanding of the hydrocarbon potential of the Faroe-Shetland Basin.

MegaSurveys are an exciting new concept that push current technology to the limit and are already providing a basis for a new era of hydrocarbon exploration, not only reducing risk in mature provinces such as the North Sea but also in frontier provinces such as the Faroe-Shetland Basin.

The first phase of the FSB MegaSurvey has been created from the merging of both oil- and service- companies 3D seismic data in and around

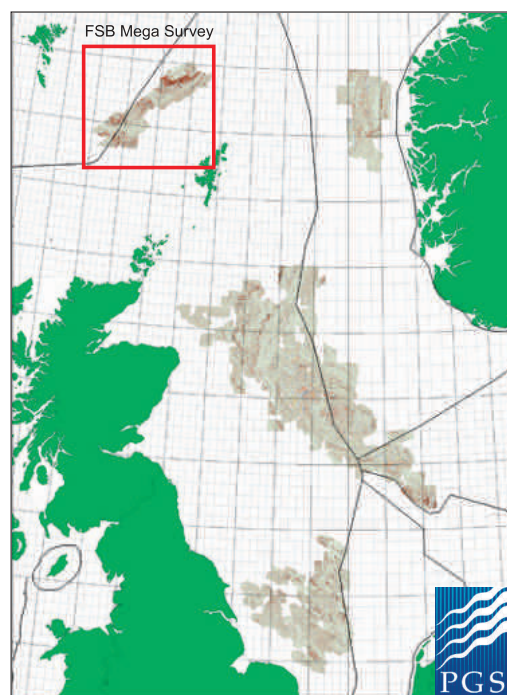


**Figure 1.** Location of the four Northwest Europe MegaSurveys.

the former “White Zone” of the Faroe-Shetland Basin. This MegaSurvey provides a continuous

dataset over an area of almost 10,000 sq km with coverage of Faroese acreage to the north and west of the Westray and Corona Ridges.

The FSB MegaSurvey is currently being expanded with the merging and interpretation of a further 10,000 sq km of proprietary and non-exclusive 3D surveys in the basin.

## The MegaSurvey Merge Process

The merging of the FSB MegaSurvey has been separated into two phases (figure 2). Phase I represents the initial merging of four PGS MC3D datasets covering an area of 9,650 sq km, 1,650 sq km of which lies within the in Faroes sector. Phase II is currently being merged and will increase the FSB MegaSurvey's full-fold coverage area to in excess of 20,000 sq km.

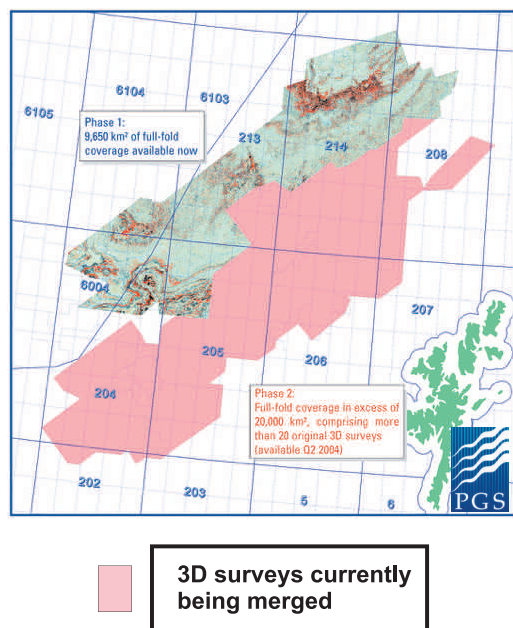


**Figure 2.** Basemap showing Phase I and II of the FSB MegaSurvey.

The MegaSurveys are based on seismic that has been released by oil companies, PGS owned seismic, and non-exclusive seismic available from other geophysical contractors. For the most part, the data is available as 3D time-migrated seismic surveys. The individual surveys are first QC'd and loaded to PetroBank. Following the initial navigation data QC, the data are output from PetroBank,

and loaded onto the PGS processing system to start the merge process. Quality control of the merges is vital and is performed by inline/cross-line analysis of both amplitude and time data in an interactive workstation review process. The different vintages and data acquisition methods that have been used imply that the seismic varies in quality. Thus, some adjustments of the data are necessary to achieve the optimal merge of all the different surveys.

After the merging process, the PetroBank contains a common regional final migration 3D dataset of consistent orientation and line / trace numbering that can be delivered in a variety of workstation formats.

## Interpretation of the MegaSurveys

It has been recognised that the vast size of the MegaSurvey projects stretch the resources of today's more asset-focused oil company. PGS Reservoir is therefore carrying out a regional interpretation of the FSB MegaSurvey data to allow oil companies to regionally review the data and then subsequently focus in on specific prospective areas.

The aim of the interpretation of the FSB MegaSurvey is to provide a consistent regional and digital interpretation across the entire area, tied to released well data. An initial pilot interpretation study was carried out on the FSB Phase I merge to determine a range of project parameters including data loading, auto tracking, gridding and mapping. This pilot work, along with experience gathered from previous PGS MegaSurvey projects, developed both a data management and interpretation methodology.

The interpretation focused on seven key regional horizons to create a consistent stratigraphic framework (figure 3):

- Seabed
- Middle Miocene Unconformity
- Top Intra Middle Eocene Fan
- Base Intra Middle Eocene Fan
- Top Balder Formation
- Base Tertiary
- Base Cretaceous Unconformity

Data from 154 released wells, which include formation tops and two-way travel times, has been

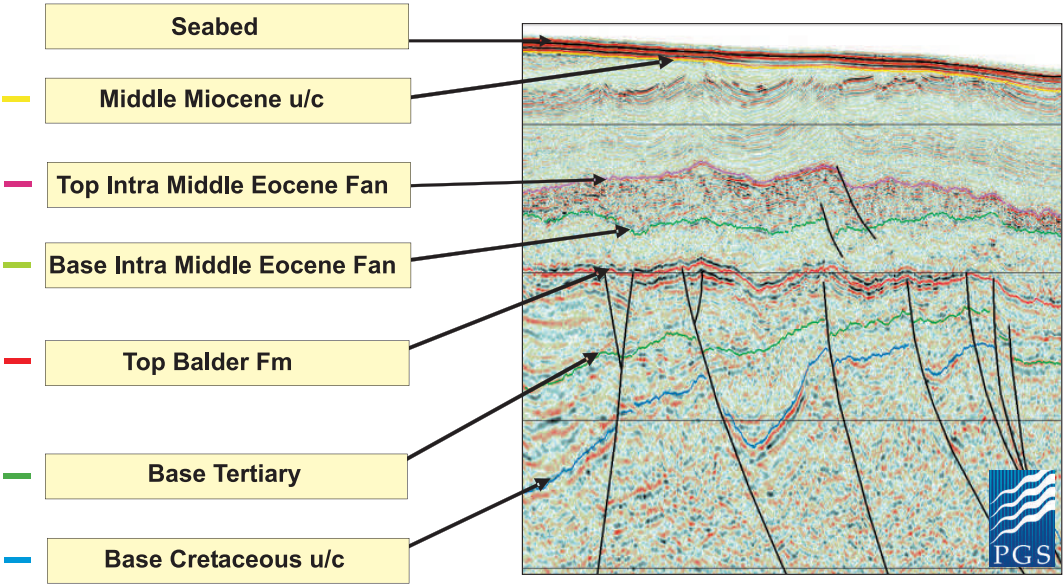


**Figure 3.** The seven regional horizons interpreted in the FSB MegaSurvey.

supplied by Aceca Geologica Ltd along with detailed facies maps. Work carried out in conjunction with Ark Geophysics Ltd involving 2D/2.5D gravity and magnetic forward modelling (figure 4) has

proved invaluable in the initial pilot interpretation, with particular respect to sub-basalt interpretation, and will be used interactively alongside more conventional seismic interpretation in Phase II.

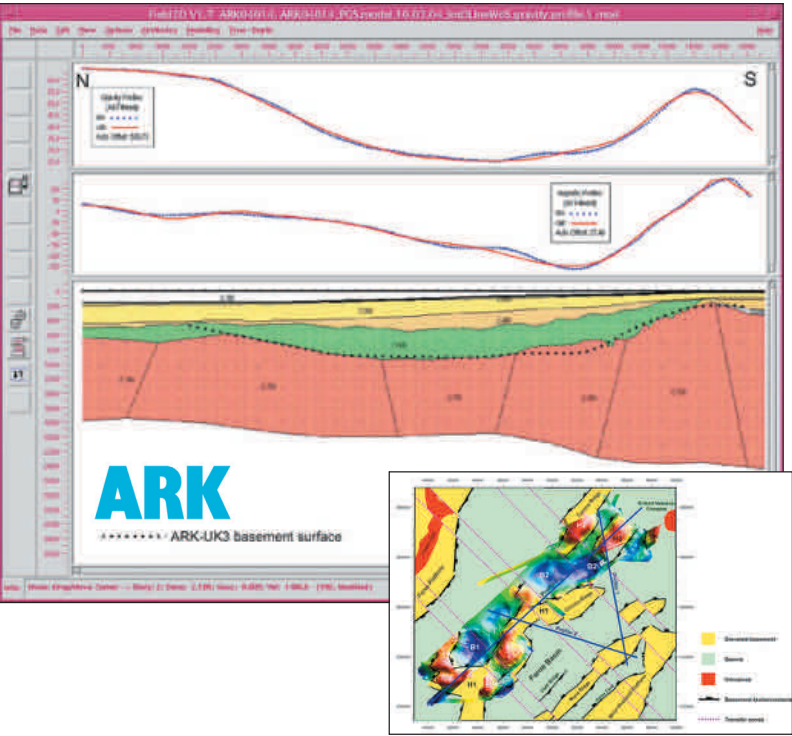


**Figure 4.** 2D/2.5D forward modelling of potential field data in conjunction with seismic data interpretation has proved to be a valuable integrated approach in the FSB MegaSurvey interpretation.



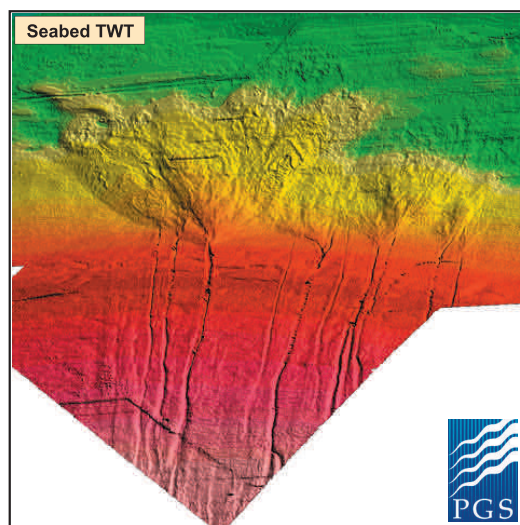


**Figure 5.** Present day basin floor fans developing at the base of the West Shetland shelf. Note the non-sinuuous incised channels on the slope.

## Geological results of the MegaSurveys interpretation

The FSB MegaSurvey allows visualisation of the subsurface on a scale and resolution that has never been available.

A structural elements map of the Faroe-Shetland Basin has been assembled based on seismic interpretation, digitally filtered gravity and magnetic data (potential field transforms) and previous work done in the area by PGS. The FSB MegaSurvey area is dominated structurally by the North Westray and Corona Ridges. These northeast-southwest trending Mesozoic structures separate the Faroe Basin and Faroe-Shetland Basin and have a big impact on the types of hydrocarbon trapping mechanisms observed in the area.

### Seabed

The seabed shows clear evidence for present day basin floor fans depositing sediments sourced from the West Shetland shelf (figure 5). These fans are fed by non-sinuuous, incised channels that bypass sediment over the shelf slope. Recent sediment drifts and contourite sedimentation can be clearly seen in the northern parts of the FSB MegaSurvey in the Faroe-Shetland Channel (figure 6). These kilometre scale, ripple-like features form as a result of the interaction between strong ocean bot-

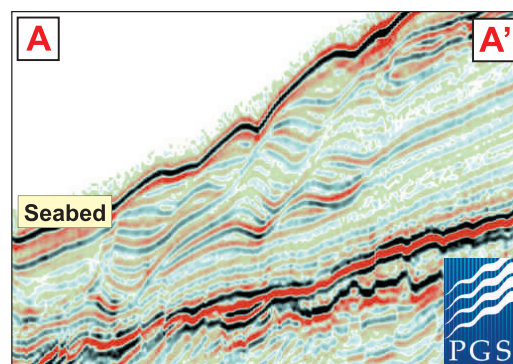
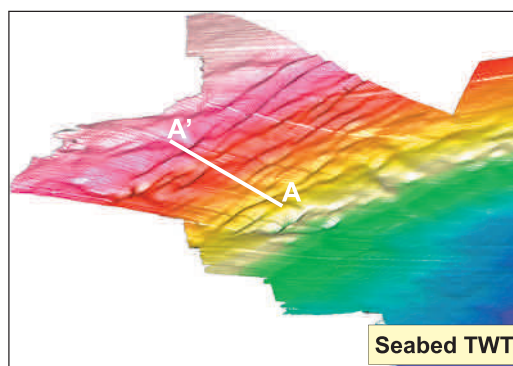


**Figure 6.** Evidence of contourite sedimentation on the seabed.

tom currents, sediment supply and the bathymetry of the continental margin.

### Middle Miocene Unconformity

The Middle Miocene Unconformity (figure 7) represents one of at least four Neogene unconformities within the Faroe-Shetland Channel. These unconformities converge to form a composite angular unconformity towards the West Shetland platform where the Neogene succession is much thinner. Figure 7 shows the Middle Miocene Unconformity horizon in the northern part of the FSB MegaSurvey. Post-early Pliocene incision can be observed on the platform slope. Dewatering has modified this shallow horizon resulting in sediment injection features and density inversion structures.

The latter (figure 8) represents a ductile equivalent of the polygonal faulting typically seen in the Central North Sea. As a result the Middle Miocene Unconformity is deformed into a series of typically one kilometre diameter, concave-downward, linked cusate domes that show polygonal plan-

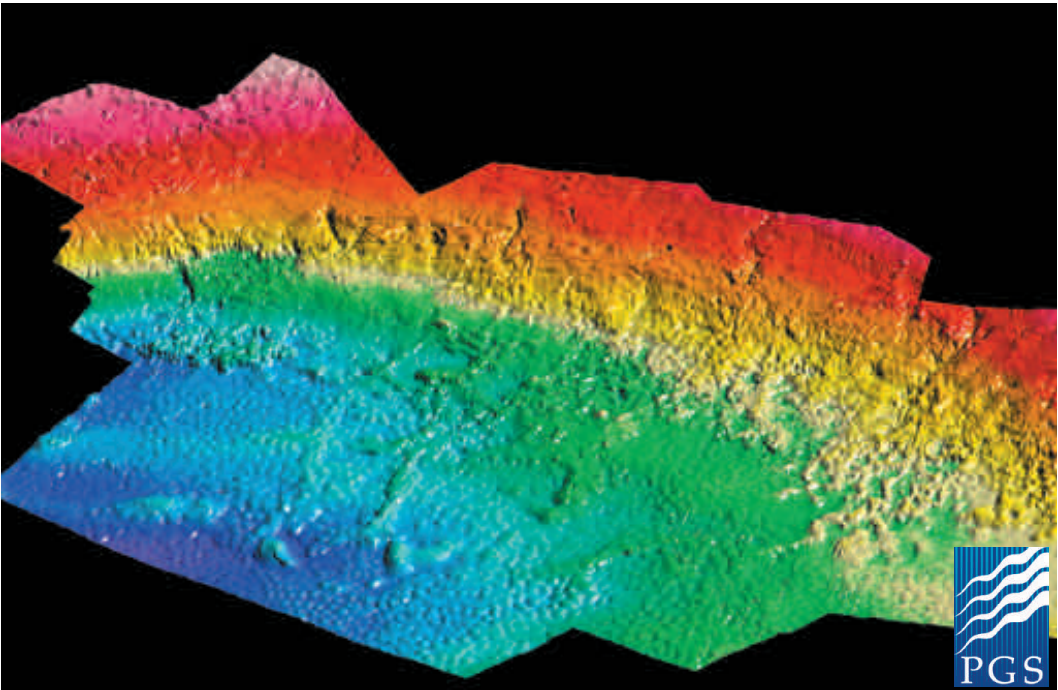


**Figure 7.** Basin scale image of the Middle Miocene Unconformity.

form geometry (Davies and Cartwright, 2002). In cross-section (see figure 8 inset seismic profile) these domes can be clearly seen along with the underlying diagenetic boundary (assumed opal A to C/T transformation).

The Middle Miocene Unconformity shows at least ten northeast-southwest trending anticlinal ridges within the FSB MegaSurvey. These formed

as a result of middle and late Miocene compression which caused contractional reactivation of the deeper Mesozoic extensional faults (Davies *et al.*, 2004).

**Eocene**

Both a top and base Intra Middle Eocene Fan horizon was picked resulting in the identification of

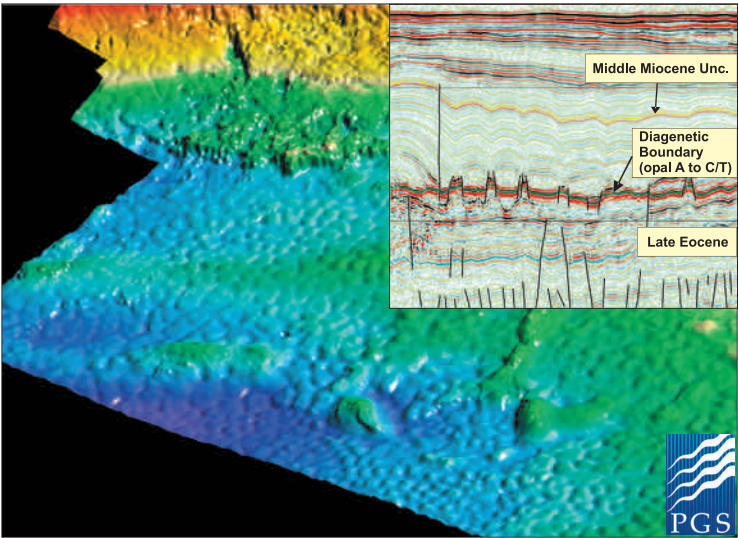


**Figure 8.** Detailed view of the Middle Miocene Unconformity showing pillow-like density inversion structures, formed partially as a result of dewatering. Inset seismic panel shows these density inversion structures in profile.

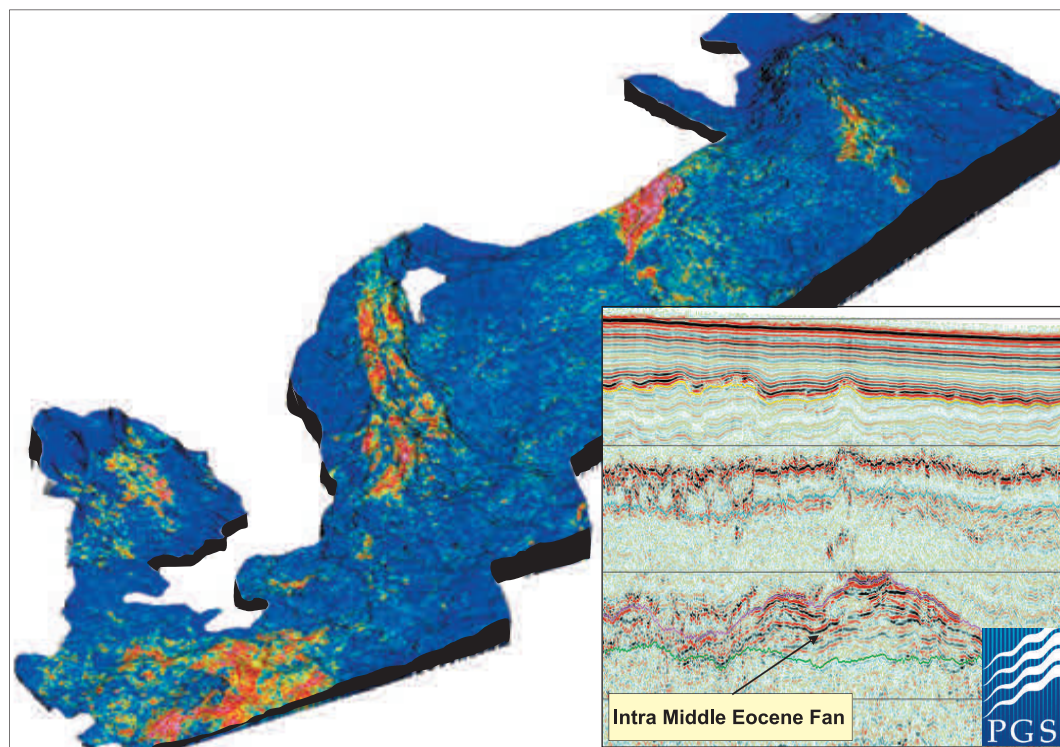


**Figure 9.** Regional RMS amplitude extraction draped over the top Intra Middle Eocene fan horizon. This image, covering approx. 7,000 sq km, shows well-developed Middle Eocene slope canyon and terminal fan systems that transported sediments off the West Shetland platform. The inset seismic profile shows a cross section perpendicular to one of the fan's axis.

four 30-100 km long slope canyons and linked terminal fans (figure 9). These fans formed in the middle Eocene during the basin's post-rift subsidence phase and transported clastic material off the West Shetland platform from the south. The slope canyons show typical confined geometries and erosional bases whereas the terminal fans, located in a more basinal setting, are less confined and have non-erosional bases. Half-graben depocenters, related to the underlying dormant Mesozoic extensional faults that form the Corona Ridge, diverted sediment transport from a north-south orientation to a northeast-southwest orientation. This change in direction broadly marks the transition between slope canyon and terminal fan facies.

The terminal fans were subsequently inverted to form northeast-southwest trending anticlinal domes as a result of the middle and late Miocene compression and differential compaction. There is therefore a spatial correspondence between potential reservoir quality sands and four-way dip closures formed as a result of Miocene inversion (Cloke *et al.*, 1999). This type of feature was de-

liberately targeted by well 214/4-1 resulting in the Tobermory gas discovery and represents an exciting future gas play in the Faroe Shetland area.

### Palaeocene and Pre-Cretaceous

The top Balder Formation and base Tertiary horizons show numerous inversion structures related to multiple phases of Tertiary inversion both in UK and Faroe waters. These features are related to contractional reactivation of the deeper Mesozoic Corona and North Westray extensional structures and have been the focus of some of the recent drilling activity in the area. In 2002 wildcat well 204/10-1 drilled the 'Cambo' prospect targeting inverted Palaeocene sediments and the deeper Mesozoic structure. Other similar structures in the area include the Rosebank-Lochnagar prospects. A top basement reflector (pre-Devonian/Carboniferous) is present in this area and is supported by potential field modelling.

Figure 10 shows a Balder Formation level RMS amplitude extraction in the northern part of the FSB MegaSurvey. An edge of basalt can be clearly



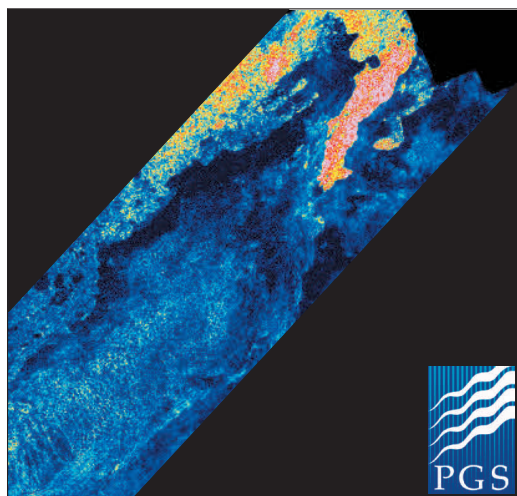


**Figure 10.** RMS amplitude extraction showing the edge of Palaeocene lavas. Amplitudes associated with individual lava flows are clearly visible towards the top of the image.

observed based on the extraction along with individual lava flows.

Seismic evidence for possible transfer zones can be seen in figure 11 and show a northwest-southeast orientation. The location of these transpressional 'pop-up' features corresponds to transfer zones regionally interpreted on gravity and magnetic data.

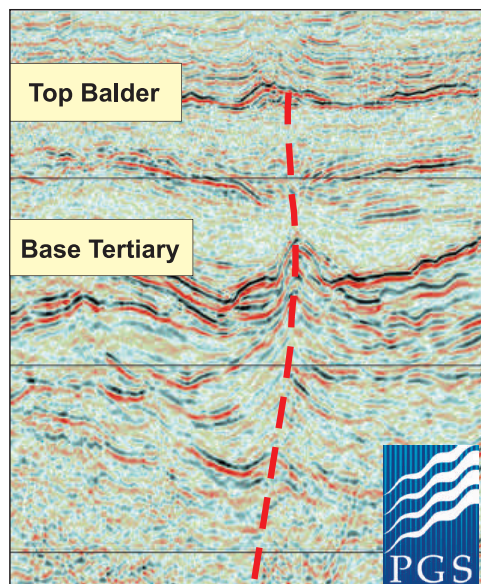


**Figure 11.** Transpressional 'pop-up' feature associated with the Victory transfer zone. These features appear to terminate at the Top Balder Formation horizon.

## MegaSurvey summary

PGS is now creating some of the world's largest ever 3D seismic data sets. Hundreds of 3D surveys from the Central North Sea (CNS), Southern North Sea (SNS), Northern North Sea (NNS) and the Faroe-Shetland Basin (FSB) have now been merged into four separate MegaSurveys. The latest merge project PGS has undertaken is the FSB MegaSurvey, covering more than 20,000 sq km. The FSB MegaSurvey brings together more than 20 separate 3D surveys and is comprised of over 1.3 terabytes of migrated, full-fold coverage seismic data. Only a few years ago such a project would not have been possible due to both software and hardware limitations.

Within North West Europe over 100,000 sq km has already been merged and interpreted. The Central North Sea MegaSurvey now exceeds 60,000 sq km, the Southern North Sea 22,000 sq km, the Northern North Sea 10,000 sq km and the Faroe-Shetland Basin 10,000 sq km (figure 1).

The PGS MegaSurvey Project also exemplifies a very successful integrated project between various parts of the PGS organization: PGS Reservoir, PGS Marine Geophysical and PGS Data Processing.

## References

- Cloke, I.R., Line, C., Davies, R.J., Ferrero, C., Mclachlan, K. and Hornafius, S. 1999. The role of inversion in the development of the petroleum system of the Faeroe-Shetland Basin. In: *Extended Abstracts of American Association of Petroleum Geologists International Conference*, September 1999.
- Davies, R.J. and Cartwright, J.A. 2002. A fossilized Opal A to Opal C/T transformation on the northeast Atlantic margin: support for a significantly elevated Palaeogeothermal gradient during the Neogene? *Basin Research* 14(4): 467-486.
- Davies, R.J., Cloke, I.R., Cartwright, J.A., Robinson, A. and Ferrero, C. 2004. Post-breakup compression of a passive margin and its impact on hydrocarbon prospectivity: An example from the Tertiary of the Faeroe-Shetland Basin, United Kingdom. *American Association of Petroleum Geologists Bulletin* 88(1): 1-20.